Understanding the Role of ZAKβ in the Maintenance and Regulation of Skeletal Muscle Function

Amy Josephine Stonadge

PhD

University of York

Biology

February 2023

Abstract

Leucine-zipper and sterile-alpha-motif kinase β (ZAKβ) is a MAPKKK and novel skeletal muscle protein first identified as part of a protein complex found at the z-disc. Loss of ZAKβ has been implicated in a muscle myopathy, whereby human patients exhibit skeletal muscle weakness and fibre atrophy, suggesting a pivotal role in muscle maintenance. To elucidate its function, a mouse $ZAK^{-/-}$ line has been characterised in detail in combination with proteomics and *in vivo* modelling.

Visibly, $ZAK^{-/-}$ mice show a much milder phenotype compared to the human condition. In $ZAK^{-/-}$ mice, histopathological data from muscle regeneration, ageing, sex, and overload conditions reveals both age and activity as drivers of this condition. $ZAK^{-/-}$ mice exhibit an increase in the percentage of slow fibres and centralised nuclei in tonically active muscles, consistent with similar observations in patients. We also observe an accumulation of the large actin cross-linking protein FLNC and the Chaperone Assisted Selective Autophagy (CASA)-associated protein BAG3, suggesting inefficient protein turnover. Overexpression of ZAKβ in adult muscle fibres is sufficient to induce fibre growth.

We performed a phosphoproteomics assay to identify putative substrates of ZAKβ kinase activity. This assay identified a significant number of proteins associated with adhesion and cytoskeletal organisation at the z-disc and costamere. The presence of both SYNPO2 and FLNC in this screen suggested a role for ZAKβ in the protein turnover mechanism of cytoskeletal adhesion factors.

Mechanical overloading of hind limb skeletal muscle was associated with the exacerbation of FLNC aggregates suggesting that ZAKβ signalling is necessary for FLNC turnover throughout the physiological response to increased mechanical stress.

We suggest a role for ZAKβ in the regulation of z-disc and costameric protein complexes, integral for the mediation of the hypertrophic response following mechanical stress, and that mislocalisation of FLNC and BAG3 underlies the pathogenic mechanisms of the ZAK-deficiency.

Table of Contents

List of Figures

List of Tables

Acknowledgements

I would like to thank my supervisors, Dr Gonzalo Blanco and Dr Betsy Pownall for their unwavering support from the very beginning. Without their patience, mentorship and guidance, this project would not have been possible. Thanks also to my thesis advisory panel members, Dr Gareth Evans and Dr Paul Pryor for their time and attention over the last four years. Their advice, comments and scrutiny gave me the perspective I needed to fully engage with my project and the wider scientific background.

Many thanks to my colleagues from both the Blanco and Pownall Labs, particularly Alexander Russell, Oscar Harrad, Tobias Cracknell, Andrew Galloway, and Ahmed Nouh. Their support throughout my time here was invaluable and their office conversations and company in the Lab enabled me to persevere even when the going got tough. Thanks also to Aitana Genzor Garbayo for her friendship and academic support. I have thoroughly enjoyed our collaboration on all things ZAK.

Thank you to the Imaging and Cytometry, and Proteomics departments within the University of York Technology Facility for your time and expertise. In addition to this, I would like to thank the Biology Infrastructure and Stores teams who were always available for training and to answer questions.

My thanks also go to Dr Chris Chase, Gillian Helm, and the University of York team who organised the LAMP-testing facility in which I spent my PIPS placement. As a consequence of this, I developed many skills that will hopefully aid me in my future career.

Finally, my friends and family were always there for me to lean on when I needed support and without whom I would never achieved what I have so far, thank you so much. But special thanks go to Rob, Mum, and Dad as I could not have done this without you, you mean the world to me.

Declaration

I declare that this thesis is a presentation of original work and I am the sole author unless explicitly highlighted. Figures adapted for use in this thesis are with the author's permission or under a Creative Commons licence and detailed in the corresponding figure legend.

LC-MS/MS and phosphoproteomic data processing was performed by Adam Dowle (University of York Biology Technology Facility), as described in text.

I give credit to an undergraduate student, Andrew Galloway, with his help in the generation of the two ZAK-deficient C2C12 stable cell lines.

Pieces of this work have been produced in collaboration with the Bekker-Jensen Lab, Copenhagen, in particular Aitana Genzor Garbayo who conducted the muscle overload experiment and provided the samples for the TA ageing cohort.

This work has not previously been presented for an award at this, or any other, University. All sources are acknowledged as References, with acknowledgement of collaborative research and discussions. Some figures have been submitted for publication: (Nordgaard *et al.*, 2022) and (Stonadge *et al.*, In review).

CHAPTER 1

INTRODUCTION

1.1 Skeletal Muscle

1.1.1 Skeletal muscle overview

Muscle is an umbrella term for a contractile tissue which is found in most multicellular organisms, from drosophila to humans. It is well known to be sub categorised into 3 defined groups. The first of which is cardiac muscle, a striated muscle responsible for sufficient contractions for the supply of oxygenated blood to the body and the return of deoxygenated blood to the lungs. This type of contraction is innervated by sympathetic and parasympathetic fibres from the autonomic branch of the peripheral nervous system (Huang *et al.,* 2017). The second muscle group is smooth muscle, found primarily in the digestive tract, in the stomach and intestines. However, it can also be found within vessels of the cardiovascular system, the renal system, the respiratory tract, and even responsible for control of the pupil and lens of the eye (Huang *et al.,* 2017). The innervation of smooth muscle varies widely by location and function. Vascular smooth muscle is primarily innervated by the sympathetic nervous system, whereas parasympathetic stimulation also plays an important role in the contraction of smooth muscle cells. The sympathetic and parasympathetic nervous systems are collectively referred to as the autonomic nervous system. The complex nature of the autonomic nervous system allows for tight unconscious control of digestions, respiratory rate, urination, heart rate, blood pressure, and many other critical body functions.

The final subgroup is skeletal muscle, and is where this report will focus. Skeletal muscle accounts for up to 50% of a human's total body weight. It is known to be the largest tissue in the human body, responsible predominantly for force generation which aids movement, circulation, and breathing (Bottinelli and Reggiani, 2000; Nader, 2005) and is therefore critical for survival. Skeletal muscle tissue itself requires substantial investment of energy in order to function. The ability to adapt this energy consumption depending on the frequency and magnitude of use gives the skeletal muscle plasticity and presents as an evolutionary advantage.

Skeletal muscle is a highly plastic and adaptive tissue which takes cues from both its external and internal environments in order to maintain its ability to produce sufficient force output. Under normal physiological conditions, muscle mass is maintained through complex and interconnected growth (hypertrophic) and wasting (atrophic) pathways, which are carefully regulated and balanced. In response to exercise, the

skeletal muscle phenotype can be dramatically altered and this shift is dependent on exercise frequency, intensity, and duration (Joyner and Coyle, 2008; Brooks, 2012). Endurance training is known to increase mitochondrial biogenesis and capillary density. These adaptive changes delay the onset of muscle fatigue during prolonged aerobic exercise (Joyner and Coyle, 2008). Resistance exercise is known to stimulate an increase in muscle mass and ultimately results in an increase in muscle strength and power through neuromuscular adaptations, increases in muscle cross-sectional area (CSA), and alterations in connective tissue (Knuttgen and Kraemer, 1987).

At a basic level, skeletal muscle converts chemical energy in the form of nutrients obtained through diet, into a mechanical output responsible for voluntary movement and maintenance of shape and form. Skeletal muscle can obtain energy through very distinct mechanisms. Firstly, anaerobic metabolism is responsible for the generation of ATP through phosphocreatine or anaerobic glycolysis (Granchi *et al.,* 2010). Intramuscular phosphocreatine is used for rapid, high-intensity contractions but is depleted extremely quickly. Anaerobic glycolysis occurs after, and refers to the breakdown conversion of glucose to pyruvate, which is converted to lactic acid in the absence of oxygen (Granchi *et al.,* 2010). Muscle glycogen stores are utilised to make glucose readily available for this process. The limiting factor in this process is the accumulation of lactic acid which is detrimental to the health of the muscle in large quantities. Aerobic metabolism is an alternative energy-producing mechanism and occurs when pyruvate is readily broken down with a surplus of oxygen, producing ATP via the Krebs cycle and electron transport chain. Glycogen stores are also used as a source of energy in aerobic metabolism, however the most abundant energy source available is fat which is responsible for resting muscle activity (Alghannam *et al.,* 2021). Under caloric restriction conditions, fewer nutrients consumed in the diet equates to less energy available for metabolism. The body's response is to release amino acids stored in the muscle for gluconeogenesis, the conversion of a non-carbohydrate substrate to glucose, or the conversion into ketogenic amino acids which can be used as fuel (Alghannam *et al.,* 2021). The release of amino acids is synonymous with a reduction in muscle mass. Under these circumstances, loss of muscle mass is beneficial in two ways, firstly by providing alternative sources of energy, and secondly by reducing the metabolic burden to the organism while nutrients are scarce.

Age-related muscle loss, also known as sarcopenia, has been shown to increase the risk of mortality in the elderly population, and often results in a poor quality of life with the need of extra assistance or care (Liu *et al.*, 2017; Tsekoura *et al.*, 2017). Muscle loss secondary to disease (cachexia) has been observed in patients suffering from diseases like cancer, diabetes, and AIDS where it demonstrates a negative correlation with disease prognosis (Bourdel-Marchasson *et al.*, 2016). Increased attention to exercise and nutrition is successful in preserving muscle function, but it is not the solution for every patient (Evans, 1999). For example, some patients with chronic kidney disease are unable to consume high protein diets (Ko *et al.*, 2017), and patients in intensive care may not be able to undertake an intensive exercise regimen.

By understanding the regulatory processes required for maintenance of muscle mass, we may be able to develop novel therapies to improve the quality and longevity of life for those suffering with muscle wasting disorders.

1.1.2 Skeletal muscle structure

Each skeletal muscle consists of thousands of individual muscle fibres (myofibres) bundled together by connective tissue, altogether known as fascicles (Figure 1.1). A myofibre is composed of multiple myofibrils, containing a number of myofilaments. The endomysium is in direct contact with and surrounds each individual muscle fibre and forms the basis of the extracellular matrix (Järvinen *et al.*, 2002; Standring, 2020). Each fascicle is surrounded by connective tissue called the perimysium, and the epimysium is the outermost connective tissue surrounding the entire skeletal muscle (Frontera and Ochala, 2015).

The tendon is critical for anchorage of the muscle to the bone, and is found at both ends of the muscle, with only one exception; the tongue. Muscles are predominantly used to connect two joints together to enact a force on the skeleton for movement, or to maintain posture and tension (McCuller *et al.,* 2023). Motor neurons innervate the muscle to allow for voluntary manipulation of skeletal muscle contraction. Additionally, the blood vessels supply the muscle with oxygen and nutrients for its metabolic activity. Skeletal muscle also serves as a mechanism to aid the circulation of venous blood to the heart (McCuller *et al.,* 2023).

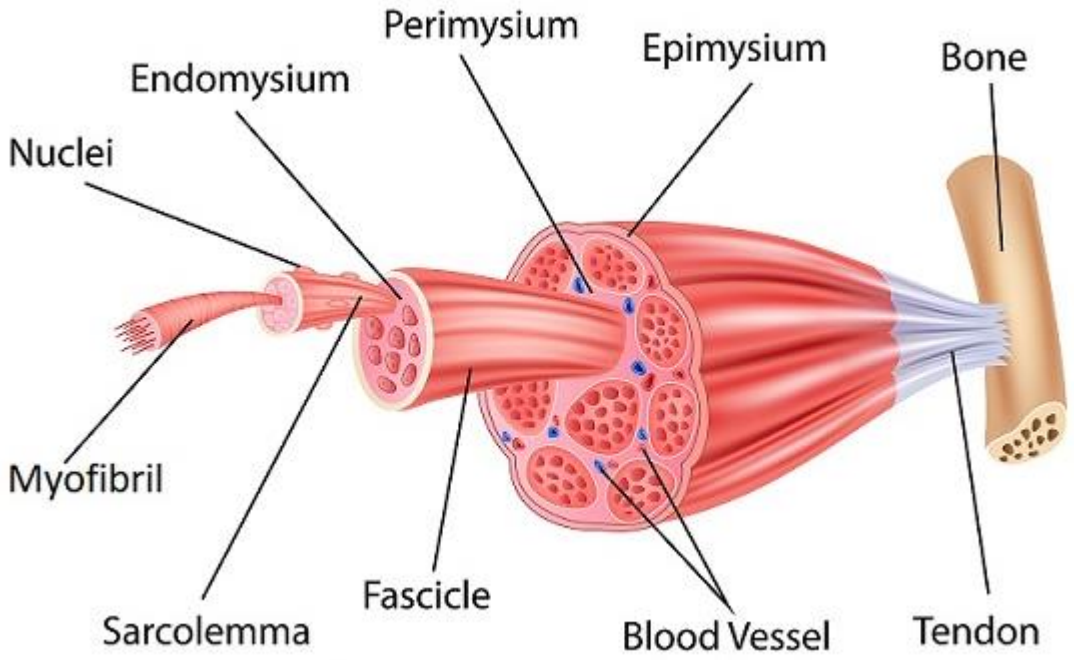

Figure 1.1: Structure of skeletal muscle. Schematic representation of the whole tissue through to individual myofibril. Each muscle fibre is composed of bundles of myofibrils into a fascicle encased by perimysium, which bundle together to form a muscle fibre. Bundles of muscle fibres comprise the whole muscle, encased in epimysium. Image taken from http://library.open.oregonstate.edu/aandp/chapter/ 10-2-skeletal-muscle/.

A skeletal muscle fibre is a multinucleated syncytium built up of consecutive contractile units called sarcomeres. The sarcomere is the basic unit of skeletal muscle and is responsible for contraction (Pham and Puckett, 2022). The sarcomere consists of two types of filaments; actin thin filaments, and myosin thick filaments. Actin (thin) filaments are anchored to the z-disc and interact with myosin (thick) filaments, which are anchored to the M line, to mediate muscle contraction at the A band where, by pulling against each other in the manner of a cross-bridge, they shorten the overall length of the sarcomere (Figure 1.2). This is known as the sliding filament theory (Huxley, 1957). Coordinated contraction of sarcomeres throughout the skeletal muscle results in the voluntary production of force throughout the musculoskeletal system.

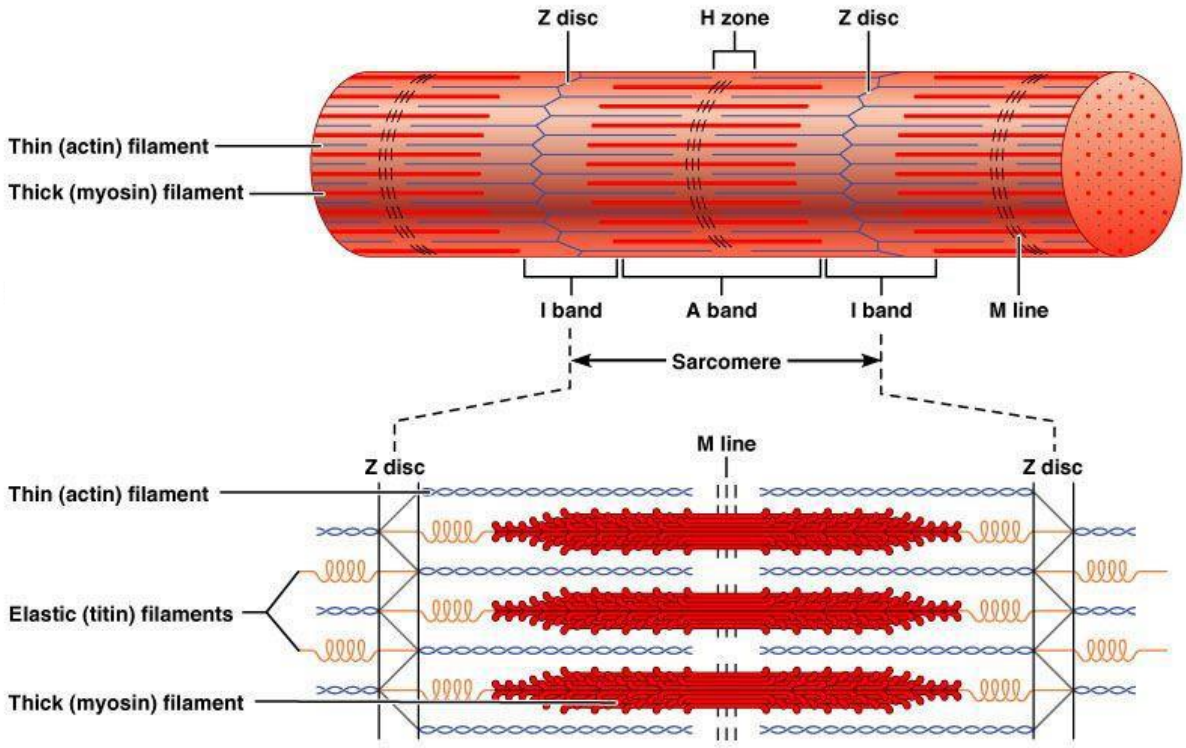

Figure 1.2: Schematic representation of the sarcomere. Actin and myosin filaments interact with each other at the A band. Myosin filaments are tethered at the M line, actin filaments anchored at the z-disc. Image obtained from https://www.pearson.com/content/dam/one-dot-com/one-dot-com/us/en/higher-ed/en/products-services/course-products/marieb-10e-info/pdf/marieb-0321927028-chapter9.pdf

1.1.3 Skeletal muscle formation

In vertebrates, skeletal muscle forms in the embryo from paraxial mesoderm, which segments into somites on either side of the neural tube and notochord (Christ and Ordahl, 1995). The ventral part of the somite, the sclerotome, will develop into cartilage and bone of the vertebral column and ribs, whereas the dorsal part of the somite, the dermomyotome, gives rise to skeletal muscle. Skeletal muscle in the limb is formed by cells derived from somites present at the level of the limb buds. The first muscle mass to form, under the dermomyotome, is the myotome, which integrates into the trunk musculature (Tajbakhsh and Buckingham, 2000). It is the mesenchymal cells of the limb which are thought to provide the positional cues for the muscle progenitor cells coming from the somite (see Christ & Ordahl, 1995). Cells that migrate from the somite have not yet activated the myogenic determination genes and it is only when they

reach the limb that they begin to express transcription factors: *MyoD* and *Myf5* (Tajbakhsh and Buckingham, 1994). From this, a coordinated signalling cascade is initiated which results in the formation of adult skeletal muscle.

In the adult vertebrate, each myofibre is formed from the differentiation and fusion of individual muscle stem cell (MuSC) progenitors, termed satellite cells, into myoblasts to form a multinucleated syncytium capable of contraction (Rochlin *et al.*, 2010). The regenerative capacity of skeletal muscle is largely attributed to the presence of these mononucleated cells that reside between the basal lamina of the extracellular matrix (ECM), and the sarcolemma (Mauro, 1961; Yin, Price and Rudnicki, 2013). Satellite cells, are responsible for rapid muscle regeneration following acute injury (Heslop *et al.*, 2002; Zammit *et al.*, 2002; Collins *et al.*, 2005; Sambasivan *et al.*, 2011). MuSCs are maintained in a mitotically quiescent state, referred to as the G_0 phase of the cell cycle, morphologically characterised by a limited amount of cytoplasm and increased heterochromatin (Schultz, Gibson and Champion, 1978; Wakayama *et al.*, 1979). Adhesion to an intact ECM maintains MuSCs in the G_0 phase of the cell cycle (Montarras, L'honoré and Buckingham, 2013). When the contact between the MuSC and the ECM is disrupted during muscle injury, MuSCs become activated (Schultz and McCormick, 1994; Tatsumi *et al.*, 1998). This can be replicated during muscle explant and culture mechanisms. The importance of the MuSC niche has been highlighted in many reports. An example of this is the role of the heparan sulphate proteoglycan syndecan 3 (SDC3), a component of the extracellular matrix (ECM), on MuSC activation. Data demonstrates *Sdc3*-null mice were unable to regulate MuSC homeostasis and replenish the MuSC pool often followed by increased MuSC migration from the resident myofibre suggesting a role for SDC3 in myogenic regulatory factor (MRF) expression and MuSC activation (Pisconti *et al.*, 2010, 2016).

Following muscle injury, MuSCs enter into the cell cycle and commit to myogenesis (Figure 1.3). MuSCs proliferate and enter a terminal G_0 phase, ultimately culminating in myoblast differentiation and subsequent fusion to damaged myofibres in order to regenerate them or the production of newly-formed myofibres (Bischoff, 1975; Konigsberg, Lipton and Konigsberg, 1975; Snow, 1977). It is critical for MuSC survival that a small population of myoblasts do not terminally differentiate, instead they re-enter the reversible G_0 state and undergo self-renewal to replenish the population of

quiescent, uncommitted MuSCs following injury-induced activation (Zammit *et al.*, 2004; Shi and Garry, 2006). Instead of differentiating, self-renewing cells exit the cell cycle and return to G_0 (Schultz and McCormick, 1994; Tatsumi et al., 1998). Skeletal muscle regeneration is highly dependent on the efficiency of MuSCs to balance quiescence and activation, and self-renewal and differentiation (Lepper, Partridge and Fan, 2011; Sambasivan *et al.*, 2011).

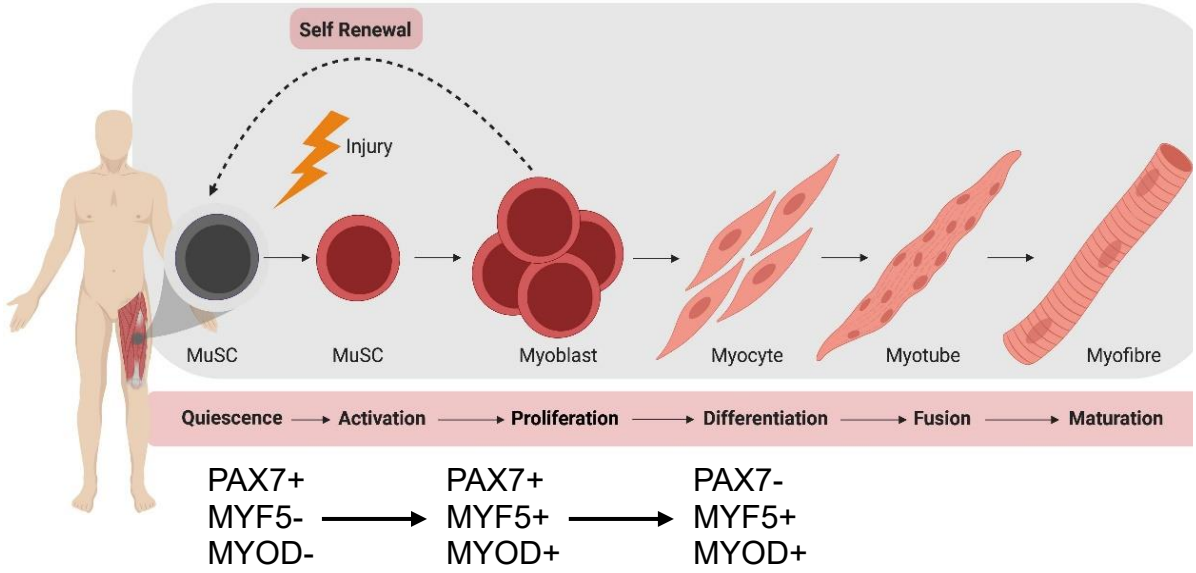

Figure 1.3: Representation of muscle stem cell (MuSC)-mediated skeletal muscle regeneration. Following injury, quiescent MuSCs expressing Pax7 are activated and undergo rapid proliferation and begin to express the myogenic regulatory factors (MRFs) MYF5 and MYOD. Some myoblasts downregulate these MRFs and re-enter quiescence. Myocytes undergo differentiation and fuse and mature to generate new muscle fibres. Adapted from Nguyen *et al.*, 2019.

The mechanisms that govern MuSC quiescence, and subsequently satellite cell activation, are poorly understood. Current understanding is that quiescent MuSCs are marked by the unique expression of the transcription factor, paired box 7 (PAX7), but do not express any other muscle-specific transcription factors known as myogenic regulatory factors (MRFs) (Seale and Rudnicki, 2000; Buckingham and Relaix, 2015). In response to injury and modulation of the ECM niche, MuSCs begin to express the MRFs MYOD and MYF5, master regulators of myogenesis (Crist, Montarras and Buckingham, 2012; Yin, Price and Rudnicki, 2013). MYOD does not directly promote

MuSC differentiation, it instead acts as a transcription factor regulating the transcription of many genes which themselves regulate differentiation. Cells begin to exit the cell cycle, committed to either to ultimately regenerate damaged muscle or re-enter quiescence and replenish the MuSC reserve pool (Kuang *et al.*, 2007). If MuSCs self-renew, they downregulate MRFs MYOD and MYF5 whilst maintaining high levels of PAX7 thus returning to quiescence. Once activated, MuSCs become myoblasts which downregulate PAX7 expression and upregulate the MRF terminal differentiation factor myogenin (Mastroyiannopoulos *et al.*, 2012). The surface of MuSCs contains many growth factor receptors such as c-Met, FGFR and IGFR. Activation of growth factor receptors results in the phosphorylation of the p38/MAPK family which phosphorylates MK2, in-turn inactivating tristetraprolin (TTP). In quiescent MuSCs, *MYOD* is normally transcribed however *MYOD* mRNA undergoes tristetraprolin (TTP)-mediated decay thus preventing MYOD protein expression (Crist, Montarras and Buckingham, 2012). Inactive TTP increases the half-life of *MYOD* mRNA and enables translation of the MYOD protein. Signalling via hepatocyte growth factor (HGF) activates the mTOR pathway which is heavily involved in MuSC activation (Laplante and Sabatini, 2013). One of the most well-known downstream targets of mTOR is the ribosomal protein S6 (RPS6) which modulates translation initiation prior to protein synthesis which is important for the cascade of events responsible for adult myogenesis (Ma and Blenis, 2009; Rodgers *et al.*, 2014).

Myogenesis progresses through the appearance of differentiated myoblasts at the periphery of the damaged myofibre. Myoblasts fuse to each other forming primordial myotubes, which then mature and eventually restore the muscle fibre (Rochlin *et al.*, 2010; Abmayr and Pavlath, 2012). A hallmark of muscle injury is muscle fibre degeneration followed by necrosis and regeneration. Successful regeneration subsequent to necrosis has been reported to depend on the preservation of the extracellular basement membrane (Caldwell, Mattey and Weller, 1990). Electron microscopy of both animal (Caldwell, Mattey and Weller, 1990) and human (Cullen and Jaros, 1988) models of muscle damage, reveals the presence of basement membrane tubes left behind following necrosis of the original fibre. Activated MuSCs adhere to the existing basement membrane which mediates the differentiation and fusion into myotubes (Mackey and Kjaer, 2017). Regenerating myotubes repopulate the empty basement membrane tube and myofibrillogenesis occurs within a new

basement membrane which ultimately replaces the original basement membrane over time (Vracko and Benditt, 1972; Sanes, Marshall and McMahan, 1978). Altogether this suggests an important role for the basement membrane in the activation of MuSCs required for regeneration, as a scaffold for adult myogenesis, and in the regulation of myofibre regeneration.

1.1.4 Skeletal muscle contraction

Each myofibril contains a continuous series of contractile units, called sarcomeres. Within the sarcomere, contractile proteins are arranged longitudinally to facilitate sarcomeric contraction and are described as thick and thin filaments.

The thin filament is primarily composed of actin which is anchored at the z-disc and oriented towards the m-line (Szikora *et al.,* 2022). Actin has polypeptide subunits, called globular actin or G actin, which bear the active sites to which the myosin heads attach during contraction. In the thin filaments, G actin subunits are polymerised into long actin filaments called filamentous, or F actin (Szikora *et al.,* 2022). Two intertwined actin filaments form the backbone of each thin filament. Each thin filament contains several regulatory proteins such as tropomyosin and troponin (Squire, 2019). Tropomyosin is a rod-shaped protein, attached to the actin core to help stiffen and stabilize it (Cooper 2002). Successive tropomyosin molecules are arranged end to end along the actin filaments, and in a relaxed muscle fibre they block myosin-binding sites on actin so that myosin heads on the thick filaments cannot bind to the thin filaments. Troponin is the name given to a protein complex found along tropomyosin molecules (Cooper, 2002). It is composed of a globular three polypeptide complex. One of its polypeptides (TnI) is an inhibitory subunit that binds to actin. Another (TnT) binds to tropomyosin and helps position it on actin. The third (TnC) binds calcium ions. (Ohtsuki and Morimoto, 2008).

The thick filament is composed of a large protein called myosin. Comprised of light and heavy chains which twist to form a helical tail, together they present binding sites responsible for interacting with actin-tropomyosin-troponin complexes which facilitates skeletal muscle contraction (Pham and Puckett, 2022). Clearly observed using electron microscopy, the overlap between the actin and myosin filaments is known as the A-band.

External to the myofibrils, but beneath the sarcolemma resides the sarcoplasmic reticulum (SR) (Rossi *et al.,* 2022). This is an elaborate structure of interconnected tubules which surround each myofibril. The SR tubules primarily run longitudinally along each myofibril, communicating with one another at the H zone (Figure 1.4). Closely associated with the SR are large numbers of mitochondria and glycogen granules, both involved in producing the energy used during contraction (Rossi *et al.,* 2022). The SR is important for the regulation of intracellular levels of calcium ions. It stores calcium and releases it on demand upon muscle fibre stimulation. At each A-I band junction, the sarcolemma protrudes into the myofibrillar interior. This generates an elongated transverse tube, called the T tubule. T tubules form triads alongside terminal cisterns of the SR (Rossi *et al.,* 2022). As T tubules are continuations of the sarcolemma, they are able to conduct nerve-initiated electrical impulses from the exterior sarcolemma deep into the muscle cell and sarcomere.

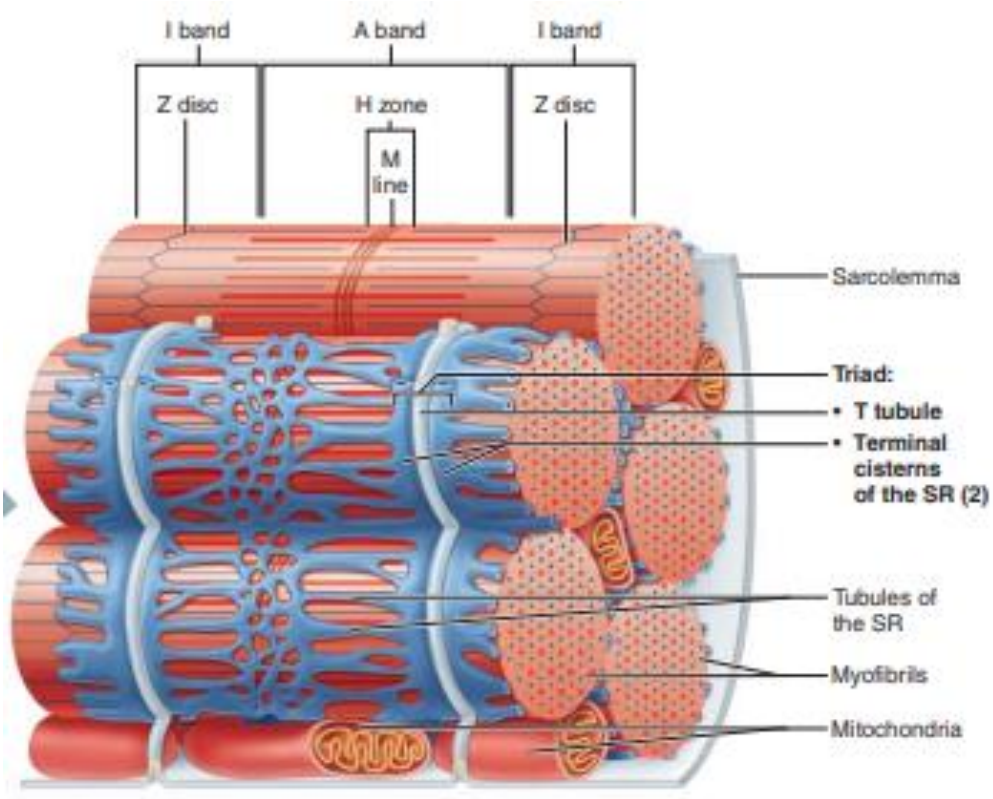

Figure 1.4: Schematic of the arrangement of the sarcoplasmic reticulum around the myofibril. Each myofibril is in contact with tubules of sarcoplasmic reticulum, T tubules, extensions of the sarcolemma, invade deep into the myofibril and assist with contraction. The triad is composed of the T tubule, and terminal cisterns of the sarcoplasmic reticulum.

Image obtained from https://www.pearson.com/content/dam/one-dot-com/one-dot-com/us/en/higher-ed/en/products-services/course-products/marieb-10e-info/pdf/marieb-0321927028-chapter9.pdf

The nerve cells that activate skeletal muscle fibres are called somatic motor neurons. These motor neurons reside in the brain or spinal cord and possess long extensions called axons which extend to the muscle cells the innervate (Zayla and Tadi, 2022). The axon of each motor neuron divides as it enters the muscle, that form a neuromuscular junction, or motor end plate, with a single muscle fibre. Each muscle fibre has only one neuromuscular junction, however they remain separated by a space filled with an extracellular substance rich in glycoproteins and collagen fibres; the synaptic cleft (Rodriguez Cruz *et al.,* 2020). When a nervous impulse reaches the end of the axon, the axon terminal releases acetylcholine (ACh) into the synaptic cleft. This diffuses across the synaptic cleft and activates ACh receptors on the muscle fibre sarcolemma (Hirsch, 2007). Activation of ACh receptors triggers an action potential. Initiation of muscle contraction is dependent on the neuromuscular junction and the generation of an action potential across the sarcolemma. Transmission of the action potential along the T tubules stimulates SR calcium channels to release Ca^{2+} into the cytosol (Figure 1.5).

When intracellular calcium levels are low, the muscle cell is relaxed, and tropomyosin molecules physically block the myosin-binding sites on actin. As Ca^{2+} levels increase, the ions bind to regulatory sites on troponin. Two calcium ions bind to troponin C, causing it to change shape and then roll tropomyosin away from the myosin-binding sites, removing the tropomyosin inhibition (Santulli, Lewis and Marks, 2017). As Ca^{2+} binds to troponin, the affinity for further binding increases, which is known as cooperativity (Ohtsuki and Morimoto, 2008). At first when myosin binds to actin, no adenosine triphosphate (ATP) is present; a transient state known as rigor. ATP then binds to myosin which decreases the affinity of the myosin head for the actin myosin-binding site causing myosin to dissociate from actin.

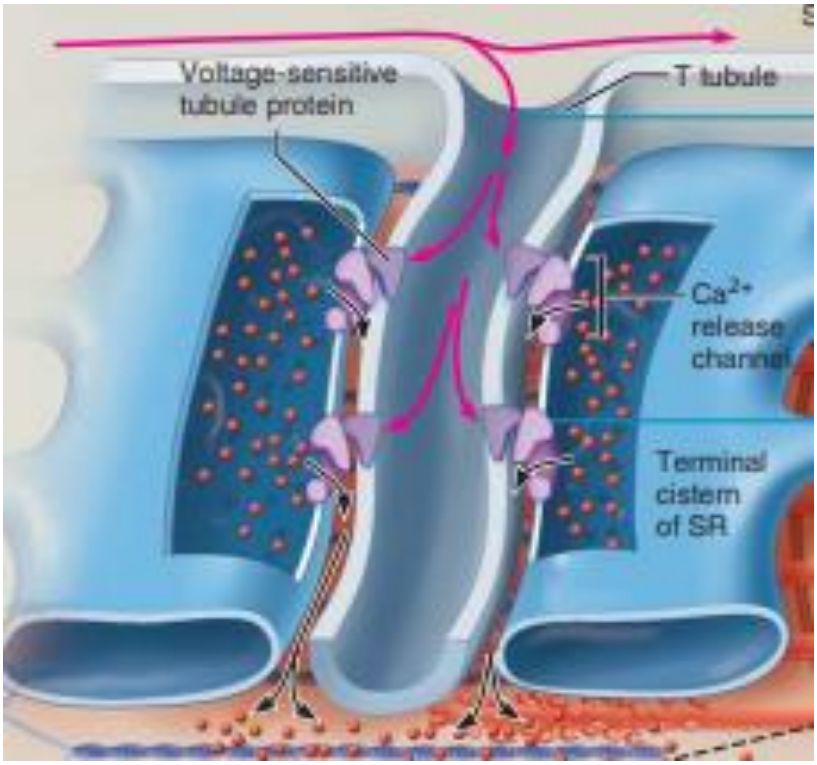

Figure 1.5: Schematic of the activation of Calcium ion channels following innervation. The action potential is transmitted via the sarcolemma and is carried into the myofibril by the T tubule. This activates voltage-gated calcium channels in the sarcoplasmic reticulum and allows the influx of calcium ions into the myofibril. Image adapted from https://www.pearson.com/content/dam/one-dot-com/one-dot-com/us/en/higher-ed/en/products-services/course-products/marieb-10e-info/pdf/marieb-0321927028-chapter9.pdf

ATP is then hydrolysed to adenosine diphosphate (ADP), providing the necessary energy for the myosin head to move and bind to the next actin binding site. This is known as the cross-bridge cycle and is responsible for pulling the actin filament towards the M-line whilst Ca^{2+} remains bound to troponin (Figure 1.6). The final stage of the cycle is when ADP is released from the myosin head where it returns to the original rigor state (Fitts, 2008). After contraction, Ca^{2+} ions are pumped back into the sarcoplasmic reticulum to return to low intracellular Ca^{2+} levels. The decrease in intracellular Ca^{2+} forces tropomyosin to resume its inhibition of the actin myosin-binding sites (Paolini *et al.*, 2007).

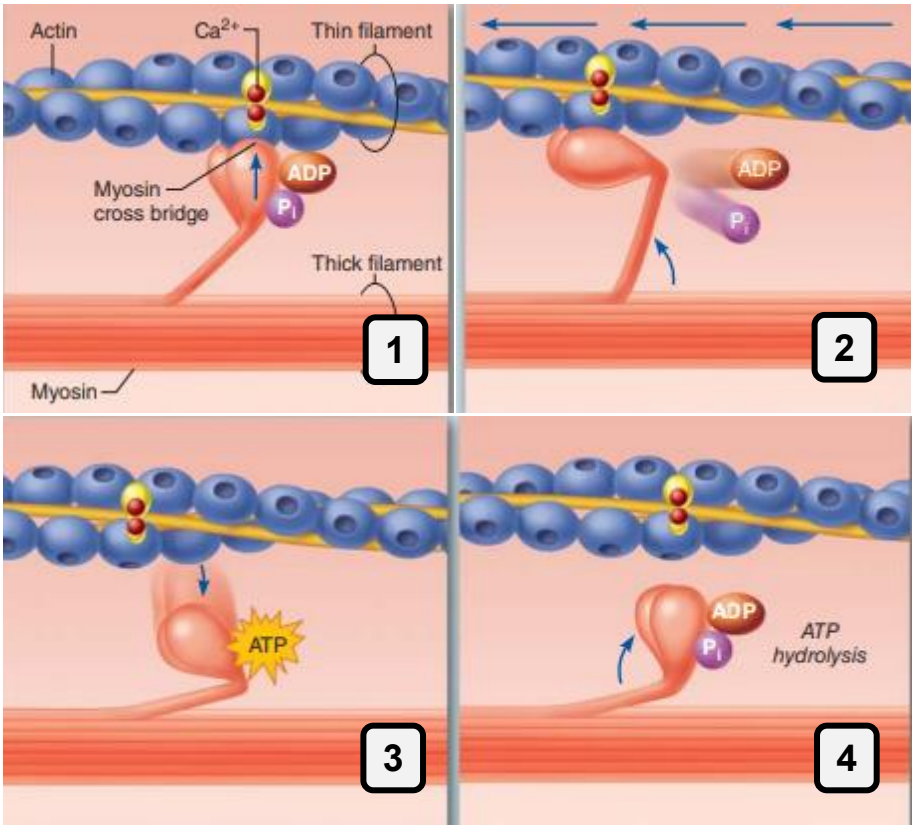

Figure 1.6: Schematic of the cross-bridge cycle. (1) Energised myosin binds to the actin-myosin binding site forming a cross bridge. (2) ATP is then hydrolysed to adenosine diphosphate (ADP) and a phosphate group. The myosin head pivots and bends, changing to its bent low-energy state. As a result, it pulls the actin filament toward the M line. (3) After ATP attaches to myosin, the link between myosin and actin weakens, and the myosin head detaches. (4) ATP is hydrolysed to adenosine diphosphate (ADP) and a phosphate group, the myosin head returns to its high-energy state. Image adapted from https://www.pearson.com/content/dam/one-dot-com/one-dot-com/us/en/higher-ed/en/products-services/course-products/marieb-10e-info/pdf/marieb-0321927028-chapter9.pdf

1.1.5 The z-disc and the costamere

The z-disc is the outermost structure of the sarcomere. It is a protein-dense crystal-like structure which acts as an anchor for the contractile machinery and maintains the structural integrity of the sarcomere. It is also an important structure for the detection and transmission of biomechanical signals.

From the z-disc, many proteins are responsible for mediating force across the sarcomere and transducing intracellular signalling responses (Figure 1.7). α-actinin is a large actin-binding protein found at the z-disc responsible for cross-linking antiparallel actin filaments (Sjöblom, Salmazo and Djinović-Carugo, 2008). By binding to both actin and other signalling molecules, α-actinin is integral for cytoskeletal organisation and mediating muscle contraction. Filamin C (FLNC) is another large z-disc protein which binds many partner proteins to once again provide structural support to the sarcomere and facilitate the mechanotransduction of sarcomeric signalling (Feng and Walsh, 2004). Loss of FLNC has been implicated in human skeletal muscle myopathies which features myofibre degeneration and protein aggregation (Dalkilic *et al.*, 2006). Myotilin is a z-disc protein critical for maintenance of sarcomeric structure by binding to both α-actinin and filamin (Salmikangas, 1999; Dube *et al.*, 2014). Through a protein complex with actin and α-actinin, myotilin stabilises actin thin filaments at the z-disc (Nandelstadh *et al.*, 2009). Four-and-half-domain-LIM Protein (FHL) localises to the z-disc but can also be found in the nucleus (Purcell *et al.*, 2004). It is thought that FHL has an important role in pathological hypertrophy facilitating the stress response through titin- and mitogen activated protein kinase (MAPK)-mediated signalling (Sheikh *et al.*, 2008). Nebulin is an extremely large protein suggested to regulate actin filament length, the mechanism for which is still largely unknown (Bang *et al.*, 2006; Witt *et al.*, 2006). Patients with nebulin mutations experience muscle weakness and hypotonia (Bang *et al.*, 2006; Witt *et al.*, 2006). Last but not least is titin, the largest structural protein in the human body. A longitudinal protein which spans the sarcomere from the M-line to the z-disc (Tskhovrebova and Trinick, 2003).

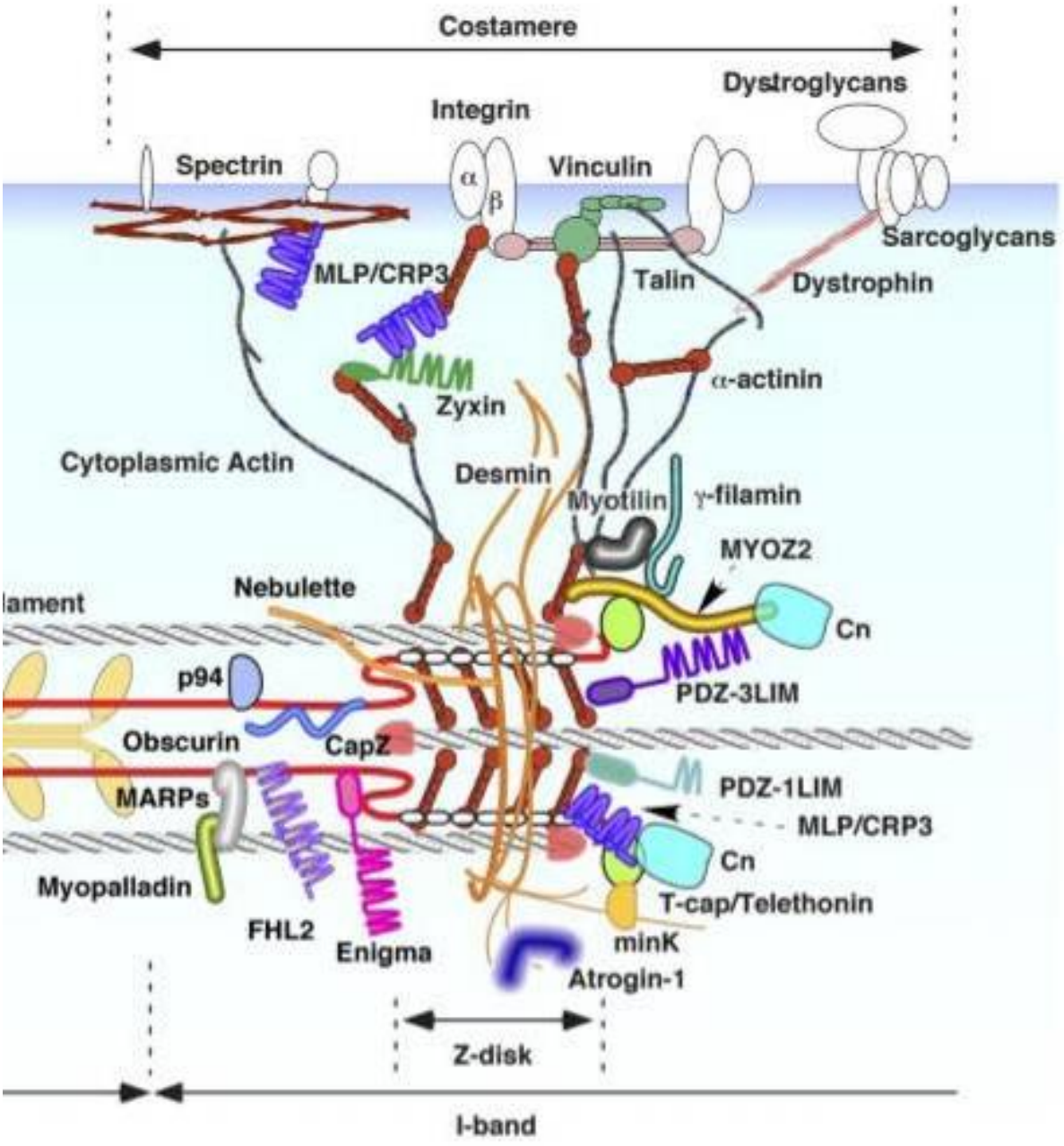

Figure 1.7: Z-disc/cytoskeletal-associated proteins and their complexes. Many proteins associated with the z-disc have been linked with intrinsic mechanical sensor sensor/signal modulator functions. These include α-actinin, Filamin C, Myotilin, Four-and-a-half-LIM protein (FHL), nebulin, and titin. These proteins in complex comprise the signalling and structural centrepiece of muscle mechanosensation and transduction. Figure taken from (Hoshijima, 2006).

As a structural protein, titin provides a molecular scaffold for many other sarcomeric proteins to bind throughout contraction and relaxation. In addition to its structural role, it is also suggested to utilise its many immunoglobulin domains as a mechanical spring to protect the sarcomere from stress-induced damage during bouts of contraction (Rief *et al.*, 1997).

The z-disc is anchored to the ECM via the costamere. This function is critical to maintain sarcomeric integrity. Described almost 40 years ago, costameres are sub-sarcolemmal protein complexes that align the z-disc with the sarcolemma (Craig and Pardo, 1983; Pardo and Siliciano, 1983). Costameric proteins form focal adhesions with the extracellular matrix (ECM) via two main complexes: the dystroglycan complex (DGC), and the integrin-vinculin-talin complex (Pardo and Siliciano, 1983; Ervasti and Campbell, 1993; Patel and Lieber, 1997) (Figure 1.8). Costameres are considered to be important hubs of mechanotransduction, whereby deregulation of costameric protein complexes is thought to underly many muscle myopathies and dystrophies (Matsumura and Campbell, 1994; Cohn and Campbell, 2000; Blake *et al.*, 2002). Additionally, FLNC interacts with sarcoglycans within the DGC promoting cytoskeletal stability (Zhang *et al.*, 2007).

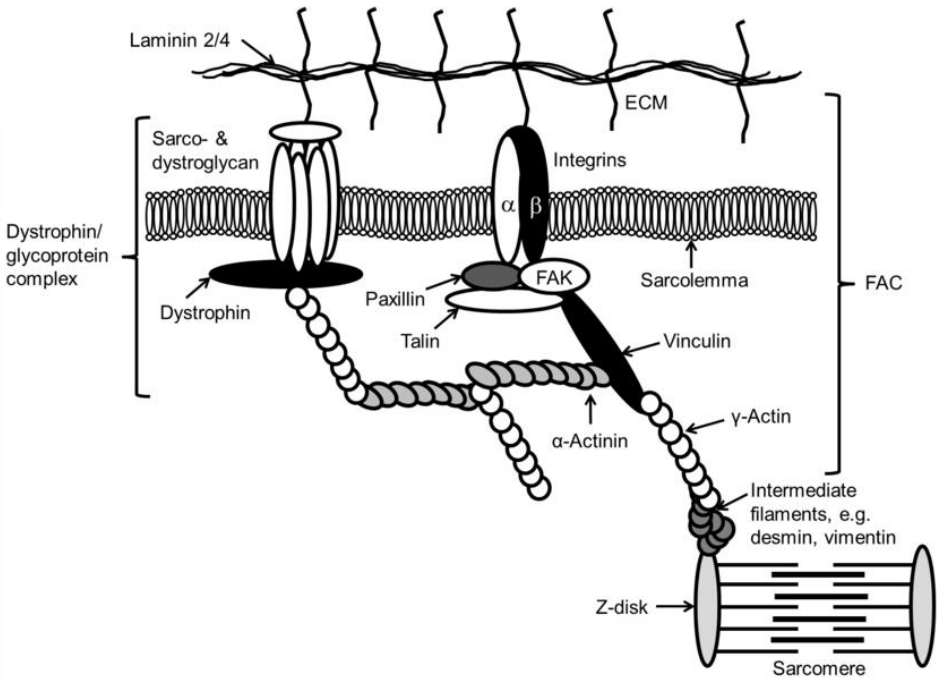

Figure 1.8: Representation of the main complexes which make up the costamere. Schematic representation of the proteins which constitute the protein complexes of the costamere. Costameres connect the z-discs to the extracellular matrix (ECM) via the

sarcolemma. The complexes which are critical for stability and signalling are the dystrophin/glycoprotein complex, and focal adhesion complex (FAC), comprised of the integrin-associated tyrosine kinase focal adhesion kinase (FAK). Figure taken from (Erskine and Degens, 2013).

1.2 Mechanisms to regulate myofibre size

1.2.1 Muscle fibre type and adaptation

Skeletal muscle composition changes from muscle to muscle depending on fibre innervation and frequency of usage. Muscles differ in contractile and metabolic properties and can be classified into four main fibre types in the mouse model, type I (slow-twitch), IIA, IIB, and IID/IIX (fast-twitch). In humans, skeletal muscles are composed of three major fibre types, slow type I, fast IIA, and fast IIX, defined by the presence of myosin heavy chain 7 (MYH7), MYH2, and MYH1, respectively (Smerdu *et al.*, 1994). In contrast to other mammalian species containing muscles with predominant slow or fast fibre type profile, most human muscles are mixed in their fibre type composition. Slow twitch muscle fibres primarily utilise oxidative phosphorylation used as the main energy source. Alternatively, fast twitch fibres utilise anaerobic phosphorylation to generate energy (Schiaffino and Reggiani, 1996; Bassel-Duby and Olson, 2006). The distribution of fibre types within a particular muscle is genetically predetermined by the gene expression program and the specific myosin heavy chain (MHC) isoform expressed. (Bottinelli and Reggiani, 2000; D'Antona *et al.*, 2006).

As a highly adaptable organ, skeletal muscle is able to respond to increased or decreased levels of demand. Signalling pathways control how the muscle fibre responds to changes in functional or metabolic demands, thus tailoring the molecular and structural phenotype to adjust to the level of use (Stewart and Rittweger, 2006). These pathways are described in Figure 1.9. Muscle fibre remodelling in response to changes in demand have been shown to be responsive to calcium-dependent signaling pathways, involving CaN-NFAT, and CaMK-HDAC- MEF-2 (McKinsey *et al.*, 2000; Calabria *et al.*, 2009), MAPKs (Shi *et al.*, 2008), myostatin (Hennebry *et al.*, 2009), and forkhead box O1 (FOXO1) transcription factor (Yuan *et al.*, 2011).

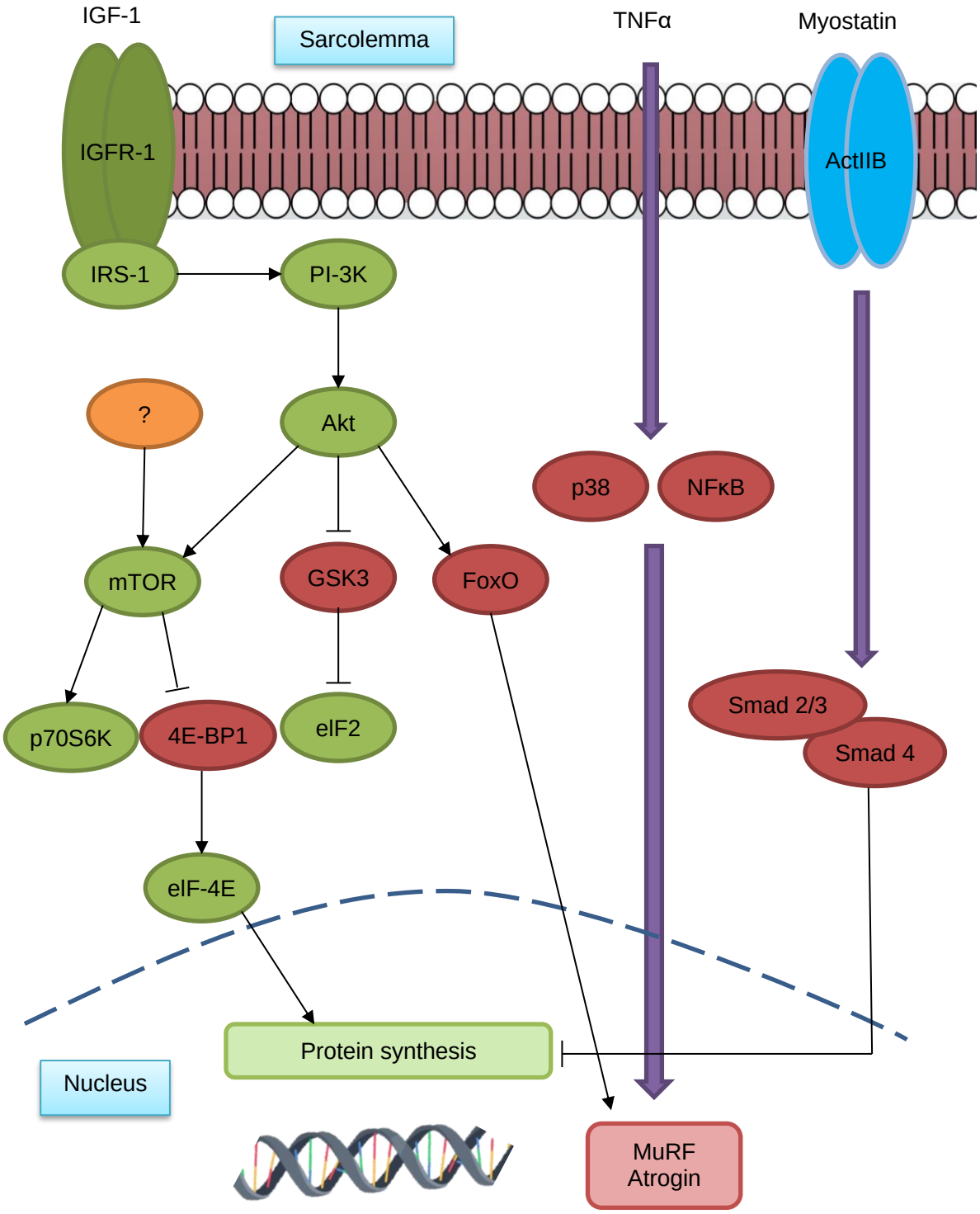

Figure 1.9: Simplified schematic of interconnected pathways responsible for skeletal muscle hypertrophy and atrophy. Up-regulators of protein synthesis are shown in green, down-regulators of protein synthesis and activators of MuRF and Atrogin are shown in red.

Some intermediates have been omitted. Orange indicates potential mechanical sensing activators of mTOR not yet identified.

1.2.2 Hypertrophy

Muscle growth can occur through two distinct mechanisms, hyperplasia and hypertrophy. Hyperplasia refers to an increase in muscle size through the formation of new muscle fibres. Skeletal muscle hypertrophy is known to increase the cross-sectional area (CSA) of skeletal muscle through a net increase in protein synthesis (Glass, 2003; Goldspink, 2003). The balance of protein synthesis to protein degradation is critical to muscle maintenance. A variety of signalling pathways are responsible for transducing cellular responses following the detection of differences in mechanical stress, nutrient availability, presence of certain growth factors, and physical activity.

1.2.3 IGF1-PI3K-Akt/PKB-mTOR

The IGF-1/PI3K/AKT signalling pathway is the canonical pathway controlling skeletal muscle hypertrophy. Initially, growth hormone (GH) is produced by the pituitary gland as a response to differences in nutrient availability and physical activity. Binding of GH with the GH-hepatic receptor stimulates the release of IGF-1 into circulation (Delafontaine, 1995; Jones and Clemmons, 1995). Circulating IGF-1 binds to its receptor (IGFR-1) on the surface of muscle fibres. Docking at the IGFR-1 receptor activates the internal tyrosine kinase domain of the receptor, resulting in autophosphorylation and subsequent activation of insulin receptor substrate (IRS-1). Activation of IRS-1 in turn phosphorylates phosphatidylinositol-3-kinase (PI-3K), activating AKT/PKB downstream (Rommel *et al.*, 2001). Activation of AKT has been shown to prevent denervation-induced atrophy (Bodine *et al.*, 2001; Pallafacchina *et al.*, 2002). AKT indirectly activates mTOR signalling through the inhibition of the tuberous sclerosis complex 1 and 2 (TSC1/2). TSC1/2 acts as a GTPase activating protein (GAP) which inhibits Ras homolog enriched in brain (RHEB) which activates mTOR signalling. mTOR is a regulator of protein synthesis and AKT phosphorylation when in complex with either Raptor, as the rapamycin-sensitive mTORC1, or Rictor, as the rapamycin-insensitive mTORC2, respectively. mTORC1 promotes protein

synthesis via phosphorylation of S6 kinase (S6K), inhibiting eIF4E-binding proteins (4EBPs) and activating other ribosomal factors involved in translation initiation and elongation, like eukaryotic translation initiation factor 4E (eIF4E) (Hara *et al.*, 1997; Inoki *et al.*, 2002).

1.2.4 Non-canonical signalling not via IGF1

The canonical mTOR signalling pathway is suggested to be the main mechanism to induce skeletal muscle hypertrophy. Recently, activation of mTOR independent of IGF-1 is now challenging this paradigm. Wortmannin inhibition of PI-3K, downstream of IGF-1 signalling, does not prevent S6K activation upon increased mechanical loading (Hornberger *et al.*, 2005). Additionally, mice lacking a functional IGFR-1 prevents IGF-1 signalling and activation of the IGF-1 dependent signalling pathway, but does not prevent initiation of a hypertrophic response following mechanical loading and subsequent S6K phosphorylation (Spangenburg *et al.*, 2008). This suggests a loading-induced hypertrophic mechanism independent of IGF-1. Whilst the IGF-1/mTOR paradigm is well understood, little is still known about the regulators of mTOR during mechanical overload. Mechanosensors are components of skeletal muscle with the capacity to sense mechanical stimuli and transduce these events into a biochemical signal (Pingel and Suhr, 2017). Some mechanosensors have been identified; integrin-linked kinase (ILK) (Mathes *et al.*, 2019), Kindlin-2 (Fermt2/KIND2) (Dowling *et al.*, 2008), Talin 1 and 2 (TLN1 and TLN2) (Conti *et al.*, 2009), Vinculin (VCL) (Shear and Bloch, 1985), and the major regulator of integrin-mediated signalling, Ilk1 (Legate *et al.*, 2006). However more work is necessary to elucidate the complex mechanisms of skeletal muscle regulation and adaptation in response to a mechanical stimulus (Figure 1.9; orange circle).

1.2.5 Myostatin-Smad3

Myostatin belongs to the transforming growth factor β (TGFβ) superfamily and ordinarily negatively regulates muscle growth (McPherron, Lawler and Lee, 1997). Studies have identified a relationship between both the myostatin and IGF-1 signalling pathways. A decrease in myostatin was accompanied by an increase in total Akt expression with subsequent pS6K activation (Morissette *et al.*, 2009; Lipina *et al.*,

2010). Decreased levels of protein synthesis was observed in cultured myotubes where myostatin was observed to inhibit AKT phosphorylation and activation (Taylor *et al.*, 2001; Trendelenburg *et al.*, 2009). Myostatin signals via activin type II receptors (ActRIIA and ActRIIB) and activin type I receptors (ALK4 and ALK5), where signal transduction is mediated by phosphorylation of Smad2 and Smad3 in complex with Smad4, also a mediator of bone morphogenic protein (BMP) signalling. Because of the crosstalk between the myostatin and BMP signalling pathways, when myostatin signalling is reduced, Smad4 is more available for BMP signalling. Increased BMP signalling leads to muscle hypertrophy (Sartori *et al.*, 2013). Interestingly, studies have shown that AKT activation downregulates the activin type II receptor Act RIIB in denervated skeletal muscle (Sartori *et al.*, 2009). Together this suggests an important and complex role of many converging pathways in the maintenance of skeletal muscle mass.

1.2.6 Atrophy

Skeletal muscle mass is maintained through the regulation of protein synthesis and degradation. An imbalance in this regulation by way of an increase in protein degradation not only results in a lack of hypertrophy, but often leads to muscle atrophy. Many triggers can induce muscle atrophy, including but not limited to denervation, disease, ageing, starvation, and immobility. These triggers initiate signalling cascades which upregulate forkhead box transcription factor (FOXO) via AKT inhibition. AKT is known to be involved in both the ubiquitin-proteosome system (UPS) and the autophagy-lysosome pathway, both of which promote protein degradation. AKT phosphorylates all 3 isoforms of FOXO; FOXO1, FOXO3, and FOXO4. As transcription factors, once the FOXO proteins are negatively phosphorylated and repressed, protein synthesis is stimulated via mTOR and glycogen synthase kinase 3β (GSK3β) (Manning and Cantley, 2007). When not actively repressed, FOXO transcription factors are involved in the transcriptional regulation of ubiquitin ligases atrogin-1/muscle atrophy F-box (MAFbx), and muscle ring finger 1 (MuRF1). Increased expression of E3 ubiquitin ligases results in the ubiquitination and target for degradation of many muscle proteins via the proteasome. FOXO transcription factors are also involved in the transcriptional regulation of microtubule-associated protein 1

light chain 3 (LC3). Together with BCL2/adenovirus E1B interacting protein 3 (BNIP3), LC3 is fundamental for protein degradation via the autophagy-lysosome pathway.

1.2.7 Ub-Proteasome

The ubiquitin-proteasome system (UPS) is a universal mechanism used to tag proteins for proteasomal degradation via the addition of the small molecule ubiquitin, a process known as ubiquitination. In this process, an E1 ubiquitin-activating enzyme ligates a ubiquitin molecule, mediating the transfer to an E2 ubiquitin-conjugating enzyme. The ubiquitin bound to the E2 ubiquitin-conjugating enzyme then complexes with an E3 ubiquitin-ligase which transfers the ubiquitin molecule onto a lysine residue of a substrate protein, thus targeting it for proteasomal degradation (Hershko and Ciechanover, 1986). It is known that the site of ubiquitination, and number of ubiquitin molecules is important for targeting proteins to different fates. Monoubiquitination has been shown to regulate DNA repair and gene expression mechanisms, whereas polyubiquitination on lysine48 targets proteins to the 26S proteasome (Passmore and Barford, 2004). Atrogin-1 and MuRF1 are 2 muscle-specific E3 ubiquitin-ligases which have been shown to be activated in muscle atrophy (Bodine and Baehr, 2014) and the expression of both are dependent on FoxO transcription factor regulation (Sandri *et al.*, 2004; Lee and Dong, 2017) which is regulated via AKT. However, Atrogin-1 and MuRF1 expression can be promoted independently of FOXO transcriptional regulation by NF-kB (Cai, McCarron and Hallenbeck, 2004) and p38 MAPK signalling (Li et al., 2005).

1.2.8 Autophagy-Lysosome

Autophagy is a distinct proteolytic mechanism to that of the UPS, one which is fundamental for the removal of damaged organelles and misfolded or damaged proteins. This mechanism is employed to break down unnecessary proteins during periods of starvation. The understanding is that the IGF-1 signalling pathway overlaps with 2 main pathways associated with autophagy. mTOR negatively regulates both unc51-like kinase-1 (ULK1), and FOXO-induced expression of autophagy-associated genes. There has since emerged conflicting evidence that mTOR has a minor role in the negative regulation of autophagy. Rapamycin treatment was shown not to induce

autophagy *in vivo*, nor was the induction of autophagy very high in cultured myotubes (Mammucari *et al.*, 2007; Zhao *et al.*, 2007). Instead it was AKT, independent of mTOR, which inhibited autophagy through FOXO3. This suggests two different mechanisms are able to inhibit autophagy; IGF-1/AKT/mTOR and IGF-1/AKT/FOXO.

1.2.9 CASA

In the case of muscle-specific proteins, misfolding or damage results in targeted degradation via an alternative, more selective, pathway. Chaperone assisted selective autophagy (CASA) is a stress-induced selective autophagy pathway which is dependent on the activity of z-disc protein BAG3 (Arndt *et al.*, 2010). CASA involves the binding of BAG3 to other co-chaperones in the identification of damaged proteins like Filamin C (FLNC) (Ulbricht and Höhfeld, 2013). This protein complex removes damaged or misfolded FLNC from the z-disc and facilitates ubiquitination by E3 ubiquitin ligase CHIP/STUB1, targeting it for autolysosomal degradation. Not only is this a means of mediating protein degradation, but BAG3 is also implicated in the HIPPO signalling pathway to promote FLNC transcription by interacting with inhibitors of YAP/TAZ (Ulbricht *et al.*, 2013). In response to resistance exercise, where muscles experience higher levels of stress and tension, components of the CASA pathway were observed to be more highly expressed (Ulbricht *et al.*, 2015). Therefore CASA is a more refined and specialised mechanism for the removal of damaged z-disc related cytoskeletal components, maintaining the integrity of skeletal muscle in response to mechanical load.

1.3 When the system goes wrong…

1.3.1 Muscle myopathies and dystrophies

Certain conditions, like illness or immobility, can cause loss of skeletal muscle mass, known as muscle atrophy (Lecker *et al.*, 1999; Bodine *et al.*, 2001; Tisdale, 2005). In contrast, resistance and strength training can increase muscle mass through muscle hypertrophy (Fry, 2004). It is clear that the regulation of muscle mass is a dynamic but acutely regulated process.

However sometimes the problem lies within the muscle. Muscle wasting diseases are caused by mutations in genes directly involved in regulating muscle function. Loss of

muscle mass results in a poor quality of life with muscle weakness and, in some cases, a shorter life expectancy (North *et al.*, 2014; Ravenscroft *et al.*, 2018).

1.3.2 Congenital myopathies

Congenital myopathies have a high prevalence within the population, estimated at 1:25,000 worldwide (Tubridy, Fontaine and Eymard, 2001), and are characterised by progressive muscle loss or weakness, histopathological abnormalities, and are observed to develop in childhood (Nance *et al.*, 2012; North *et al.*, 2014). Based on clinical phenotype and histopathological evidence, congenital myopathies can be classified into several distinct groups and are caused by mutations in specific genes. The subdivisions of congenital myopathy include: nemaline myopathy, central core myopathy, multiminicore myopathy, centronuclear myopathy, congenital fibre type disproportion myopathy, myotubular myopathy, and myosin storage myopathy (North *et al.*, 2014).

Nemaline myopathy is also known as rod myopathy because of the characteristic presence of rod-like structures within the muscle fibre. These rod-like structures are primarily composed of structural proteins like α-actinin, actin, and other z-disc-associated proteins (Fardeau, 1994). The most common variant of this myopathy is characterised by weakness of both core and peripheral muscles of the trunk, limbs, and face which is slowly progressive and causes moderate delay of motor control (Ryan *et al.*, 2001).

Core myopathy encompasses both central core myopathy and multiminicore myopathy. Central core myopathy is characterised by the presence of individual central “cores”; defined as rounded structures within the muscle fibre which have a limited oxidative activity (Dubowitz and Everson Pearse, 1960). Multiminicore myopathy is defined as the presence of numerous smaller cores in more of a diffuse pattern (Engel, Gomez and Groover, 1971). Patients present a heterogenous range of symptoms but primarily exhibit muscle hypotonia and weakness, respiratory problems, some level of scoliosis, and spinal stiffness (Cauwer *et al.*, 2002; Jungbluth, 2007).

Centronuclear myopathy is so called due to the presence of large centralised nuclei present in muscle fibres. The appearance of these nuclei are similar to that of nascent

myotubes, which gives its name to one of the centronuclear myopathy subtypes; myotubular myopathy (Spiro, Shy and Gonatas, 1966). Myotubular myopathy is an X-linked variant of centronuclear myopathy where patients, usually boys, are macrosomic, a baby who is born much larger than average for their gestational age, and commonly found to have other malformations which accompany this during development. Many patients are unable to survive longer than one year after birth due to respiratory insufficiency (Herman *et al.*, 1999). Female carriers are in general asymptomatic themselves, but mild symptoms may develop in childhood which is thought to be a result of an X-chromosome inactivation defect (Tanner *et al.*, 1999). In comparison with myotubular myopathy, symptoms of autosomal centronuclear myopathy develop later in life, from childhood to early adulthood. Patients present muscle hypotonia with muscle weakness of the trunk and facial muscles. Many cases which present themselves as a centronuclear myopathy have no known genetic diagnosis, therefore it is clear that many more genes important for muscle function are yet to be identified (Fattori *et al.*, 2015).

Congenital fibre type disproportion myopathy (CFTD) is primarily characterised by a clear disproportionate difference in fibre size between type I and type II fibres. Here. a large proportion of type I fibres are found to be 35-40% smaller than type II fibres, which presents in patients as muscle hypotonia with muscle weakness and delayed motor development (Clarke, 2011).

Mutations in a myosin heavy chain β (MHC-β) isoform which is expressed in type I skeletal muscle fibres are known to result in a variety of myopathies including myosin storage myopathy (Tajsharghi *et al.*, 2003), distal myopathy (Laing *et al.*, 1995), CTFD (Ortolano *et al.*, 2011), and multiminicore myopathy (Cullup *et al.*, 2012). The clinical presentation is moderate with a slow progressive weakness that eventually affects respiration and skeletal formation (Fiorillo *et al.*, 2016).

1.3.3 Muscle dystrophies

Muscular dystrophies are a group of genetic disorders characterised by progressive loss of muscle mass and subsequent weakness. Mutations which occur in genes which encode muscle proteins subsequently interfere with production of integral

proteins responsible for muscle stability. Deficient or absent glycoproteins within the muscle fibre membrane confer a diverse range of disease presentations (Allen, Whitehead and Froehner, 2016). Based on the age of onset, genetic cause, and disease characteristics, muscular dystrophies can be further sub categorised into 9 groups, with some overlapping symptoms. These include: Duchenne muscular dystrophy, Becker muscular dystrophy, myotonic dystrophy, facioscapulohumeral muscular dystrophy, limb-girdle muscular dystrophy, Emery-Dreifuss muscular dystrophy, oculopharyngeal muscular dystrophy, congenital muscular dystrophy, and distal muscular dystrophy.

Of the muscular dystrophies, Duchenne muscular dystrophy (DMD) is the most common; affecting about 100 newborn boys each year in the UK, with about 2,500 males living with the condition (Venugopal and Pavlakis, 2022). Symptoms appear in early postnatal development when movement and ambulation appears delayed or more difficult. DMD patients are usually in need of wheelchair assistance by the age of 11 years old and generally have a shorter life expectancy caused by severe respiratory failure. DMD is caused by a mutation within the coding region of the dystrophin gene, located on the X chromosome. Dystrophin, a 427kDa protein, forms part of the dystroglycan-complex (DGC) and is fundamental for anchorage of z-disc contractile and structural proteins to the costamere (Hoffman, Brown and Kunkel, 1987; Ervasti and Campbell, 1991).

Becker muscular dystrophy is closely related to DMD, but is generally less severe. Because of this, the average age of diagnosis is much later than that of DMD, usually around 11 years of age. Muscle weakness is an early symptom, which progresses until the use of a wheelchair is necessary in their 40’s or 50’s. Like that of DMD, Becker muscular dystrophy is caused by a mutation in the dystrophin gene which instead results in the production of a truncated dystrophin protein conferring partial functionality of the protein (Malhotra *et al.*, 1988).

Distal muscular dystrophies is a name given to a group of rare progressive genetic muscle disorders characterised by muscle atrophy and progressive muscle weakness in the distal limbs; the forearm and hand, and the lower leg and feet. Many genes have been implicated in distal muscular dystrophy and some of these include: MYH7, Titin,

Dysferlin, FLNC, VCP, Matrin 3, Anoctamin 5, Nebulin, Telethonin, and GNE (Dimachkie and Barohn, 2014).

1.3.4 Myofibrillar myopathy

The origins of the term “Myofibrillar myopathy” (MFM) began in the late 1990’s as a way of classifying diseases which present with patterns of myofibrillar dissolution associated with accumulations of abnormal proteins (Bleecker *et al.*, 1996; Nakano *et al.*, 1997). Electron microscopy of abnormal fibres reveals disintegration of myofibres which originates at the z-disc (Selcen, 2011). The clinical presentation of MFM appears to be quite heterogeneous, although it often affects distal muscles, and features elements of cardiomyopathy and neuropathy, also making it a neuromuscular disorder. MFM shares many symptoms with other muscular dystrophies, as some were in fact first reported as such (Markesbery *et al.*, 1974; Hauser, 2000). Genes found mutated which are known to result in MFM are: Desmin (Muñoz-Mármol *et al.*, 1998), ab-crystallin (Reilich *et al.*, 2010), myotilin (Hauser *et al.*, 2002), ZASP (Selcen and Engel, 2005), Filamin C (Vorgerd *et al.*, 2005), BAG3 (Selcen *et al.*, 2009), and FHL1 (Selcen *et al.*, 2011).

MFMs are muscle myopathies with variable characteristics and morphological features. However, the one common feature is that of the z-disc pathology. The underlying pathology of all MFMs implicates z-disc proteins as causes of the disease. However the genetic causes of many other muscular dystrophies have yet to be identified. Therefore this makes the understanding of the structure and function of skeletal muscle all the more important to identify potential disease-associated proteins, key players in muscle regulation, and their implications in disease pathogenesis.

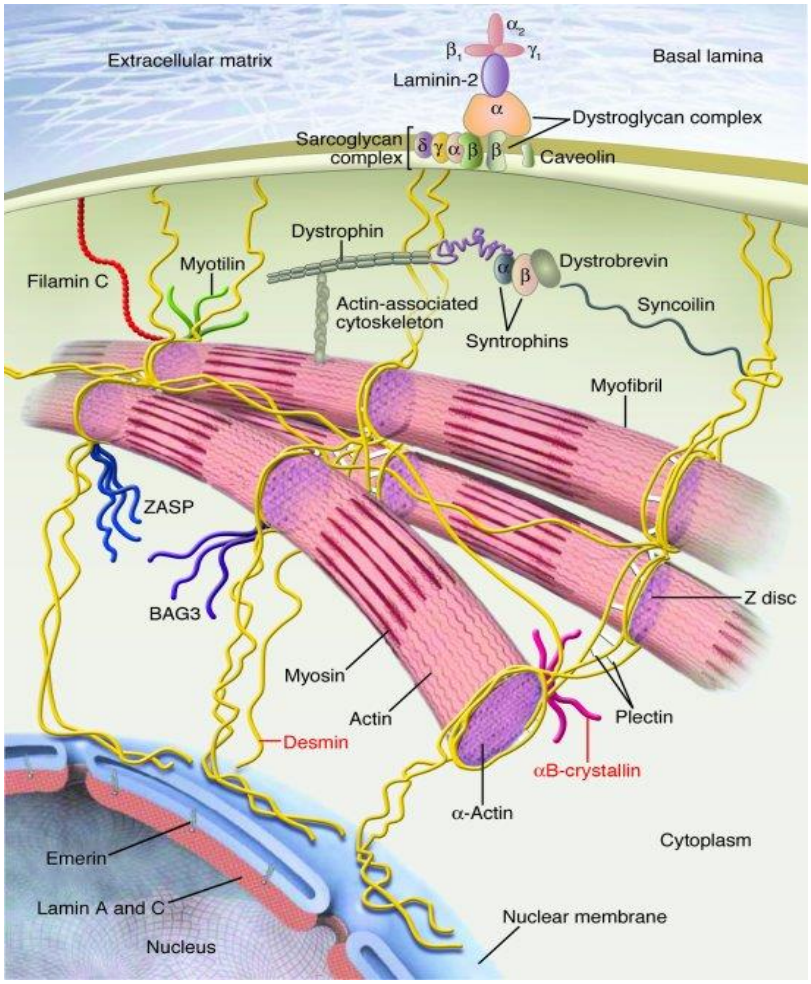

Figure 1.10: Molecular architecture of z-disc/costamere-associated proteins involved in skeletal myopathies. Mutations in sarcomeric and cytoskeletal proteins such as desmin, plectin, myotilin, filamin C, αB-crystallin, Z band alternatively spliced PDZ-motif protein (ZASP), and BCL2-associated athanogene 3 (BAG3) have been shown to cause neuromuscular disorders resulting predominantly in myofibrillar myopathy. Figure taken from (Goldfarb and Dalakas, 2009).

1.4 The KY protein

1.4.1 The KY mouse

A mutation within the Kyphoscoliosis Peptidase (*Ky*) gene in mice gave rise to the *ky/ky* mouse lacking a functional KY protein which went on to develop secondary thoracic-lumbar kyphoscoliosis (Dickinson and Meikle, 1973; Blanco *et al.*, 2001). Structurally it contains a protease/transglutaminase domain (Baker *et al.*, 2010) which is thought to be functionally inactive (O. Harrad, University of York; pers comm) but

may act as a mediator of protein interactions (Anantharaman, Koonin and Aravind, 2001), and a nuclear localisation signal (NLS) at the N-terminus which is specific only to primates (O. Harrad, University of York; pers comm). The protein itself is thought to interact with filamin C (FLNC), myosin-binding protein (MYBPC1), and Immunoglobulin-like and Fibronectin type III domain containing 1 (IGFN1) (Beatham *et al.*, 2004) in a complex at the z-disc (Baker *et al.*, 2010). The phenotype of the *ky/ky* mice was attributed to a GC deletion in the Ky gene that introduces a premature stop codon (Blanco *et al.*, 2001). The kyphoscoliosis which arises from this mutation is caused by a weakening of the postural paraspinal muscles that prevents the mouse from completing the placing reflex when held above a ledge (Blanco *et al.*, 2001). Contrary to the adult mouse, the neonatal mouse does not exhibit any phenotype. This is representative of a progressive disorder exacerbated by increased postnatal mechanical load. In the first 4 weeks of life, the tonically active muscles of the soleus, gracilis, and spinal muscles begin to atrophy with high levels of necrosis, regeneration, and accumulation of autophagic vesicles (Bridges *et al.*, 1992). In the adult mouse, slow muscles are predominantly affected. Despite this, total muscle mass is consistently lower in *ky/ky* mice than their wildtype (WT) counterparts (Maréchal, Coulton and Beckers-Bleukx, 1995). Increasing mechanical load through resistance exercise or synergistic ablation is a paradigm used to measure the ability of a muscle to detect increased load and respond accordingly by initiating the hypertrophic response. Interestingly, loss of KY protein results in a prevention of type IIa and type IIb fibres to coordinate this hypertrophic response, indicative of a role of KY in tension-induced hypertrophy (Blanco *et al.*, 2001). This data suggests that *ky/ky* skeletal muscle cannot adapt to increased mechanical load and the increase in ratio of type I slow fibres observed in the soleus muscle of these *ky/ky* mice is an adaptation attempting to increase resistance to fatigue and reduce potential future damage (Blanco *et al.*, 2001). Thought to be a consequence of tension-induced damage of cytoskeletal and z-disc proteins, and a hallmark of myofibrillar myopathies, the *ky/ky* mouse exhibits significant protein aggregations of damaged FLNC (Beatham *et al.*, 2004), BAG3 (Jokl *et al.* 2018), and XIN (Beatham *et al.*, 2006). This is suggested to be a pathological sign of an innate vulnerability of the muscle to withstand forces of contraction and subsequent inability to manage the degradation and synthesis of the cytoskeletal proteins critical to maintain sarcomeric structure throughout repeated

bouts of contraction. Therefore, KY is hypothesised to be important for the efficient degradation of these large structural z-disc proteins.

1.4.2 KY mutations in humans

Loss of function of *KY* in human patients has been known to cause myofibrillar myopathy 7 (MFM7). Many independent cases of patients associated with mutations in the *KY* gene have been reported with MFM phenotypes. Each patient presented with significant overlap in the pathological and clinical phenotypes, however inbred pedigrees in some families and accumulation of other damaging mutations is thought to account for some of the variability observed. These mutations are summarised in Appendix - Supplementary Figure 1.

The first human case of a MFM associated with loss of function of KY was in a young girl presenting with walking difficulties and moderate muscle weakness (Hedberg-Oldfors *et al.*, 2016). Whole exome sequencing (WES) showed that the patient had a one base deletion within the KY gene, NM_178554.6:c.1071delG;p.(Thr358LeufsTer3), resulting in a frameshift, introduction of a premature stop codon, producing a smaller truncated protein. She exhibited contractures of the shoulder, hip, elbow, plantar, and feet alongside a slight lumbar lordosis. Immunohistochemistry of muscle biopsies showed variable type I and type II fibre size, with centralised nuclei, small fibres expressing embryonic myosin heavy chain (eMyHC), and z-disc thickening and formation of small nemaline rods on electron microscopy. As in the *ky/ky* mouse, and phenotypic of this MFM, aggregations of FLNC and XIN were also observed.

The second case of a KY-associated MFM occurred in 2 brothers with a mutation in exon 6 the *KY* gene NM_178554.6:c.405C>A;p.(Tyr135Ter) resulting in a premature stop codon suggested to cause nonsense-mediated mRNA decay (Straussberg *et al.*, 2016). Both of the brothers suffered from muscle weakness, with atrophy of the peripheral limb muscles and of the tongue. Both exhibited a degree of kyphosis, more evident in the younger brother who also displayed intellectual and speech impairments. Internally, split fibres, centralised nuclei, necrosis and regenerating fibres were just some of the myopathic phenotypes observed in the muscle fibres of these

patients. FLNC aggregations were observed, consistent with the *ky/ky* mouse and the previous patient.

Twelve individuals from 3 families from a single consanguineous tribe were studied after showing signs of early onset progressive spastic paraplegia. Genetic analysis revealed a frameshift mutation NM_178554.6:c.51_52insTATCGACATGTGCTG TATCTATCGACAT;p. (Val18TyrfsTer56) with loss of function. All patients exhibited atrophy of the tongue, small fibres, centralised nuclei, lower limb spasticity, hyperreflexia, an inability to walk using their heel, and a progressive kyphoscoliosis developing with age (Yogev *et al.*, 2017).

WES of a single male patient identified a nonsense mutation in the *KY* gene NM_178554.6:c.415C>T;p.(Arg139Ter) which resulted in loss of function of the KY protein (Ebrahimzadeh-Vesal *et al.*, 2018). This patient exhibited equinovarus foot deformity, lower limb muscular weakness, mild scoliosis, and joint contracture.

A complex neurological disorder of four individuals was investigated by WES in order to find the underlying cause. Sequencing revealed a missense mutation, the only case that did not result in total loss of function. All patients shared an equinovarus foot deformity phenotype, progressive muscle weakness, and toe-walking (Arif *et al.*, 2020). Unfortunately the patients declined further invasive blood or biopsy testing.

The implication of KY in both human disease and the phenotype observed in the *ky/ky* mouse further emphasises the critical function of KY in the maintenance of skeletal muscle.

1.4.3 KY and CASA

Previously, KY has been shown to be necessary for tension-induced hypertrophy (Blanco *et al.*, 2001). As a result of this, the presence of FLNC aggregates in both human patients (Hedberg-Oldfors *et al.*, 2016; Straussberg *et al.*, 2016) and in the *ky/ky* mouse (Beatham *et al.*, 2004) suggest an increase in damaged cytoskeletal proteins and subsequent mislocalisation. Additionally, FLNC is known to be a client of the BAG3-mediated CASA pathway responsible for protein degradation (Ulbricht *et*

al., 2013). Therefore there emerged a possible dual role for KY in the maintenance of skeletal muscle whereby a KY-associated impairment of CASA is responsible for inefficient protein degradation and turnover of misfolded FLNC, as KY and FLNC interact at the z-disc (Beatham *et al.*, 2004; Baker *et al.*, 2010), and muscle instability caused by the loss of KY results in an increase in the levels of damaged structural proteins. Furthermore, loss of functional KY protein results in an inability of skeletal muscle to undergo a hypertrophic response following increased mechanical load (Blanco *et al.*, 2001). Therefore, not only are FLNC aggregates indicative of MFM pathology, but it is an indication of an impaired CASA pathway.

The association between KY and CASA was strengthened using 3 different models of KY loss of function. The first model utilised KY-deficient C2C12 myotubes which exhibited increased levels of *BAG3* and *FLNC* transcripts (Jokl *et al.*, 2018). These same transcripts were consistently upregulated in the muscle of the Zebrafish KY-knockout model. Resistance exercise imposed on these fish using increased viscosity of swimming medium did not produce the expected increase in *BAG3* and *FLNC* transcripts that their wildtype siblings produced, as the basal levels of these transcripts were already higher in the mutant fish (Jokl *et al.*, 2018). Investigation of transcript levels within the exterior digitorum longus (EDL) muscle of *ky/ky* mice also showed an elevation of *BAG3* transcript expression, in correlation with elevated BAG3 in the insoluble fraction of soleus muscle protein extracts, and impairment in BAG3 turnover in the soleus muscle. Altogether this suggests a role for KY in maintaining muscle mass and stability via the BAG3-mediated CASA protein degradation pathway, although the specific nature of this interaction is yet to be determined.

1.5 IGFN1

1.5.1 Structure, variants, and interacting partners

Immunoglobulin-like and Fibronectin type III domain containing 1 (IGFN1) was identified as a KY-interacting protein at the z-disc through a yeast two-hybrid (Y2H) screen using KY as bait (Baker *et al.*, 2010). It is a large skeletal muscle protein found to localise at the z-disc, but does some nuclear localisation (Mansilla *et al.*, 2008; Baker *et al.*, 2010). Full length IGFN1 is extremely large and consists of 11 immunoglobulin (IG) and fibronectin type 3 (FN3) domains separated either side of an

unstructured region, in a similar structure to that of titin or myomesin (Rief *et al.*, 1997; Schoenauer *et al.*, 2005; Baker *et al.*, 2010). Full length IGFN1 contains multiple putative ATG start sites which can produce multiple shorter IGFN1 isoform variants through alternative splicing like that of IGFN1_V1 which lacks the unstructured region (Baker *et al.*, 2010). Conservation of the *IGFN1* gene between human and mouse is high, with respect to the region coding for the IG and FN3 domains. Conservation of the unstructured region is highly variable, suggesting that this region is not as important for the function of the protein as the organised regions (Baker *et al.*, 2010). Instead, unstructured regions like this have been shown to be important for mechanical stretching which allows for protein binding upon mechanically-induced conformational changes which expose previously hidden protein binding sites (Dyson, Jane Dyson and Wright, 2005). This offers a potential role for IGFN1 in mediating a cellular response following mechanical stress and tension. Its position at the z-disc makes it highly likely to behave in a similar fashion to that of titin or myomesin in maintaining the structural integrity of the sarcomere during repetitive bouts of contraction and relaxation.

IGFN1 contains many globular IG and FN3 domains either side of the unstructured region, suggested to be likely candidates for targets of protein interactions. A Y2H assay using IGFN1 as bait identified FLNC, titin, and actin as interacting proteins; FLNC also being an interacting protein of KY (Baker *et al.*, 2010). Not only are all of these proteins critical components of sarcomeric organisation, but they are implicated in pathways associated with mechanotransduction, hypertrophy, and protein degradation.

1.5.2 IGFN1 and Atrophy

Muscle denervation is well known for causing muscle atrophy, and is used as a model to induce fibre atrophy *in vivo* (Pellegrino and Franzini, 1963). Analysis of denervated muscles reveals a significant increase in *IGFN1* expression. The atrophy resulting from muscle denervation was proposed to be a consequence of IGFN1-mediated downregulation of protein synthesis by negatively regulating eEF1A activity (Mansilla *et al.*, 2008). In contrast, *IGFN1* transcript was found to be significantly lower in muscles which have undergone myostatin-inhibited increase in muscle mass

(Rahimov *et al.*, 2011), and found once again to be increased in models of muscle atrophy when myostatin signalling is overactivated using adenoviral overexpression *in vivo* (Chen *et al.*, 2014). These findings provide a tangible link between IGFN1 as a z-disc protein, and the regulation of atrophy signalling *in vivo*, contrary to the IGFN1-interacting protein, KY, which is thought to mediate hypertrophy/protein turnover pathways.

1.6 ZAK

1.6.1 Genomic/Proteomic features

Leucine Zipper-and Sterile Alpha Motif-Containing Kinase (ZAK; also known as MRK, AZK, MAP3K20, MLTK, or MLTK7) was first identified in relation to the control of cell cycle checkpoints in cancer biology (Gotoh, Adachi and Nishida, 2000; Liu *et al.*, 2000; Bloem *et al.*, 2001; Gross *et al.*, 2002). The *ZAK* gene, located on human chromosome 2q31.1 (mouse chromosome 2C3) is subject to alternative splicing; thus yielding two isoforms: *ZAKα* and *ZAKβ* (Figure 1.11 A). These protein isoforms share a 331 amino acid region of homology at the N-terminus, encoding the highly conserved serine/threonine (Ser/Thr) kinase domain, and a leucine zipper domain (Gross *et al.*, 2002). The ZAKα isoform is longer than its alternative, translated from the whole 20 exon sequence and comprising 803 amino acids. Conversely, ZAKβ is translated from the same first 11 exons as ZAKα, with an alternatively spliced exon 12. The resulting protein is shorter than ZAKα and is formed of 454 amino acid residues (Gotoh, Adachi and Nishida, 2000). The isoforms diverge at the C-terminus, where ZAKα contains a sterile alpha motif domain known to aid oligomerisation (Peterson *et al.*, 1997) and protein-protein interactions (Ponting, 1995), and two ribosome-binding domains that together serve as a molecular sensing module (Vind *et al.*, 2020). ZAKα has been implicated in ribotoxic stress but is unlikely to have a role in fully differentiated skeletal muscle since *ZAKβ* is the only ZAK isoform present in fully differentiated adult skeletal muscle in both humans and mice. On the other hand, the unique C-terminal region of ZAKβ encodes a highly acidic domain with no known function, except for 2 distinct domains, a sensory and C-terminal domain (CTD) which does not respond to ribotoxic stress (Vind *et al.*, 2020), but instead has been shown to respond to mechanical perturbation of cytoskeletal stress fibres caused by osmotic shock or cellular compression in U2OS cells (Nordgaard et al., 2022). Under these conditions, ZAKβ

activates by self-phosphorylation, relocates and colocalises with stress fibres through its unique C-terminal region which leads to p38 activation (Nordgaard et al., 2022). Interestingly, repeated contractions of Tibialis anterior (TA) muscle also lead to acute p38 activation in a ZAKβ-dependent mechanism (Nordgaard et al., 2022), confirming the *in vitro* findings in a physiologically relevant model.

BLAST analysis revealed that the Ser/Thr kinase domain is highly conserved between members of the mitogen-activated protein triple kinase (MAPKKK) family. According to Gross et al., 2002 the DNA sequence within this region shares 52% and 47% homology with human mixed lineage kinases MLK2 and MLK1 respectively. The term mixed lineage kinase (MLK) is derived from the 11 conserved subdomains that are found in all protein kinases, of which; subdomains 1-8 are homologous to Ser/Thr kinases, whereas subdomains 9-11 are similar to those found in tyrosine kinases (Gallo and Johnson, 2002). All MLKs appear to act as mitogen-activated protein kinase kinase kinases (MAPKKKs). In the case of ZAK, the protein kinase domain is preferential to ser/thr phosphorylation targets. Both ZAK protein isoforms are highly conserved between mice and humans (Figure 1.11 B&C).

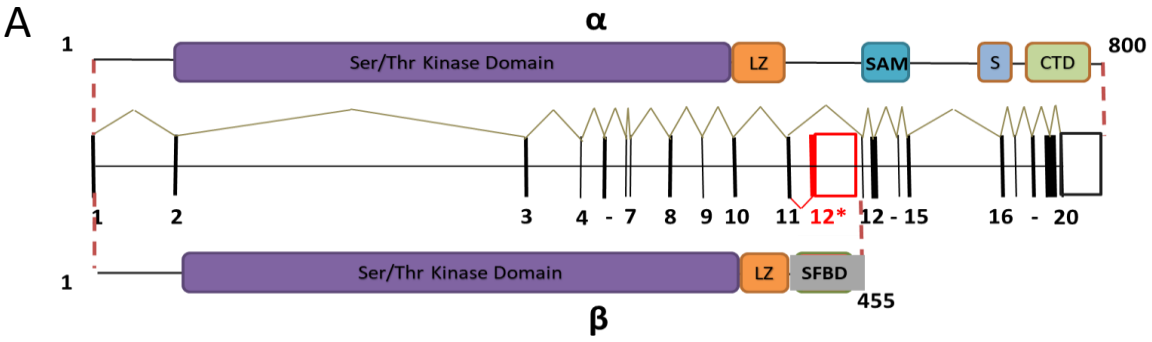

B

```
CLUSTAL O(1.2.4) multiple sequence alignment


sp|Q9NYL2|M3K20_HUMAN       MSSLGASFVQIKFDDLQFFENCGGGSFGSVYRAKWISQDKEVAVKKLLKIEKEAEILSVL 60
sp|Q9ESL4|M3K20_MOUSE       MSSLGASFVQIKFDDLQFFENCGGGSFGSVYRAKWISQDKEVAVKKLLKIEKEAEILSVL 60
                            ************************************************************

sp|Q9NYL2|M3K20_HUMAN       SHRNIIQFYGVILEPPNYGIVTEYASLGSLYDYINSNRSEEMDMDHIMTWATDVAKGMHY 120
sp|Q9ESL4|M3K20_MOUSE       SHRNIIQFYGVILEPPNYGIVTEYASLGSLYDYINSNRSEEMDMEHIMTWATDVAKGMHY 120
                            ************************************************:***********

sp|Q9NYL2|M3K20_HUMAN       LHMEAPVKVIHRDLKSRNVVIAADGVLKICDFGASRFHNHTTHMSLVGTFPWMAPEVIQS 180
sp|Q9ESL4|M3K20_MOUSE       LHMEAPVKVIHRDLKSRNVVIAADGVLKICDFGASRFHNHTTHMSLVGTFPWMAPEVIQS 180
                            ************************************************************

sp|Q9NYL2|M3K20_HUMAN       LPVSETCDTYSYGVVLWEMLTREVPFKGLEGLQVAWLVVEKNERLTIPSSCPRSFAELLH 240
sp|Q9ESL4|M3K20_MOUSE       LPVSETCDTYSYGVVLWEMLTREVPFKGLEGLQVAWLVVEKNERLTIPSSCPRSFAELLH 240
                            ************************************************************

sp|Q9NYL2|M3K20_HUMAN       QCWEADAKKRPSFKQIISILESMSNDTSLPDKCNSFLHNKAEWRCEIEATLERLKKLERD 300
sp|Q9ESL4|M3K20_MOUSE       QCWEADAKKRPSFKQIISILESMSNDTNLPDQCNSFLHNKAEWRCEIEATLERLKKLERD 300
                            **************************.***:**************************

sp|Q9NYL2|M3K20_HUMAN       LSFKEQELKERERRLKMWEQKLTEQSNTPLLPSFEIGAWTEDDVYCWVQQLVRKGDSSAE 360
sp|Q9ESL4|M3K20_MOUSE       LSFKEQELKERERRLKMWEQKLTEQSNTPLLPSFEIGAWTEDDVYFWVQQLVRKGESSVE 360
                            ******************************************* *********:**.*

sp|Q9NYL2|M3K20_HUMAN       MSVYASLFKENNITGKRLLLLEEEDLKDMGIVSKGHIIHFKSAIEKLTHDYINLFHFPPL 420
sp|Q9ESL4|M3K20_MOUSE       MSGYASLFKENNITGKRLLLLEEEDLKDMGIVSKGHIIHFKSAIEKLTHDYLNLFHFPPL 420
                            ** ***********************************************:********

sp|Q9NYL2|M3K20_HUMAN       IKDSGGEPEENEEKIVNLELVFGFHLKPGTGPQDCKWKMYMEMDGDEIAITYIKDVTFNT 480
sp|Q9ESL4|M3K20_MOUSE       IKDSGGEPEENEEKIVNLELVFGFHLKPGTGPQDCKWKMYMEMDGDEVAITYIKDVTFNT 480
                            ************************************************:************

sp|Q9NYL2|M3K20_HUMAN       NLPDAEILKMTKPPFVMEKWIVGIAKSQTVECTVTYESDVRTPKSTKHVHSIQWSRTKPQ 540
sp|Q9ESL4|M3K20_MOUSE       SLPDAEILKMTKPPFVMEKWIVGIAEDQTVECTVTYENDVRTPKLTKHVHSIQWDRTKPQ 540
                            .************************:.**********.****** *********.*****

sp|Q9NYL2|M3K20_HUMAN       DEVKAVQLAIQTLFTNSDGNPGSRSDSSADCQWLDTLRMRQIASNTSLQRSQSNPILGSP 600
sp|Q9ESL4|M3K20_MOUSE       DEVKAVQLAIQTLFSSSEGNPGSRSDSSADCQWLDTLRMRQIASHTSLQRSQSNPILGSP 600
                            **************:.*:*************************:***************

sp|Q9NYL2|M3K20_HUMAN       FFSHFDGQDSYAAAVRRPQVPIKYQQITP-VNQSRSSSPTQYGLTKNFSSLHLNSRDSGF 659
sp|Q9ESL4|M3K20_MOUSE       FFPYFANQDSYAAAVRRTQTPVKYQQITPSINPSRSSSPTQYGLSRNFSSLNLSSRDSGF 660
                            ** :* .********** *.*:******* :* ***********::*****:*.******

sp|Q9NYL2|M3K20_HUMAN       SSGNTDTSSERGRYSDRSRNKYGRGSISLNSSPRGRYSGKSQHSTPSRGRYPGKFYRVSQ 719
sp|Q9ESL4|M3K20_MOUSE       SSLN-DSSSERGRYSDRSRNKYYRGSVSLNSSPKGRYGGKSQHSTPSRERYSGKFYRLPQ 719
                            ** * *:*************** ***:******:***.********** ** *****: *

sp|Q9NYL2|M3K20_HUMAN       SALNPHQSPDFKRSPRDL--HQPNTIPGMPLHPETDSRASEEDSKVSEGGWTKVEYRKKP 777
sp|Q9ESL4|M3K20_MOUSE       SALNTHQSPDFKRSPNDHDRRVPRTIPGMPLHPETASKAGEEESRVSEGGWTKVEYRKKT 779
                            **** **********.*   : *.*********** *:*.**:*:************** 

sp|Q9NYL2|M3K20_HUMAN       HRPSPAKTNKERARGDHRGWRNF      800
sp|Q9ESL4|M3K20_MOUSE       HRQLSAKTSKERTRGNYRGRRNF      802
                            **   ***.***:**:.** ***
```

C

```
CLUSTAL O(1.2.4) multiple sequence alignment

sp|Q9NYL2-2|M3K20_HUMAN      MSSLGASFVQIKFDDLQFFENCGGGSFGSVYRAKWISQDKEVAVKKLLKIEKEAEILSVL      60
sp|Q9ESL4-2|M3K20_MOUSE      MSSLGASFVQIKFDDLQFFENCGGGSFGSVYRAKWISQDKEVAVKKLLKIEKEAEILSVL      60
                             ************************************************************

sp|Q9NYL2-2|M3K20_HUMAN      SHRNIIQFYGVILEPPNYGIVTEYASLGSLYDYINSNRSEEMDMDHIMTWATDVAKGMHY      120
sp|Q9ESL4-2|M3K20_MOUSE      SHRNIIQFYGVILEPPNYGIVTEYASLGSLYDYINSNRSEEMDMEHIMTWATDVAKGMHY      120
                             ****************************************:***************

sp|Q9NYL2-2|M3K20_HUMAN      LHMEAPVKVIHRDLKSRNVVIAADGVLKICDFGASRFHNHTTHMSLVGTFPWMAPEVIQS      180
sp|Q9ESL4-2|M3K20_MOUSE      LHMEAPVKVIHRDLKSRNVVIAADGVLKICDFGASRFHNHTTHMSLVGTFPWMAPEVIQS      180
                             ************************************************************

sp|Q9NYL2-2|M3K20_HUMAN      LPVSETCDTYSYGVVLWEMLTREVPFKGLEGLQVAWLVVEKNERLTIPSSCPRSFAELLH      240
sp|Q9ESL4-2|M3K20_MOUSE      LPVSETCDTYSYGVVLWEMLTREVPFKGLEGLQVAWLVVEKNERLTIPSSCPRSFAELLH      240
                             ************************************************************

sp|Q9NYL2-2|M3K20_HUMAN      QCWEADAKKRPSFKQIISILESMSNDTSLPDKCNSFLHNKAEWRCEIEATLERLKKLERD      300
sp|Q9ESL4-2|M3K20_MOUSE      QCWEADAKKRPSFKQIISILESMSNDTNLPDQCNSFLHNKAEWRCEIEATLERLKKLERD      300
                             *************************.***:**************************

sp|Q9NYL2-2|M3K20_HUMAN      LSFKEQELKERERRLKMWEQKLTEQSNTPLLLPLAARMSEESYFESKTEESNSAEMSCQI      360
sp|Q9ESL4-2|M3K20_MOUSE      LSFKEQELKERERRLKMWEQKLTEQSNTPLLLPLSARMSEESYFESKTEESNSAEMSCQI      360
                             *********************************:************************

sp|Q9NYL2-2|M3K20_HUMAN      TATSNGEGHGMNPSLQAMMLMGFGDIFSMNKAGAVMHSGMQINMQAKQNSSKTTSKRRGK      420
sp|Q9ESL4-2|M3K20_MOUSE      TAASNGEGHGMNPGLQAMMLMGFGDVFSMNKAGAVLHSGMQINMQAKQNSSKTTCKRRGK      420
                             **:**********.**********:*********:*****************.*****

sp|Q9NYL2-2|M3K20_HUMAN      KVNMALGFSDFDLSEGDDDDDDDGEEEDNDMDNSE        455
sp|Q9ESL4-2|M3K20_MOUSE      KVNMALGFSDFDLSEGDDDDH-DGDDAENDVDNSE        454
                             ******************. **:: :**:****
```

Figure 1.11: Conservation of ZAK in mouse and human. (A) The domain structure of both ZAK isoforms associated with alternative splicing of the *ZAK* gene. The alternative eon 12 associated with ZAKβ is shown in red. (B) Amino acid clustal alignment of human and mouse ZAKα protein. (C) Amino acid clustal alignment of human and mouse ZAKβ protein.

1.6.2 ZAK signalling

Transcriptomic analyses reveal a diverse expression pattern in mouse tissues for both *ZAK* isoforms (Bloem *et al.*, 2001; Gross *et al.*, 2002). Interestingly, transcript analysis identified isoform exclusivity of *ZAKβ* in both human (Vasli *et al.*, 2017) and mouse skeletal muscle (X Li, University of York; pers comm). This raised an interesting question as to the nature of the role of ZAKβ in skeletal muscle. It was previously established that IGFN1 interacts with many components of the z-disc (Figure 1.12). A Y2H study using the first 3 domains of IGFN1 as bait identified interactions with ZAKβ, FHL2, and PDLIM3. A Y2H using domains 4-11 as bait identified MYBPC1, MYOM2, FLNC, ACTA1, and TTN as interacting targets of IGFN1 (Baker *et al.*, 2010). The identification of ZAKβ in association with the KY protein complex including KY, IGFN1,

and FLNC which all share z-disc localisation, places ZAKβ at the heart of skeletal muscle mechanosensation and transduction pathways (Beatham *et al.*, 2006; Baker *et al.*, 2010).

ZAK overexpression has been shown to activate a multitude of signalling cascades. For instance, *Zakα* overexpression has been shown to have a hypertrophic effect on cultured cardiomyoblasts thought to be a consequence of TGFβ signalling (Huang *et al.*, 2004; Hsieh *et al.*, 2015). Expression of the *Zakβ* isoform in the same model has also shown an increase in protein synthesis (Bloem *et al.*, 2001). Furthermore, cardiac-specific expression in a transgenic mouse showed an increase in total cardiac mass, fibrosis, and fetal gene expression (Christe *et al.*, 2004). ZAK has been shown to preferentially activate ERK6/p38γ and JNK respectively via their endogenous activators MKK3/MKK6, and MKK4/MKK7 (Gross *et al.*, 2002). The implication of p38γ and JNK signalling could be highly relevant in muscle maintenance as they are very important for myogenesis (Burks and Cohn, 2011), maintenance of fibre type (Shi *et al.*, 2008; Foster, Tidball and Wang, 2012), fibre adaptation (Smythe and Forwood, 2012), and expression of regulatory transcription factors (Brennan *et al.*, 2022). However these overexpression models have not specifically informed us on the physiological function of ZAKβ in skeletal muscle. It appears that ZAKβ is a potential early mediator/regulator of tension-induced mechanical stress; however the mechanism of activation and how ZAKβ senses this stress is not yet understood. Similarly, p38 has been used as a readout of ZAKβ activation in many experiments, however the nature of this signalling and direct output of ZAKβ activation in skeletal muscle remains to be determined.

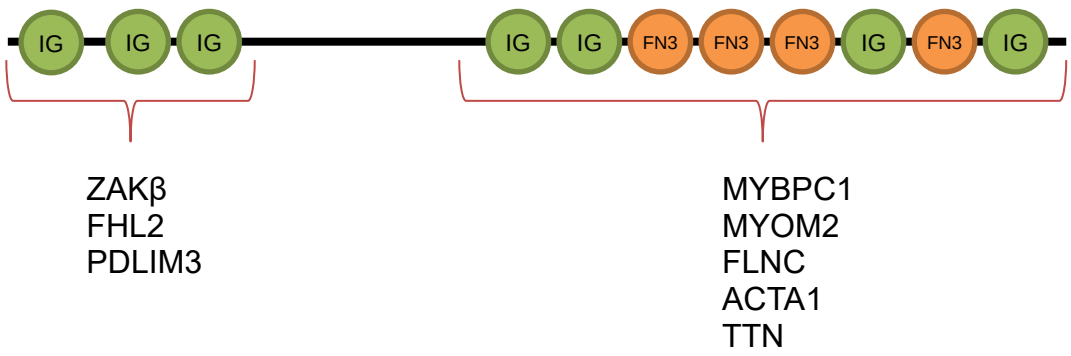

Figure 1.12: Schematic of the results of the interacting partners of IGFN1 using a yeast two-hybrid. Domains 1-3 were used as bait and identified ZAKβ, FHL2, and PDLIM3.

Domains 4-11 were used as bait and identified MYBPC1, MYOM2, FLNC, ACTA1, and TTN. Figure adapted from Baker *et al.*, 2010.

1.6.3 ZAK-associated congenital myopathy in humans

Next generation sequencing (NGS), and whole exome sequencing (WES) has been fundamental for the identification of the genetic cause of debilitating myopathies caused by mutations in proteins fundamental for sarcomeric integrity. Recently these methods have been utilised to identify and diagnose mutations in both the *KY* and *ZAK* genes (Hedberg-Oldfors *et al.*, 2016; Straussberg *et al.*, 2016; Vasli *et al.*, 2017; Yogev *et al.*, 2017; Ebrahimzadeh-Vesal *et al.*, 2018; Arif *et al.*, 2020; Ahmad *et al.*, 2022). The mutations identified in *ZAK* patients were the first direct association of a stress-induced mixed lineage kinase and a skeletal muscle myopathy, supporting the hypothesis that ZAK has an important role in the maintenance of muscle function and mass. These mutations are summarised in Appendix - Supplementary Figure 2.

Pathogenic mutations in the *ZAK* gene have been shown to clinically cause a centronuclear myopathy with fibre disproportion (CNM6 [MIM: 617760]). First described in 2017, autosomal recessive mutations in 3 consanguineous families in different ethnic backgrounds were identified and analysis revealed mutations included 2 homozygous frameshift mutations and one homozygous nonsense mutation (Vasli *et al.*, 2017). All affected individuals developed symptoms in infancy or early childhood which manifested as slow progressive muscle weakness, fibre size variation, a predominance of type I slow fibres, and increased levels of centralised nuclei (Vasli *et al.*, 2017). Recently, more individuals with deleterious *ZAK* mutations have been identified, all exhibiting progressive muscle weakness, a mild scoliosis, and delayed motor development; a pathology phenotypically similar to that of cases presenting with *KY* mutations (Ahmad *et al.*, 2022). The association between a human myopathy and a signalling protein with links to the z-disc and therefore important mechanotransduction pathways poses an intriguing prospect for another regulatory protein in skeletal muscle maintenance.

1.7 Hypotheses and Objectives

1.7.1 Hypotheses

Previously, ZAK was identified as an interacting protein of IGFN1; a member of the KY protein complex at the z-disc. However, the function of ZAK in skeletal muscle has not yet been defined. Based on the literature detailed above, several hypotheses regarding the role of ZAK were outlined at the start of this project (Figure 1.13). The initial hypotheses are as follows:

- **ZAKβ is a signalling protein**

One of the simplest hypotheses regarding the role of ZAKβ is that it acts as a signalling protein. As a protein which contains a Ser/Thr kinase domain thought to be upstream of JNK and p38 signalling modules makes it an ideal candidate to perform such a role.

- **ZAKβ interacts with cell adhesion complexes**

Previous data suggested a role for the ZAKβ interacting protein IGFN1 in myoblast fusion and actin remodelling via the actin nucleating protein COBL. The suggested interaction between ZAKβ and IGFN1/COBL may facilitate a role for ZAKβ as an modulator of adhesion complexes critical for myoblast fusion.

- **ZAKβ is a mechanosensor**

Loss of ZAKβ in patients results in muscle atrophy. ZAKβ may act as a sensor of mechanical tension at the z-disc and modulate the response of skeletal muscle to facilitate hypertrophy. This hypothesis overlaps with the previous hypothesis and would require interactions with relevant adhesion complexes at the z-disc. The association of ZAKβ with IGFN1, KY, and FLNC provides a possible mechanism to facilitate hypertrophic signalling following the detection of increased mechanical stress.

- **ZAKβ interacts with the CASA pathway**

Preliminary data at the outset of this project suggested a remarkable similarity in pathology of the ZAK-deficient patient when compared to that of the KY patient. In the *ky/ky* mouse, this phenotype is considered a disorder which affects the CASA protein degradation pathway.

1.7.2 Objectives

In order to explore this in more detail, the objectives set out at the beginning of the project were as follows:

- **Characterization of the ZAK-KO mouse pathology**

Characterisation of the ZAK-KO mouse pathology from whole organism to skeletal muscle-specific abnormalities. This will inform on the similarities between patients identified with ZAK loss of function and that of the novel ZAK-KO mouse generated as a model for the human myopathy. Validation of this preclinical model is key to future therapeutic developments. This work will help identify the general role of ZAKβ in skeletal muscle.

- **Determining the role of ZAKβ in skeletal muscle hypertrophy**

Previous ZAK overexpression models have demonstrated fibre hypertrophy in cardiomyocytes. In ZAK patients, loss of ZAK causes muscle atrophy. If loss of ZAK causes atrophy and ZAKβ is a genuine regulator of hypertrophy, overexpression of ZAKβ may result in the opposite effect. Here, we will investigate the effects of overexpression of ZAKβ in skeletal muscle, and determine the role of ZAKβ in the hypertrophic response in both ZAK-KO and *ky/ky* mouse models.

- **Identification of ZAKβ activators and effectors**

Given what is known about ZAKβ, a MAPKKK stress kinase which is activated in response to mechanical stress with a potential role in muscle hypertrophy, focus was placed on identification of the direct effectors of ZAKβ signalling. To get insights into the potential roles of ZAKβ in skeletal muscle we will be using an adapted

phosphoproteomics protocol to identify the immediate downstream targets of ZAKβ phosphorylation.

- **Examining the role of ZAKβ under physiological stress**

ZAKβ has been shown to become activated in response to mechanical stress *in vivo*. Therefore, it is imperative to understand the type(s) of mechanical stress which ZAKβ is most responsive to. Potential roles for ZAKβ in muscle regeneration, acute hypertrophy response and muscle adaptation to endurance will be exposed by subjecting the ZAK$^{-/-}$ mouse to focal muscle injury, ablation of synergistic muscles and long-term exercise, respectively.

As new evidence was obtained the objectives above were kept under constant development to allow for the exploration of new and interesting avenues of research. This will be discussed in the following chapters.

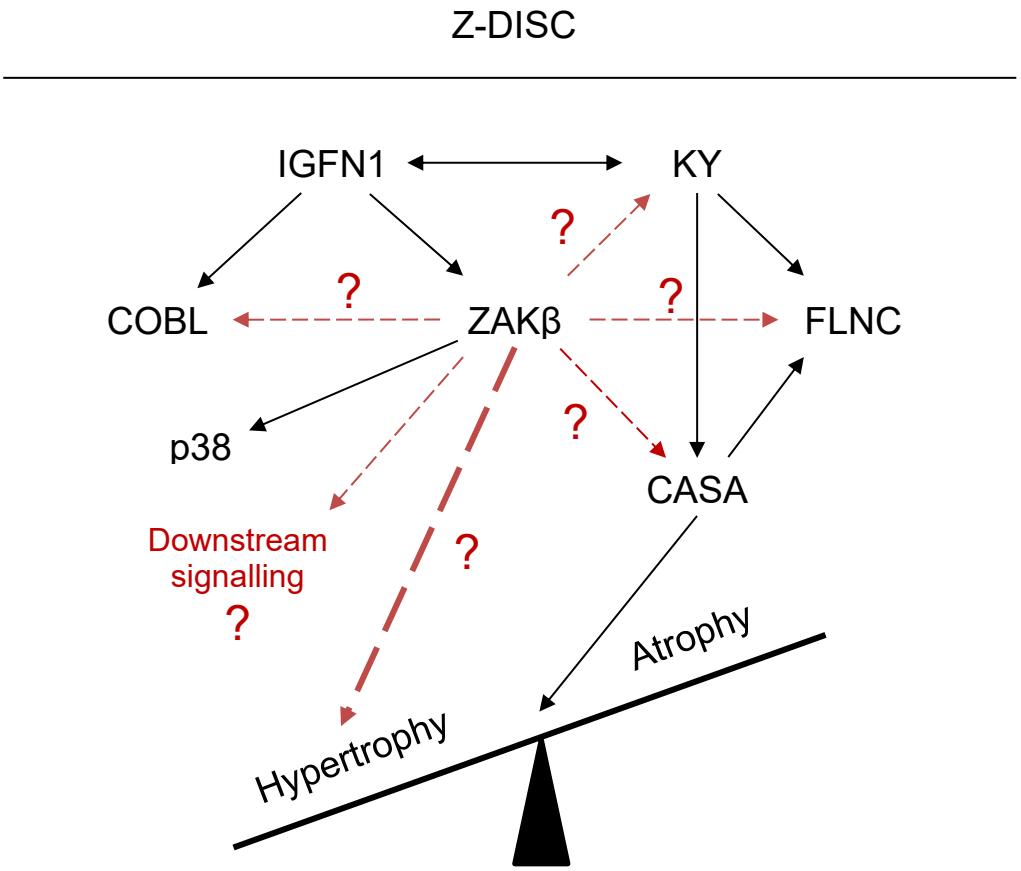

Figure 1.13: Summary of the lines of investigation for the role of ZAKβ in skeletal muscle. Black lines indicate known relationships. Red dashed lines indicate proposed relationships.

CHAPTER 2

MATERIALS AND METHODS

2.1 Buffers and Reagents

Name	Composition	Source
DMEM	DMEM + 4.5 g/L D-Glucose, + L-Glutamine, + Pyruvate	Gibco, Life Technologies (S41966-029)
Cell culture growth media (GM)	10% Fetal Bovine Serum (FBS), 100 U/mL Penicillin/Streptomycin in DMEM	Produced in lab
Cell culture differentiation media (DM)	2% Fetal Bovine Serum (FBS), 100 U/mL Penicillin/Streptomycin in DMEM	Produced in lab
Cell culture freezing media (DM)	Complete growth medium supplemented with 5% (v/v) DMSO	Produced in lab
10x Tris-Glycine Western running buffer	25 mM Tris, 192 mM Glycine, 0.1% w/w SDS, in ddH_2O	Produced in lab
10x Western transfer buffer	25 mM Tris, 192 mM Glycine, in ddH_2O. Diluted 1:2:7, 10x transfer buffer:methanol:ddH_2O	Produced in lab
Western washing buffer (PBST)	1x PBS supplemented with 0.1% v/v TWEEN20	Produced in lab
5x Kinase Assay Buffer	50 mM Tris (pH 7.2), 125 mM β-glycerophosphate, 250 mM KOH, 10 mM EGTA, 1.25 mM Na_3VO4, 50 mM $MgCl_2$ and 2 mM DTT, in ddH_2O	Produced in lab
DNA extraction solution 1	0.05 M NaOH	Produced in lab
DNA extraction solution 2	0.08 M Tris-HCl and 0.2 mM EDTA	Produced in lab
Nonidet P-40 Buffer	10 mM Tris HCl, 10 mM NaCl, 3 mM $MgCl_2$, 0.5% Nonidet P-40	Produced in lab
Urea lysis buffer	100 mM Tris (pH 7.4), 8 M Urea, 1 mM Na_3VO_4, 2.5 mM $Na_4P_2O_7$, and 1 mM β-glycerophosphate	Produced in lab
DTT reducing solution	19.25 mg/mL DTT in ultra-pure water	Produced in lab
IAM Alkylating solution	19 mg/mL iodoacetamide in ultra-pure water	Produced in lab
Alcian Blue stain	0.02% (w/v) Alcian blue 8GX (Sigma-Aldrich), 70% EtOH, 30% glacial acetic acid	Produced in lab
Alizarin Red stain	0.005% (w/v) Alizarin red (Sigma-Aldrich) in 0.5% KOH (w/v)	Produced in lab
Mowiol + DAPI	24 g analytical grade glycerol (Sigma #G-6279), 9.6 g Mowiol 4-88 (Fluka, #81381 (through Sigma)), 24 mL distilled water, 48 mL 0.2 M Tris buffer, pH 8.5, DAPI (ThermoScientific, 62248;1:1000)	Produced in lab

2.2 Bacterial cell culture

2.2.1 Bacterial strains

For the expression of recombinant DNA plasmids, XL1-Blue subcloning-grade competent cells (Agilent, 200130) were transformed with the desired constructs according to manufacturer's guidelines.

Genotype:

recA1 endA1 gyrA96 thi-1 hsdR17 supE44 relA1 lac [F´ proAB laclq ZΔM15 Tn10 (Tetr)]

2.2.2 Bacterial cell culture

Transformed cells were grown in Lysogeny broth (LB; 10 g NaCl, 10 g Tryptone, and 5 g of Yeast Extract in 1 L ddH_2O). The appropriate antibiotic was added prior to use. Bacterial growth performed in a 37˚C incubator whilst shaking (200 rpm) overnight (ON).

LB agar (28 g of CM3 Nutrient Agar (Culture Medium; Oxoid CM0003B) in 1 L of ddH_2O) enriched with the appropriate antibiotic was used to generate agar plates for the growth of transformed bacteria in order to select for colonies expressing only the target plasmid. Plates were incubated ON at 37˚C.

Ampicillin antibiotic stocks (100 mg/mL) were dissolved in autoclaved sterilised ddH_2O, aliquoted, and stored at -20˚C for long-term storage. Ampicillin stocks were diluted 1000-fold for final concentration: 100 µg/mL. Kanamycin antibiotic stocks (50 mg/mL) were dissolved in autoclaved sterilised ddH_2O, aliquoted, and stored at -20˚C for long-term storage. Kanamycin stock solutions were diluted 1000-fold for final concentration: 50 µg/mL)

Transformed bacterial colonies were preserved in glycerol stocks (1:1 v/v with sterile 50% glycerol) and stored at -80˚C.

2.2.3 Bacterial transformation

Bacterial transformation was conducted according to the protocol specified by the manufacturer (Agilent Technologies, 200130). 50 uL of competent cells were used per construct. Cells were incubated with β-mercaptoethanol on ice for 10 minutes, followed by a further incubation with 2 uL of ligated DNA or 0.5 uL of pUC18 control plasmid for 30 minutes on ice. Reactions were heat pulsed at 42°C for 45 seconds with an immediate incubation on ice for 2 minutes. 450 uL of preheated LB broth was added to each transformation reaction and incubated at 37°C for 1 hour whilst shaking at 225-250 rpm. Transformed cells spread onto an LB agar plate inoculated with appropriate antibiotic and incubated ON at 37°C.

2.2.4 DNA extraction from bacterial cultures

A 5 mL starter culture of LB broth containing selective antibiotic was inoculated with a single colony of transformed *E. coli* and incubated for 8 hours at 37°C whilst shaking at 250-300 rpm. The 5 mL of starter culture was added to 45 mL of LB broth and incubated at 37°C ON whilst shaking at 250-300 rpm. The 50 mL of overnight culture was then added to 700 mL of fresh warm LB Broth inoculated with antibiotic and left to shake ON at 37°C shaking at 200 rpm. The DNA was extracted using Nucleobond Midiprep extraction kit (Macherey-Nagel™; 740410) according to the manufacturer's instructions. The large overnight culture was pelleted by centrifugation at 8000 rpm for 30 minutes and the supernatant was discarded. The pellet was resuspended in resuspension solution and lysed by adding 10 mL of lysis solution followed by neutralisation after 5 minutes with neutralisation solution. The neutralised solution was centrifuged at max speed for 15 minutes and the supernatant added to a column prepared with equilibration solution. The column was washed once with wash solution prior to elution of the DNA. The DNA was precipitated and concentrated with isopropanol, centrifuged at max speed for 30 minutes, and washed with 70% ethanol. The pellet was left ON to air dry and resuspended in an appropriate volume of TE Buffer or sterile distilled water depending on the application.

2.2.5 DNA quantification

DNA was quantified using the NanoDrop (ThermoScientific; NanoDrop™ One/One^{C}; ND-ONEC-W) available from the University of York Technology Facility. A concentration of 1 ug/uL was determined as the minimum concentration threshold for electroporations.

2.3 Mammalian cell culture

2.3.1 Mammalian cell lines

The following cell lines were used in this work:

- C2C12 (ATCC; CRL-1772) – An immortalised mouse muscle myoblast cell line from the thigh muscle of the C3H mouse line (Yaffe and Saxel, 1977)
- Cos7 (ATCC; CRL-1651) – An immortalised fibroblast cell line from the kidney of the African green monkey (Gluzman, 1981)

2.3.2 Mammalian cell culture

Prior to use, all reagents were pre-heated to 37˚C in a sterile water bath. All cells were cultured in an incubator at 37˚C with exposure to 5% CO_2. All procedures performed in a laminar flow hood.

2.3.2.1 Proliferation

Aliquots of cell lines were thawed at 37˚C in water bath and immediately resuspended in Growth media (GM) (see Table 2.1 Buffers and Reagents). Cells were transferred to flasks GM and incubated at 37˚C and 5% CO_2. Cells were cultured using either T25 (using 4 mL of GM) or T75 (using 9 mL of GM) cell culture flasks until culture had reached 70-80% confluency. To subculture the cells, cells were first rinsed twice with 1x PBS and incubated with 0.05% trypsin-EDTA (Sigma, 59427C) at 37˚C until complete detachment. Trypsinisation was stopped by adding an equivalent volume of GM and a subpopulation of cells were transferred into new flasks or cell culture plates

containing pre-warmed GM. For applications requiring accurate measures of cell density, the population was quantified using a haemocytometer and then seeded at the necessary cell density.

2.3.2.2 Freezing

For long-term storage of cell lines, cell lines were trypsinised as described above followed by centrifugation at 1500 rpm for 10 minutes. The resultant pellet was resuspended in freezing media (FM) (see Table 2.1 Buffers and Reagents), aliquoted into cryotubes, and stored at -80˚C or liquid nitrogen.

2.3.2.3 C2C12 Differentiation

Cells were cultured in GM until they reached 100% confluency whereby the culture medium was changed from GM to differentiation media (DM) (see Table 2.1 Buffers and Reagents) to induce C2C12 myoblast differentiation, fusion, and myotube formation. DM was changed daily until the required time had been reached.

2.3.3 Mammalian transfection

Cells were seeded in either 6-well or 24-well plates in GM, 2 mL per well (6-well plate) or 0.5 mL per well (24-well plate). Transfections were performed according to manufacturer's guidelines when cells reached 80% confluency. TransIT-X2 (Mirus Bio; MIR 6000) transfection reagent was used in the transfection of both C2C12 and Cos7 cells. After 48 hours, cells were fixed, clonally selected, or processed for differentiation analyses. For fixation, transfected cells were washed twice with pre-warmed 1x PBS, and fixed with either 4% paraformaldehyde (PFA) for 10 minutes, or ice cold acetone:methanol (1:1) for 20 minutes. After fixation, cells were washed twice with 1x PBS and then with ddH_2O. Cells are then ready for immunostaining and microscopy. If further processing is delayed, cells can also be stored in 1x PBS at 4 °C for up to 2 weeks.

2.3.4 Immunofluorescence of cells

Fixed cells were permeabilised by incubation with 4% Bovine serum albumin (BSA) in 1x PBS supplemented with 0.1% triton-X100 for 30 minutes. This was followed with blocking using 4% BSA in 1x PBS for 1 hour and overnight (ON) incubation with primary antibodies at an appropriate concentration at 4˚C. Cells were incubated with appropriate secondary antibodies for 2 hours following 3x PBS washes. Cells were further washed 3x with 1x PBS, followed by a final wash with ddH_2O. Cells cultured on coverslips were mounted onto slides with Mowiol+DAPI. For cells cultured directly onto plastic, the bottom of the plastic dish was removed by cutting it using specialised laser equipment in order to isolate the bottom of the well and mounted with a coverslip using Mowiol+DAPI (see Table 2.1 Buffers and Reagents).

For the labelling of actin, fixed and permeabilised cells were washed twice in 1x PBS before phalloidin (either: Phalloidin CruzFluor 488 Conjugate, Santa Cruz, sc-363791. Or: Rhodamine Phalloidin, Cytoskeleton, PHDR1) was added, and the cells incubated for 30 minutes in the dark. Cells were then washed, and slides/coverslips mounted with Mowiol+DAPI as above.

2.3.5 Immunofluorescence of sections

Snap-frozen muscle tissue was first sectioned using a cryostat machine to a thickness of 10 µm, and slides were stored at -80°C. Slides were removed from -80°C and left to thaw at RT until condensation had evaporated. Blocking was performed in 4% BSA in 1x PBS. Sections were incubated with the following primary antibodies ON at 4°C; 1:100 anti-MyHC1 (A4.840, DSHB), 1:100 anti-MyHC2a (SC-71, DSHB) 1:150 anti-FLNC (RR90, gift from Peter Van der Ven), 1:150 anti-BAG3 (10599-1-AP, Proteintech), and 1:80 anti-MYOT (RS034, Novocastra) in blocking solution. Sections were subject to 3x 5 min washes in 1x PBS and incubated with the following secondary antibodies at RT for 1 h; 1:150 goat anti-mouse IgG-FITC (F9006, Sigma), 1:150 goat anti-mouse IgM-TRITC (SAB3701196, Sigma), 1:150 goat anti-mouse IgA-FITC (F9006, Sigma), goat anti-rabbit IgG-alexafluor594 (R37117, Invitrogen), and goat anti-mouse IgG-alexafluor594 (R37121, Invitrogen). Sections were again subject to 3x 5 min washes in 1x PBS. Slides were mounted with Mowiol mounting medium with DAPI. A coverslip was added and compressed avoiding the formation of air bubbles.

2.3.6 Scratch wound assay

Cells were grown to 100% confluency in a 6-well plate. A 200 µL pipette tip was used to scrape a single vertical line through the cells from the growth surface (0 hr). Cells were imaged every 3 hours for a total of 24 hours using an Evos XL core microscope (Thermofisher, AMEX1000). For quantification of wound closure, three replicates per cell line, per time point, were taken and averaged. An average distance travelled wound closure was then calculated compared to the initial wound distance at 0 hr.

2.4 CRISPR/Cas9 targeting in C2C12 cell line

2.4.1 Constructs

Pre-designed vectors were purchased from VectorBuilder. ZAKβ CRISPR/Cas9 KO plasmid (Vectorbuilder, VB191031-4552uqf) was obtained for CRISPR/Cas9 targeting (Figure 2.1). Specific target sites within exons 2 and 3 of ZAKβ were identified and targeted using 2 gRNAs:

- $gRNA_1$ = 5'-GGAGTGTGTATCGAGCCAAA-3'
- $gRNA_2$ = 5'-CCAACTATGGCATCGTCAC-3'

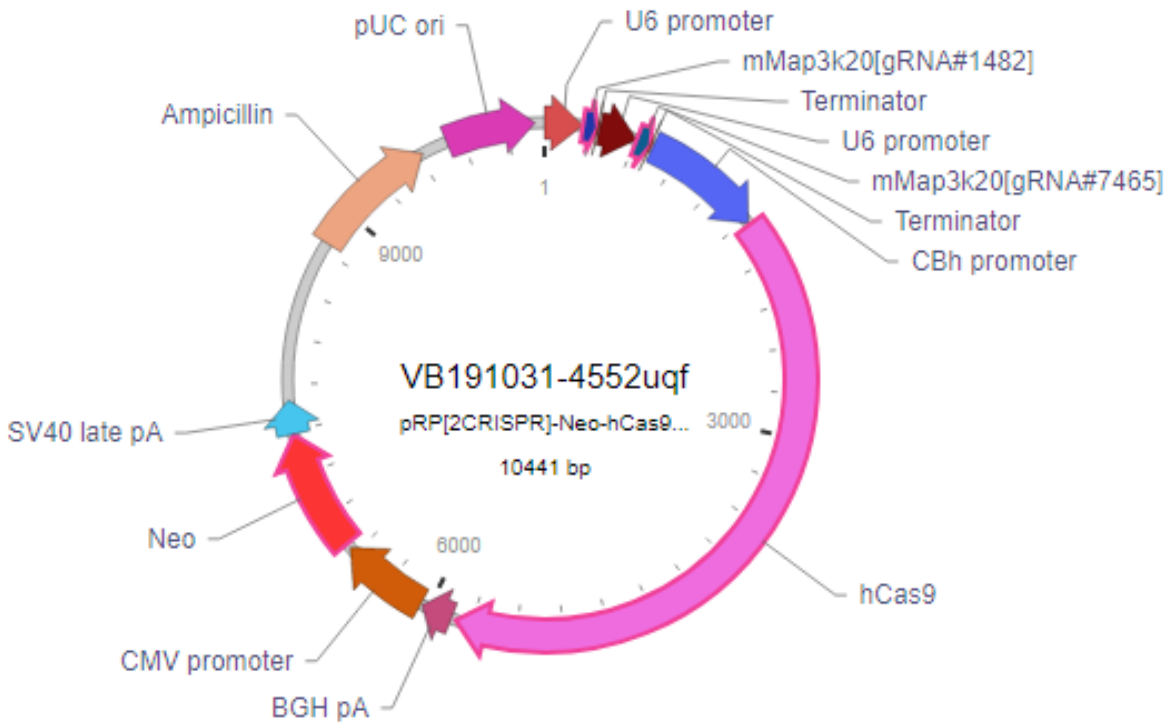

Figure 2.1: Vector map of ZAKβ CRISPR/Cas9 KO Plasmid: ZAKβ CRISPR/Cas9 KO Plasmid (VB191031-4552uqf) with 2 gRNA sequences targeting exons 2 and 3. (1) gRNA1 = GGAGTGTGTATCGAGCCAAA
(2) $gRNA_2$ = CCAACTATGGCATCGTCAC

2.4.2 Confirmation of vector identity by purification and linearisation

With the help of a Stage 3 project student, Andrew Galloway, a glycerol of *E. coli* containing the ZAKβ CRISPR/Cas9 KO Plasmid (VB191031-4552uqf) (Figure 2.1) was cultured on LB agar (as previously described) containing ampicillin for bacterial selection. Vector DNA was extracted via miniprep, purified, and quantified. Restriction digests were used to confirm the vector identity (*NcoI*, New England BioLabs, R0193) and then to linearise the vector for ease of transfection (SacII, New England BioLabs, R0157) (Figure 2.2A). Restriction digest cocktails were made as per manufacturer's instruction before being left overnight, at 37°C. The restriction cocktails were run on 0.7% agarose gel alongside with the undigested vector (Fig 2.2B) and compared with predicted restriction enzyme digests created using Serial cloner 108 (v 2.6.1).

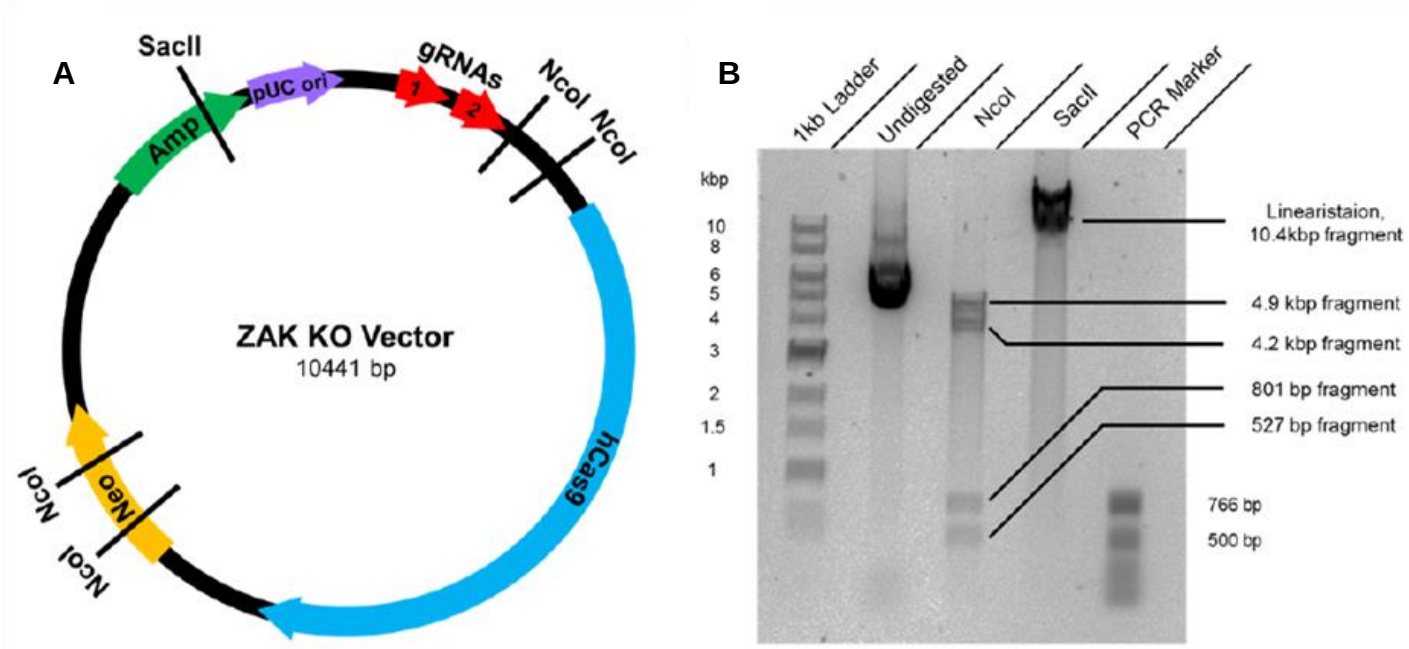

Figure 2.2: Restriction digest of ZAKβ CRISPR/Cas9 KO vector (VB191031-4552uqf). (A) Schematic of the ZAKβ CRISPR/Cas9 KO vector (VB191031-4552uqf) mapped with restriction sites of the 2 restriction enzymes NcoI and SacII. (B) Agarose gel electrophoresis of undigested vector (Lane 2), NcoI-digested vector (Lane 3) and SacII-digested vector (Lane 4).

2.4.3 Transfection and clonal selection

SacII-linearised ZAKβ CRISPR/Cas9 KO vector (VB191031-4552uqf) was transfected into wild type (WT) C2C12 cells using TransIT-X2 system as described above. After 48 hrs the GM was replaced with GM + neomycin (1.5 mg/mL). Transfected cells were then maintained at 37°C in a humidified 5% CO_2 incubator. Media was changed every two days until the formation of resistant colonies. Resistant colonies were re-seeded in a 96-well plate via serial dilution (Figure 2.3), to identify individual clones. Cells were observed and wells in which single colonies formed were selected for expansion, differentiation, and analysis.

2.4.4 Sequencing of clones

Cultures of WT, ZAK-KO-C10 (KOC10) and ZAK-KO-D9 (KOD9) were grown in T25 flasks as described above. Genomic DNA was extracted using Qiagen DNAeasy extraction kit for tissue according to the manufacturer's instructions. PCR using genomic DNA was performed using the following primers:

- Exon 2 Forward: 5’-GATTCGGCATTTCTTCTCTTTCC-3’
- Exon 2 Reverse: 5’-AGTTCGACGACTTGCAGTTT-3’
- Exon 3 Forward: 5’-CTCAGTCACAGAAACATCATCC-3’
- Exon 3 Reverse: 5’-CAGTAGCACACAACAGAACC-3’

The amplicon was subject to TOPO-TA cloning using TOPO™ TA Cloning™ Kit for Sequencing (Invitrogen™, K461020). Following TA cloning, DNA was transformed into competent *E. coli* and cultured. DNA was extracted from successful colonies, purified, and sent for sequencing using the forward primers above using GATC sequencing (Eurofins).

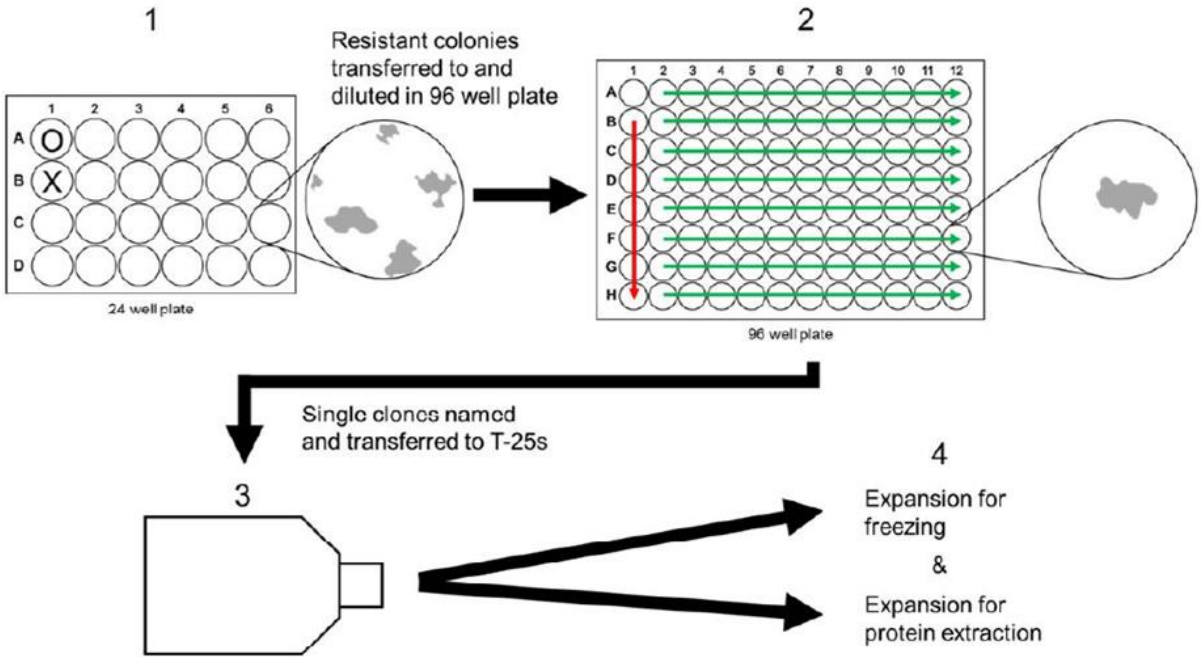

Figure 2.3: Schematic representation of serial dilution of resistant C2C12 colonies to obtain single ZAK-KO C2C12 colonies. (1) A 24-well plate of wild type C2C12 cells was transfected with ZAKβ CRISPR/Cas9 KO vector (VB191031-4552uqf). O = Untransfected control to evaluate effect of neomycin treatment. X = Transfected control not treated with antibiotic. (2) Resistant colonies were subject to serial dilution using a 96-well plate. Cells were introduced into well A1, diluted 1:1 vertically (Red arrow), and then again 1:1 horizontally (Green arrows). (3) Single colonies were removed and re-seeded into T25 flasks and expanded for freezing, protein extraction and for evaluation of differentiation and fusion capabilities (4). Adapted from Stage 3 Research Project Report.

2.5 Protein Analysis

2.5.1 Protein extraction from C2C12 cells

Cells placed on ice and washed twice in ice-cold 1x PBS. A sufficient volume of RIPA buffer (Sigma, R0278) + Protease inhibitor cocktail (PI) (Sigma; P8340) was added in order to aspirate the cells in an aqueous solution. The surface of the cell culture flask was scraped until all cells were detached from the surface. Cell solution was subjected to 5x 5 s pulses of sonication with a 1 minute rest on ice between each pulse. Cell lysate was centrifuged at 15,000 x g for 15 minutes at 4˚C. The supernatant was collected, aliquoted, and stored at -80˚C.

2.5.2 Protein extraction from mouse tissue

Tissues snap-frozen in liquid nitrogen-cooled isopentane were powderised using a mortar and pestle. Powder was placed into an Eppendorf and suspended in an adequate volume of RIPA buffer/PI solution. Tissue solution subjected to 10x 5s pulses of sonication, with a 1 minute rest on ice in-between, and centrifuged at 15,000 x g for 20 minutes at 4˚C. The supernatant was collected, aliquoted, and stored at -80˚C.

2.5.3 SDS-PAGE

Samples were prepared for SDS-PAGE by combining with 4x NuPAGE LDS buffer (Invitrogen; NP0008), 10x NuPAGE Reducing Agent (Invitrogen; NP004), and ddH_2O (optional depending on loading volume). Samples denatured by heating at 75˚C for 10 minutes prior to loading onto an 8 or 10% Polyacrylamide gel, depending on the size of the protein of interest. Between 10 and 20 µL was loaded per well. Gel running buffer was supplemented with NuPage antioxidant (NP0005) prior to sample loading.

Gels were typically run at 160V using a Mini-PROTEAN Tetra Cell System (Biorad) until the protein ladder had sufficiently separated (Protein Ladder Pageruler Prestained; Thermo Scientific; S26616).

2.5.4 Transfer and Western blotting

Transfer was performed using the wet transfer method (Mini Trans-blot cell; Biorad) onto a nitrocellulose membrane, 1 h at 100V. Ponceau S (Sigma, P7170-1L) staining was used to confirm complete protein transfer by incubation with transferred nitrocellulose membrane at RT for 20 minutes and washed by ddH_2O before being imaged. Remaining Ponceau S staining was removed by ddH_2O prior to blocking in western blocking buffer (see Table 2.1) for 1h at RT with constant shaking.

Membranes were incubated with primary antibodies diluted in blocking buffer ON at 4˚C with constant shaking. Unbound primary antibody was removed following 3x 10 minute washes in washing buffer. Membranes then incubated with HRP-conjugated secondary antibody for 1 h at RT. Unbound antibody removed following another 3x 10 minute washes in washing buffer.

The final membrane was incubated in Western Chemiluminescent HRP Substrate (Merck Millipore; 11556345) for 1 minute prior to visualisation. Exposure to X-ray film was used to detect luminescence resulting from the HRP reaction, which was developed using a Xograph film developer.

2.6 LC-MS/MS of muscle tissue

2.6.1 Sample Preparation

Tibialis anterior muscle from wild type C57Bl/6 mice was collected and snap-frozen in liquid nitrogen-cooled isopentane. Protein was extracted using the protocol as stated above. Skeletal muscle lysate was kept on ice and used fresh for the remainder of processing.

2.6.2 FSBA treatment and kinase assay

Skeletal muscle tissue lysed in RIPA buffer (as previously described) and treated with 5 mM 5’-4-fluorosulphonylbenzoyladenosine (FSBA; Sigma, F9128) solubilised in DMSO and incubated at 30°C for 1 hour. The samples then desalted using either ThermoFisher Scientific Zeba™ Spin Desalting Columns with 7 kDa molecular weight cutoff or Millipore Amicon ultrafiltration columns with a 3 kDa molecular weight cutoff.

When using the ultrafiltration columns, samples were diluted 1:10 with Nonidet P-40 buffer (see Table 2.1 Buffers and Reagents) and protease inhibitors. Following desalting, samples diluted 1:5 with 5x kinase assay buffer (see Table 2.1 Buffers and Reagents) and 10 µCi [γ-32P]ATP (Perkin Elmer. NEG002H250UC). 5 µg of recombinant ZAKβ (Medical research council protein production unit (MRC PPU, DU 42048) was added and samples were assayed at 30°C for 3 hours.

For 1D SDS-PAGE analysis of skeletal muscle lysate treated with FSBA, [γ-32P] ATP and recombinant ZAKβ protein the above protocol was used to assay the in vitro kinase activity of the recombinant ZAKβ protein. These reactions were stopped using 4x NuPAGE LDS buffer and 10x NuPAGE Reducing Agent. Samples were electrophoresed using a 10% Polyacrylamide gel at 200V for 1 hour or until the dye had run off the gel. Protein loading assessed using SafeBlue (NBS Biologicals, NBS-SB1L). X-ray film (Insight Biotechnology, sc-201696) was placed over the gel encased in acetate, and exposed for 5 days before being developed.

2.6.3 LC-MS/MS preparation and running

Mass spectroscopy was performed by Adam Dowle at the University of York, Department of Biology Technology Facility.

Following the assay with ATP (Sigma, A26209) and recombinant ZAKβ protein, proteins were precipitated using 4x ice-cold acetone and left at -20°C overnight. Samples were then pelleted for 10 minutes at 15,000x g. Once the supernatant was removed, the pellet was left to air dry. The pellet was resuspended in urea lysis buffer using sonication. 0.0364x the sample volume of DTT reducing solution (see Table 2.1 Buffers and Reagents) was added to the samples and incubated at 55°C for 30 minutes. The samples were then cooled to 4°C for 10 minutes. 0.1x the sample volume of IAM Alkylating solution (see Table 2.1 Buffers and Reagents) was added and incubated in the dark at RT for 15 minutes. Samples were then diluted 4x with 50 mM ammonium bicarbonate and 1:50 (protease:protein m:m) protease (Trypsin and Lys-C mix). Samples were incubated ON at 37°C.

For peptide desalting, ON samples were acidified in 0.1% TFA. C18-E cartridges (Phonomenex) were loaded with 100% acetonitrile. The cartridge was then

conditioned with 2 mL of 80% acetonitrile/0.1% TFA. Equilibration of the cartridge was performed using 2 mL of 0.1% TFA. Samples were loaded onto the cartridge using moderate pressure and flow rate. Column was washed with 2x 0.25 mL of 0.1% TFA. Phosphopeptides were eluted with 2x 0.2 mL of 80% acetonitrile/0.1% TFA and collected into an Eppendorf tube. Samples were subsequently dried using SpeedVac using moderate heat.

LC-MS/MS was performed over a 60 minute acquisition with elution from a 50 cm EasyNano PepMap column onto a Fusion Orbitrap Fusion Tribrid mass spectrometer using a Waters mClass nanoUPLC. LC-MS chromatograms were imported into PEAKSX-Studio for peak picking and peptide identification. Data were searched against the mouse subset of the UniProt database with the following criteria specified: Enzyme, trypsin; Max missed cleavages, 2; Fixed modifications, Carbamidomethyl (C); Variable modifications, Oxidation (M), Deamidated (NQ), Gln->pyro-Glu (N-term Q), Glu->pyro-Glu (N-term E), Acetyl (Protein N-term) Peptide tolerance, 3 ppm (# 13C = 1); MS/MS tolerance, 0.5 Da; Instrument, ESI-TRAP. These data are filtered to 1% false discovery rate (FDR) for identification. Complete mass spectrometry data sets and proteomic identifications are available to download from MassIVE (MSV000090935), [doi:10.25345/C5TB0Z08V] and ProteomeXchange (PXD037832). Phosphopeptides from 5 samples were analysed with 5 biological replicates. Samples comprised of ZAKβ recombinant protein-treated contrasted with untreated negative control. Samples were compared qualitatively using the following criteria. Acceptance of sample group protein identifications as significant to the control group protein identification probability of greater than 95% in at least three of five biological replicates.

2.6.4 Analysis of direct results

The full complement of phosphopeptides identified in the FSBA phosphoproteomics screen were a combination of significant phosphopeptides with high probability of confidence being present in all 5 biological replicates, and phosphopeptides identified in fewer than 5 replicates with reduced confidence. The complete data was processed in R (v4.0.3), using an adapted version of a phosphoproteomics script, originally provided by Dr Gareth J O Evans, to produce a list of significant phosphopeptides.

Generation of the list of significant phosphopeptides was necessary to identify the potential targets of ZAKβ for further processing.

2.6.5 Extrapolation of results and further analysis

The list of direct phosphopeptides was loaded into the PSSMSearch website (http://slim.icr.ac.uk/pssmsearch/) to generate a position-specific scoring matrix (PSSM) as well as a consensus sequence using the default settings. The PSSM was then cross-referenced against the entire mouse proteome of Mus musculus within the PSSMSearch website. The list of predicted substrates of ZAKβ, and targets found during the FSBA experiment were combined into one list, where duplicate gene entries were removed. The resultant list was cross referenced against a mouse skeletal muscle proteome (Krystkowiak, Manguy and Davey, 2018) for gene ontology (GO) and KEGG analyses using GProfiler.

2.6.6 RNA sequence data analysis

RNA sequencing data was provided by Simon Bekker-Jensen's lab in Denmark. Muscles were snap-frozen in liquid nitrogen and homogenized twice for 2 min at 30 Hz using Tissuelyser II (Qiagen). Total RNA was isolated using the TRIzol reagent. Total RNA was sent to BGI Europe for RNA sequencing. Here, a polyA-selected mRNA library was prepared from the total RNA and subjected to PE100 sequencing with 20 M pair reads using the DNBSEQ platform. Low-quality reads were filtered with SOAPnuke 1.5.2 and the remaining reads were mapped to version GCF_000001635.26_GRCm38.p6 of the Mus musculus genome. After alignment using Bowtie2 2.2.5, the expression level of each gene was calculated by RSEM 1.2.12, and differential expression analysis was performed using DESeq2 1.4.5 with the parameters fold change ≥2 and adjusted P value ≤ 0.001. KEGG analyses were then performed on the differentially expressed genes (DEGs) identified in tibialis anterior (TA) and soleus muscle, of WT control and $ZAK^{-/-}$. Fastq RNA sequencing files were deposited in the NCBI BioProject database under accession code: PRJNA816072 (https://www.ncbi.nlm.nih.gov/bioproject/ ?term=PRJNA81607

2.7 *In vivo* analysis

2.7.1 *In vivo* Electroporation

Mice were injected with 10 µL of 0.4 U/µL hyaluronidase in sterile saline (0.9% solution) intramuscularly into the tibialis anterior one hour prior to the procedure. Pre-operative analgesia was simultaneously administered subcutaneously (50 µg/mL Bupravet, 2 µL/g of body weight). DNA constructs (20 µL of ~1 µg/µL) were loaded into sterile insulin syringes (BD Medical™ BD Micro-Fine Insulin Syringes). Mice were placed inside an anaesthetic chamber with 2.5% isoflurane in O_2 supplied using an appropriate anaesthetic machine. When tail and pedal reflexes were lost, mice were moved to a heated pad (37 °C) where they remained anaesthetised using a face mask, again tail and pedal pinches were performed to assess the depth of the anaesthesia. The surgical site was shaved and sterilised prior to the procedure. Surgery was performed to expose the tibialis anterior via anterior incision. Once exposed, the DNA was injected intramuscularly into the Tibialis Anterior followed by the placement of the electrodes. The electrodes delivered 20 pulses, each 20 ms in duration, at 1 Hz via a NEPA21 Electroporator (SONIDEL™ Ltd.). The incision was closed using tissue glue (Vetbond™) and inspected for quality of closure. Following the procedure, mice were placed in a holding cage and observed during recovery for signs of pain. Once recovered from the anaesthetic, electroporated mice were returned to their home cage and placed back in their experimental room.

2.7.2 Sample preparation and fixation of electroporated muscle samples

Mice were sacrificed after 8 days following the electroporation procedure. The Tibialis Anterior muscle was dissected from the mouse and placed in pre-cooled 4% PFA for 15-20 minutes, followed by washing in 1x PBS. Fixed samples were viewed under a fluorescent microscope to determine whether the whole mount presented successful transfection. Samples were subsequently snap frozen in liquid nitrogen-cooled isopentane in preparation for cryostat sectioning and stored at -80 °C.

2.7.3 Haematoxylin and eosin staining (H&E)

Snap fresh frozen muscle tissue was first sectioned using a cryostat machine and slides were stored at -80 °C. Slides were removed from -80 °C and left to thaw at RT until condensation had evaporated. Slides were fixed in acetone for 10 seconds and then incubated in Gill's Hematoxylin for 2 minutes. Slide was then washed in tap water for 1 minute. Sections were incubated in Scott's water for 1 minute and subsequently washed again in tap water for 1 minute. Afterwards, the sections were incubated in eosin for 45 seconds and then washed in tap water for 1 minute. Sections were washed first in 70% ethanol for 1 minute, then in 100% ethanol for 1 minute, and finally in HistoClear (National Diagnostics) for an additional 1 minute. Slides were mounted with Histomount medium and a coverslip and compressed to prevent the formation of air bubbles.

2.7.4 Fibre typing

Snap-frozen muscle tissue was first sectioned using a cryostat machine, and slides were stored at -80°C. Slides were removed from -80°C and left to thaw at RT until condensation had evaporated. Blocking was performed in 4% Bovine Serum Albumin (BSA) in 1x PBS. Sections were incubated with the following primary antibodies ON at 4°C; 1:100 anti-MyHC1 (A4.840, DSHB) and 1:100 anti-MyHC2a (SC-71, DSHB) in blocking solution. Sections were subject to 3x 5 min washes in 1x PBS and incubated with the following secondary antibodies at RT for 1 h; 1:150 goat anti-mouse IgG-FITC (F9006, Sigma) and 1:150 goat anti-mouse IgM-TRITC (SAB3701196, Sigma). Sections were again subject to 3x 5 min washes in 1x PBS. Slides were mounted with Mowiol mounting medium with DAPI. A coverslip was added and compressed avoiding the formation of air bubbles.

2.7.5 $BaCl_2$ treatment

Barium chloride ($BaCl_2$) was selected as the method of injury as the levels of inflammatory cells return to basal levels quicker when compared to notexin or freezing injury models (Hardy *et al*., 2016). WT and $Zak^{-/-}$ mice (8 weeks) were anaesthetized with 2% isoflurane. To injure the leg, intramuscular (IM) injections of $BaCl_2$ (1.2% in

sterile saline, 30 µL) delivered to the tibialis under general anaesthesia. The tibialis muscle from the contralateral leg remained uninjured. 5 replicates were performed per condition. Injections were performed on control and Zak$^{-/-}$ mice. 3 uninjured mice used as non-injured controls. After the procedure mice were left for 4, 7, 12, and 28 days post injection (dpi) to recover. Mice were euthanized by cervical dislocation and the injured tibialis was isolated and snap frozen in isopentane for sectioning. Cross sections of tibialis were obtained at proximal, central and distal levels along the long axis of the muscles, H&E stained and imaged as described

2.7.6 Rapamycin electroporation

Daily IP injections of rapamycin (2 mg/kg) dissolved in DMSO with 2% carboxymethylcellulose were administered over the course of 11 days. On day 4, mice were electroporated with ZAK constructs into the tibialis as previously described. On day 12, muscles mice were sacrificed and muscles snap frozen and sectioned for IF analysis.

2.7.7 Synergistic ablation

WT and *Zak*$^{-/-}$ mice (30 weeks) were anaesthetized with 2% isoflurane. To mechanically overload the soleus muscles, the distal third of the gastrocnemius muscle is removed from one leg, leaving the soleus muscle intact. The gastrocnemius muscle from the contralateral leg remains intact and acts as a control. After the procedure mice were left for 2 weeks in individually housed cages. Immediately after the surgical procedure and 6, 12, 18 and 24 hours after the surgery, each mouse is injected with analgesics (buprenorphine - Temgesic, 0.05–0.1 mg / kg). In addition, the mice are injected with Carprofen immediately after surgery (when still anesthetized) and 24 hours after surgery. After 14 days, the mice were euthanized by cervical dislocation and the soleus (sham and overloaded) muscles were isolated and embedded in OCT compound and frozen in liquid nitrogen-cooled isopentane and then stored at -80°C for further analysis.

2.8 Skeletal preparation of whole organism

$ZAK^{-/-}$ and WT mice were sacrificed at 24 and 28 weeks old respectively and fixed in 10% neutral buffered formalin (Sigma-Aldrich, HT501128) for 48 hours. Samples were rinsed with ddH_2O and left for 24 hours with gentle shaking. Both samples were post-fixed in 70% ethanol for 5 days, with the ethanol solution refreshed daily. Following post-fixing, specimens were dissected. This process involved removal of the skin, eyes, visceral organs and adipose tissue between the scapulas and behind the neck. Specimens were placed in two changes of 95% ethanol ON at RT to dehydrate and further fix the remaining tissue. The ethanol solution was replaced with 100% acetone for a further 2 days to fix the specimens and remove excess adipose tissue. Specimens were stained with Alcian blue stain solution (see Table 2.1 Buffers and Reagents) for 4 days. Samples were washed with ethanol/glacial acetic acid (7:3) for 1 hour and fixed in 100% ethanol ON at RT. Specimens were rinsed in ddH_2O for 3 days before being incubated with 1% trypsin (in ddH2O containing 30% sodium borate) for 24 hours. Digested specimens were subjected to staining with Alizarin red stain (see Table 2.1 Buffers and Reagents) for 48 hours. Specimens were transferred to 1% KOH clearing solution for 2 days followed by decreasing gradients of 1% KOH to Glycerol to further clear the specimens, i.e 3:1, 1:1, 1:3, and 100% glycerol at 2 days per step. Specimens were stored in 100% glycerol prior to imaging.

2.9 Polymerase Chain Reaction (PCR)

2.9.1 DNA extraction from ear notches

Ear notch samples were taken by the animal facility that the mice were housed in. DNA extraction was performed using a HotSHOT protocol. Ear notch samples from control and $ZAK^{-/-}$ mice were incubated with 80 µL of DNA extraction solution (see Table 2.1 Buffers and Reagents) 1 for 1 h at 90˚C. The solution was then neutralised following the addition of 20 µL of DNA extraction solution 2 (see Table 2.1 Buffers and Reagents). The combined solution was vortexed for 1 minute prior to 10x 5s pulses of high-level sonication, cooling in ice between each pulse. For each 30 µL PCR reaction, 1 µL of lysate was used.

2.9.2 PCR

PCR reactions prepared using the following reagents:

- 15 uL 2x PCR Master Mix (Thermo Scientific, K0171)
- 1 uL 10 µM Forward Primer
- 1 uL 10 µM Reverse Primer
- 1-3 uL DNA
- Make up to 30 uL with PCR water (Thermo Scientific, R0581)

Reactions were performed using Geneamp 9700 Thermocycler (Applied Biosciences) according to the following program:

95˚C [10mins]

95˚C [30secs]
60˚C [30secs] } 37 cycles
72˚C [30secs]

72˚C [10mins]

6˚C [∞]

PCR products were mixed with 6x Gel loading dye (New England BioLabs; B7024) prior to loading onto a TBE gel containing 1.8% agarose and SYBRsafe (Invitrogen, S33102; 1:10,000), and subsequently run along with an appropriate DNA ladder (New England BioLabs; N3234) in TBE buffer for 40 minutes at 100V. Gels were visualised using a BioRad EZ GelDoc system.

Excess primers, nucleotides, and enzymes were removed from PCR amplicons using a PCR purification kit (Qiagen, 28106) as per manufacturer's instructions.

2.9.3 Agarose gel electrophoresis

Products were mixed with 6x DNA loading dye (New England Biolabs, B7024S) and loaded on an agarose gel (agarose percentage dependent on the size of the DNA for analysis) containing 1:10,000 v/v dilution of SYBRsafe. Electrophoresis was

performed using a BioRad power pack with a voltage of typically 100V, but dependent on the size of the DNA. Bands were then visualised using the EZ Gel Doc Imager (BioRad).

2.9.4 DNA sequencing

Sequencing of PCR products was performed using the GATC Biotech Light Run sequencing service according to their instructions regarding sample and primer concentrations and volumes.

2.9.5 Confirmation of *Zak* mutation in mice

The forward and reverse PCR primers were designed to flank the coding region of exon 2 within the ZAK genomic sequence (Figure 2.4A). A single base thymine deletion should be situated within this region, whereby introducing a premature stop codon. The PCR of the DNA obtained from control (WT) and ZAK$^{-/-}$ (KO) mice should amplify a region of 305 bp (WT mice) or a region of 304 bp (KO mice). Figure 2.4B demonstrates that the PCR reaction with WT and KO DNA was both successful and exhibits strong amplification.

Figure 2.4: Validation of the PCR primers designed to flank the single base deletion within exon 2 of *Zak*. (A) Representative image of where the forward and reverse primers (grey) were targeted. The start codon of exon is underlined. Red text indicated the intronic non-coding DNA sequence where the PCR primers were designed to bind. Black text signifies the entirety of exon 2. Highlighted in yellow with red text is the single base which is deleted in the ZAK$^{-/-}$ mutant. (B) PCR products of the forward and reverse primers listed here run on an agarose gel for gel electrophoresis. We demonstrate the successful amplification of the 305 bp amplicon (WT) and 304 bp amplicon (KO).

As a result of the positive validation of the forward and reverse primers, the PCR products were sent for sequencing using LightRun Sequencing services. The results of which are shown in Figure 2.5. The asterisk (*) replaces adenosine, which is complementary to the missing thymine on the leading strand.

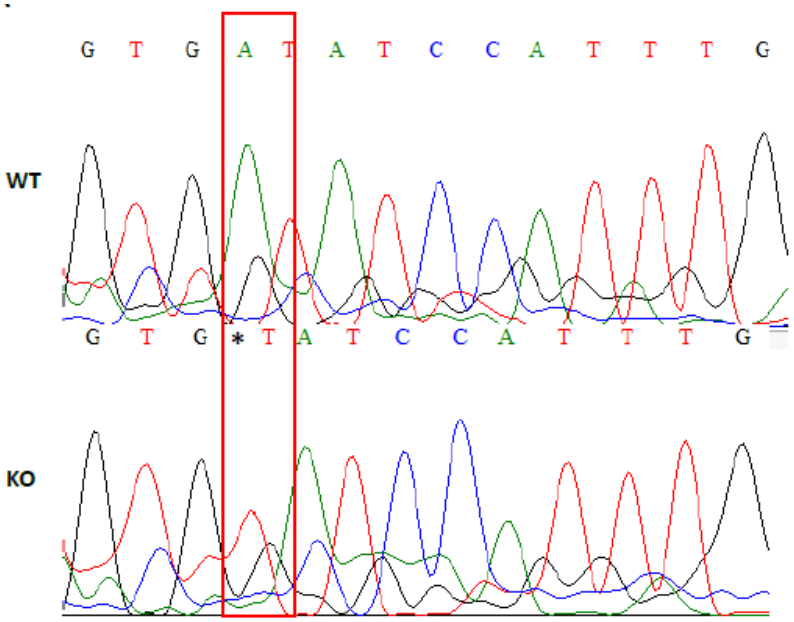

Figure 2.5: Validation of the single base deletion of ZAK-null mouse colony using DNA sequencing. DNA sequencing of the reverse complementary strand of the *Zak* genomic sequence. The red box highlights the position of the mutation across both WT and KO sequences. The asterisk (*) replaces the missing adenosine not present in the KO mutant.

2.10 Cloning of miniTurbo-ZAKβ-GFP

2.10.1 DNA Miniprep

Minipreps were performed using the QIAprep Spin Miniprep Kit (Qiagen, 27104) according to the manufacturer's instructions.

2.10.2 NEBuilder High-Fidelity DNA Assembly for miniTurbo-ZAKβ-GFP

ZAKβ was previously cloned into the pDEST47_tdtomato vector using the Gateway Cloning system (Xiang Li). The vector was linearised using a *NotI* single restriction digest. MiniTurbo was amplified from 3xHA-miniTurbo-NLS_pCDNA3 using primers that left complementary overhangs to the digest sites

- Forward 3xHA-miniTurbo-NLS_pCDNA3 primer: TACAAAAAAGCAGGCTCCGCGCCACCATGTACCCGTATG
- Reverse 3xHA-miniTurbo-NLS_pCDNA3 primer: TTCTTAAAGTTAAACAAGGCCTTTTCGGCAGACCGCAG

The PCR product and digested vector were then assembled using the NEBuilder High-Fidelity DNA Assembly Cloning system (New England Biolabs, E5520S) Assembly Master Mix according to manufacturer's instructions. The resulting vector was then transformed into One Shot chemically competent *E. coli*.

2.10.3 Validation of positive clones

Colonies were validated using both *NheI* and *SalI* restriction digestions described in Chapter 7. The fused vector was transfected into both Cos7 and C2C12 cell lines to test for transfection efficiency, fluorescence, and the ability to biotinylated as described above.

2.10.4 Assessment of biotinylation

After 24 hr post-transfection, GM was replaced with GM supplemented with 500 µM of biotin and left to incubate with the cells for 20 mins at 37 ℃. The reaction was stopped

by placing the cells on ice and cells were washed with 3x 1x PBS washes, followed by fixation with 4% PFA as previously described. Cells were permeabilised using 0.1% Triton-X100 in 1x PBS for 10 mins followed by blocking with 3% horse serum (HS) in 1x PBS at RT for 45 mins. Cells were washed once with 1x PBS and incubated with Streptavidin-FITC (Biolegend; 405201) conjugated antibody (1 µg/mL) in blocking solution containing 1% HS in 1x PBS for 1 hr in the dark. Cells were washed and mounted as described previously.

2.11 Mice

2.11.1 Mouse husbandry

All experiments were performed in accordance with The Animals (Scientific Procedures) Act 1986, the project licence (P3FF2D943) and valid personal licences (I6C1CA88C). All experimental procedures performed following approval of the University of York Ethics Committee. Mice were sacrificed using Schedule 1 killing methods stated in ASPA 1986, generally using a rising concentration of CO2, followed by cervical dislocation to confirm death. Mice were housed in IVC cages, with free access to food, water and exercise.

2.11.2 Generation of ZAK knockout mice

Generation of Cas9 mRNA and sgRNA was performed as previously described (Yang et al, 2014) by the Vivian Li lab at the Francis Crick Institute. In vitro transcription of Cas9 mRNA was done using the mMESSAGE Machine T7 Kit and MEGAclear kit following the manufacturer's instruction. sgRNA was transcribed using the MEGAshortscript T7 kit, as per the kit protocol. C57BL/6 X CBA(F1) female mice were used as embryo donors and foster mothers. Superovulated female mice (7–8 weeks old) were mated to males, and fertilised embryos were collected from oviducts. Cas9 mRNAs (10 ng from a 100 ng/µL stock) were injected into zygotes, and sgRNA (25 ng from 50 ng/µL stock) was injected into the cytoplasm of fertilized eggs with well-recognized pronuclei in M2 medium. Genotyping was performed by targeted gene sequencing in the Illumina Miseq System according to the manufacturer's instructions.

- Forward: 5′-tcgtcggcagcgtcagatgtgtataagagacagtttctgaactcatcgggcct-3′;
- Reverse: 5′-gtctcgtgggctcggagatgtgtataagagacagttgggaaggagcctcatgga-3′

FastQ reads were mapped to the Mus musculus genome version 9 (mm9). Several alleles were successfully germline transmitted. Animals harbouring Mutation 2 (M2) were maintained as $ZAK^{-/-}$ mouse strains. The $ZAK^{-/-}$ M2 mouse strain was imported into the York Animal Facility to be used in this project.

2.12 ZAK patient

The patient originated from France and sample collection was performed with written informed consent from the patient and participating family members, according to the Declaration of Helsinki.

2.13 Statistical analysis

2.13.1 Statistics

Statistical analysis of data was performed using SPSS (IBM). Data were tested for normality using the Shapiro-Wilk test. Unpaired two-tailed Student's t-tests were used for single comparisons and ANOVA for multiple comparisons with the Tukey HSD multiple comparison test for post-hoc identification of significantly different means.

2.13.2 Muscle Analysis

To measure the effect of loss of function of ZAK on soleus and TA muscle regeneration in vivo, 10x magnification images were captured using a Leica brightfield microscope. The number of fibres displaying centralised nuclei was expressed as a percentage of the total number myofibres to create one single data point per image. Comparison of percentage of centralised nuclei determined from full coverage of soleus (n=3) and TA muscles (n=6). An average of the percentage of fibres with centralised nuclei was calculated across three mice per condition. Soleus muscle fibre size determined from complete coverage of soleus muscle (n=3). TA fibre size determined from a minimum sample of 2000 fibres from sections taken at the same level (n=6). Data was compared

using either the Student's t-test, or one-way ANOVA test followed by a Bonferroni HSD post hoc test. P values less than 0.05 were deemed significant.

For fibre typing of soleus muscle sections, relative numbers of type I and type IIa fibres were determined manually by counting the total of fibres expressing each myosin isoform. The fibre cross-sectional area was calculated as an average of three individual muscles. To avoid regional fibre size variation in the TA muscle to confound comparisons, a scale factor (average area of electroporated: average area non-electroporated) was obtained from at least three electroporated regions within the muscle, which were then averaged to produce a single data point per muscle.

For morphological analyses of H&E stained sections, 10x magnification images were captured using the Leica brightfield microscope (DM2500), camera and imaging software (SPOT Insight FireWire; Diagnostic instruments). Centralised nuclei were counted manually. The number of fibres displaying centralised nuclei was expressed as a percentage of the total number of myofibres to create one single data point per muscle. An average of the percentage of fibres with centralised nuclei was calculated across three mice per genotype. Data were compared using a one-way ANOVA test followed by a Tukey's HSD post hoc test. P values less than 0.05 were deemed significant.

To measure the effect of loss of function of ZAK on TA muscle regeneration in vivo in response to $BaCl_2$-induced injury, 10x magnification images were captured using a Leica brightfield microscope from 28 days post-injury muscles. The fibres displaying centralised nuclei were used as a proxy for injured muscle fibres undergoing regeneration (54). 28 dpi TA fibre size was determined from a measurement of all centro-nucleated fibres (minimum of 750 fibres per section) from sections taken at the same level (n=4). Data was compared using the Student's t-test. A p value less than 0.05 was deemed significant.

2.13.3 ImageJ processing

Immunofluorescence images were imported into ImageJ for image adjustment. Brightness and contrast levels were used to optimise the image for downstream processing.

2.13.4 Quantification of fusion index

Cell lines C2C12 (parental control) KOC10 and KOD9 (deleted for ZAKβ) cells were grown to confluency and differentiated. Fusion index was calculated as a percentage of α-actinin +'ve structures with 3+ nuclei divided by the total number of α-actinin +'ve structures per field (Li *et al.*, 2017). A minimum of 3 fields were obtained for each replicate, a minimum of 3 replicates were tested per cell line.

2.13.5 Quantification of bands on Western blot

Band intensity of western blots was quantified using ImageJ. Fold changes to the control sample were calculated, and data were compared using the statistical test described in the figure legends.

2.14 Antibodies

Table 2.2 Primary Antibodies

Antibody	Supplier	Product code	WB concentration	IF concentration
Anti-GAPDH	Sigma	G9295	1:50000	N/A
Anti-COBL	Sigma	HPA019167	1:300	1:150
Anti-Myosin Heavy Chain Type I (slow)	DSHB	A4.840	N/A	1:100
Anti-Myosin Heavy Chain Type IIa (fast)	DSHB	SC-71	N/A	1:100
Anti-ZAK	Proteintech	14945-1-AP	1:1500	N/A
Anti-FLNC	Gift from Peter Van der Ven	RR90	N/A	1:150
Anti-BAG3	Proteintech	10599-1-AP	N/A	1:150
Anti-MYOT	Novocastra	RS034	N/A	1:80

Phalloidin CruzFluor 488 Conjugate	Santa Cruz	sc-363791	N/A	1:150
Rhodamine Phalloidin	Cytoskeleton	PHDR1	N/A	1:150
Streptavidin-FITC	Biolegend	405201	N/A	1 µg/mL
Anti-α-actinin	Abcam	EA-53	1:300	1:250

Table 2.3 Secondary Antibodies

Antibody	Supplier	Product code	WB concentration	IF concentration
AlexaFluor 488 anti-rabbit	Invitrogen	R37116	N/A	1 drop per ml
AlexaFluor 488 anti-mouse	Invitrogen	R37120	N/A	1 drop per ml
Goat anti-mouse IgG-FITC	Sigma	F9006	N/A	1:150
Goat anti-mouse IgM-TRITC	Sigma	SAB3701196	N/A	1:150
Goat anti-mouse IgA-FITC	Abcam	Ab97234	N/A	1:150
AlexaFluor 594 anti-rabbit IgG	Invitrogen	R37117	N/A	1 drop per ml
AlexaFluor 594 anti-mouse IgG	Invitrogen	R37121	N/A	1 drop per ml
Anti-mouse IgG-HRP	Santa Cruz	Sc-2314	1:10000	N/A
Anti-rabbit IgG-HRP	Abbkine	A21020	1:10000	N/A

CHAPTER 3

Results

CHARACTERISATION OF SKELETAL MUSCLE IN THE ZAK$^{-/-}$ MOUSE

3.1 Introduction

Recently, mutations in *ZAK* were identified in patients affected by a congenital myopathy. First described in 2017, autosomal recessive mutations in 3 consanguineous families in different ethnic backgrounds were identified and analysis revealed mutations included 2 homozygous frameshift mutations and one homozygous nonsense mutation (Vasli *et al.*, 2017). The presentation of the subsequent pathology resulted in skeletal muscle weakness and atrophy (Vasli et al., 2017). Further characterisation of these patients revealed a fibre-size variation, predominance of type I (slow) fibres, and the presence of centralised nuclei. Examination of heart function using ECG and ultrasound showed no cardiac abnormalities, suggesting skeletal muscle is the primary target tissue of the disease. Other patients with mutations in *ZAK* are affected by developmental limb defects (Spielmann et al., 2016). However, the mutations identified in these patients are gain-of-function mutations within the C-terminal SAM domain (Spielmann et al., 2016). Historically, the SAM domain is known to aid oligomerisation (Peterson et al., 1997) and protein-protein interactions (Ponting, 1995). The SAM domain is only present in the longer ZAKα isoform which is shown not to be expressed in skeletal muscle (Nordgaard et al., 2022). The loss of function mutations that result in a congenital myopathy are located within the N-terminal region of the protein, common to both isoforms and results in complete loss of both ZAKα and ZAKβ (Vasli et al., 2017).

A few $ZAK^{-/-}$ mouse lines have been generated in an attempt to understand the function of this protein. One group attempted to generate CRISPR/Cas-mediated knockout mice for both ZAK isoforms. This appeared to fail because of embryonic lethality due to severe cardiac oedema and growth retardation (Spielmann et al., 2016). This was an unexpected finding considering the identification of six patients with *ZAK* mutations presenting a myopathy phenotype (Vasli et al., 2017). In contrast to this, another group successfully generated a CRISPR/Cas-mediated knockout mouse for both *ZAK* isoforms which was not embryonically lethal (Nordgaard et al., 2022).

This chapter describes the experiments conducted to confirm and characterise the ZAK-deficiency in this ZAK$^{-/-}$ mouse line, in order to assess the suitability of this line to recapitulate the human pathology and therefore learn about the human condition.

3.2 Protein expression of ZAKβ in mouse tissue

Early publications describing the identification of the two *Zak* isoforms reported that the transcript length of each isoform does not correlate to that of the molecular weight of the protein. Due to the presence of a large 3'-untranslated region (3'-UTR) of about 5.6 kb, the RNA band for ***Zakβ*** (7.5 kb) is much larger than that of *Zak*α (3.8 kb) (Gross et al., 2002; Bloem et al., 2001). The RNA profile of each isoform appeared to be highly tissue specific. Levels of ***Zakβ*** RNA were highest in heart and skeletal muscle, with a predominance of *Zak*α in most other tissues sampled (Gross et al., 2002; Bloem et al., 2001). Based on what was established at transcriptional level, we wanted to establish the expression pattern of each isoform at protein level in different tissues.

Firstly, we looked at protein expression of both ZAK isoforms in skeletal muscle (Figure 3.1A). Immunostaining using a ZAK-specific polyclonal antibody (14945-1-AP, Proteintech) via pre-incubation to remove non-specific binding confirmed the loss of function mutation in the CRISPR/Cas-mediated ZAK-knockout mice (ZAK$^{-/-}$) and demonstrated the exclusivity of this isoform within skeletal muscle at protein level.

Secondly, we evaluated the expression of ZAK isoforms in different tissues (Figure 3.1B). The results demonstrated that the expression pattern of ZAK isoforms largely reflects the previous observations at transcript level. Striated muscle like skeletal and cardiac muscle primarily expresses ZAKβ, whereas other tissues and organs especially ones containing smooth muscle, appear to express either both, or primarily ZAKα (https://www.proteinatlas.org/ENSG00000091436-MAP3K20/tissue, Figure 3.1B). These data suggest ZAKβ must have an important tissue-specific role in striated muscle.

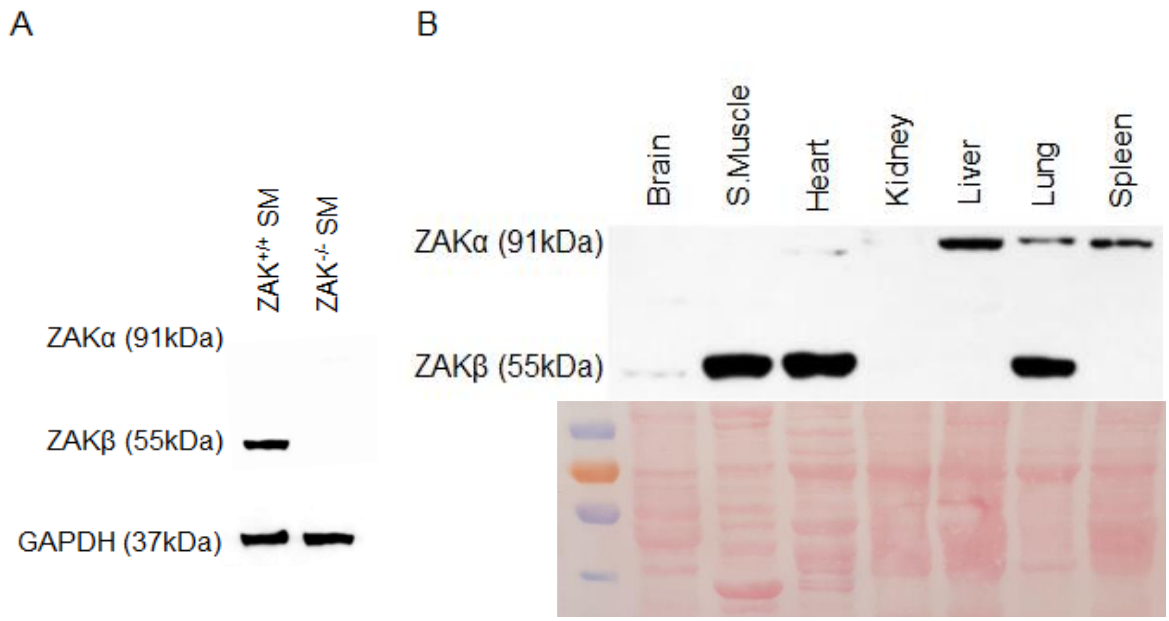

Figure 3.1: **ZAKβ is the only isoform expressed in skeletal muscle.** Analysis of the expression of ZAK isoforms using immunoblotting. (A) Expression of ZAK isoforms in skeletal muscle of control ($ZAK^{+/+}$) and ZAK KO ($ZAK^{-/-}$) mouse skeletal muscle. (B) Expression of ZAK isoforms in the indicated tissues of control mice (Top). Equal loading was estimated using ponceau red staining (Bottom) following inconclusive GAPDH staining.

3.3 The ZAK-null mouse does not exhibit a secondary spinal deformity

ZAKβ is a MAPKKK and novel skeletal muscle protein first identified as an interacting partner of the KY protein complex found at the z-disc (Baker et al., 2010). The z-disc itself is a very important structure within striated muscle, maintaining structural integrity during contraction and facilitating the transduction of signals critical to respond to mechanical demand and stress (Faulkner *et al.*, 2001; Pyle and Solaro, 2004; Constantin, 2014). The *ky/ky* mutant mouse exhibits a striking spinal deformity, which is secondary to myofibre degeneration within postural skeletal muscle (Blanco et al., 2001). This severe kyphoscoliosis results in an inability to carry out the placing reflex in mice. In humans, loss of *ZAKβ* has been implicated in a muscle myopathy, whereby human patients exhibit skeletal muscle weakness and fibre atrophy (Vasli et al., 2017). KY-deficient patients often required surgical correction of hypercontracted tendons in the lower limb. This is not the case for the milder myopathy affecting ZAK-deficient patients. Considering the interaction between ZAKβ and the KY protein complex, it is possible that the $ZAK^{-/-}$ mouse also presents a similar, but potentially milder, skeletal phenotype to that of the *ky/ky* mouse.

We wanted to characterise the ZAK$^{-/-}$ mouse to determine the extent of the effect of the loss of ZAK. A skeletal prep was performed on both a 22 week old control mouse and ZAK$^{-/-}$ mouse (Figure 3.2). Initial analysis revealed no obvious visual abnormalities between the two specimens (Figure 3.2; Panels 1,3). Further to this, looking specifically at the skeletal formation, again the ZAK$^{-/-}$ mouse does not appear to exhibit any spinal abnormalities compared with its WT counterpart (Figure 3.2; Panels 2,4). A physical abnormality, such as kyphoscoliosis observed in *ky/ky* mice, would be apparent in an aged mouse (Blanco et al., 2001). This suggests that the loss of ZAK results in a less severe phenotype to that of the *ky/ky* mouse, in accordance with data from human patients.

Figure 3.2: The ZAK$^{-/-}$ mouse exhibits no skeletal abnormalities. (Left 2 panels) The control (ZAK$^{+/+}$) mouse before and after skeletal preparation. (Right 2 panels) ZAK-knockout (ZAK$^{-/-}$) mouse before and after the skeletal prep. Alizarin red (red) depicts mineralised bone and Alcian blue (blue) illustrates cartilage. There is no visible evidence of any secondary spinal deformity associated with loss of skeletal muscle function in the 22 week female ZAK$^{-/-}$ mouse, i.e. kyphosis, lordosis or scoliosis. Skeletal prep performed on one biological replicate per genotype of which were non-littermates. No kyphosis detected on all mice used throughout the project of both young and old mice.

3.4 Pathological changes within ZAK$^{-/-}$ skeletal muscle

Although we saw no discernible phenotype at whole organism level, we do know that *ZAKβ* is highly expressed in skeletal muscle. Therefore, delving further into how skeletal muscle specifically is affected by the loss of ZAK, we explored the presence of damage and regeneration within the ZAK$^{-/-}$ soleus muscles in comparison with WT controls. Histochemical staining of soleus muscle cross-sections was performed to

ascertain the level of muscle regeneration in ZAK$^{-/-}$ mice, using centralised nuclei as a proxy (Figure 3.3A). Further staining against embryonic myosin to confirm newly regenerating myofibres was attempted, however was unsuccessful. H&E staining of soleus muscle cross-sections resulted in two interesting findings. The first was that at 8 weeks, muscles of ZAK$^{-/-}$ males and females exhibited significantly more centralised nuclei than their WT counterparts. Even at this early age, this suggests that the pathological slow-type soleus muscle of the ZAK$^{-/-}$ has higher levels of regeneration (Figure 3.3B). As the ZAK$^{-/-}$ mice aged, the percentage of centrally nucleated fibres also increased (Figure 3.3B). These data suggest that postural muscles, like the soleus, must be unable to withstand the pressures of mobility and maintenance of tension against gravity, thus initiating a cycle of fibre degradation and regeneration. The second interesting point is that at 22 weeks, not only did ZAK$^{-/-}$ muscles display significantly more centrally-nucleated fibres than at 8 weeks, but 22 week males had significantly more muscle fibre regeneration than 22 week females. These two results suggest that ZAK$^{-/-}$ females may be more resistant to the effect of the loss of ZAK. Nevertheless, despite there being significantly less fibre regeneration than their male counterparts, the muscle regeneration in both 22 week males and female ZAK$^{-/-}$ was significantly higher than that of the 22 week controls (Figure 3.3B). These data suggest that ZAK is important for muscle maintenance and function.

The distribution of myosin heavy chain (MHC) isoforms in skeletal muscle is characteristic of every muscle and defines its overall slow, fast or mixed properties. Muscle degradation and changes in innervation status often results in muscle weakness and fibre-type transformations (Weeds et al., 1974; Stréter et al., 1973). The expression of MHC isoforms in the ZAK$^{-/-}$ mutant were characterised by immunofluorescence in both control and ZAK$^{-/-}$ soleus muscle (Figure 3.4A). We observed a progressive shift of type IIa-to-type I fibres in older ZAK$^{-/-}$ soleus muscle (Figure 3.4B). Measurements of fibre proportions at 8 weeks of age showed no significant difference between genotypes (Figure 3.4B).

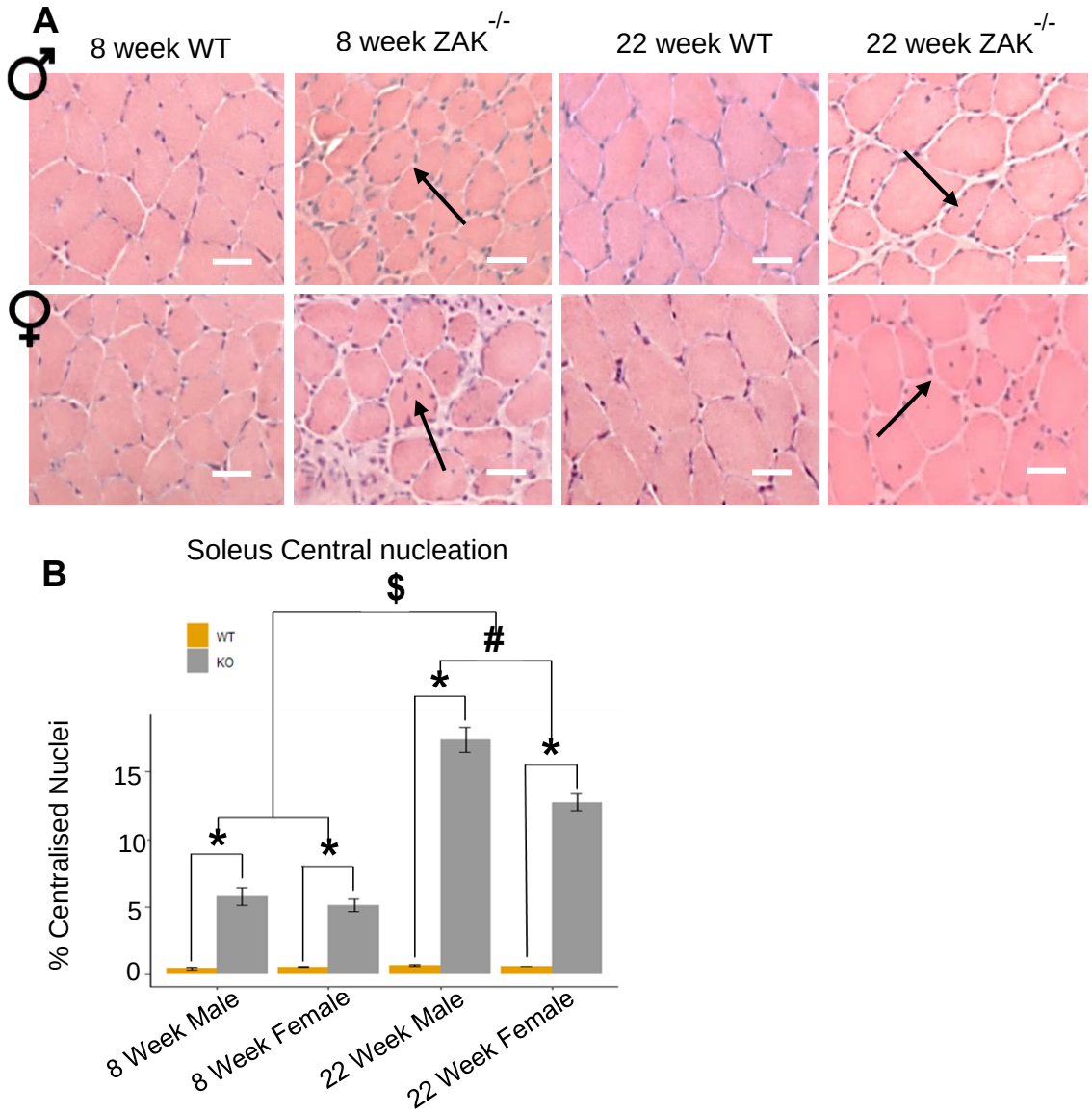

Figure 3.3: Loss of ZAKβ results in muscle regeneration in slow-twitch soleus muscle. Loss of function of ZAKβ results in increased muscle regeneration in aged mice with a significant gender bias. (A;a-h) H&E staining of 8/22 week soleus muscle sections from ZAK control ($ZAK^{+/+}$) and ZAK-knockout ($ZAK^{-/-}$) male/female mice (n=3). Centralised nuclei (purple; black arrows) used as a proxy for regenerating myofibres. (B) Increased levels of regeneration were detected in $ZAK^{-/-}$ mice at 8 and 22 weeks. Calculated as percentage of number of fibres with centralised nuclei / total number of fibres across entire soleus muscle. One-way ANOVA; * represents $p<0.001$ significance between genotypes, # represents $p<0.01$ significance between 22 week $ZAK^{-/-}$ males and females, and $ represents $p<0.01$ significance between 8 and 22 week $ZAK^{-/-}$ males and females.

A

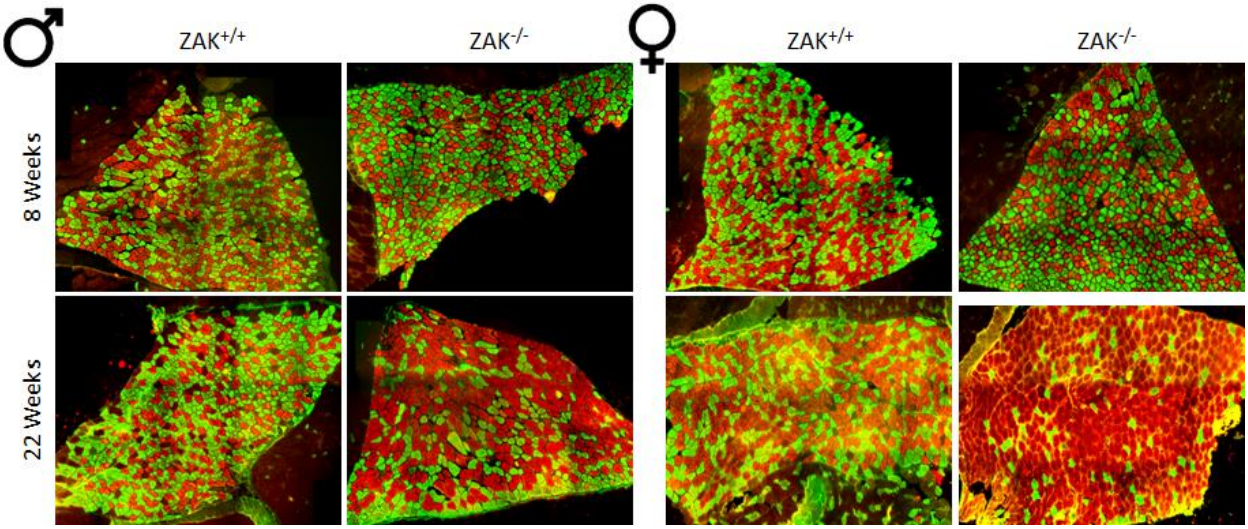

B

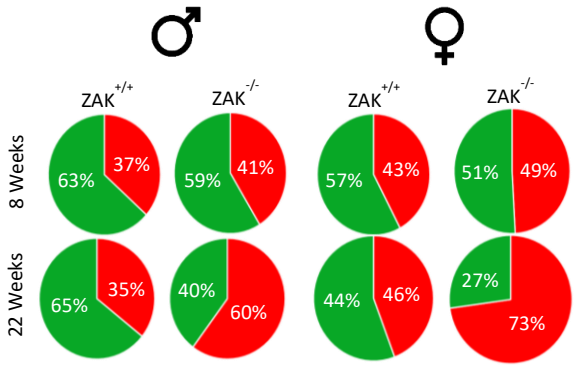

C

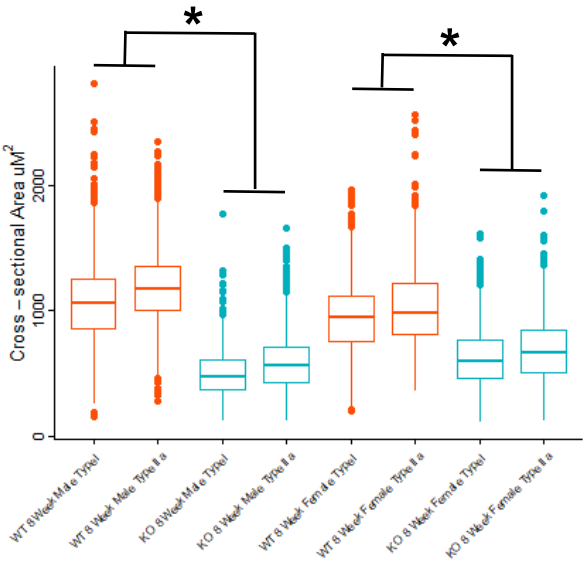

D

		WT				ZAK$^{-/-}$			
		8 wk male	8 wk female	22 wk male	22 wk female	8 wk male	8 wk female	22 wk male	22 wk female
WT	8 wk male		x	x	x	x	0.007	<0.001	<0.001
	8 wk female	x		x	x	x	x	<0.001	<0.001
	22 wk male	x	x		0.047	x	0.002	<0.001	<0.001
	22 wk female	x	x	0.047		x	x	<0.001	<0.001
ZAK$^{-/-}$	8 wk male	x	x	x	x		x	<0.001	<0.001
	8 wk female	0.007	x	0.002	x	x		0.012	<0.001
	22 wk male	<0.001	<0.001	<0.001	<0.001	<0.001	0.012		0.001
	22 wk female	<0.001	<0.001	<0.001	<0.001	<0.001	<0.001	0.001	

Figure 3.4: Loss of ZAKβ results in a fast-to-slow fibre type switch in slow-twitch soleus muscle. (A) Immunofluorescence of cross-section of mouse soleus muscle stained for type I (red, A4.849; DSHB) and type IIa (green, SC-71; DSHB) fibres using anti-myosin isoform specific antibodies in soleus muscle. Categories of age (8/22 week), sex and genotype ($ZAK^{+/+}$ and $ZAK^{-/-}$) are annotated. Sections measure 12 µm in thickness. (B) Pie charts depicting the relative counts type I (red) fibres in relation to type IIa (green) fibres in soleus muscle. 22 week $ZAK^{-/-}$ muscles show a predominance of type I fibres. (C) Cross-sectional area of type I and type IIa fibres in soleus from 8-week-old WT (Orange) and $ZAK^{-/-}$ (Blue) male and female mice. (* = $p<0.001$ in non-parametric Kruskal-Wallis test using Dunn's multiple comparison test). One-way ANOVA; ***represents $p<0.001$. Error bars = mean +/- Standard Error. (D) Statistic table describing the significant pairwise comparisons of the fibre typing analysis.

Interestingly, despite a lack of obvious secondary phenotype, the soleus muscle showed a progressive adaptation towards a slow fibre phenotype which appeared more apparent in females. This adaptation may be sufficient and necessary to compensate for the loss of ZAK. Fast to slow fibre type switching enhances metabolic activity and oxygen consumption in skeletal muscle which produces greater fatigue resistance (Herbison *et al.*, 1982; Boyer et al., 2019). Cross sectional analysis of soleus of soleus showed atrophy affecting both type I and IIa fibres (Figure 3.4C).

We isolated fast (Tibialis anterior; TA) and slow (soleus) twitch muscles from the lower hind limb of 3 mice. Immunohistochemical staining of soleus muscle sections revealed a severe and progressive increase in basal levels of regeneration (Figure 3.3B). In contrast to the changes in soleus described above, sections of TA muscle stained with H&E did not exhibit any significant difference in the levels of regeneration between control and $ZAK^{-/-}$, using centralised nuclei as proxy (Figure 3.5A&B). Fibre typing of the TA was attempted using anti-Myosin Heavy chain immunostaining specific for Type IIa and IIb, however this was not quantified due to unsuccessful Type IIb staining.

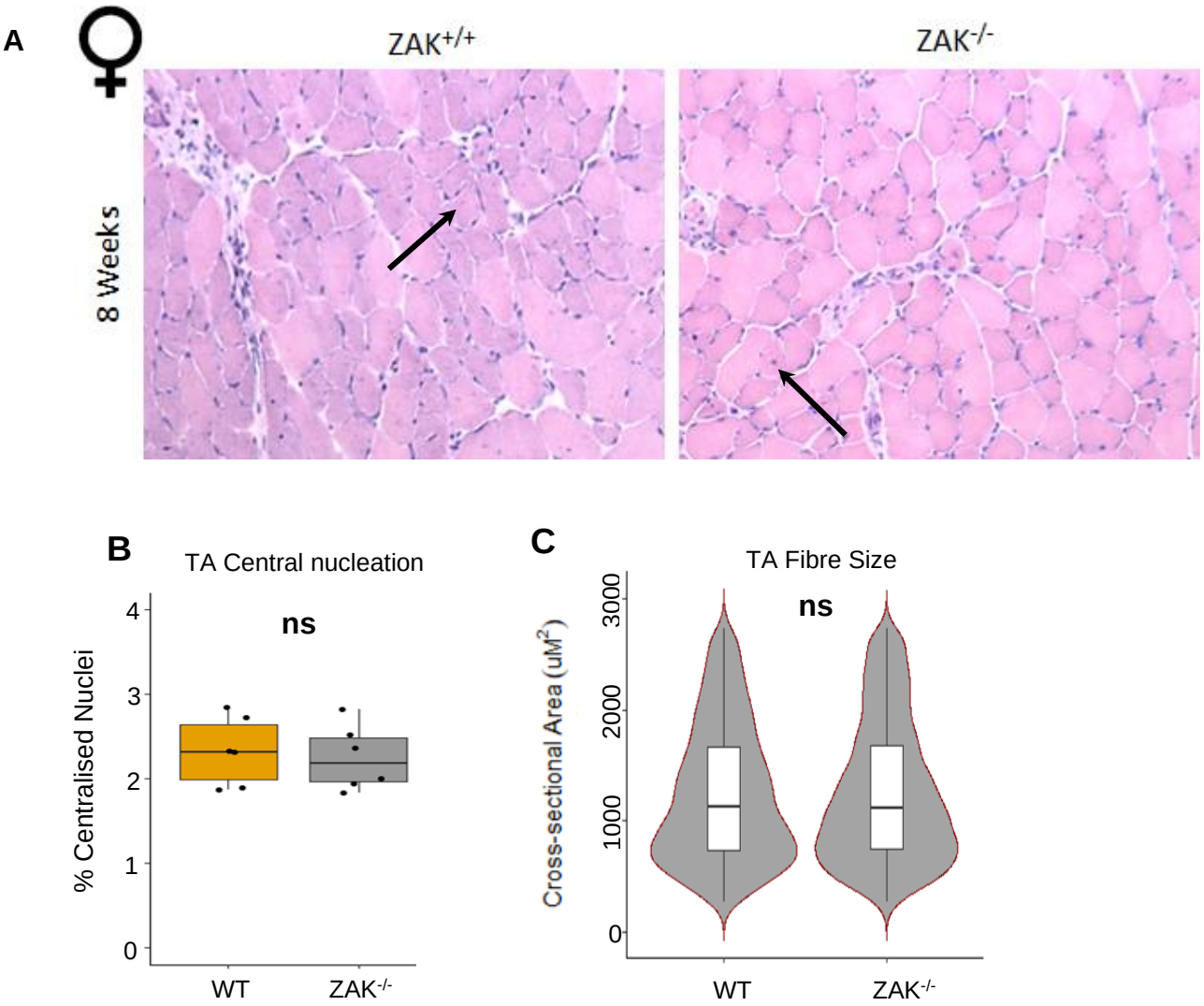

Figure 3.5: Pathological differences in tibialis anterior in the ZAK$^{-/-}$ mouse. (A) H&E staining of 8 week tibialis anterior muscle sections from control (Left; ZAK$^{+/+}$) and ZAK-KO (Right; ZAK$^{-/-}$) female mice. The presence of centralised nuclei (black arrows) was used as a proxy for regenerating myofibres. (B) No regeneration was detected in female ZAK$^{-/-}$ mouse TA muscle. Calculated as percentage of number of fibres with centralised nuclei / total number of fibres (n=6). Independent t-test; (ns = non-significant). (C) Cross-sectional area of tibialis anterior muscle fibres from 8-week-old WT and ZAK$^{-/-}$ female mice (ns = non-significant) (n=6) analysed using sampling of 5 images per muscle. Box and whiskers within violin plot representative of mean and interquartile range.

The progressive nature of this pathology, exhibited solely in soleus muscle of ZAK$^{-/-}$ mice and worsens with age, suggests that it is not a developmental disorder, but rather linked to muscle use and an innate insufficiency to cope with gravitational and mechanical demand. The TA muscle is responsible for the control of the ankle and

inversion of the foot (Maharaj *et al.*, 2019). As this phenotype is not observed in ZAK$^{-/-}$ TA muscle, it is possible that tonically active muscles are more susceptible to the loss of ZAK protein than phasic muscles.

Congenital myopathies cause a plethora of phenotypes, ranging from mild to extremely destructive. One such phenotype is skeletal muscle atrophy, the result of an imbalance between protein synthesis and degradation in favour of degradation. As a result, other phenotypes happen (scoliosis, regeneration, etc.). In many cases of myopathies, instability within the muscle itself results in an increase in damaged proteins in need of degradation, and thus the muscle atrophies. We looked at two different muscles, the TA and the soleus. Both are very different in terms of frequency of use. In order to evaluate muscle fibre size and quality, we measured the cross-sectional area (CSA) of both the TA and soleus muscles in control and ZAK$^{-/-}$ mice. We identified that the CSA of TA myofibres is no different in the ZAK$^{-/-}$ to that of the control (Figure 3.5C). Whereas the soleus exhibited a significant reduction in CSA between the ZAK$^{-/-}$ and the control consistently across fibres expressing both myosin heavy chain isoforms type I (slow) and type IIa (faster) (Figure 3.3C). These findings altogether suggest that the loss of ZAKβ primarily affects slow muscle. This appears not to be fibre-type specific, instead an intrinsic problem with the type of muscle.

3.5 Discussion

Skeletal muscles consist of a heterogeneous mixture of type I (oxidative, slow) and type IIa/b/x (glycolytic, fast) myofibers. The proportion of these myofibers vary from muscle to muscle depending on the nature, location, and function. For example, slow-twitch tonically-active muscle like the soleus comprises primarily of type I and IIa myofibres (Augusto, Padovani and Campos, 2004). Type I myofibers are mitochondria-rich and rely mostly on β-oxidation for energy production. Whereas, type IIa/b/x myofibers are more dependent on glycolytic pathways for energy production (Scott *et al.*, 2001). Prolonged increases of skeletal muscle activity, such as during endurance exercise, has long been known to lead to a variety of biochemical and biophysical adaptations, including fibre-type transformations (Andersen and Henriksson, 1977; Green et al., 1979). Interestingly, ZAK has also been found to be highly activated following maximal intensity muscle contractions (Potts et al., 2017).

However, this skeletal muscle plasticity is not limited to just healthy muscles. It has also been observed that muscles affected by muscle-specific disorders also exhibit fibre-type transformations (Vihola et al., 2003; Celegato et al., 2006; Webster et al., 1988). From these data presented here, we observe increased levels of regeneration (Figure 3.3A&B) and a progressive predominance of type I fibres (Figure 3.4A&B) in ZAK$^{-/-}$ mice. This is indicative of an adaptation to preserve muscle function whereby switching to a more oxidative phenotype attempts to preserve the integrity of the muscle fibre for longer (Boyer et al., 2019). Taken together, this suggests a role for ZAKβ in the maintenance of skeletal muscle and also in response to increased load and demand which is in keeping with its classification as a stress response kinase (Gross et al., 2002; Tosti et al., 2004).

According to the neuromuscular homepage, the human ZAK deficiency identified by Vasli *et al.* caused by nonsense-mediated mRNA decay, is classified as a centronuclear myopathy, a type of congenital myopathy with a predominance of type I fibres and centralised nuclei (Neuromuscular Home Page, http://neuromuscular.wustl.edu; Vasli *et al.,* 2017). Genetic ablation of the *Zak* gene in mice causes a subtle pathology in skeletal muscle, most pronounced in a slow muscle like soleus, and not so much in fast muscle like the tibialis anterior (Figure 3.5). However, unlike most other centronuclear myopathies, human patients did not exhibit a predominant facial weakness characteristic of that specific subtype of congenital myopathy (Vasli et al., 2017). Additionally, electron microscopy analysis of ZAK-deficient human muscle biopsies reveal central nuclei, tightly surrounded by myofibrils, but not by membranes and organelles characteristic of centronuclear myopathies (Neuromuscular Home Page, http://neuromuscular.wustl.edu; (Vasli et al., 2017). Still, there was a pathology observed in the skeletal formation of ZAK-deficient patients which was not observed in the mouse model. Across the six patients, clinicians observed spinal deformities ranging from mild-to-moderate scoliosis with additional hyperlordosis all of which not necessitating correctional surgery (Vasli et al., 2017). These organismal differences may reflect a higher abundance of intermediate skeletal muscle types throughout the human body, whereas mouse muscles are predominantly of the fast type in which we did not observe the same pathology.

Altogether, this information both validates the ZAK$^{-/-}$ mouse as a model of the ZAK loss of function in humans, and yet raises interesting questions regarding the clinical nature and classification of this myopathy.

CHAPTER 4

Results

ECTOPIC EXPRESSION OF ZAKβ CONSTRUCTS *IN VITRO* AND *IN VIVO*

4.1 Introduction

The KY protein is an important protein for the maintenance of tonically active postural skeletal muscle. Mutations within the *KY* gene underlie a skeletal muscle myopathy characterised by progressive weakness, atrophy, and contractile deficiencies (Maréchal et al., 1996, Blanco *et al.*, 2001; Straussberg *et al.*, 2016). The usual hypertrophic response to mechanical loading observed in wild-type (WT) mice is not detected in mice lacking functional KY protein, suggesting it is important for mechanosensation and adaptation to mechanical demands (Blanco *et al.*, 2001). It is suggested that the location of KY at the z-disc makes it an ideal candidate to perform such actions.

A yeast two-hybrid (Y2H) of KY further identified IGFN1 as an interacting protein (Beatham *et al.*, 2004). From this interaction assay and further characterisations, a z-disc based KY protein complex comprising KY, FLNC and IGFN1 was proposed (Baker *et al.*, 2010). IGFN1 domain composition is similar to other sarcomeric proteins such titin, filamin C or myosin binding protein C, essentially composed of a variable number of repetitive globular domains. In skeletal muscle, IGFN1 was detected at both the z-disc and the nucleus (Baker *et al.*, 2010). This data, together with what is known regarding KY function and localisation, places the KY protein complex in one of the most vital components of sarcomeric maintenance.

The function of IGFN1 is unknown. Using IGFN1 as bait, a Y2H revealed ZAKβ as an interacting partner (Baker *et al.*, 2010). The *Zak* gene encodes 2 distinct isoforms, *Zakα* and *Zakβ* (Gotoh, Adachi and Nishida, 2001). The two isoforms illustrated in figure 4.1 share homology at the N-terminus, which includes serine/threonine kinase domain between residues 16 and 227, and leucine zipper between residues 287 to 322. The C-termini differ after residue 331 and are thought to direct their distinct functions. ZAKα contains a sterile alpha motif (SAM) domain (residues 337-408), which is usually involved in protein-protein interactions (Ponting, 1995), although not necessary for ZAKα oligomerisation (Huang *et al.*, 2004). Mutations in the SAM domain of ZAKα produces split-foot and abnormal nail phenotypes in human patients (Spielmann *et al.*, 2016), and is therefore suggested to be important in limb development. ZAKα has been shown to mediate MAPK activation in the presence of ribotoxic stress through ribosome-binding sensor domains in its C-terminus (Vind *et*

al., 2020), including a “sensing domain” (residues 670-713) and a c-terminal domain (CTD; residues 774-800). When expressed in cardiomyoblasts, ZAKα has also been shown to increase actin fibre organisation and overall cell size, suggesting a role for ZAKα in cardiomyoblast hypertrophy through actin organisation (Huang *et al.*, 2004). The relationship between ZAKβ and the KY protein complex was an intriguing finding as ZAKβ transcripts were previously found to be up-regulated in the muscles of *ky/ky* mice (Blanco *et al.*, 2004). Moreover, ZAKβ is a stress-activated MAP3K thought to have a role in cardiac hypertrophy whereby transgenic overexpression of ZAKβ in mouse hearts results in an increase in cardiac weight to body weight ratio (Gross *et al.*, 2002; Christe *et al.*, 2004). On the other hand, the specific functions of the C-terminus of ZAKβ were unknown. Therefore, to gain insights into possible roles for ZAKβ, I first looked at protein localisation *in vitro* and *in vivo*.

.

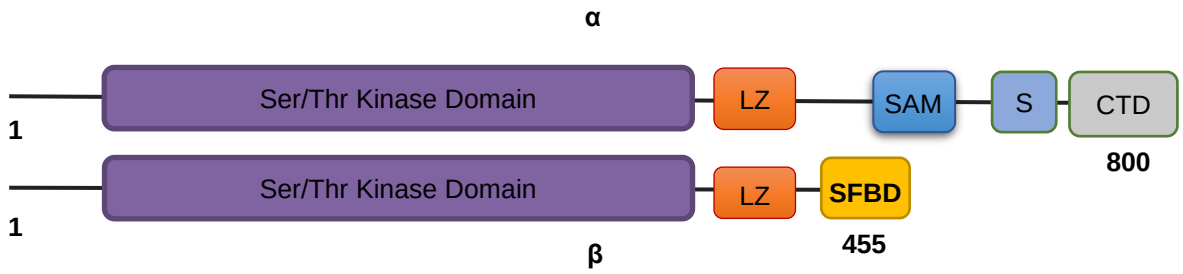

Figure 4.1: Domain composition of ZAK isoforms ZAKα and ZAKβ. Illustration of the domain composition of ZAK isoforms. Both ZAK isoforms are identical at the N-terminus, sharing both the serine/threonine kinase domain and leucine zipper domain. Different C-termini represented by a sterile alpha motif (SAM) domain followed by a sensor (S) and C-terminal domain (CTD) in ZAKα (Vind *et al.*, 2020), while the ZAKβ C-terminal region is thought to contain a stress fibre binding domain (SFBD) (Nordgaard et al., 2022)

4.2 Wild-type, kinase-dead, and constitutively active ZAKβ-tdTomato subcellular localisation in skeletal muscle

The association between ZAKβ, and the KY protein complex is one of a compelling relationship between a stress-activated MAP3K and proteins found located at the z-disc and critical to its integrity. To test whether ZAKβ itself would also localise to the z-disc in a similar fashion to KY or IGFN1, tdTomato-tagged ZAKβ was electroporated

into mouse Tibialis anterior (TA) muscle and left to express for eight days. Despite being expressed at high levels in skeletal muscle, endogenous ZAK was unable to be detected using the anti-ZAK antibody (X Li, University of York; pers comm). The results showed that ZAKβ colocalises with α-actinin at the z-disc. α-actinin is both a component of the z-disc and used a marker for z-disc striations (Figure 4.2). A caveat of this protocol is the incompatibility of the α-actinin primary antibody with the fixation procedure for electroporated skeletal muscle prepared for sectioning. Despite this, this result confirms the expression pattern of ZAKβ in skeletal muscle as one primarily at the z-disc presumably through its interaction with the z-disc partner IGFN1.

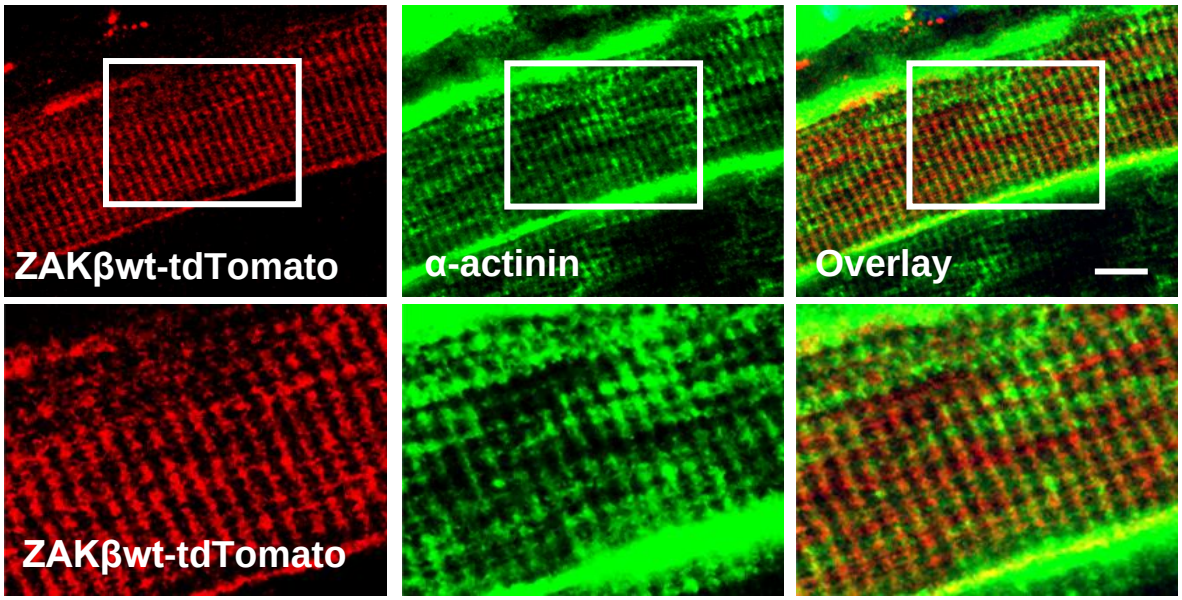

Figure 4.2: ZAKβ localises to z-discs in fully differentiated adult mouse skeletal muscle. Representative images of WT mouse Tibialis muscle electroporated with ZAKβwt-tdTomato counterstained for a-actinin exhibits a definitive striated pattern consistent with z-disc striations. Bottom 3 panels are magnified images of top 3 panels identified by white rectangles. Scale bar representative of 10μm (n=3).

To evaluate the effect of kinase domain activity on the subcellular localisation *in vivo*, DNA constructs encoding ZAKβdn-tdTomato (ZAKβ dominant negative; kinase dead) and ZAKβca-tdTomato (ZAKβ constitutively active) (Figure 4.3) were electroporated into the Tibialis anterior muscle of WT mice (Figure 4.4). Generated previously by

Huang *et al.* 2004, autophosphorylation was observed at higher levels in the ZAKβca overexpressing cells as the glutamic acid substitutions mimic phosphorylation events (Maciejewski et al., 1995). Conversely, no autophosphorylation took place in the case of ZAKdn after substitution of the catalytic lysine ablates catalytic activity (Hu et al., 2011). After co-staining for the z-disc marker a-actinin, z-disc localisation was observed in muscles electroporated with both constitutively active and dominant negative ZAKβ. This suggests that a functional kinase domain is not required for z-disc localisation.

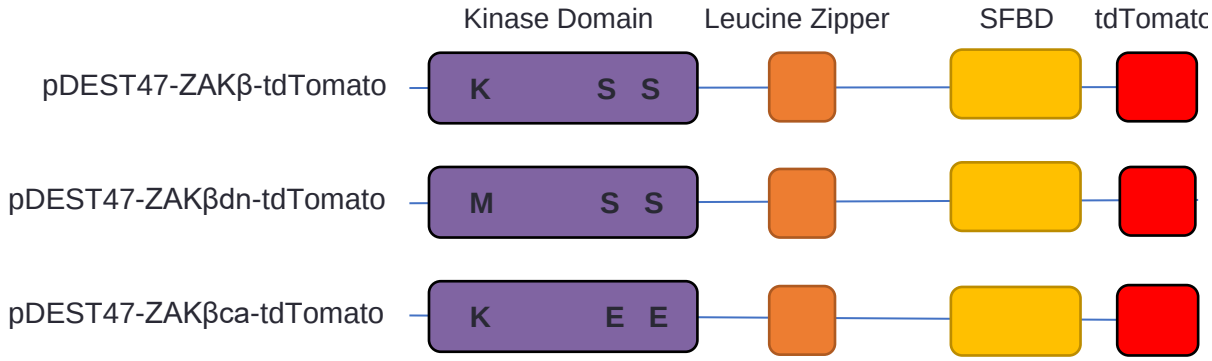

Figure 4.3: Kinase dead and constitutively active variants of ZAKβ. pDEST47-ZAKβ-tdTomato encodes the wild type ZAKβ protein, the conserved residues of the kinase domain are shown (green box). tdTomato (red box) is attached via the C-terminus. pDEST47-ZAKβdn-tdTomato holds a single substitution (K45M) at the start of the kinase domain. pDEST47-ZAKβca-tdTomato holds a double substitution (S230E & S234E) at the end of the kinase domain (Huang *et al.*, 2004). This was performed previously by Xiang Li in the Blanco Lab.

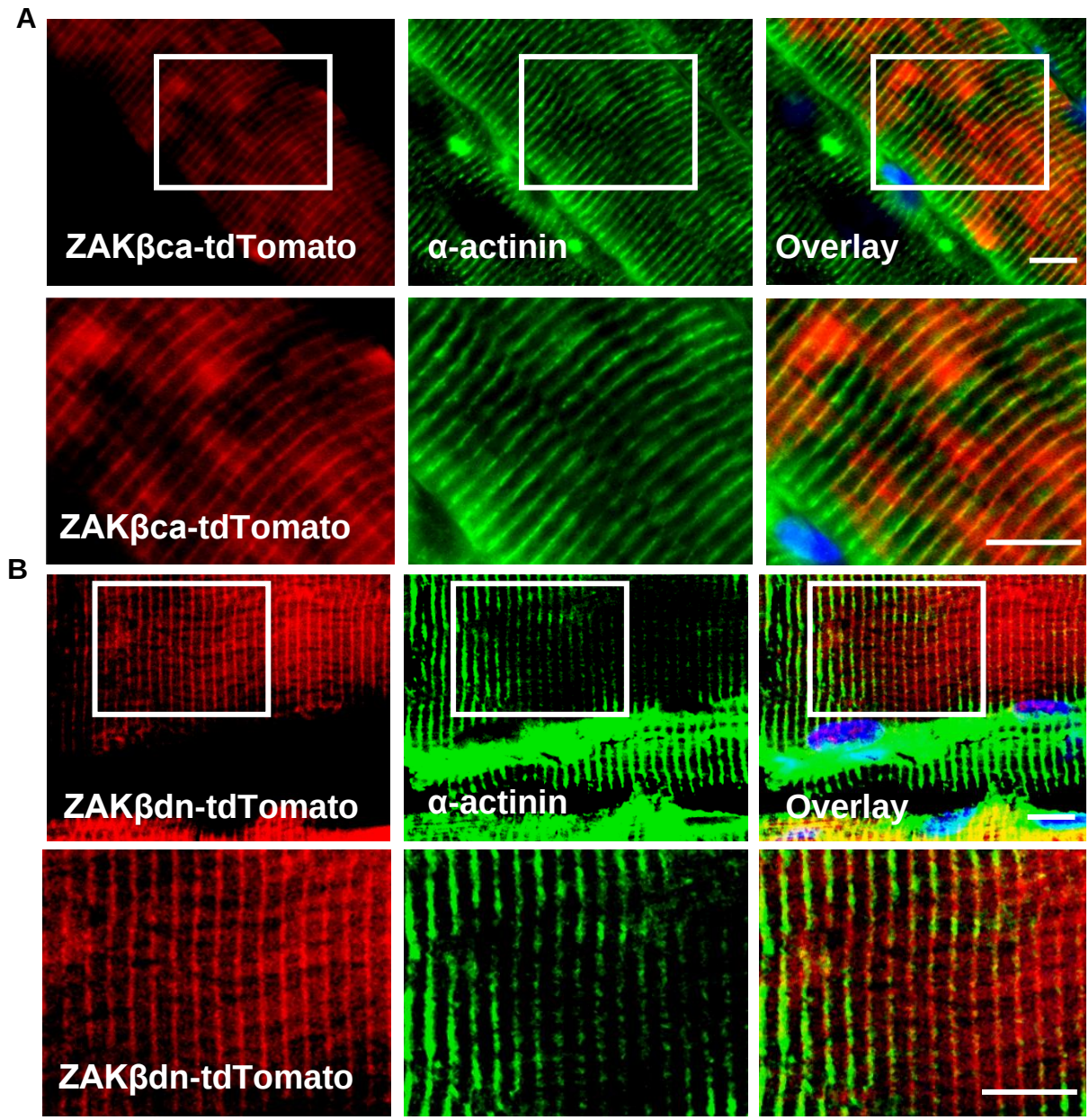

Figure 4.4: ZAKβ localises to the z-disc in fully differentiated adult mouse skeletal muscle irrespective of kinase domain activity. (A) Representative images of WT mouse Tibialis muscle electroporated with ZAKβca-tdTomato counterstained for a-actinin exhibits a striated pattern consistent with ZAKβwt. Bottom 3 panels are magnified images of white rectangle area. Scale bar representative of 10μm (n=3). (B) Representative images of WT mouse Tibialis muscle electroporated with ZAKβdn-tdTomato counterstained for a-actinin exhibits the same striated pattern. Bottom 3 panels are magnified images of white rectangle area. Scale bar representative of 10μm (n=3).

4.3 ZAKβ-GFP and ZAKβ(1-332)-GFP subcellular localisation in C2C12 myotubes

In vitro cellular models have been used for many years to mimic and perturb cellular processes and phenotypes in order to define key players in those processes. The C2C12 cell line is an immortalised myoblast cell line isolated from adult mouse leg muscle (Yaffe and Saxel, 1977). When cultured in high serum conditions (10%), these cells proliferate. In low serum (<2%), or at high confluency (95-100%), these proliferating cells differentiate into myocytes which eventually fuse to form myotubes. By fusing, multinucleated myotubes develop a striated pattern and are capable of contraction. This remarkable property of C2C12 cells makes them an ideal model for the study of early myogenesis, fusion, differentiation, and primitive structure formation.

The unique C-terminal region of ZAKα has been shown to be critical for localisation and detection of stalled ribosomes in its role in the remediation of ribotoxic stress (Vind *et al.*, 2020). The ZAKβ C-terminal region, unique to this isoform, was hypothesised to play an important role in its localisation and function. Experiments using truncated proteins identified a possible stress fibre binding domain (SFBD) within the C-terminus (Nordgaard *et al.*, 2022). Using ZAKβ(wt) and truncated ZAKβ(aa1-332) constructs fluorescently labelled with GFP (Figure 4.5), proliferating C2C12 cells were transfected and cultured in low serum conditions for 14 days to form primitive myotubes (Figure 4.6).

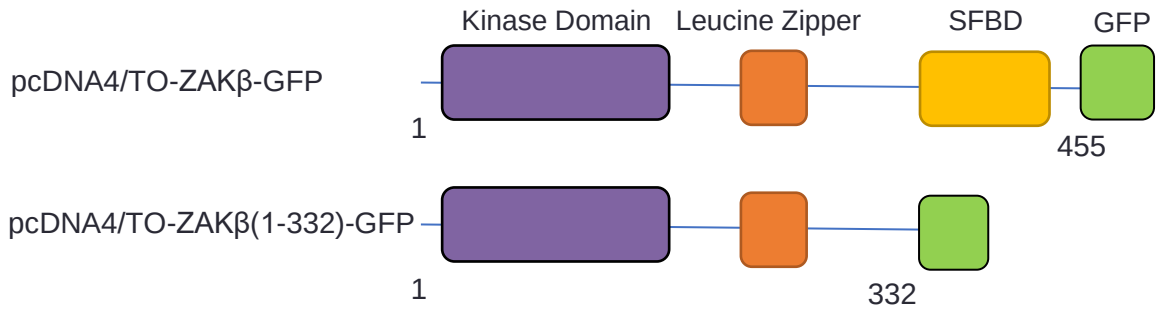

Figure 4.5: Schematics of recombinant wild type pcDNA4/TO-ZAKβ-GFP construct and pcDNA4/TO-ZAKβ-GFP (1-332) deletion construct. Mutagenesis of the C-terminal region to eliminate the SFBD C-terminal domain. This was performed previously by the Bekker-Jenson Lab.

The myotubes were imaged to identify the expression pattern of GFP-labelled ZAKβ and ZAKβ(1-332)-GFP lacking the SFBD. Myotubes positive for ZAKβ-GFP exhibited a striated pattern which colocalises with α-actinin, the z-disc marker (Figure 4.6, white arrows). This suggests that in an early model of muscle fibres, the C2C12 myotube, the SFBD is fundamental for z-disc localisation.

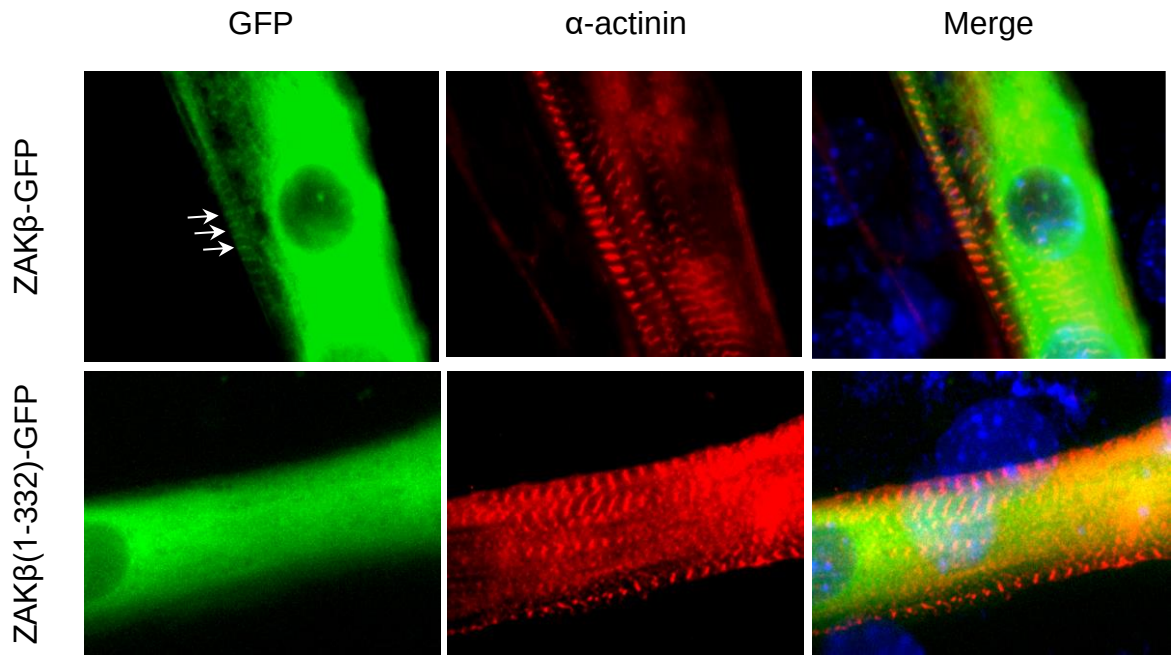

Figure 4.6: C2C12 myotubes exhibit loss of ZAKβ-specific striated pattern when SFBD is lost. 14 day post differentiation of C2C12 myoblasts transfected with either pcDNA4/TO-ZAKβ-GFP or pcDNA4/TO-ZAKβ(1-332)-GFP. Myotubes expressing pcDNA4/TO-ZAKβ(1-332)-GFP exhibit loss of classical striated pattern associated with ZAKβ. Striations are specific for z-disc as represented by α-actinin staining. Between 4 and 15 myotubes analysed per replicate, 3 replicates per condition.

4.4 ZAKβ-GFP and ZAKβ(1-332)-GFP subcellular localisation in skeletal muscle

Use of a C2C12 cellular model can be useful as this cell line is moderately easy to manipulate. However, it will never be a true substitute for the *in vivo* system which is supported by extrinsic factors, a cellular niche, and a basement membrane. An electroporation was performed with the same GFP-tagged ZAKβ constructs (Figure 4.5) in WT mouse TA muscle. These muscles were dissected, sectioned, and stained once again with α-actinin as a z-disc marker. Interestingly, whilst ZAKβ-GFP exhibited

the classical z-disc localised striated pattern, ZAKβ(1-332)-GFP also displayed z-disc localisation (Figure 4.7). This result is contrary to what was observed in the C2C12 myotubes and suggests in this *in vivo* model, that the SFBD does not exclusively determine the localisation of the protein.

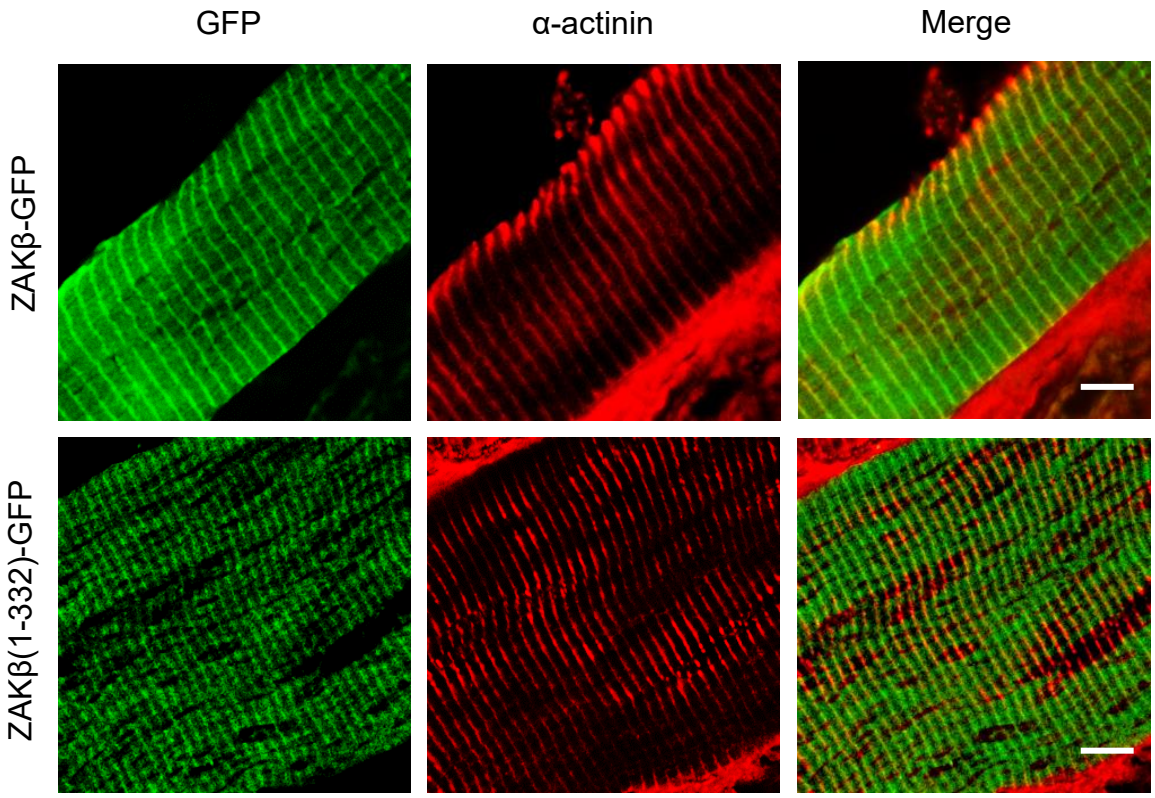

Figure 4.7: Electroporated WT TA muscle does not exhibit loss of ZAKβ-specific striated pattern when SFBD is lost. Representative images of WT tibialis muscle electroporated with either pcDNA4/TO-ZAKβ-GFP or pcDNA4/TO-ZAKβ(1-332)-GFP. Longitudinal representative merged images of pcDNA4/TO-ZAKβ-GFP or pcDNA4/TO-ZAKβ(1-332)-GFP (green) and α-actinin (red) both exhibit classical striated pattern associated with ZAKβ. Striations are specific for z-disc as represented by a-actinin staining. Scale bar representative of 10μm (n=5).

Fully differentiated skeletal muscle contains endogenous ZAKβ which has been shown to dimerise using the leucine zipper (LZ) domain (Gross *et al.*, 2002). As the ZAKβ(1-332)-GFP only lacks the SFBD, it was considered that the LZ domain may have been responsible for the localisation of the truncated construct to the z-disc by dimerising with endogenous ZAKβ. To eliminate endogenous ZAKβ as a factor in the localisation

of fluorescently labelled ZAKβ, the same electroporation was performed in ZAK$^{-/-}$ mice. TA muscle electroporated with GFP-alone, ZAKβ-GFP, and ZAKβ(1-332)-GFP were sectioned and imaged to identify the fluorescent expression pattern of each construct (Figure 4.8). It appeared as though this was not the case. Not only was the construct lacking the SFBD still showing a striated pattern, consistent with full-length ZAKβ, but the removal of endogenous ZAKβ by using the ZAK$^{-/-}$ mouse did not prevent z-disc localisation. This suggests that the presence of the kinase domain is sufficient to provide this z-disc localization *in vivo*, and that the *in vitro* result is most probably caused by insufficient terminal differentiation.

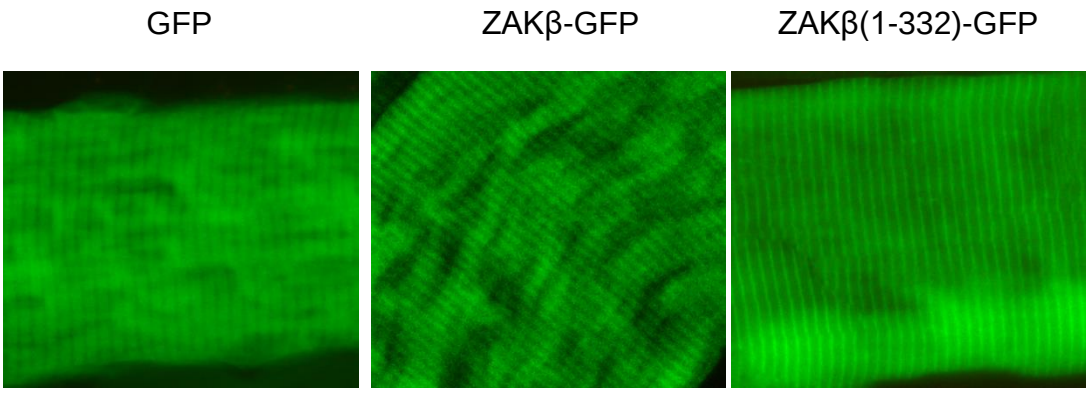

Figure 4.8: Electroporated ZAK$^{-/-}$ TA muscle does not exhibit loss of ZAKβ-specific striated pattern when SFBD is lost. Representative images of WT tibialis muscle electroporated with either pcDNA4/TO-ZAKβ-GFP or pcDNA4/TO-ZAKβ(1-332)-GFP. Longitudinal representative merged images of pcDNA4/TO-ZAKβ-GFP or pcDNA4/TO-ZAKβ(1-332)-GFP (green) exhibit classical striated pattern associated with ZAKβ. Striations not observed in longitudinal sections of muscle expressing pcDNA4/TO-GFP. (n=5)

4.5 Discussion

In this chapter, the subcellular localisation of ZAKβ was investigated in WT mouse skeletal muscle. In addition to this, mutagenised and deletion variants of ZAKβ were investigated in both C2C12 myotubes and fully differentiated adult WT and ZAK$^{-/-}$ mouse skeletal muscle. Data generated during the course of this project identified a potential stress fibre binding domain (SFBD) contained within the final 123 residues of the ZAKβ protein (Nordgaard *et al.*, 2022). In the C2C12 muscle myoblast cell line, myotubes exhibited a striated pattern when transfected with ZAKβ-GFP, but not with

ZAKβ(1-332)-GFP (Figure 4.6). This suggested that the SFBD contained within the C-terminal region of ZAKβ is important for z-disc localisation, as these early striated structures form the basis of the dense crystal-like z-disc structure found in fully differentiated adult skeletal muscle. In WT mouse skeletal muscle, ZAKβ was also shown to localise to the z-disc and was not influenced by mutations within the kinase domain rendering it inactive (Figure 4.4), or loss of the SFBD (Figure 4.7, 4.8). Because ZAKβ and IGFN1 are known interacting partners, and both appear to localise to the z-disc, this suggests that the z-disc is an important component in the relationship between ZAKβ and its interacting partners and signalling pathways. A summary of these findings can be found in Figure 4.9.

The identification of the SFBD was through transfections in a non-muscle cell line, U2OS cells. Here ZAKβ was shown to colocalise with Lamin A/C at stress fibres, which is unique to that of the ZAKβ isoform (Nordgaard *et al.*, 2022). The z-disc is known to share compositional overlap with these cellular stress fibres, therefore ZAKβ was thought to localise to z-discs in a muscle-like model such as C2C12 myoblasts. To an extent, this was confirmed. It was only when employing the most physiologically relevant model, electroporation in adult skeletal muscle that this hypothesis of a SFBD was shown not to be correct. The difference observed in the skeletal muscle could be a result of a number of factors present in the skeletal muscle niche, such as a higher level of sarcomeric structure, expression of more structural proteins, the presence of ZAKβ-interacting proteins, and extrinsic factors that could enable correct ZAKβ localisation even in the absence of a functional SFBD. All of these factors influence how proteins behave, and therefore how the cell behaves *in vivo* (Cornelison, 2008; McNeill *et al.*, 2014). The primitive state of the C2C12 myotube without a basal lamina or cellular niche may allow for a more realistic idea of how ZAKβ localises in the presence/absence of the SFBD however may not be entirely relevant in the context of adult muscle, being just a semi-artificial *in vitro* model of myogenesis.

Another point to consider is the composition of TA muscle which was used in this electroporation protocol. TA muscle consists of a mix of type IIa /IIb fast muscle fibres, fibres which do not appear as affected by the loss of ZAKβ when compared with the type I/IIa slower fibres of the soleus. It would be an interesting experiment to confirm the same results in slow muscle fibres as what has been observed in fast muscle

fibres. However, to do so would require exposure and electroporation of the soleus muscle which is very small and unlikely to respond well to the protocol.

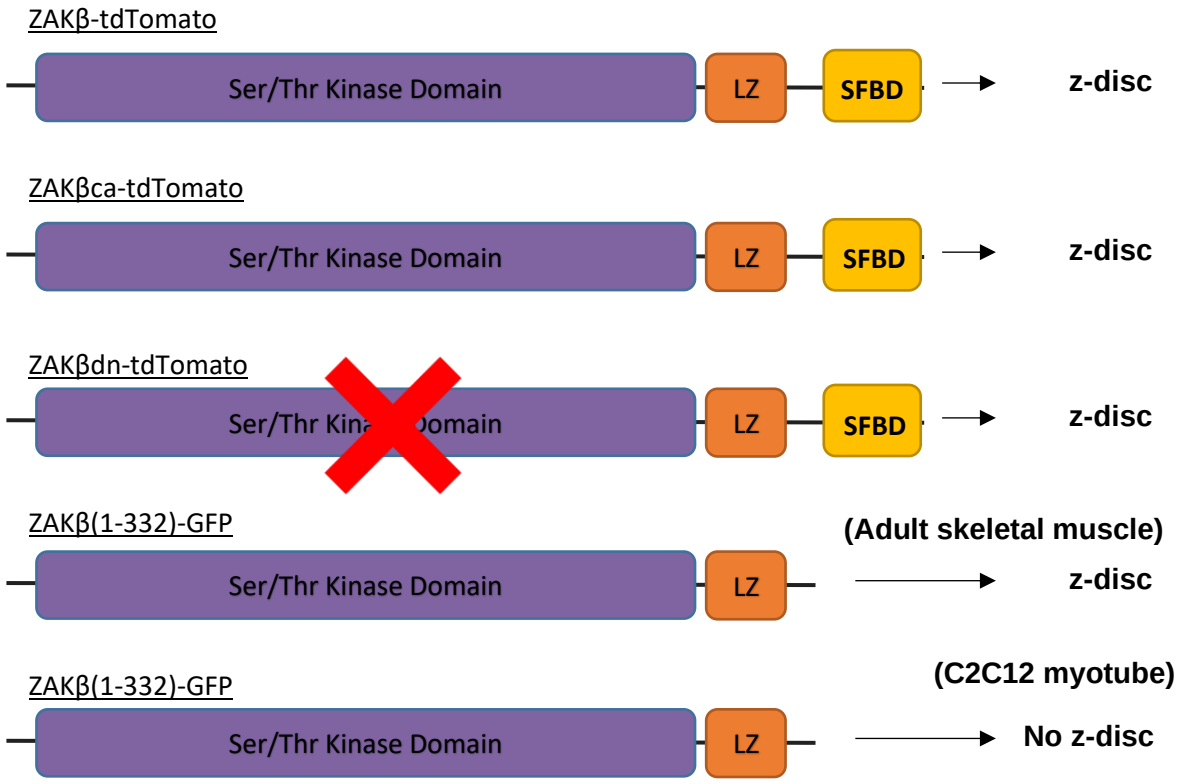

Figure 4.9: Localisation summary of ZAKβ constructs. Electroporation of ZAKβ-tdTomato, ZAKβca-tdTomato, ZAKβdn-tdTomato, and ZAKβ(1-332)-GFP into adult skeletal muscle resulted in clear z-disc localisation. Loss of the SFBD in C2C12 myotubes differentiated from myoblasts transfected with ZAKβ(1-332)-GFP resulted in loss of the z-disc localisation.

CHAPTER 5

Results

THE EFFECT OF ZAKβ OVEREXPRESSION ON MUSCLE FIBRE CROSS-SECTIONAL AREA

5.1 Introduction

Recently, *ZAKβ* has been implicated in a rare cases of congenital myopathy, where human patients lacking both *ZAK* isoforms exhibit skeletal muscle weakness and atrophy (Vasli *et al.*, 2017). This is concordant with histopathological evidence that includes skeletal muscle fibre size variation, predominance of type I fibres and centralised nuclei. The resulting myopathy from loss of function of ZAKβ is the first example of a direct association between a stress kinase signalling protein and a clinical myopathy in skeletal muscle.

The KY protein has demonstrated its importance in maintaining sarcomeric integrity. Loss of KY results in a myopathic phenotype characterised by muscle weakness and fibre atrophy unable to respond to increased mechanical loading (Maréchal, Coulton and Beckers-Bleukx, 1995; Blanco *et al.*, 2001). Transcriptomic analysis of *ky/ky* skeletal muscle reveals an upregulation of *Zakβ*, suggesting a potential coordination between the signalling pathway of ZAKβ, and that of KY. The nature of such an interaction remains unknown; however, these 2 proteins share IGFN1 as an interacting partner which may play a role as scaffold and mediator (Baker et al., 2010).

Post-translational modifications (PTM) regulate many complex and important signalling pathways and cellular processes, ultimately facilitating intracellular signalling and muscle function. One of the most abundant and important types of PTM is protein phosphorylation, which is known to cause subsequent activation or inhibition of enzymes via specific allosteric changes to the protein structure. This may result in changes in subcellular localisation and interactions with other proteins. Previous experiments have determined ZAKβ as being a MAPKKK stress kinase within the MAPK signalling cascade (Gross et al., 2002). MAPK signalling cascades are activated either as a result of a series of interactions between subsequent kinase components or through the formation of a signalling complex that is mediated by a scaffold protein (Morrison and Davis, 2003; Whitmarsh, 2006). Interestingly, ZAK has previously been reported to preferentially activate the ERK6/p38γ and JNK MAPK signalling cascades via the respective endogenous MAPKKs MKK3/6 and MKK4/7 (Kyriakis and Avruch, 2001; Gross *et al.*, 2002).

ZAKβ is thought to be required for canonical TGFβ signalling (Nyati *et al.*, 2016), a pathway important for regulating hypertrophic signalling. ZAKβ overexpression induces hypertrophic growth in cardiomyoblasts *in vitro*, via the TGFβ dependent pathway (Huang *et al.*, 2004; Hsieh *et al.*, 2015). This hypertrophic growth coincided with an increase in protein synthesis, once again implicating downstream proteins such as p38, JNK and ERK in ZAKβ signalling (Bloem *et al.*, 2001). It must be noted that these results are acquired primarily from overexpression/ectopic expression models which are not entirely physiologically relevant to ascertain the role of ZAKβ in skeletal muscle. From a muscle perspective however, the potential involvement of p38, JNK, and TGFβ is very compelling, as all are important factors in myogenesis and development (Perdiguero et al., 2007; Delaney et al., 2017; Xie et al., 2018; Brennan et al., 2021).

Muscle hypertrophy is primarily dependent on the activation of the mTOR signalling pathway. mTOR itself is a serine/threonine kinase capable of sensing both environmental and intracellular cues to initiate and coordinate downstream cellular processes such as growth, differentiation, autophagy or cell survival, and metabolism (Laplante and Sabatini, 2012). The mTORC1 complex consists of mTOR regulatory protein raptor associated with the AKT substrate (PRAS40), the DEP domain-containing mTOR-interacting protein (DEPTOR), and the mammalian lethal with SEC13 protein 8 (mLST8) (Hara *et al.*, 1997; Inoki *et al.*, 2002). This complex in particular is rapamycin-sensitive and controls protein synthesis through S6 kinase (S6K) activation, and 4E-binding protein 1 (4EBP1) inhibition (Pallafacchina *et al.*, 2002; Ma and Blenis, 2009). Rapamycin has been used in many experiments to pharmaceutically inhibit the mTORC1 complex for suppression of the hypertrophic response (Kline *et al.*, 2007; Choi, Yang and Kim, 2019; Ogasawara *et al.*, 2019). Therefore, rapamycin can also be used experimentally to determine whether a hypertrophic response is mTOR-dependent.

5.2 The effect of wild-type, kinase-dead, and constitutively active ZAKβ-tdTomato on skeletal muscle fibre cross-sectional area

Muscle use is intrinsically linked with changes to metabolism, muscle repair, and adaptation to exercise. Since the loss of ZAKβ causes atrophy, we decided to test

whether upregulation of the pathway by overexpression of ZAKβ would have the opposite effect. We sought to overexpress ZAKβ through electroporation of ZAKβ-tdTomato in mouse TA muscle (Figure 5.1A; panels A-C). Cross-sectional analysis was performed only on transfected/untransfected fibres within the same region of the muscle as a result of the high levels of size variation throughout the complete muscle section. Comparisons between mice were not possible without normalising the data due to large fibre size variation between individual mice. The analysis of the fibre area was performed using ImageJ software (Fiji version) using wheat germ agglutinin (WGA) stained muscle sections, whereby each positive fibre (Red) was manually outlined and compared with the negative (untransfected) fibres. Fibre cross sectional area was calculated as an average of three individual muscles. To avoid regional fibre size variation in the TA muscle to confound comparisons, a scale factor (average area of transfected: average area untransfected) was obtained from at least three transfected regions within the muscle, which were then averaged to produce a single data point per muscle. Normalised data was collated and analysed using a Student's t-Test. After 8 days, this resulted in a dramatic (more than 50%) increase in the cross-section area of electroporated fibres (Figure 5.1B). This suggested that ZAKβ indeed has a role in the mediation of hypertrophic signalling in skeletal muscle.

We then sought to further over-activate the same pathway or prevent ZAKβ signalling through electroporation of constitutively active and dominant negative ZAKβ in mouse TA muscle to test whether this effect is caused by activity of the ZAKβ kinase domain. DNA constructs (Figure 4.3) encoding both ZAKβdn-tdTomato (ZAKβ dominant negative; kinase dead) and ZAKβca-tdTomato (ZAKβ constitutively active) were electroporated into the Tibialis anterior (TA) muscle of WT mice (Figure 5.1; panels D-I). After 8 days, this resulted in an increase in fibre cross-sectional area in a manner dependent on ZAKβ kinase activity. Overexpression of ZAKβdn-tdTomato did not produce such an increase as observed with ZAKβ(wt) or ZAKβ(ca). Not only does this confirm the previous observations that ZAKβ is sufficient to induce a hypertrophic response, but it further confirms that a functionally active kinase domain is required for this effect.

A

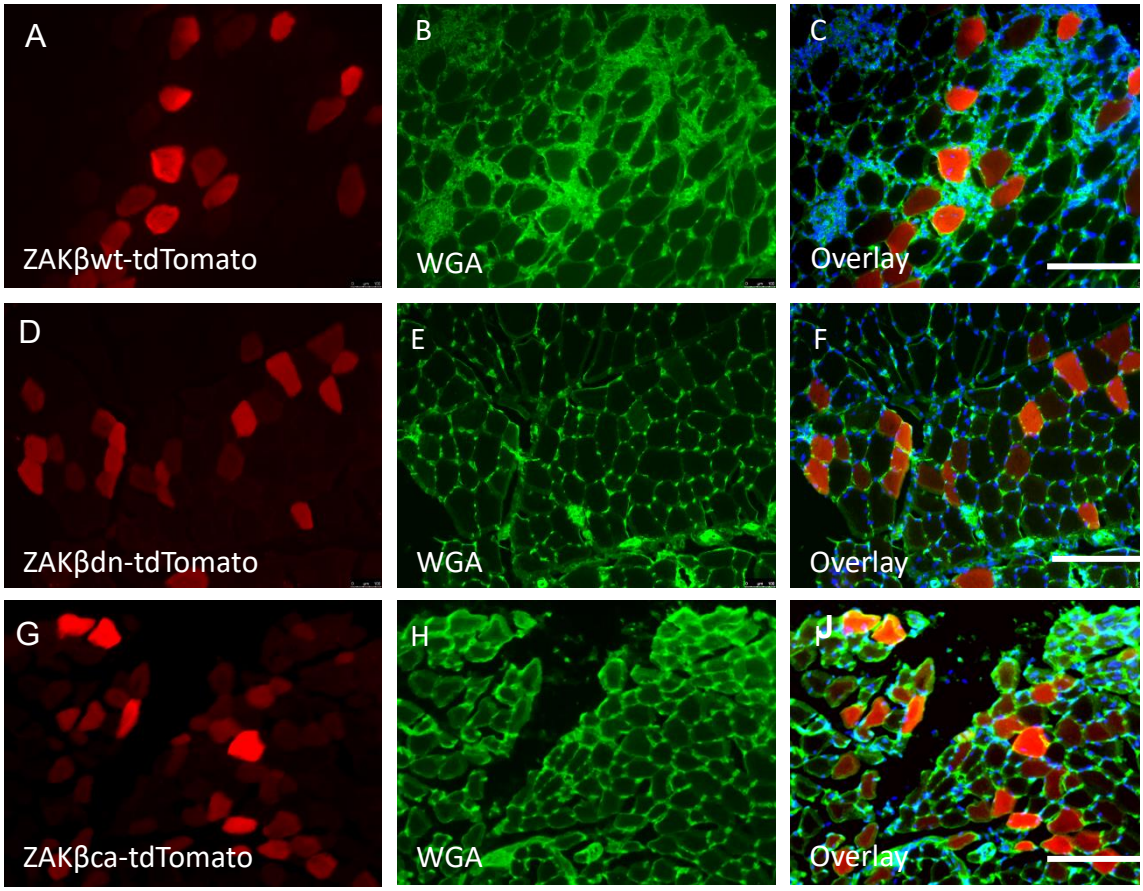
A
ZAKβwt-tdTomato
B
WGA
C
Overlay
D
ZAKβdn-tdTomato
E
WGA
F
Overlay
G
ZAKβca-tdTomato
H
WGA
J
Overlay

B

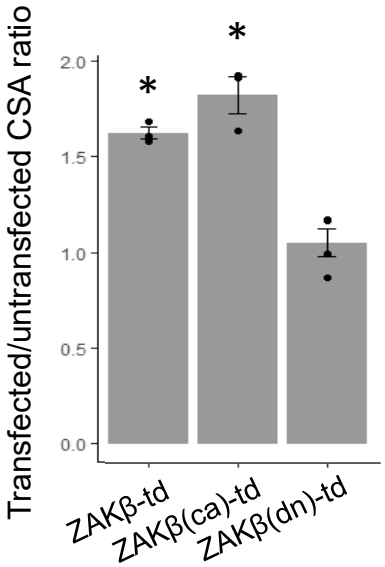
Transfected/untransfected CSA ratio
2.0
1.5
1.0
0.5
0.0
*
*
ZAKβ-td
ZAKβ(ca)-td
ZAKβ(dn)-td

Figure 5.1: Overexpression of a functional ZAKβ kinase domain is sufficient to induce muscle fibre hypertrophy *in vivo*. (A) Electroporated tibialis anterior muscle fibres of WT mice expressing pDEST47-ZAKβ-tdTomato (Top 3 panels), pDEST47-ZAKβdn-tdTomato (Middle 3 panels) or pDEST47-ZAKβca-tdTomato (Bottom 3 panels). Scale bar = 250 µm. (B) Bar graph depicts fibre size comparisons, measured as cross-sectional area (CSA) of transfected (red) and untransfected (black) fibres, between pDEST47-ZAKβdn-tdTomato, pDEST47-ZAKβwt-tdTomato, and pDEST47-ZAKβca-tdTomato. CSA of transfected fibres normalised to average area of untransfected fibres within the field of view. Muscle fibres transfected with either pDEST47-ZAKβwt-tdTomato or pDEST47-ZAKβca-tdTomato displayed an increase in fibre size in comparison to fibres transfected with pDEST47-ZAKβdn-tdTomato. Kruskall-Wallis non-parametric test with Dunn multiple comparisons post hoc test, * represents $p<0.001$. Scale bar = 100 µm. Error bars = mean +/- Standard Error (n=3).

We next electroporated ZAKβ-GFP and its SFBD-deleted counterpart (ZAKβ(1-332)-GFP) into the TA muscles of ZAK-KO mice to test if the kinase domain alone was sufficient to cause the hypertrophic effect. This was performed in the same way as previously mentioned, and positively electroporated muscles were sectioned, and stained with WGA (Figure 5.2A). Cross sectional area (CSA) was measured for each of the constructs and a ratio was calculated from the untransfected fibres. As expected, GFP had no impact on CSA, whereas muscles electroporated with ZAKβ-GFP or ZAKβ(1-332)-GFP did indeed cause an increase in fibre CSA, indicative of fibre hypertrophy (Figure 5.2B). This confirms that overexpression of the kinase domain alone is sufficient to cause an increase on CSA.

5.3 Determining whether ZAKβ-induced hypertrophy is mTOR-dependent

Such apparent muscle hypertrophy is generally associated with signalling via the mTOR pathway. We thus decided to investigate whether the observed hypertrophy was associated specifically with mTOR signalling, and thus representative of the muscle growth observed following increased mechanical load/ resistance exercise. One way of ascertaining whether ZAKβ-mediated hypertrophy was mTOR-dependent, was to inhibit mTOR signalling via the natural mTOR inhibitor, rapamycin.

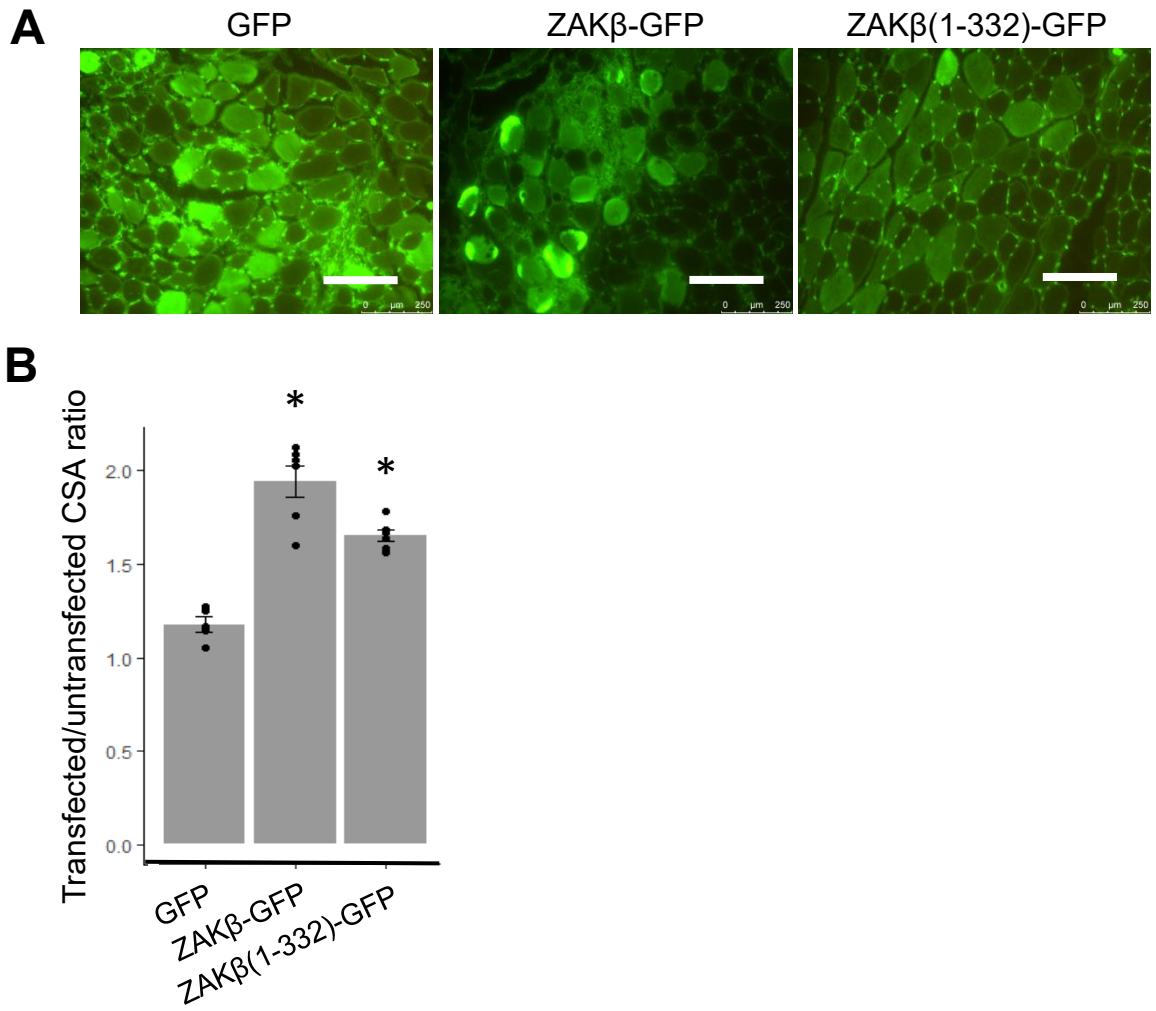

Figure 5.2: ZAKβ-induced fibre hypertrophy using ZAKβ-GFP or ZAKβ(1-332)-GFP is not affected by lack of endogenous ZAKβ. (A) Electroporated tibialis anterior muscle fibres of ZAK KO mice expressing pcDNA4/TO-GFP (Left), pcDNA4/TO-ZAKβ-GFP (Middle), or pcDNA4/TO-ZAKβ(1-332)-GFP (Right). Scale bar = 250 µm. (B) Bar graph depicts fibre size comparisons, measured as cross-sectional area (CSA) of transfected (Green) and untransfected (Black) fibres, between pcDNA4/TO-GFP, pcDNA4/TO-ZAKβ-GFP, and pcDNA4/TO-ZAKβ(1-332)-GFP. CSA of transfected fibres normalised to average area of untransfected fibres within the field of view. Muscle fibres transfected with either pcDNA4/TO-ZAKβ-GFP or pcDNA4/TO-ZAKβ(1-332)-GFP displayed an increase in fibre size in comparison to fibres transfected with pcDNA4/TO-GFP. Kruskall-Wallis non-parametric test with Dunn multiple comparisons post hoc test, * represents $p<0.001$ (n=5).

Rapamycin was administered systemically via intraperitoneal (IP) injection over a period of 12 days, during which mouse TA muscle was electroporated with either ZAKβ(wt)-tdTomato or ZAKβ(ca)-tdTomato and left to express for 8 days (Figure 5.3A). As before, muscles electroporated with functional ZAKβ in the absence of rapamycin showed an increase in fibre CSA. When treated in the presence of the inhibitor, muscle fibres failed to have the same response with regards to the CSA of rapamycin-treated muscle fibres electroporated with ZAKβ(wt)-tdTomato or ZAKβ(ca)-tdTomato. The CSA of inhibited ZAKβ-overexpressing fibres was non-significant from that of the non-transfected control fibres (Figure 5.3B). This result is highly significant in the identification of the exact nature of ZAKβ signalling in skeletal muscle. This suggests that ZAKβ overexpression causes mTOR-dependent hypertrophy; the canonical signalling pathway associated with skeletal muscle hypertrophy, via its kinase domain.

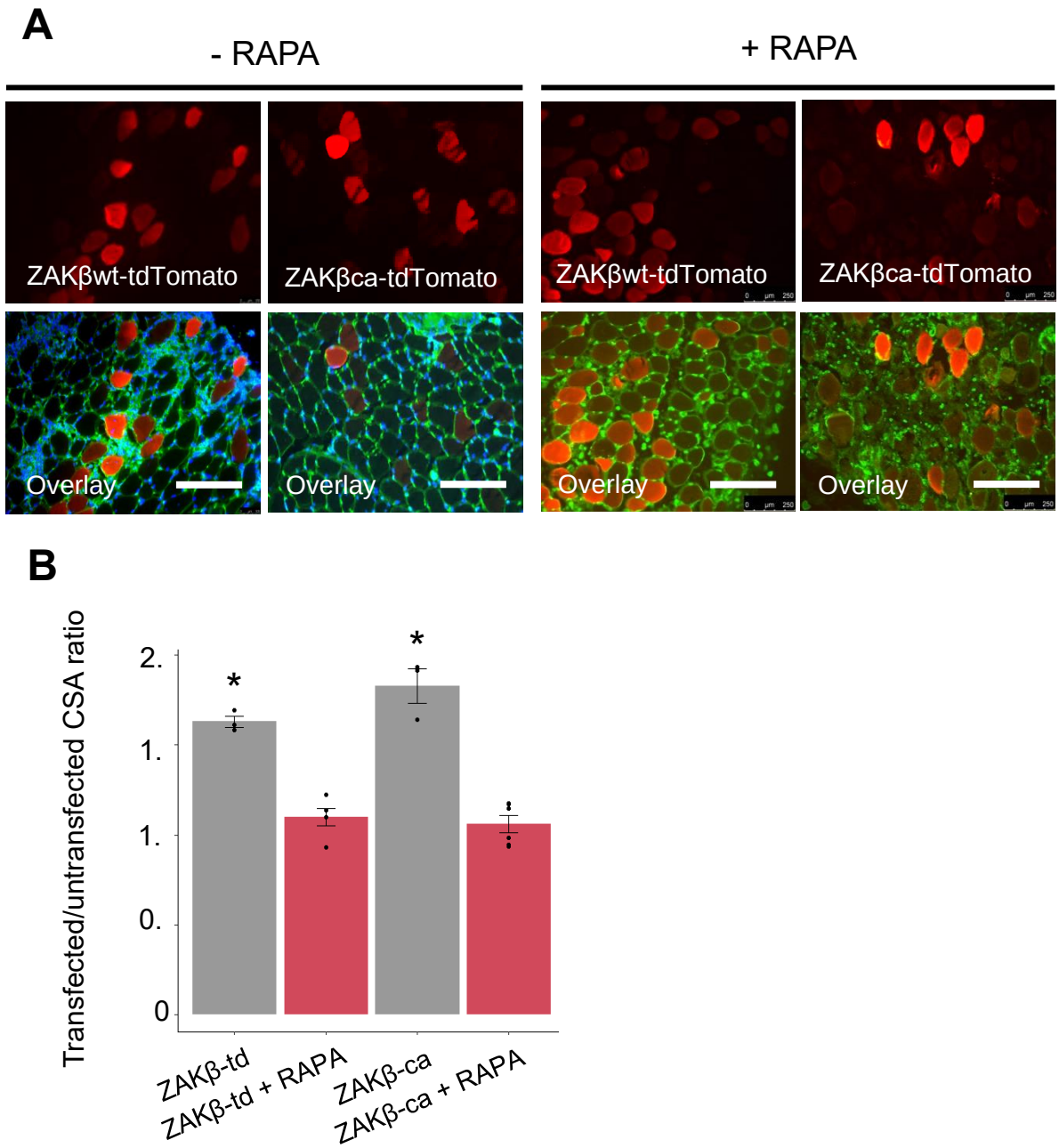

Figure 5.3: ZAKβ-induced hypertrophy is mTOR-dependent. (A) Electroporated tibialis anterior muscle fibres of WT mice expressing either pDEST47-ZAKβ-tdTomato (Left), or pDEST47-ZAKβca-tdTomato (Right) in the presence (Right 4 panels)/absence (Left 4 panels) of rapamycin. Scale bar = 250 µm. (B) Bar graph depicts fibre size comparisons, measured as cross-sectional area (CSA) of transfected (red) and untransfected (black) fibres, between pDEST47-ZAKβwt-tdTomato, and pDEST47-ZAKβca-tdTomato in muscles treated with or without rapamycin. CSA of transfected fibres normalised to average area of untransfected fibres within the field of view. Between 6 and 23 fibres measured per field. Muscle fibres transfected with either pDEST47-ZAKβwt-tdTomato or pDEST47-ZAKβca-tdTomato in the

absence of rapamycin displayed an increase in fibre size. Muscles treated with rapamycin did not see such an effect. Kruskall-Wallis non-parametric test with Dunn multiple comparisons post hoc test, * represents $p<0.001$ (n=6).

5.4 Characterisation of the relationship between KY and ZAKβ using the ky/ky mouse model

Connected by the potential scaffolding protein IGFN1, ZAKβ and KY both have proved to be important for sarcomeric stability. Loss of either protein results in a muscle myopathy characterised by muscle weakness and atrophy. However, the myofibrillar myopathy in humans which develops following the loss of KY presents as more severe than that of the ZAK patient, and is also observed in the respective mouse models. KY and ZAKβ appear to be forever linked together as interacting partners of the KY protein complex, further strengthened by the fact that ZAKβ transcripts are upregulated in the *ky/ky* mouse skeletal muscle, suggesting a crossover or redundancy in their respective signalling networks. From previous experiments, it was clear that loss of KY prevents mechanical load-induced hypertrophy (Maréchal, Coulton and Beckers-Bleukx, 1995; Blanco *et al.*, 2001). We also knew that ZAKβ was able to produce this effect just by overexpression alone in both WT and $ZAK^{-/-}$ mouse models (Figures 5.1 & 5.2). Therefore, we decided to investigate whether ZAKβ was able to compensate for the loss of KY in the atrophied TA muscle of *ky/ky* mice. To do so, we performed the same electroporation protocol with ZAKβ(wt)-tdTomato and ZAKβ(ca)-tdTomato as above in *ky/ky* mice, and allowed for expression over 8 days-post procedure (Figure 5.4A). Once again, muscles transfected with ZAKβ(wt)-tdTomato or ZAKβ(ca)-tdTomato increased CSA of WT muscle fibres. However, electroporation of ZAKβ(wt)-tdTomato or ZAKβ(ca)-tdTomato in the TA of *ky/ky* mice did not have the same effect (Figure 5.4B). Able to induce hypertrophy in WT tissue when overexpressed and cause muscle atrophy when absent suggests that ZAKβ regulates muscle size. Furthermore, ZAKβ was unable to initiate a hypertrophic response in muscles deficient in KY protein, suggesting a role for KY downstream of ZAKβ important for hypertrophic signalling via mTOR.

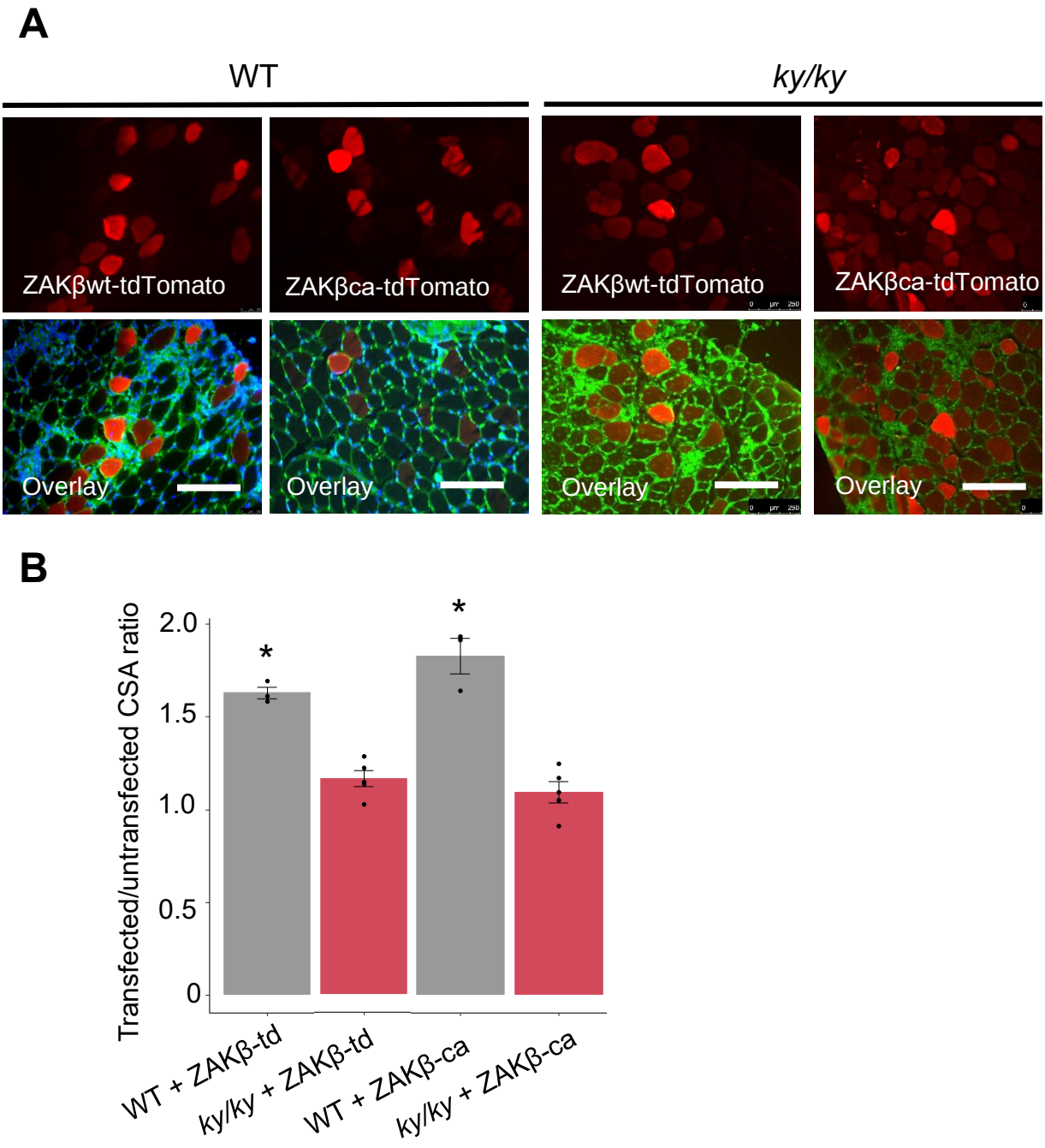

Figure 5.4: Loss of KY is sufficient to prevent ZAKβ-induced fibre hypertrophy. (A) Electroporated tibialis anterior muscle fibres of WT (Left) or *ky/*ky (Right) mice expressing eitherpDEST47-ZAKβ-tdTomato (Left), or pDEST47-ZAKβca-tdTomato (Right). Scale bar = 250 µm. (B) Bar graph depicts fibre size comparisons, measured as cross-sectional area (CSA) of transfected (red) and untransfected (black) fibres, between pDEST47-ZAKβwt-tdTomato, and pDEST47-ZAKβca-tdTomato in both WT and *ky/*ky muscles. CSA of

transfected fibres normalised to average area of untransfected fibres within the field of view. Muscle fibres transfected with either pDEST47-ZAKβwt-tdTomato or pDEST47-ZAKβca-tdTomato in WT tibialis displayed an increase in fibre CSA. *ky/*ky muscles electroporated with pDEST47-ZAKβwt-tdTomato or pDEST47-ZAKβca-tdTomato did not see such an effect. Kruskall-Wallis non-parametric test with Dunn multiple comparisons post hoc test, * represents $p<0.001$ (n=6).

5.5 Discussion

ZAKβ is found in most tissues of the body, suggesting that its role is generally important for cellular function. Skeletal muscle is a tissue where the role of ZAKβ can be more functionally investigated as it is the only ZAK isoform expressed. ZAK loss of function (LOF) is also associated with skeletal muscle pathology in mice and humans (Vasli *et al.*, 2017). Histological analysis of muscle biopsies of human patients carrying the deleterious mutation within the kinase domain of *ZAK* showed evidence centralised nuclei tightly surrounded by myofibrils and sarcoplasmic disorganisation (Vasli *et al.*, 2017).

Of the two isoforms, only ZAKβ is found in muscle. *ZAK* is an unusual gene in which it encodes two very distinct MAPKKKs that are activated upstream by very different stimuli. ZAK as a MAP3K stress kinase has been implicated in the activation of p38γ, JNK and ERK signalling cascades (Bloem *et al.*, 2001; Gotoh, Adachi and Nishida, 2001; Gross *et al.*, 2002; Christe *et al.*, 2004). Similar to other MAPK signal transducers, the levels of active ZAK require tight regulation. Overexpression of ZAK in a hepatoma cell line results in apoptosis and overexpression in myofibres *in vivo* results in cellular hypertrophy as we observe here (Liu *et al.*, 2000).

Collectively, our data suggest that the functional outcome of ZAKβ activation is related to hypertrophic signalling. These findings go hand in hand with the observed general muscle atrophy in human patients (Vasli *et al.*, 2017) and specific atrophy in our mouse model (Figure 3.3C). Contraction-induced MAPK signalling has recently been associated with this dichotomy (Lessard *et al.*, 2018). Under normal circumstances, myostatin suppresses the SMAD2 transcription factor. Upon increased mechanical demand induced by contraction of the muscle fibre, activated JNK phosphorylates

SMAD2 which aids its dissociation from myostatin inhibition (Figure 5.5). Mice lacking functional JNK proteins are unable to undergo hypertrophy following resistance exercise. ZAKβ was identified originally as a MAP3K with the ability to preferentially activate both the p38 and JNK signalling cascades (Gallo and Johnson, 2002; Yang, 2002). This putative signalling network offers a potential explanation for the hypertrophy-associated increase in fibre CSA when ZAKβ is overexpressed, as a potential mediator of JNK-associated hypertrophic signalling (Figure 5.5).

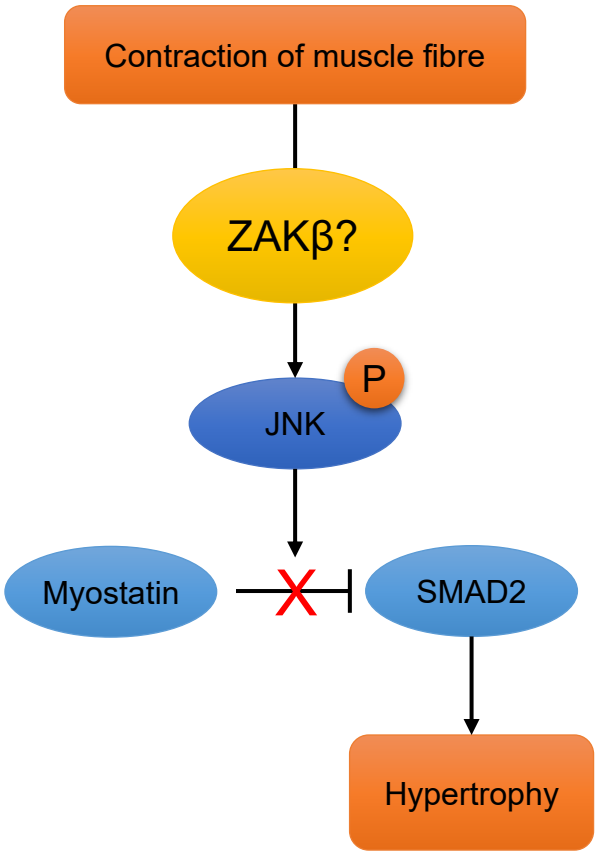

Figure 5.5: Schematic detailing the potential role for ZAKβ in non-canonical JNK signalling. The myostatin inhibition of SMAD2 is relieved by activated JNK. Activation of JNK can occur via contraction of the muscle fibre. As a stress-induced MAPKKK know to act upstream pf JNK, ZAKβ may have a role in the activation of JNK following mechanical stress and thus may activate hypertrophic mechanisms as a result.

Increased load or demand on skeletal muscle results in the stretch-induced stress response which ultimately leads to increased protein synthesis and adaptation of the muscle fibre to withstand future demand. Regulation of actin dynamics plays a key role in skeletal muscle hypertrophy. When hypertrophy is induced by mechanical stress, actin reorganisation increases at the barbed end, which is beneficial for the construction of new sarcomeres. These new sarcomeres are added in parallel to the existing sarcomeres and increase the overall cross sectional area of the myofibre (Johnson and Klueber, 1991; Farup *et al.*, 2012; Gaikis *et al.*, 2013). ZAKα has been shown to increase actin organisation in cardiomyoblasts (Huang *et al.*, 2004) and increase actin polymerisation affecting cardiac hypertrophy (Christe *et al.* 2004). The effect on fibre CSA with ZAKβ overexpression may act in a similar fashion to that of nebulin and N-WASP which are both required for IGF-1-induced muscle hypertrophy and actin filament formation in myofibrillogenesis via actin nucleation (Takano *et al.*, 2010). ZAKβ could be responsible for initiating a signalling cascade that ultimately results in hypertrophic growth via an increase in cytoskeletal organisation and protein synthesis.

CHAPTER 6

Results

A PHOSPHOPROTEOMIC APPROACH FOR THE IDENTIFICATION OF DIRECT SUBSTRATES OF ZAKβ

6.1 Introduction

Protein phosphorylation is both a post-translational modification, and a mechanism of regulation extremely important in cellular processes such as: protein synthesis and degradation, cell division and growth, signal transduction, and both development and ageing (McCance *et al.*, 2019). As a consequence of tightly controlled kinase and phosphatase activity, specific enzymes and receptors are activated/deactivated due to phosphorylation/dephosphorylation events and these are one of the most important post-translational modifications in cellular biology (X. Li *et al.*, 2013). Protein kinases in particular are known to regulate signalling processes (McCance *et al.*, 2019). They function by mediating the binding of a phosphate group to specific protein substrates which remains covalently bound after the conversion of ATP to ADP within the kinase domain. In order to identify the overall role of an uncharacterised protein kinase, large-scale screening methods for downstream targets directly phosphorylated by the kinase of interest have been implemented. Previously, whole-cell or tissue lysates have been used to detect perturbations in global phosphorylation levels, however this does not allow for the association of a kinase of interest with direct phosphorylation events without additional enquiries (Holt *et al.*, 2009). As a consequence, a simplified assay that identifies the direct downstream phosphorylation targets of a particular protein was developed (Knight *et al.*, 2012).

Activation of TGFβ, p38 and JNK signalling pathways are associated with ectopic overexpression of both ZAKα and ZAKβ *in vitro* and *in vivo*, which has been shown to cause cardiac cell hypertrophy (Bloem *et al.*, 2001; Christe *et al.*, 2004; Huang, Chueh, *et al.*, 2004; Huang, Kuo, *et al.*, 2004; Hsieh *et al.*, 2015). While these pathways are involved in myogenesis (Burks and Cohn, 2011; MacDonald and Cohn, 2012) and myofibre adaptation (Foster, Tidball and Wang, 2012; Boyer *et al.*, 2019), these overexpression models have not specifically informed us on the exact physiological function of ZAKβ in skeletal muscle. More recently, the isoform-specific C-terminal domains of ZAKα and ZAKβ have been shown to provide functional specificity. ZAKα has been implicated in ribotoxic stress (Vind *et al.*, 2020). ZAKα performs this function through two ribosome-binding domains in its C-terminus that serve as a molecular sensing module. However, ZAKα is unlikely to play a relevant role in skeletal muscle, since ZAKβ is the only protein isoform present in skeletal muscle in humans (Vasli *et*

al., 2017) and mice (Figure 3.1A), in agreement with previous findings at transcriptional level (Bloem *et al.*, 2001). ZAKβ does not respond to ribotoxic stress (Vind *et al.*, 2020). ZAKβ has been shown to respond to mechanical perturbation of cytoskeletal stress fibres caused by osmotic shock or cellular compression in U2OS cells through the action of a stress-fibre binding domain (SFBD) at the C-terminus (Nordgaard et al., 2022). Under these conditions, ZAKβ autophosphorylates, relocates to stress fibres through its unique C-terminal domain, and results in p38 activation (Nordgaard et al., 2022). Interestingly, repeated contractions of Tibialis anterior (TA) muscle also lead to acute p38 activation in a ZAKβ-dependent mechanism (Nordgaard et al., 2022. It would therefore appear that ZAKβ is an early mediator of a contraction-induced mechanical stress, but the mechanism(s) by which ZAK senses these stimuli are not known. Likewise, while p38 has been shown an effective reporter of ZAKβ activation in the above experiments, the direct downstream targets of ZAKβ in skeletal muscle are yet to be determined.

Here I describe a simple approach for substrate mining that can be used to identify direct, *ex vivo*, downstream substrates of ZAKβ, adapted from Knight *et al*. 2012. As a brief overview, the technique is different from other phosphoproteomics analyses as the skeletal muscle lysate is pre-treated to inactivate all endogenous kinases, followed by an *in vitro* assay using an exogenous kinase of interest, concluding with quantitative mass spectrometry (MS) to identify phosphorylation sites specific to the added kinase, which in this case is ZAKβ.

This approach can be used alongside biologically relevant information to identify and determine the direct downstream targets of ZAKβ, and shed light on its potential role in skeletal muscle.

By using this technique, we were able to identify many novel substrates of ZAKβ that suggest potential roles for ZAKβ other than in the classical MAPK signalling cascade. This leads us to propose that ZAKβ has a role in the modulation of z-disc and costameric-based protein adhesion complexes critical for muscle fibre maintenance.

6.2 Development of a direct phosphoproteomics assay

In an attempt to clarify what could be the major role of ZAKβ in skeletal muscle we performed a phosphoproteomics assay to identify direct targets of ZAKβ kinase activity (Figure 6.1A). For this, recombinant active ZAKβ was obtained from the Medical Research Council Protein Production Unit (MRC PPU), and tested for activity using an *in vitro* kinase assay with radioactively-labelled ATP (32P-γ-ATP) (Figure 6.1B; lane 5). Then, muscle extracts were treated with either 5'-4-fluorosulfonyl benzoyl adenosine (FSBA) dissolved in DMSO, or DMSO as control, to irreversibly inhibit all endogenous kinases. As an ATP analogue, FSBA covalently binds to a conserved lysine residue critical for catalytic function and occupies the ATP binding site. This irreversibly inhibits the kinase from interacting with ATP molecules and as a result, the kinase loses all activity. As FSBA is a potent inhibitor of all kinases, it must be sufficiently removed before the addition of the recombinant protein.

Skeletal muscle lysate treated with FSBA was desalted using either Thermofisher Zeba spin desalting column with a 7 kDa molecular weight cut-off (Figure 6.1C; lanes 1&2), or Millipore Amicon ultrafiltration columns with a 3 kDa molecular weight cut-off (Figure 6.1C; lanes 3&4) to remove all unbound FSBA inhibitor. Use of the Thermofisher Zeba spin column resulted in non-selective removal of many proteins within the 15-170 kDa range unlike that of the Millipore Amicon Ultrafiltration column. Therefore, the latter was used for desalting FSBA-inhibited skeletal muscle lysate going forward. Skeletal muscle lysate inhibited using FSBA, and subsequently desalted, was tested for endogenous kinase activity using an in vitro kinase assay (Figure 6.1B; lanes 1-3). Once the FSBA treatment proved effective at inhibiting all endogenous kinase activity, the kinase-dead skeletal muscle lysate was subject to a kinase assay using recombinant active ZAKβ kinase. This provided the evidence that treatment of kinase-dead skeletal muscle lysate with ZAKβ would be sufficient to phosphorylate downstream targets (Figure 6.1B; lane 4).

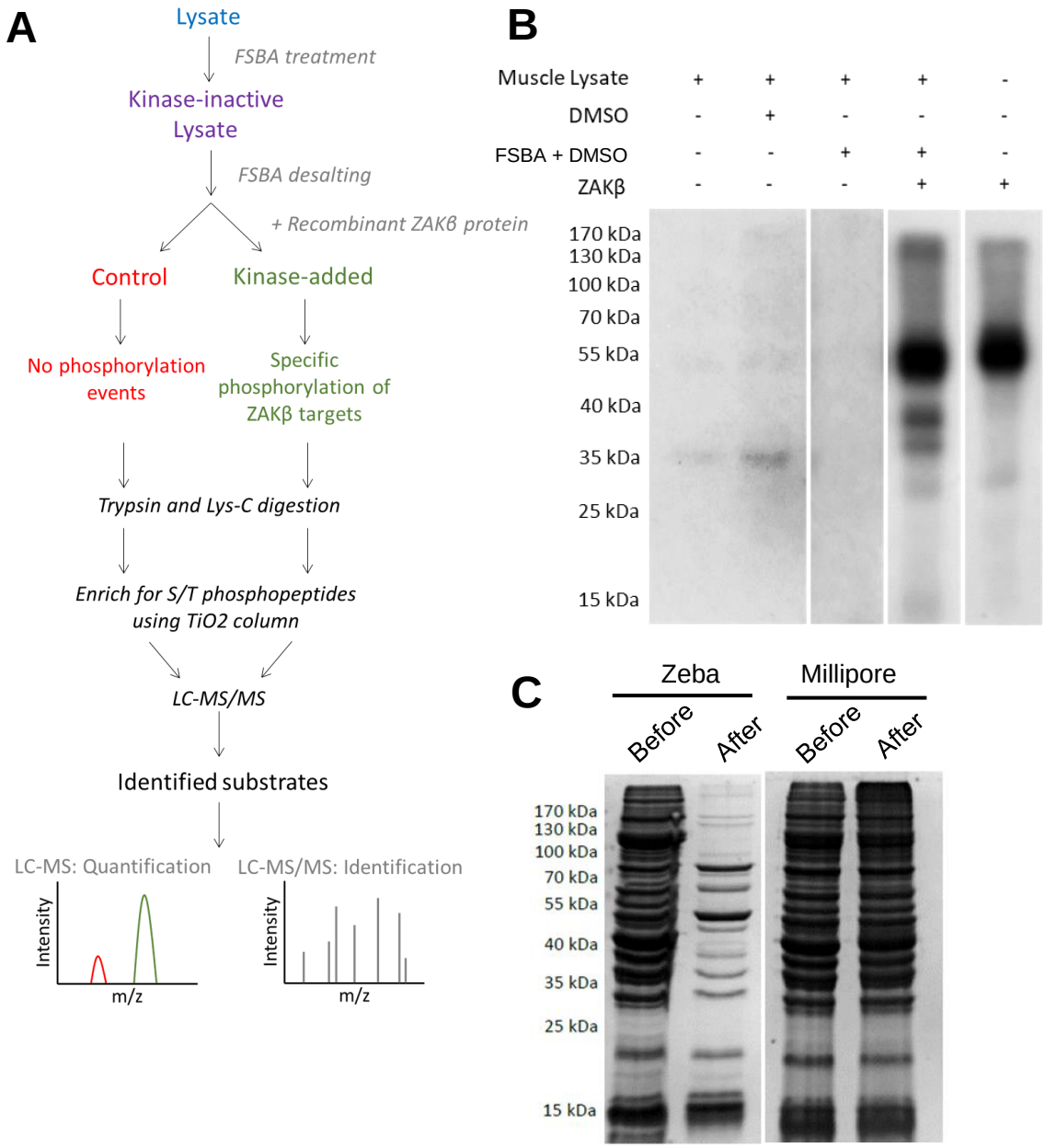

Figure 6.1: Whole cell lysate *ex vivo* kinase assay identifies direct ZAKβ substrates using LC-MS/MS. (A) Phosphoproteomics workflow utilising the inhibitor, 5'-4-fluorosulphonylbenzoyladenosine (FSBA). Control samples (red) used to assess background phosphorylation levels of phosphorylated proteins in the sample treated with recombinant ZAKβ (green). Workflow adapted from Knight et al. 2012. (B) Radioactive kinase assay used as a quality control step to assess kinase activity. Samples treated with 32P-γ-ATP were separated using an SDS-PAGE gel. Phosphorylated proteins detected using radiography film specific for the radioactively-labelled ATP. Skeletal muscle lysate (lane 1) was treated with either dimethyl sulphoxide (DMSO) (lane 2) or FSBA solubilised in DMSO (lane 3). Recombinant ZAKβ was added to skeletal muscle lysate treated with

FSBA and desalted using Thermofisher Zeba spin desalting 7K column, to assess the ability to phosphorylate its direct substrates (lane 4). As ZAKβ is a protein kinase which auto phosphorylate, activity of the recombinant ZAKβ protein was assayed (lane 5). (C) Mouse Tibialis Anterior skeletal muscle lysate treated with FSBA and desalted using either the Thermofisher Zeba spin desalting 7K column (LEFT) or the Millipore amicon 3K ultrafiltration column (RIGHT). Samples were assayed before and after desalting using SDS-PAGE separation, and then subjected to staining with Safeblue to determine relative protein concentration.

6.3 Use of a direct phosphoproteomics assay to identify direct downstream targets of ZAKβ

Following on from this, we used our FSBA-based phosphoproteomic assay to identify the immediate downstream targets of ZAKβ, whereby recombinant ZAKβ was added to a kinase-dead skeletal muscle lysate and subsequent phosphopeptides were detected by LC-MS/MS which was performed by Adam Dowle at the University of York Biology Technology Facility (see Materials and Methods 2.6.3 for details) (Figure 6.1A). The following criteria were applied to determine presence or absence in each treatment/control group: 1) Inclusion required protein identification probability of greater than 95% in at least three of five biological replicas; 2) Exclusion required protein identification probability of less than 95% in all five biological replicas. The phosphoproteomic assay alone yielded a list of 114 S/T phosphopeptides from 48 individual proteins presented in Table 6.1. This list is curated without ZAKβ autophosphosites as these can sometimes present with a different target sequence to those of downstream substrates. We detected five sites on ZAKβ that likely result from autophosphorylation (S58, S61, T226, S230, and S302). Of these, S302 has been shown to be differentially phosphorylated in tumours (Mertins *et al.*, 2014). Complete mass spectrometry data sets and proteomic identifications are available to download from MassIVE (MSV000090935), [doi:10.25345/C5TB0Z08V] and ProteomeXchange (PXD037832). GO-term enrichment analysis showed that genes associated with cytoskeletal constituents were highly represented using the GO-term of Molecular function with a P-value of 3.650E-5 (Table 6.2). It has been identified previously that ZAKβ is likely to be involved with regulation of actin dynamics (Christe et al., 2004)

and that ZAKβ is a z-disc protein (Figure 4.2) which interacts with cytoskeletal and structural components of the z-disc/costamere (Baker *et al.*, 2010).

Table 6.1: List of proteins identified as direct targets of recombinant ZAKβ.

Gene symbol	Gene/Protein
Ahnak	AHNAK nucleoprotein (desmoyokin)
Atp5f1a	Atp synthase, h+ transporting, mitochondrial f1 complex, alpha subunit 1
Bin1	Myc box-dependent-interacting protein 1;
Cavin2	aveolae-associated protein 2
Cavin4	Caveolae-associated protein 4
Chchd3	Coiled-coil-helix-coiled-coil-helix domain-containing protein 3
Ckm	Creatine kinase M-type
Ckmt2	Creatine kinase S-type
Clint1	Clathrin interactor 1
Cnpy2	Canopy FGF signalling regulator 2
Col1a2	Collagen alpha-2(I) chain
Cox6b1	Cytochrome c oxidase subunit 6B1
Eef2	Elongation factor 2
Endod1	Endonuclease domain-containing 1 protein
Eno3	Enolase 3
Etfb	Electron transfer flavoprotein subunit beta
Fhl1	Four and a half lim domains 1
Gapdh	Glyceraldehyde-3-phosphate dehydrogenase
Got2	Glutamatic-oxaloacetic transaminase 2
H2afv	H2A.Z histone variant 2
H2afz	H2A.Z variant histone 1
Hbb-b1	Hemoglobin, beta adult s chain
Hspd1	60 kDa heat shock protein
Kif5b	Kinesin-1 heavy chain
Ldhb	L-lactate dehydrogenase b chain
Map2k1	Dual specificity mitogen-activated protein kinase kinase 1
Mapt	Microtubule-associated protein tau
Mb	Myoglobin
Mbp	Myelin basic protein
Mmgt1	Membrane magnesium transporter 1
Myh1	Myosin, heavy polypeptide 1
Myh3	Myosin, heavy polypeptide 3
Mylpf	Myosin light chain, phosphorylatable, fast skeletal muscle
Pax1	Paired box protein Pax-1
Pax9	Paired box protein Pax-9
Pdlim5	Lim domain-binding protein 3; PDZ and LIM domain protein 5
Pgam2	2,3-bisphosphoglycerate-dependent phosphoglycerate mutase
Phf2	Lysine-specific demethylase
Prx	Periaxin
Synpo2	Synaptopodin-2

Tnks1bp1	Tankyrase 1 binding protein 1
Togaram2	TOG array regulator of axonemal microtubules protein 2
Ttn	Titin
Tuba1a	Tubulin alpha-1A chain
Tuba1b	Tubulin alpha-1B chain
Tuba3b	Tubulin alpha-3B chain
Tuba4a	Tubulin alpha-4A chain
Tubb3	Tubulin beta-3 chain

Table 6.2: List of GO:MF enriched pathways identified using the initial FSBA screen of direct ZAKβ targets.

GO:MF ID	Description	P-value
GO:0005200	Structural constituent of the cytoskeleton	3.650E-5
GO:0036094	Small molecule binding	4.893E-4
GO:0019899	Enzyme binding	1,296E-4

Supramolecular membrane assemblies represent a major biochemical feature of contractile fibres. As examples, they include the dystrophin-glycoprotein complex (DGC) of the sarcolemma and the abundant actomyosin machinery with its regulatory troponin-tropomyosin system. This complexity has been previously acknowledged in proteomics studies (for a review see Ohlendieck, 2011). Since we have focused on total extracts, our samples contain mostly soluble muscle proteins, which may have negatively affected the quantity of proteins identified in the initial FSBA experiment (Figure 6.1A). By leaving the insoluble fraction behind, only the direct soluble ZAKβ targets were identified by LC-MS/MS. To improve the resolution of the data, a position specific scoring matrix (PSSM) was generated from the 15-mer phosphopeptide sequences of the initial FSBA experiment (Figure 6.2B). By cross referencing the ZAKβ consensus sequence with the mouse proteome (Krystkowiak, Manguy and Davey, 2018), further putative ZAKβ targets were identified. From this, 1449 phosphopeptides from 1200 different proteins were identified (Figure 6.2). KEGG analysis of this extended list of putative direct ZAKβ targets demonstrated an enrichment of proteins involved with focal adhesion (p-value: 4.429E-5), ECM-receptor interactions (p-value: 1.022E-5), and cell adhesion molecules (p-value: 5.280E-5) (Table 6.3). These putative substrates have previously known associations with proteins already identified through interaction analyses of ZAKβ such as filamin C

(Beatham *et al.,* 2004; Baker *et al.,* 2010; Maruyama *et al.,* 2020), Four-and-a-half LIM domain Protein 1 (Baker *et al.,* 2010), IGFN1 (Baker *et al.,* 2010), AHNAK (Baker *et al.,* 2010), and COBL (Cracknell *et al.*, 2020). Moreover, this list of direct targets of ZAKβ include many components of z-disc/costameric protein complexes responsible for maintaining structural integrity of the sarcomere (Table 6.4), providing additional support that these targets are relevant and that their phosphorylation could be critical for myofibre function.

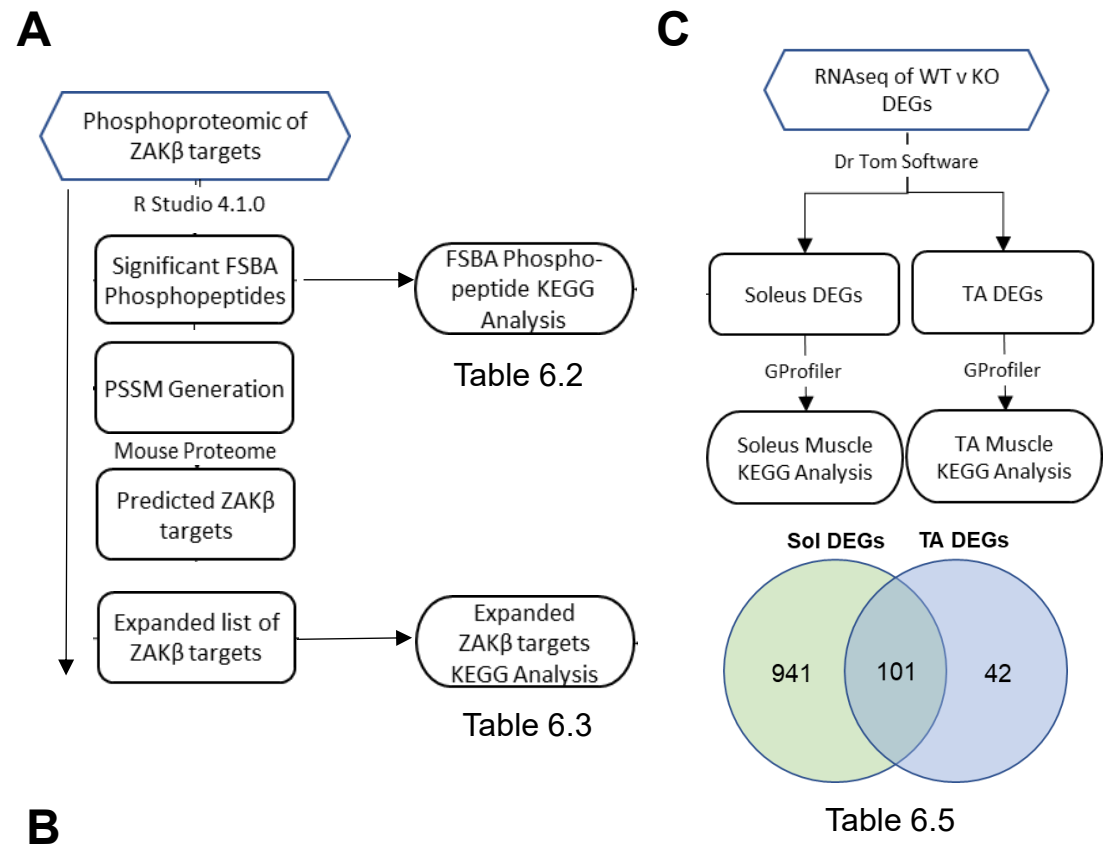

Figure 6.2: Extrapolation of FSBA phosphoproteomics using a position specific scoring matrix to identify additional novel ZAKβ targets plus cross-comparison with RNAseq data. (A) The experimental output from the initial phosphoproteomics identified 48

significant proteins suggested to be directly phosphorylated by ZAKβ (Table 6.1). (B) Using the specific phosphopeptide 15-mer sequences from these proteins, a PSSM was generated. As a consensus sequence for ZAKβ-targeted phosphorylation, this PSSM was cross-referenced against the mouse proteome to expand the list of putative ZAKβ targets (Table 6.3). This expansion yielded a further 1200 targets which were subject to KEGG analysis. (C) RNAseq data provided to us by the Bekker-Jensen lab, showing differentially expressed genes (DEGs) in both the soleus and TA muscles were subject to KEGG analyses (Table 6.5).

Table 6.3: List of KEGG pathways enriched in predicted ZAKβ targets.

KEGG Term ID	Description	P-value
KEGG:04510	Focal adhesion	4.429E-5
KEGG:04512	ECM-receptor interaction	1.022E-4
KEGG:04514	Cell adhesion molecules	5.280E-4

Table 6.4: Genes associated with cell adhesion and actin organisation identified as predicted ZAKβ targets.

Gene Symbol	Gene/Protein
Nexn	Nexillin
Synm	Synemin
Prx	Periaxin
Fhl1	Four-and-a-half LIM domain Protein 1
FLNA/B/C	Filamin A/B/C
IGFN1	Immunoglobulin-like and fibronectin type 3 domain containing 1
AHNAK	Neuroblast differentiation-associated protein; desmoyokin
Ank2	Ankyrin 2
Dmd	Dystrophin
Tjp1	Tight junction protein 1
Ttn	Titin

6.4 Pathological changes within ZAK$^{-/-}$ skeletal muscle

We next wanted to discern whether the putative targets identified using the ZAKβ consensus target sequence were physiologically relevant in vivo. RNAseq data provided by Simon Bekker-Jensen's lab in Denmark was analysed using Dr. Tom software, a powerful web-based tool for RNAseq analysis

(https://www.bgi.com/global/dr-tom/). Fastq RNA sequencing files were deposited in the NCBI BioProject database under accession code: PRJNA816072 (https://www.ncbi.nlm.nih.gov/bioproject/?term=PRJNA81607). These datasets included control and ZAK$^{-/-}$ muscle tissue from the pathological soleus and non-pathological tibialis anterior (TA). Differentially expressed genes (DEGs) datasets were compared and analysis revealed that the soleus muscle contained 1042 DEGs in comparison with 143 in the TA, with an overlap of 101 genes (Figure 6.2). Enrichment using GO: Biological processes of TA DEGs identified only proteins associated with cell adhesion. Similarly, the same analysis of the soleus DEGs revealed strong enrichment for genes associated with cell adhesion, amongst others (Table 6.5). As cell adhesion appears highly enriched in both the TA and soleus muscle DEGs, this suggests that the other genes enriched in the soleus muscle are likely primarily involved in the pathology of the soleus muscle as they are not found differentially expressed in the non-pathological TA. This suggests that cell adhesion plays a role in the pathology attributed to the loss of ZAK, but is exacerbated in muscles of a slow profile. Taken together, these data appear to show that ZAKβ modulates components of the z-disc and costameric protein complexes which we find are deregulated in the ZAK-KO mouse model.

Table 6.5: List of GO:BP enriched pathways identified using the differentially expressed genes between control and ZAK-KO soleus muscle.

GO:BP ID	Description	P-value
GO:0051239	Regulation of multicellular organismal process	3.68E-26
GO:0030334	Regulation of cell migration	8.13E-21
GO:0051241	Negative regulation of multicellular organismal process	1.07E-20
GO:2000145	Regulation of cell motility	1.19E-19
GO:0040012	Regulation of locomotion	6.37E-19
GO:0051270	Regulation of cellular component movement	7.86E-19
GO:0007155	Cell adhesion	1.95E-17
GO:0022510	Biological adhesion	2.28E-17

6.5 Validation of ZAKβ phospho-targets

IGFN1 is a z-disc protein of unknown function with repeats of globular domains similar to many other sarcomeric proteins. It is thought that IGFN1 interacts both with ZAKβ (Baker *et al.*, 2010) and the actin nucleating protein COBL (Cracknell *et al.*, 2020) at the z-disc. As a result of this investigation, it appears as though COBL is a direct downstream target of ZAKβ phosphorylation. It is therefore plausible that using IGFN1 as a scaffold protein, ZAKβ modulates the activity of COBL via phosphorylation and that in the absence of ZAK, inadequate actin remodelling results in weaker muscle fibres. Previously, it was discovered that COS7 cells overexpressing COBL exhibit large membrane accumulations of polymerised actin, termed hereafter as actin "ruffles" (Ahuja *et al.*, 2007). To test this, we first transfected COS7 cells with COBL and detected the formation of ruffles as previously described (Cracknell *et al.*, 2020). This provides a convenient readout to test the ability of ZAKβ to modulate COBL activity (Figure 6.3A&B; white arrows). While COBL ruffles were abolished in cells transfected with both ZAKβ and COBL, transfection with GFP instead failed to have the same effect (Figure 6.3C). This suggests that ZAKβ modulates the activity of COBL via phosphorylation, as suggested by the phosphoproteomics assay.

We next wanted to investigate whether the expression of COBL was influenced by ZAKβ. To do so, we generated day 14-differentiated C2C12 cell protein lysate from control, COBL-KO (KO23), and $ZAK^{-/-}$ KOD9 and KOC10 cell lines. We were unable to test skeletal muscle for COBL expression due skeletal muscle lysate due to issues extracting COBL in the lysate with confidence. The C2C12 cell lysate was then subject to Western blot for the identification of COBL protein (Figure 6.3D). Here we identified the expected COBL band as seen for WT C2C12s was missing in both cell lines lacking ZAK. This suggests that ZAK may have a role in the stabilisation of COBL. Further analysis is necessary to identify if this is the same *in vivo*.

In addition to COBL, IGFN1 has also previously been shown to interact with both KY and Filamin C (FLNC) in what was called the "KY protein complex", at the z-disc (Beatham *et al.*, 2004; Baker *et al.*, 2010). FLNC was further identified as a direct target of ZAKβ in the targeted phosphoproteomic screen and turnover of FLNC has been found to be disrupted in the soleus muscle of *ky/ky* mice (Beatham *et al.,* 2004). Considering this information, FLNC emerged as an interesting target to look at further in $ZAK^{-/-}$ tissue.

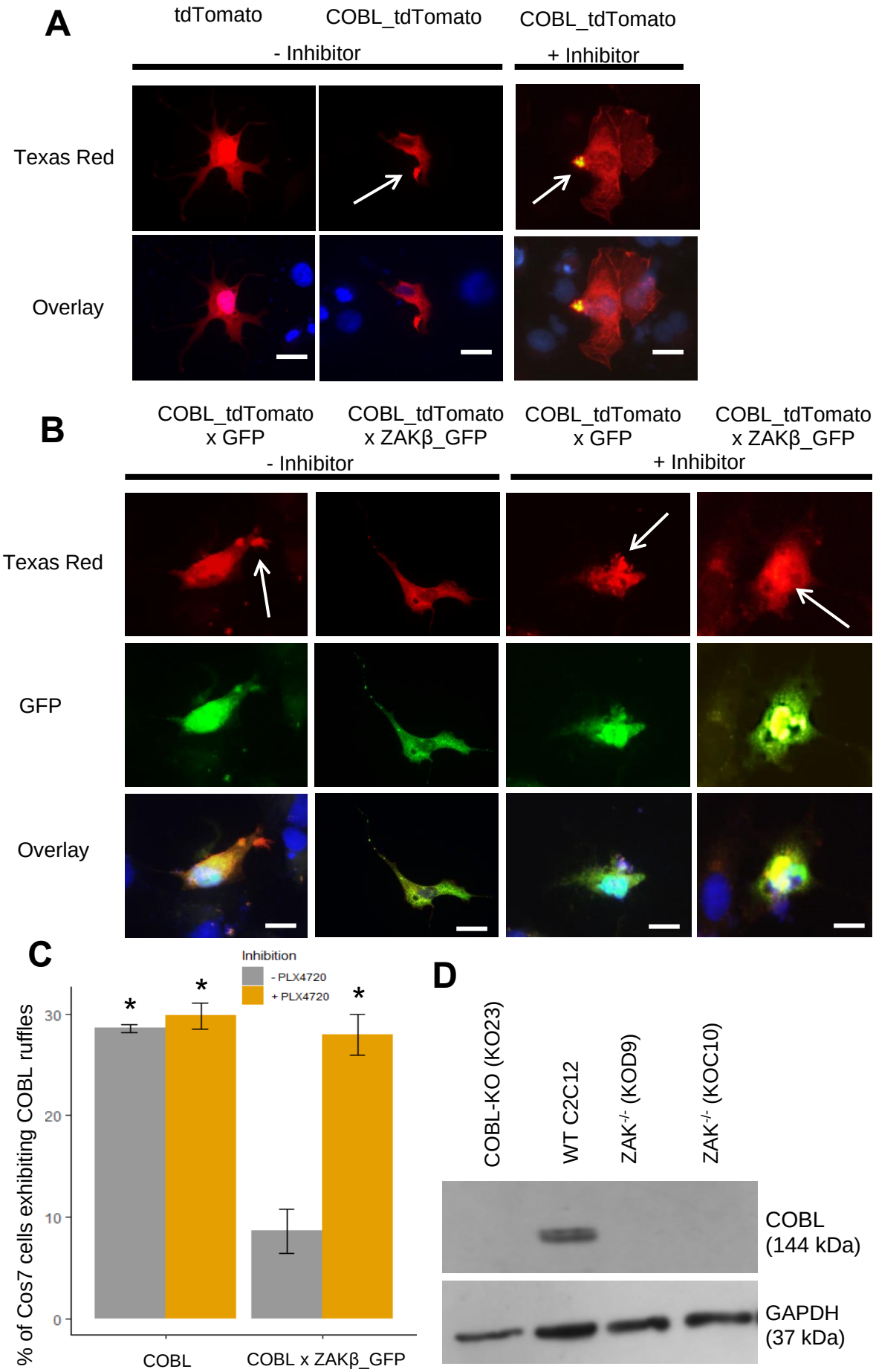
A
tdTomato
COBL_tdTomato
COBL_tdTomato
- Inhibitor
+ Inhibitor
Texas Red
Overlay
B
COBL_tdTomato x GFP
COBL_tdTomato x ZAKβ_GFP
COBL_tdTomato x GFP
COBL_tdTomato x ZAKβ_GFP
- Inhibitor
+ Inhibitor
Texas Red
GFP
Overlay
C
Inhibition
- PLX4720
+ PLX4720
% of Cos7 cells exhibiting COBL ruffles
0
10
20
30
COBL
COBL x ZAKβ_GFP
D
COBL-KO (KO23)
WT C2C12
ZAK-/- (KOD9)
ZAK-/- (KOC10)
COBL (144 kDa)
GAPDH (37 kDa)

Figure 6.3: ZAKβ inhibits COBL-mediated ruffle formation in COS7 cells. (A) Representative images of COS7 cells co-transfected with pDEST47-COBL-tdTomato or tdTomato in the presence/absence of ZAK inhibitor, PLX4720. Arrow indicates the presence of actin ruffles. Scale bar = 25 µm. (B) Representative images of COS7 cells co-transfected with pDEST47-COBL-tdTomato, GFP, or pDEST47-ZAKβ-GFP in the presence/absence of ZAK inhibitor, PLX4720. Arrow indicates the presence of actin ruffles. Scale bar = 25 µm. (C) Analysis and quantification of the presence of membrane ruffles in COS7 cells transfected with pDEST47-COBL-tdTomato, GFP, or pDEST47-ZAKβ-GFP. Cells co-transfected with ZAKβ-GFP and COBL-tdTomato displayed significantly fewer ruffles compared to cells co-transfected with GFP and COBL-tdTomato. (* = $p<0.01$; One way ANOVA with Bonferroni post hoc test). Error bars = mean +/- Standard Error (n=4, minimum 20 cells per replicate). (D) Western blot showing the expression of COBL across COBL KO C2C12 cell line (KO23), WT C2C12 cell line, and two ZAK KO C2C12 cell lines (KOD9 & KOC10). Loading assessed via GAPDH.

The actin-crosslinking protein FLNC ordinarily becomes damaged throughout repeated bouts of muscle contraction (Wackerhage *et al.*, 2019). The myofibre resolves this by upregulating protein breakdown of damaged FLNC and synthesis of new functional FLNC protein which is integral for muscle hypertrophy (Wackerhage *et al.*, 2019; Martin *et al.*, 2021). In cases of muscle myopathies, an imbalance in protein turnover results in an increase in damaged proteins and muscle atrophy (Sandri, 2013). The KY mutation results in a myofibrillar myopathy, which is characterised by a progressive disintegration of muscle fibres and formation of protein aggregates (Blanco *et al.*, 2004; Kley *et al.*, 2013; Straussberg *et al.*, 2016). The presence of FLNC aggregates is considered a hallmark of myofibrillar myopathies and is observed with KY-associated myofibrillar myopathy (Straussberg *et al.*, 2016). ZAKβ is a protein associated with z-disc proteins like KY and FLNC, both of which are known to cause myofibrillar myopathies when mutated. The pathology of the ZAKβ-associated myopathy observed here appeared to be a milder version of the KY-associated myopathy. In addition to being abnormally distributed in KY-deficient myofibres, FLNC was identified as a putative phosphorylation target of ZAKβ. An investigation was launched to determine whether FLNC expression was abnormal in muscles of $ZAK^{-/-}$ mice. Immunofluorescence using an antibody against FLNC was performed on soleus

muscle cross sections of control and ZAK$^{-/-}$ mice of both males and females at both 8 and 22 weeks-old to visualise FLNC distribution *in vivo* (Figure 6.4A).

FLNC immunostaining showed increased reactivity in some fibres in the ZAK$^{-/-}$ soleus muscle for both 8 week and 22 week male and female mice (Figure 6.4A; white arrows). Observation of FLNC aggregates within the muscle fibres of ZAK$^{-/-}$ mice does suggest that there is an accumulation of FLNC which is not localised to the z-disc where it is normally located, moreover it is indicative of inefficient turnover of damaged protein.

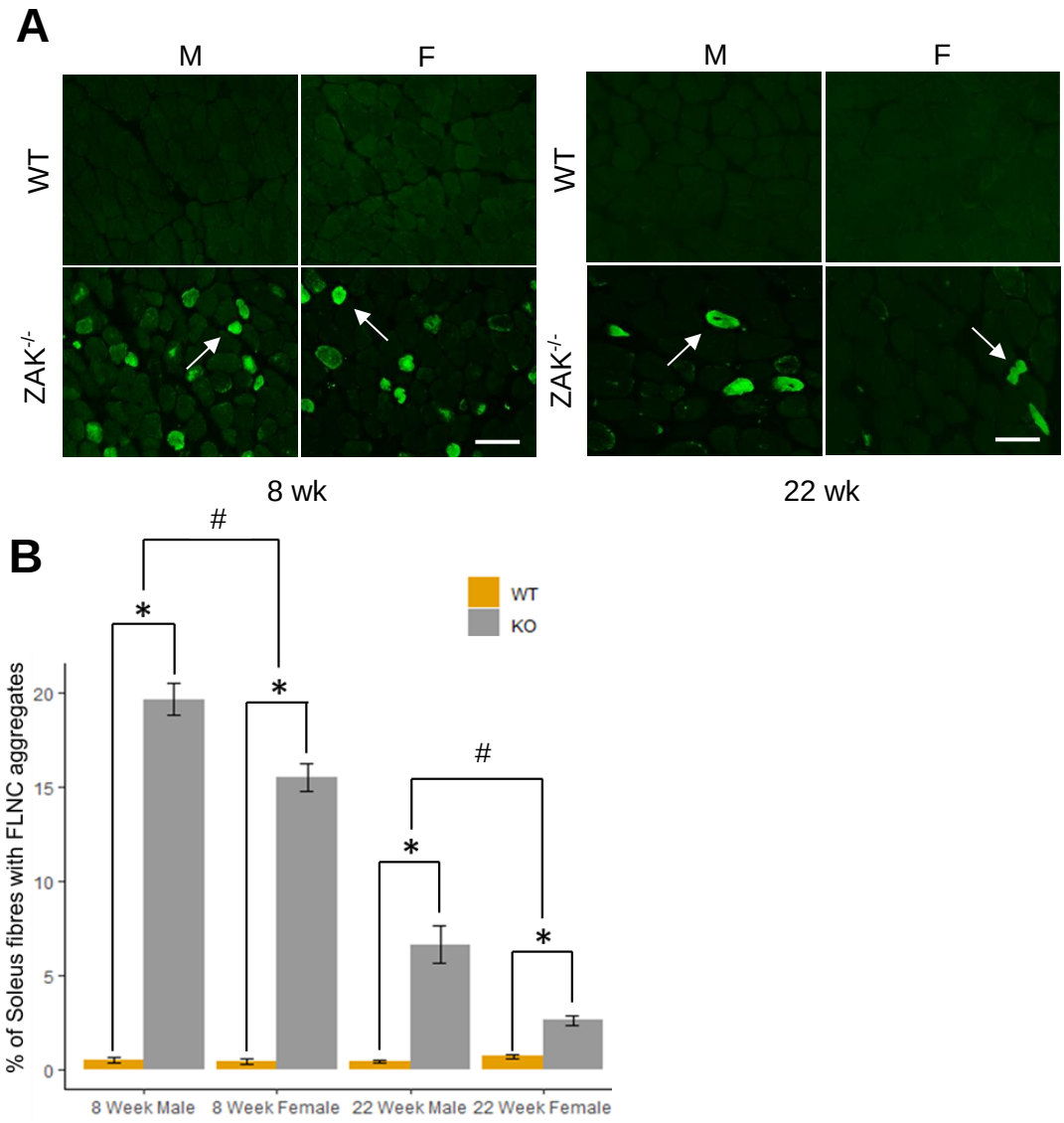

Figure 6.4: ZAK LOF impedes efficient turnover of actin crosslinking protein, FLNC. (A) Immunofluorescence images of Soleus muscle cross sections of 8 and 22-week-old male and female, control and ZAK$^{-/-}$ mice stained with anti-FLNC (RR90). FLNC aggregation is observed only in the ZAK$^{-/-}$ mouse (white arrows) Scale bar represents 100 µm. (B)

Quantification of the percentage of soleus muscle fibres exhibiting FLNC aggregations suggests that the loss of ZAKβ causes intracellular accumulation of FLNC at both 8 and 22 weeks, a hallmark of myofibrillar myopathy (n=3). One way ANOVA; (*p < 0.05). FLNC aggregates were observed to significantly decrease with age and sex. One way ANOVA; (*)p < 0.05 between genotypes, (#)p < 0.05 between sexes). Coverage of entire soleus muscle. Error bars = +/- standard error.

Interestingly, as the mice age, there appears to be a significant reduction in the percentage of fibres exhibiting FLNC aggregates (Figure 6.4B). This suggests that the vulnerability within the muscle is resolved over time and that the fibre may become progressively more capable of successful protein turnover. Additionally, this reduction in FLNC aggregation is also consistent between males and females at both timepoints, as females appear to exhibit fewer FLNC aggregates than their male counterparts at both 8 and 22 weeks of age (Figure 6.4B). This further suggests that males are more susceptible to the loss of ZAK than females, exhibited by the exacerbation of the pathological effects observed in the ZAK mutant.

Damaged FLNC is a target of the BAG3-mediated chaperone assisted selective autophagy (CASA) pathway and accumulations of FLNC are known to indicate the presence of pathology and inefficient protein turnover via the BAG3-mediated CASA pathway (Leber *et al.*, 2016; Ruparelia *et al.*, 2016). We therefore wanted to determine whether or not the accumulation of FLNC in soleus muscle was a consequence of impaired BAG3-mediated protein turnover via CASA. To do so, both soleus and TA muscle cross-sections were immunostained with antibodies against both FLNC and BAG3 (Figure 6.5). We had already established the presence of FLNC aggregates in soleus muscle (Figure 6.4). When co-stained for BAG3 in these same muscle sections, we observed high levels of co-localisation between the pre-established FLNC aggregates and the newly-identified BAG3 aggregates in the soleus (Figure 6.5A). On the contrary, TA muscle cross sections did not show any presence of FLNC or BAG3 aggregates. Some aberrant FLNC/BAG3 staining was observed in the $ZAK^{-/-}$ whereby the seemingly ringed fibres were only present in the WT.

This suggests that once again, slow twitch muscle like the soleus is inherently more vulnerable to the loss of ZAK than that of fast twitch muscle like the TA. As FLNC is a known target for BAG3-mediated protein breakdown (Ulbricht *et al.*, 2013), the

presence of both FLNC and BAG3 aggregates in soleus muscle cross-sections is indicative of an impairment to CASA-specific protein turnover.

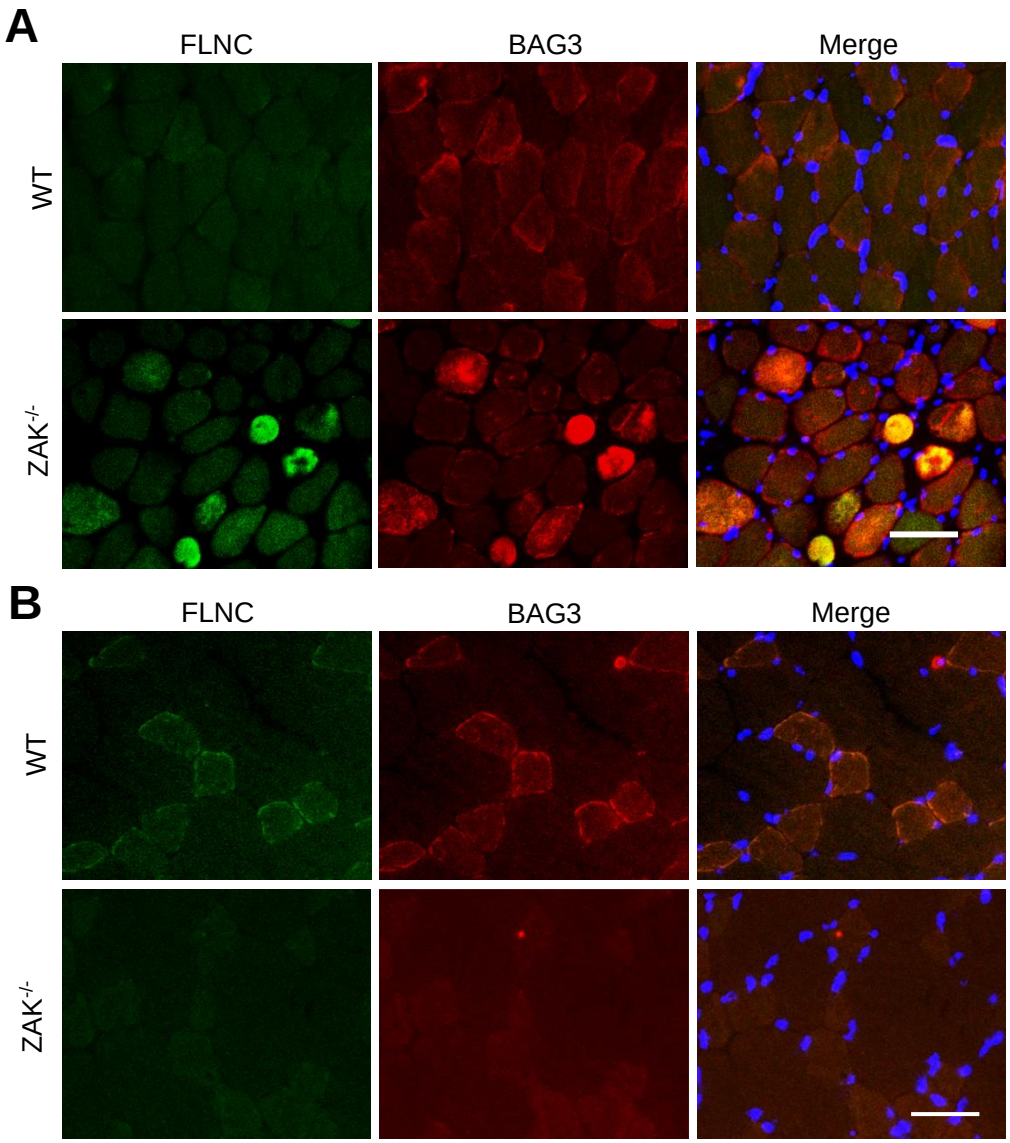

Figure 6.5: ZAK results in accumulation and co-localisation of both the CASA-associated proteins, BAG3 and FLNC. (A) Representative immunofluorescence images of FLNC/BAG3 co-localisation in 8-week WT and ZAK$^{-/-}$ soleus muscle. (B) Representative immunofluorescence images of TA muscle cross sections of 8-week-old WT and ZAK$^{-/-}$ female mice stained with anti-FLNC (RR90) and anti-BAG3. Comparisons of soleus and TA muscles suggest that loss of ZAK results in a pathology more evident in slow-type muscle. Scale bar represents 100 µm. Coverage of entire TA muscle. Independent t-test; (*$p < 0.05$).

The observations above suggest that ZAKβ may have a role in protein turnover through the CASA mechanism. Alternatively, ZAKβ may have a role in stabilising costameric complexes, leading the accumulation of damaged crosslinking proteins such as FLNC in the absence of ZAKβ.

6.6 ZAK patients exhibit abnormal aggregations of myofibrillar myopathy markers

Phenotypic analyses of the $ZAK^{-/-}$ mouse revealed a high similarity in disease pathology with the ZAK patient (Vasli *et al.,* 2017). The disease pathology in the $ZAK^{-/-}$ mouse suggests that aggregates of damaged FLNC in conjunction with abnormal localisation of the CASA-associated co-chaperone BAG3 are caused by aberrant protein turnover. As the $ZAK^{-/-}$ mouse is purely a model for the human myopathy, we wanted to determine whether the ZAK-associated human myopathy involves aberrant expression of z-disc proteins. To test the relevance of the findings above in the ultra-rare recessive human condition associated with ZAK-deficiency, we analysed a biopsy sample from a previously described congenital myopathy patient (Vasli *et al.,* 2017). This patient carries a truncating variant in the ZAK gene in homozygosity (c.490?491delAT, p.Met164fs*24, using reference sequence NM_133646) (Vasli *et al.,* 2017).

We first looked at FLNC as this was a protein which interacts with the KY protein complex, accumulates in mouse soleus muscle (Figure 6.6A), and is thought to be phosphorylated downstream of ZAKβ. After staining for FLNC, we found a handful of myofibres with an abnormal expression pattern of FLNC, similar to the phenotype of the $ZAK^{-/-}$ mouse. Such aggregates were not observed in the control and were thought to be an accumulation of damaged FLNC.

We next wanted to identify whether the abnormal FLNC was being targeted for degradation. We did this by counterstaining for BAG3, a co-chaperone in the CASA mechanism (Figure 6.6B). Here we saw colocalisation between the abnormal FLNC aggregates and that of BAG3, suggesting the damaged FLNC was being targeted for degradation via BAG3-mediated CASA.

As a hallmark of myofibrillar myopathies (Sandri, 2013), damaged myotilin is a large z-disc protein often found contained within protein aggregates (Selcen, 2008; Can *et al.*, 2014; Fichna, *et al.*, 2018).

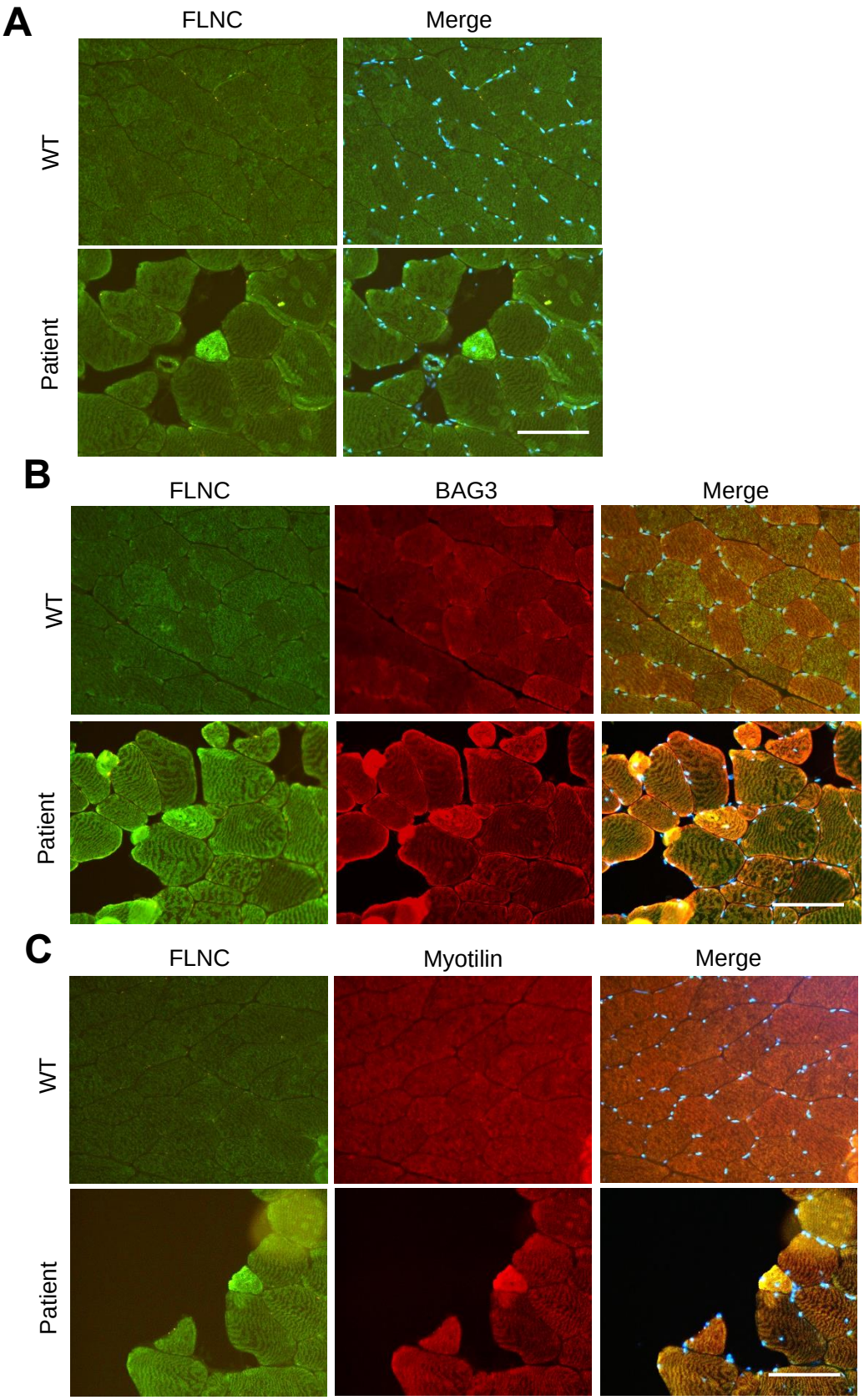
A
FLNC
Merge
WT
Patient
B
FLNC
BAG3
Merge
WT
Patient
C
FLNC
Myotilin
Merge
WT
Patient

Figure 6.6: ZAK patient exhibits abnormal aggregations of FLNC, BAG3, and Myotilin. (A) Skeletal muscle biopsies from control and patients IF stained with anti-FLNC (RR90). FLNC aggregation is observed only in the patient (white arrow) Scale bar represents 250 μm. (B) Skeletal muscle biopsies from control and patients IF stained with anti-FLNC (RR90) and BAG3 (10599-1-AP; Proteintech). FLNC and BAG3 colocalise only in the patient (white arrow) Scale bar represents 250 μm. (C) Skeletal muscle biopsies from control and patients IF stained with anti-FLNC (RR90) and Myotilin (RS034; Novocastra). FLNC and myotilin colocalise only in the patient (white arrow). Skeletal muscle biopsies obtained from patients included in Vasli *et al.,* 2017, and sectioned by Norma Romero from the Institute of Myology in Paris. Scale bar represents 250 μm.

We next wanted to ascertain whether the protein aggregates containing FLNC also contained other markers of myofibrillar myopathies. We did so by counter staining with myotilin (Figure 6.6C). From this we observed colocalization between ZAK and myotilin within the protein aggregates which was suggestive of two possible things. Like with the mice, ZAK may be important for the turnover of large z-disc proteins like FLNC and myotilin, or it has an important role in the initial stabilisation of these proteins.

6.7 Discussion

6.7.1 ZAKβ and the Costamere

From the mouse characterisations, we were unable to discern an obvious role for ZAKβ, nor its mechanism of action. We conducted a direct phosphoproteomic assay with the intention of identifying putative immediate downstream phosphorylation targets of ZAKβ (Figure 6.1A; 6.2). Mining of this data, in combination with data collected from RNAseq analysis of differentially expressed genes (DEGs) between the wild-type (WT) and $ZAK^{-/-}$ mouse, has allowed us to further understand what is seemingly an elusive role for ZAKβ in the maintenance of skeletal muscle.

Our phosphoproteomics data suggest that genes involved in cell adhesion, amongst other processes, are putative targets of ZAKβ phosphorylation (Table 6.2). In conjunction with this, the RNAseq data of DEGs deregulated in the $ZAK^{-/-}$ mouse suggests that in both the non-pathological Tibialis anterior (TA) and pathological soleus, the loss of ZAKβ significantly affects the expression of genes that regulate cell adhesion and actin organisation (Table 6.4), further evidenced by the effect of ZAKβ

on the ability of the actin nucleator COBL to mediate actin ruffle formation (Figure 6.3). A possibility is that when ZAK is not present in skeletal muscle, the expression of proteins that ZAKβ may directly phosphorylate is deregulated. These proteins are those that we observe in both the phosphoproteomics data and the DEGs within the soleus.

At a glance, many of the putative ZAKβ downstream targets form adhesion and structural complexes at the costamere/z-disc such as ankyrin, dystrophin, filamin, nexilin, and titin. The costamere is vitally important for skeletal muscle integrity as it provides the mechanical link between the extracellular matrix and the force-producing area of the sarcomere, acto-myosin complex anchored to the z-disc (Craig and Pardo, 1983; Pardo and Siliciano, 1983). Costameres were first identified using the canonical focal adhesion protein, vinculin, which was proposed to aid the anchorage of the Z-disc to the plasma membrane (Craig and Pardo, 1983; Pardo and Siliciano, 1983). Since then, many more proteins have been identified as components of the costameric complex, such as talin (Zemljic-Harpf, Manso and Ross, 2009), α-actinin (Wachsstock, Wilkins and Lin, 1987), paxillin (Quach and Rando, 2006), integrin (Patel and Lieber, 1997), and dystrophin (Porter *et al.*, 1992). The functional importance of costameres to skeletal muscle integrity has been highlighted in recent years through investigations into the genetic causes of certain myopathies and muscular dystrophies caused by loss of function of costameric proteins (Matsumura and Campbell, 1994; Cohn and Campbell, 2000; Blake *et al.*, 2002). One of the most well-recognised of these conditions is Duchenne muscular dystrophy (DMD), whereby mutations in the dystrophin gene lead to abnormal and insufficient mechanotransduction in the skeletal muscle of patients (Porter *et al.*, 1992; Kumar *et al.*, 2004). The resulting dystrophy is life-limiting and severely debilitating. Interestingly, dystrophin was identified as a putative target of ZAKβ.

Further evidence of the interaction of ZAKβ with costameric protein complexes was identified very recently when ZAK demonstrated to negatively regulate cancer cell extrusion in RasV12-transformed cells by modulating the activity of Paxillin, Myosin, and Filamin (Maruyama *et al.*, 2020). In this study, ZAK was shown to be a key regulator in cell competition between normal and RasV12-transformed cells of the pancreatic membrane by negatively regulating the activity and localisation of

downstream regulators: Paxillin, Myosin, and Filamin. This study however was unable to discern the exact substrates of ZAK to elicit these effects (Maruyama *et al.*, 2020). Nevertheless, this further supports the idea that ZAKβ may act as a modulator of components important for costameric structure and signal transduction.

Another potential target of ZAKβ is α7 integrin, which was found as a direct phosphorylation target of ZAKβ and also differentially expressed in the ZAK patient. The α7 integrin isoform is the most common isoform in skeletal muscle (Collo, Starr and Quaranta, 1993). It usually heterodimerises with the β1 isoform (Belkin *et al.*, 1997), the resultant transmembrane receptor has an extremely important role in cell adhesion at the costamere (Huveneers and Danen, 2009). Particularly, α7 integrin mutations have been associated with congenital myopathies (Hayashi *et al.*, 1998). Hereby we suggest a mechanism for ZAKβ as an activator of α7 integrin upon detection of stress, and thus critical for their interaction with other associated proteins, such as Focal adhesion kinase (FAK) (Graham, Gallagher and Cardozo, 2015) leading to increased protein synthesis and myofiber hypertrophy via mTOR. Costameres are thought to be involved in the generation of the hypertrophic response (Li *et al.*, 2013). Phosphorylation of FAK is known to induce skeletal muscle hypertrophic signalling through Akt/mTOR, ERK1/2, and JNK (Nadruz *et al.*, 2005; Graham, Gallagher and Cardozo, 2015). Both the overexpression of α7 integrin and FAK respectively are known to induce muscle hypertrophy in vivo (Franchini, Clemente and Marin, 2009; Zou *et al.*, 2011; Graham, Gallagher and Cardozo, 2015). Similarly, I have shown that overexpression of ZAKβ *in vivo* increases skeletal muscle fibre cross-sectional area (Figure 5.3). Supporting this data, we have observed muscle atrophy in the soleus muscle of the $ZAK^{-/-}$ mouse (Figure 3.3) in accordance with muscle atrophy in the $ZAK^{-/-}$ human (Vasli *et al.*, 2017). This suggests that ZAKβ may have a role in supporting the normal function of the costamere and disruption of the complexes found here may affect the typical hypertrophic signalling networks initiated upon detection of mechanical stress.

Interestingly, it appears as though the atrophy observed in the soleus is not observed in the TA muscle. This suggests that the muscle vulnerability is not a global issue, instead it appears to be determined by the intrinsic functions of the muscles themselves. We have determined previously that the soleus muscle exhibits a fibre-type shift and expresses a predominance of slow-myosin heavy chain isoforms (Figure

3.4). It is hypothesised that this is a result of the tonically active muscle adapting to constant stress by becoming more oxidative and fatigue-resistant (Herbison *et al.*, 1982). Remarkably, costamere protein composition varies in different fibre types (Shear and Bloch, 1985; Bozyczko *et al.*, 1989; Flück *et al.*, 2002). Due to their physiologically critical role in maintenance of myofibrillar attachment at the z-disc (Pardo and Siliciano, 1983), costamere component regulation is thought to reflect the necessary cytoskeletal remodelling and fibre-type adaptation that accompanies differential load mechanosensing of myofibrillar stress (Schiaffino and Reggiani, 2011; Li *et al.*, 2013). This may explain the phenotypic differences between the slow-type soleus, and the faster-type muscle of the TA, and also why we may observe an amelioration in the presence of FLNC aggregates as the $ZAK^{-/-}$ mice age and become more fatigue-resistant (Figure 6.4).

6.7.2 ZAKβ and the KY Protein complex

The history of ZAKβ sees it identified by independent research groups as a MAP3K (Gross *et al.*, 2002; Tosti *et al.*, 2004) that interacts with IGFN1, a member of the KY protein complex, located at the z-disc in fully differentiated skeletal muscle (Beatham *et al.*, 2004; Baker *et al.*, 2010). Our phosphoproteomic data has revealed FLNC, another protein associated with the KY protein complex (Beatham *et al.*, 2004; Baker *et al.*, 2010), as a putative phosphorylation target of ZAKβ. This would suggest that ZAKβ has a role in the functionality of these proteins. It has previously been observed that loss of function of KY results in a pathological mutation in both humans and mice (Blanco *et al.*, 2001, 2004; Straussberg *et al.*, 2016). Interestingly, the upregulation of ZAKβ in the EDL muscle of the ky/ky mouse suggests a potential role for ZAKβ upstream of KY. The role of ZAKβ has yet to be determined, however one possibility is that ZAKβ signalling is mediated by KY at the z-disc. This may explain why, when KY is not present, levels of ZAKβ mRNA may be upregulated (Blanco *et al.*, 2004). This altogether provides a further functional connection between the ZAKβ and the KY protein complex.

Analysis of DEGs upregulated in the absence of ZAK in humans revealed that levels of IGFN1 are 5-times higher in one of the ZAK-deficient human patients, further supporting the hypothesis that ZAKβ is involved in regulating components of the KY protein complex (Vasli *et al.*, 2017). The splice variant of IGFN1, IGFN1_v1, is critical for C2C12 myoblast differentiation and fusion *in vitro* (Li *et al.*, 2017). In conjunction

with focal adhesion-associated downstream phosphorylation targets of ZAKβ, this links the two interacting proteins of IGFN1 and ZAKβ with a role in modulation of adhesion complexes. Additionally, not only is Filamin C a predicted target of ZAKβ, but aggregates of FLNC were observed in both the ky/ky and ZAK$^{-/-}$ mouse soleus muscles (Figure 6.4, Jokl *et al.*, 2018).

Thanks to the yeast-2-hybrid screens of both KY and IGFN1, and further functional analyses, we know that ZAKβ is associated with KY, IGFN1, and FLNC as the KY protein complex at the z-disc (Beatham *et al.*, 2004; Baker *et al.*, 2010). Loss of function of KY results in a moderately severe pathology in mice and humans, with increased damage of structural proteins integral for z-disc and costameric stability, subsequent loss of functionality of these proteins, and consequential muscle weakness (Blanco *et al.*, 2001, 2004; Straussberg *et al.*, 2016). Loss of IGFN1 *in vitro* has been shown to impede normal fusion and differentiation processes critical during early myogenesis (Li *et al.*, 2017). Furthermore, mutations within the Filamin C gene result in filaminopathies which result in accumulations of misfolded FLNC protein and subsequent muscle weakness and pathology (Kley *et al.*, 2013). Unsurprisingly, these key players in the KY protein complex all appear to share a similar functionality to that of ZAKβ.

C2C12 cells lacking functional IGFN1 display fusion and differentiation defects and were partially rescued with the reintroduction of IGFN1_V1 overexpression (Li et al., 2017). As myoblast fusion still occurs in the IGFN1-KO cell line, it is plausible that IGFN1 is a contributing factor of myoblast fusion however not an essential component. Instead, IGFN1 is perhaps a scaffold for interacting protein partners to bind during mechanical tension. IGNF1 and actin were determined to be interacting partners in the Y2H assay (Baker *et al.*, 2010). This supports the observation in IGFN1-KO myoblasts which sees a difference in globular (G) to filamentous (F) actin ratios (Cracknell *et al.*, 2020). LC-MS/MS was used to identify protein interacting targets of IGFN1 in a pull-down assay. This revealed the actin nucleating protein cordon bleu (COBL) as a interacting protein of interest (Cracknell *et al.*, 2020). This interaction is thought to facilitate the role of IGFN1 in actin remodelling and may explain the increase in G:F actin ratios in IGFN1-KO C2C12 myoblasts. Additionally, IGFN1 has been shown to interact with ZAKβ (Baker *et al.*, 2010), and Eukaryotic translation elongation factor 1A (eEF1A) (Mansilla *et al.*, 2008). The identification of COBL and BAG3 as direct substrates of ZAKβ was very exciting, following their previous associations with IGFN1

and KY respectively. As an actin nucleator, COBL has been shown to be critical for polymerisation of actin at focal adhesions and neuronal cell protrusions (Ahuja *et al.*, 2007). BAG3 has also been reported to regulate the actin cytoskeleton, and control cell motility and cell adhesion via Rac activity, in addition to interacting with PDZGEF2 to regulate integrin-mediated cell adhesion (Iwasaki *et al.*, 2007, 2010). Altogether, this enhances the credibility that these proteins are all key players in the same pathways that overall govern the integrity of significant structural players as well as on the ability to adapt their protein turnover to the actual physiological demands.

Here, we suggest that these proteins are intrinsically linked through established interaction networks and all localise to the z-disc, the hub of mechanosensation and transduction, with close proximity to costameric protein complexes. From these data, in conjunction with previous studies, emerges a compelling relationship between ZAKβ, KY, IGFN1, and FLNC as transducers of the stress response and regulators of skeletal muscle maintenance through cell adhesion signalling networks and BAG3-mediated protein turnover.

6.7.3 ZAKβ and FLNC turnover

The relationship between autophagy and muscle integrity is complex, with the de-regulation of autophagy contributing to myopathy in different contexts (Jokl and Blanco, 2016). The KY mutation results in an increase in the level of BAG3, although the mechanism remains unclear (Jokl *et al.*, 2018). The KY mutation results in a myofibrillar myopathy, which is characterised by a progressive disintegration of muscle fibres and formation of protein aggregates (Kley *et al.*, 2013; Straussberg *et al.*, 2016). Filamin C is a target of the BAG3-mediated chaperone assisted selective autophagy (CASA) pathway, and accumulations of FLNC are known to indicate inefficient protein turnover via the BAG3-mediated CASA pathway (Leber *et al.*, 2016; Ruparelia *et al.*, 2016). We have shown that in slow twitch muscle, like the soleus, that damaged FLNC co-localises with BAG3, a co-chaperone within the CASA protein degradation pathway. Ordinarily, this process would result in full breakdown of the entire protein complex involving BAG3 and other proteins like SYNPO2, HSC70, HSPB8, CHIP, and p62. Instead we observe an accumulation of BAG3 colocalising with FLNC (Figure 6.5). We also know that the expression of SYNPO2 is 2.5-times higher in biopsies of a ZAK patient than in a control (Vasli *et al.*, 2017). This suggests a muscle-specific impairment within the mechanism of protein turnover when ZAKβ is lost.

In summary, we have generated a non-exhaustive list of potential targets of ZAKβ phosphorylation in addition to cross-referencing this with the list of DEGs in the $ZAK^{-/-}$ mouse. From this, and that of the DEGs in the $ZAK^{-/-}$ human patients, we reveal an over-representation of genes associated with cell adhesion and proteins found as typically part of the z-disc and costameric protein complexes. Amongst these, the actin filament crosslinking protein FLNC emerged as an interesting target, as FLNC aggregates are a hallmark of the KY-associated muscle conditions (Straussberg *et al.*, 2016). We confirmed the presence of FLNC aggregates in soleus muscle from the $ZAK^{-/-}$ mouse, suggesting the ZAK-associated myopathy overlaps with other myofibrillar myopathies, in which aggregates containing a small set of z-disc proteins is a common observation.

We hypothesise that ZAKβ phosphorylates components of the z-disc and costameric protein adhesion and signalling complexes, and the KY protein complex, both thought to be important for normal muscle function. As a result, we suggest ZAKβ regulates the activity and stability of proteins involved in actin organisation and cell adhesion at the costamere. From what we have discovered, we propose that loss of ZAK causes sarcomeric instability, whereby many proteins responsible for maintaining the structure of the sarcomere become damaged. These damaged proteins accumulate within the fibre and contribute to muscle weakness. We know from other disease models, accumulation of large damaged proteins is detrimental to the health of the organ (Davies, 1987; Davies, Lin and Pacifici, 1987; Williams *et al.*, 2006; Voisine, Pedersen and Morimoto, 2010). The consequences of these aggregates in this scenario are 2-fold. Firstly, the mere presence of protein aggregates results in myofibre weakness through loss of structure and adhesion, and an obstruction to the normal function of the contractile apparatus. But secondly, and arguably more importantly, reduced protein degradation of these damaged proteins is also associated with impaired synthesis of new functional replacement proteins (Figure 6.7), thus exacerbating the level of protein accumulation, atrophy, and muscle weakness (Homma *et al.*, 2006; Selcen *et al.*, 2009; Kathage *et al.*, 2017).

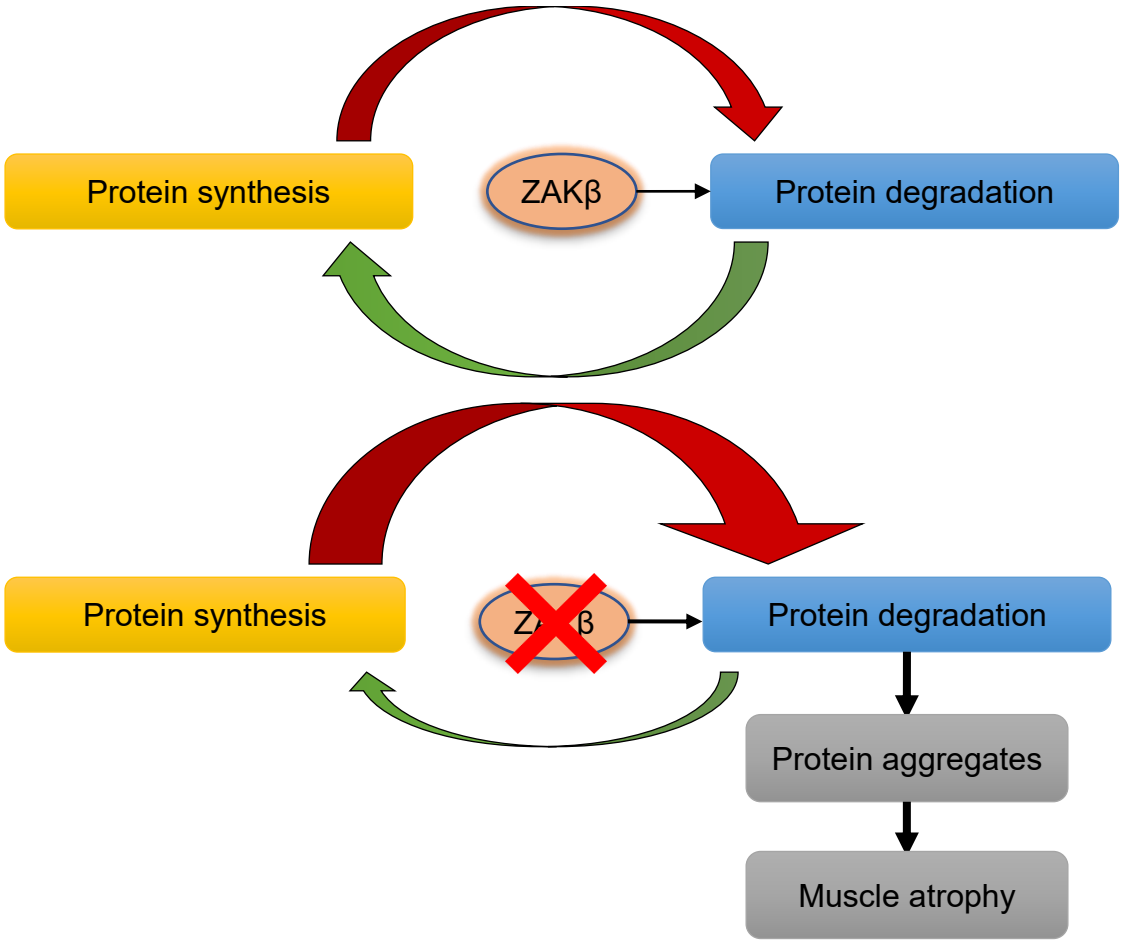

Figure 6.7: Schematic representing the imbalance of protein turnover and consequences of the loss of ZAK. Impaired protein degradation results in an impairment to the mechanisms which govern the synthesis of new functional protein. Reduced synthesis of functional protein results in the build-up of protein aggregates and overall muscle weakness.

We know that one of the most obvious phenotypes of the pathology caused by the KY mutation is the presence of FLNC/BAG3 aggregates with an upregulation of clients of the CASA pathway (Jokl *et al.*, 2018). These functional components of the CASA pathway have now been identified in association with the ZAK mutation and thus is a common pathological readout conserved between ZAKβ and KY myopathies. It is from this that we hypothesise that ZAKβ modulates both clients and players of the CASA pathway through phosphorylation.

CHAPTER 7

Results

GENERATION OF A miniTURBO-ZAKβ-tdTomato CONSTRUCT FOR PROXIMITY LIGATION ASSAY

7.1 Introduction

ZAKβ belongs to a MAP3K family of serine/threonine kinases responsible for induction of p38 and JNK signalling (Gross *et al.*, 2002; Nordgaard *et al.*, 2022). Phosphoproteomics analysis of ZAKβ downstream targets suggests that ZAKβ preferentially phosphorylates proteins associated with focal adhesion or cell adhesion with an abundance of z-disc components.

Here we generated a ZAKβ-tdTomato construct capable of biotinylation of proximal proteins for the identification of interacting partners and the validation of direct ZAKβ phosphorylation targets.

7.2 Generation of the miniTurbo-ZAKβ-tdTomato construct

Phosphoproteomics analysis of the immediate downstream targets of ZAKβ suggests that it preferentially phosphorylates components of the actin cytoskeleton and proteins involved in its (re)organisation. It is important to validate these interactions in order to develop an understanding of the way ZAKβ behaves in response to a stress stimulus. Recent advances in proximity-based labelling had led to the development of a novel protocol using a biotin ligase enzyme to specifically label short-lived, transient interactions and map the full complement of protein–protein interactions *in vitro* by adding biotin onto nearby interacting proteins (Branon *et al.*, 2017).

For this method to work, the protein of interest must be fused to that of a biotinylating enzyme. Originally, two enzymes were commonly used for this purpose: BirA-R118G (also known as “BioID”), a point mutant of *Escherichia coli* (*E. coli*) biotin ligase (Choi-Rhee, Schulman and Cronan, 2004; Roux *et al.*, 2012), and APEX2, an engineered variant of soybean ascorbate peroxidase (Rhee *et al.*, 2013; Lam *et al.*, 2015). Unfortunately, the low catalytic activity of these enzymes has made it difficult to apply in a wide range of biological contexts. For instance, one of the few *in vivo* studies performed using BioID required biotin addition for 7 days (Uezu *et al.*, 2016), which is not feasible for protein interaction mapping.

More recently, the production of TurboID and miniTurbo has allowed for the biotin-tagging of transient interactions in as little as two hours (Branon *et al.*, 2017). They each have unique properties and can be useful in different applications. TurboID is the most active, and used when the priority is to maximise biotinylation yield and sensitivity/recovery (Branon *et al.*, 2017). However, this enzyme produces a small amount of promiscuous biotinylation prior to the application of exogenous biotin, suggesting that TurboID can utilise low levels of biotin present in cells and organisms. Alternatively, miniTurbo is used when the priority is to restrict promiscuous biotinylation to a specific window of time as despite a slight reduction in activity, it gives much less background than TurboID in the absence of exogenous biotin addition. Furthermore, miniTurbo (28 kDa) is 20% smaller than TurboID (35 kDa), which may decrease the probability of poor transfection or negative impact on the trafficking and/or function of the proteins to which it is fused. As ZAKβ is a kinase and interaction events may be transient, being able to detect these short-lived interactions will be quite important. Therefore, in this study we intended to fuse ZAKβ to miniTurbo.

We generated a pDEST47-3xHA-miniTurbo-ZAKβ-tdTomato fusion vector using NEBuilder® HiFi recombinase DNA assembly (Figure 7.1). The miniTurbo module was introduced to the ZAKβ-tdTomato vector at the N-terminus following unsuccessful cloning of miniTurbo at the C-terminus whereby the fluorescent tag was not identifiable after transfection. The destination plasmid pDEST47-ZAKβ-tdTomato was linearised using the restriction enzyme *Not*I, and the 3xHA-miniTurbo insert was amplified using modified HiFi DNA Assembly primers (Figure 7.1; Steps 1 & 2). The restriction enzyme-digested linearised pDEST47-3xHA-miniTurbo-ZAKβ-tdTomato destination vector (8.4 kb) and successful 3xHA-miniTurbo insert PCR amplification (0.9 kb) was confirmed using gel electrophoresis (Figure 7.2).

The resulting plasmid (Figure 7.3A) was used to transform highly competent *E. coli* and spread on agar plates. DNA from the resulting colonies was extracted and digested using two additional restriction enzymes, *Sal*I and *Nhe*I. The digested DNA separated on an agarose gel and visualised for the predicted fragments (Figure 7.3B). From the *Sal*I-digestion gel, only 4 colonies were observed to have the three-band pattern (Figure 7.3C). The 4 colonies identified also were positive for the two-band

pattern expected from the *Nhe*I-digestion (Figure 7.3D). From this, 4 clones were purified to test transfection efficiency and performance *in vitro*.

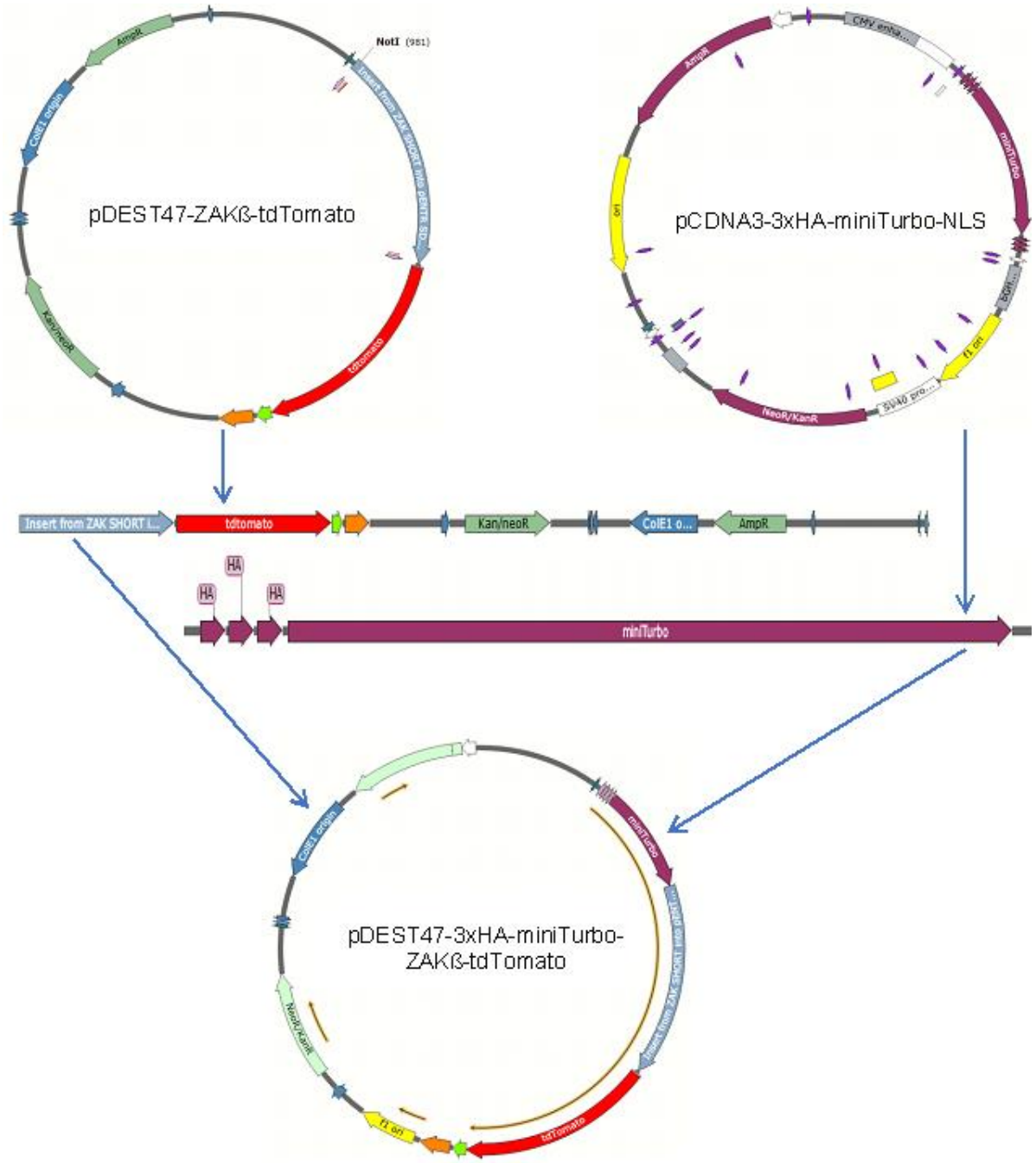

Figure 7.1: Illustration of NEBuilder HiFi DNA cloning. Recipient plasmid: pDEST47-ZAKβ-tdTomato, 8.399 kb. (1) Recipient plasmid linearised using *NotI* at the N-terminus of ZAKβ. Donor vector: pCDNA3-3xHA-miniTurbo-NLS, 6.338 kb. (2) Insert (0.904 kb) amplified using:

- Forward primer: 5'-TACAAAAAAGCAGGCTCCGCGCCACCATGTACCCGTATG-3'

- Reverse primer: 5’-TTCTTAAAGTTAAACAAGGCCTTTTCGGCAGACCGCAG-3’

(3) Overlapping homologous sequences used in HiFi cloning are included in the primer sequence. Fusion vector, pDEST47-3xHA-miniturbo-ZAKβ-tdTomato contains all components in the correct ORF, 9.265 kb.

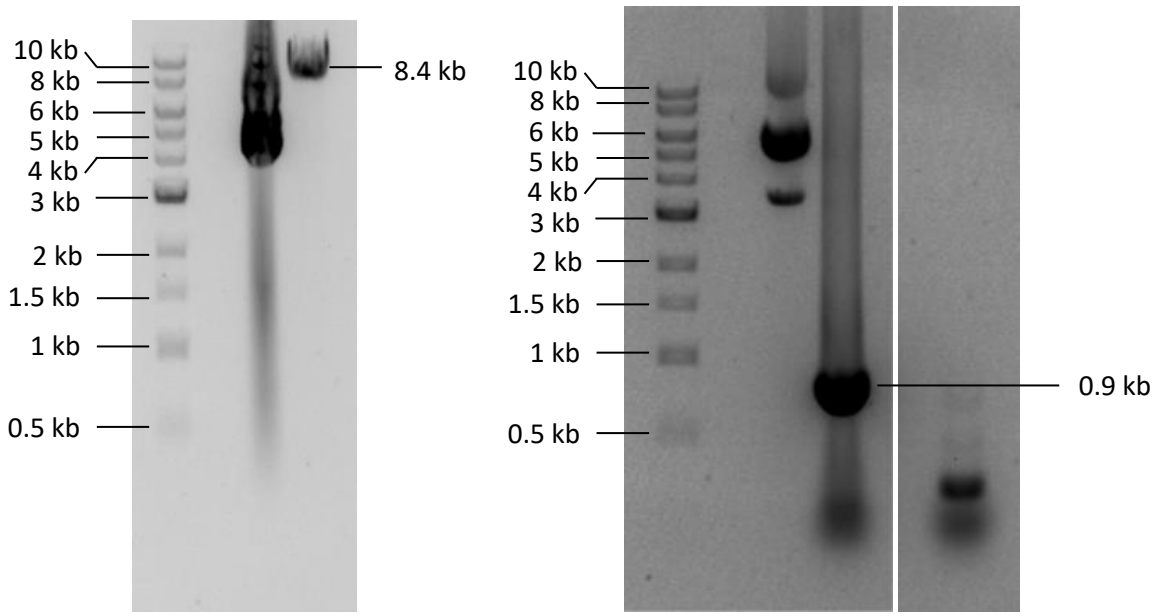

Figure 7.2: Linearisation and PCR amplification of the recipient vector and donor insert. (Left) pDEST47- ZAKβ-tdTomato, 8.399 kb linearised by *NotI* restriction enzyme. (Right) Insert from donor vector pCDNA3-3xHA-miniTurbo-NLS (0.904 kb) amplified using:

- Forward primer: 5’-TACAAAAAAGCAGGCTCCGCGCCACCATGTACCCGTATG-3’
- Reverse primer: 5’-TTCTTAAAGTTAAACAAGGCCTTTTCGGCAGACCGCAG-3’

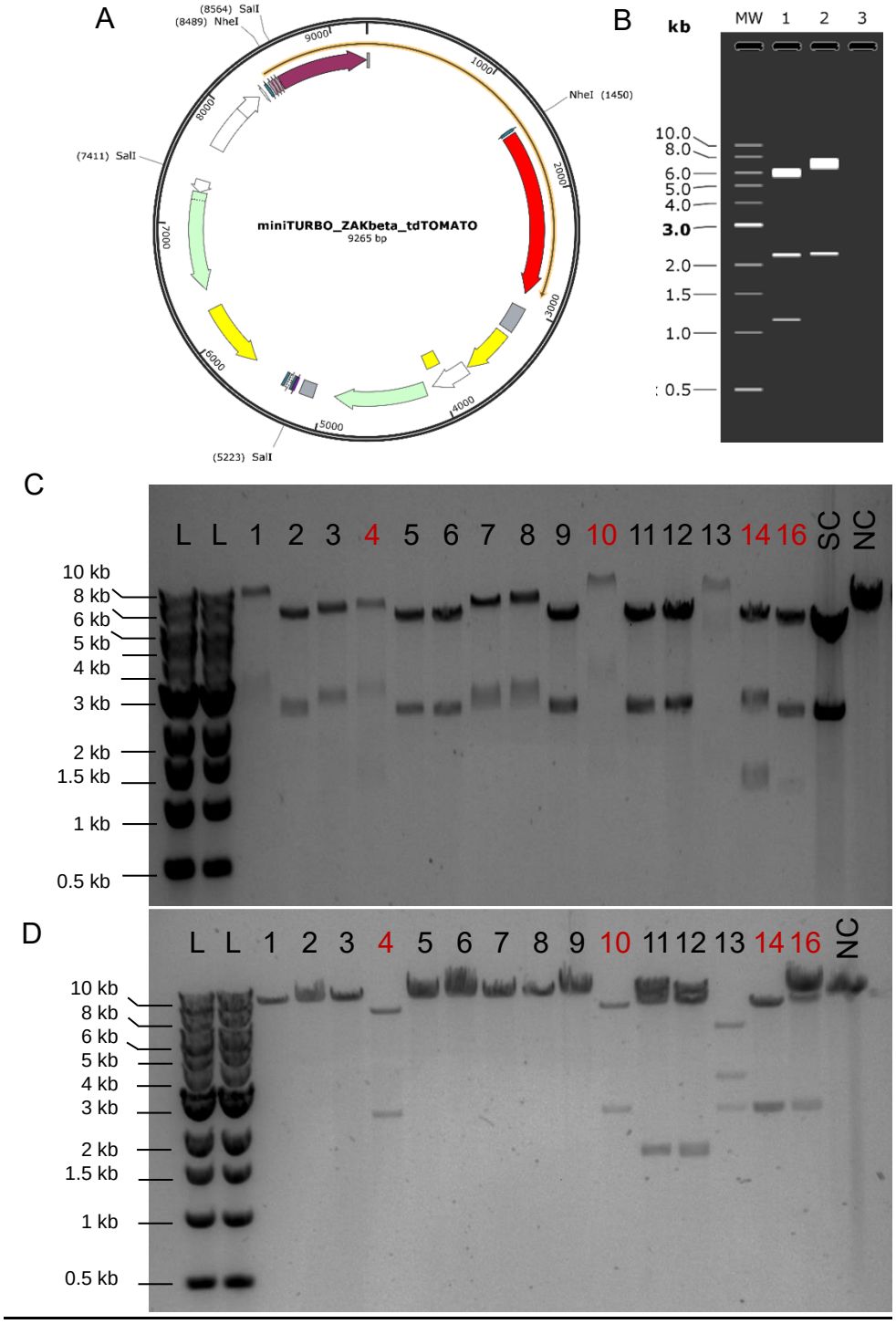

Figure 7.3: *SalI* and *NheI* restriction digestions confirmed insertion of miniTurbo in HiFi destination pDEST47-ZAKβ-tdTomato plasmid. (A) 9.3 kb pDEST47-mTurbo-ZAKβ-tdTomato plasmid with *SalI* (x3) and *NheI* (x2) restriction sites. (B) Lane 1: Successful digestion with *SalI* would produce three fragments: 5.9 kb, 2.2 kb, and 1.1 kb. Lane 2: Digestion with *NheI* would produce two fragments: the 7.0 kb and 2.2 kb. (C) Agarose gel electrophoresis of *SalI*-digested purified HiFi transformant plasmid (SC = *SalI* Control

digested pDEST47-ZAKβ-tdTomato plasmid, NC = *NotI* digested pDEST47-ZAKβ-tdTomato template). (D) Agarose gel electrophoresis of *NheI*-digested purified HiFi transformant plasmid (NC = *NotI* digested pDEST47-ZAKβ-tdTomato template). Lanes 4, 10, 14 and 16 represent successful integration of the miniTurbo insert (Red).

7.3 Transfection efficiency in COS7 cells

The next step was to confirm transfection in a cell line classically easy to manipulate like the COS7 cell line. Here the construct was checked for fluorescence, indicating that the construct had been ligated in frame and confirming the electrophoresis results, and transfection efficiency. All 4 clones identified as correct from the electrophoresis were transfected into COS7 cells (Figure 7.4). From this we observed successful transfection, as shown by the bright red cells, and a diffuse expression no different to that of previous ZAKβ expression in COS7 cells.

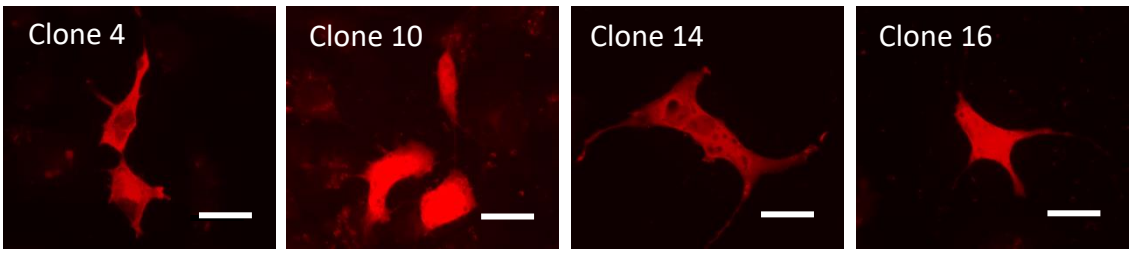

Figure 7.4: Transfected miniTurbo-ZAKβ-tdTomato construct exhibits normal expression and fluorescence in COS7 cells. Representative images of COS7 cells transfected with each of the 4 positive clones identified in the restriction digest: clones 4, 10, 14, and 16. Each clone was positive for tdTomato fluorescence indicating the fluorophore was intact. The expression pattern was diffuse, with mainly cytoplasmic localisation which was not any different from transfection with ZAKβ-tdTomato. As these were deemed clones, only one was used in subsequent transfections. Scale bar = 100 µm.

7.4 Evaluation of biotin-labelling in C2C12 cell line

The final step in the validation of this construct was to assay the ability of miniTurbo to biotinylate in the presence of exogenous biotin after transfection with pDEST47-3xHA-miniTurbo-ZAKβ-tdTomato, and for no biotinylation to be detected specifically in untransfected cells. Because C2C12 cells are a muscle myoblast cell line, the C2C12 cell line was chosen for this transfection. C2C12s were transfected with pDEST47-3xHA-miniTurbo-ZAKβ-tdTomato and treated with and without biotin for 1 hr prior to fixation. Biotin was detected using a streptavidin-FITC conjugated probe and was analysed for colocalisation with the pDEST47-3xHA-miniTurbo-ZAKβ-tdTomato construct. Successful transfection was again observed in this cell line (Figure 7.5). Treatment with biotin and labelling with streptavidin-FITC allowed for visualisation of miniTurbo activity. Biotinylation was detected in cells transfected with pDEST47-3xHA-miniTurbo-ZAKβ-tdTomato, untransfected cells were negative for streptavidin-FITC. Finally, as control for endogenous biotin, pDEST47-3xHA-miniTurbo-ZAKβ-tdTomato-transfected cells were negative for biotinylation. Altogether, this suggests that this would be a good model to detect interacting partners of ZAKβ and validate possible direct phosphoproteomics candidates of ZAKβ activity.

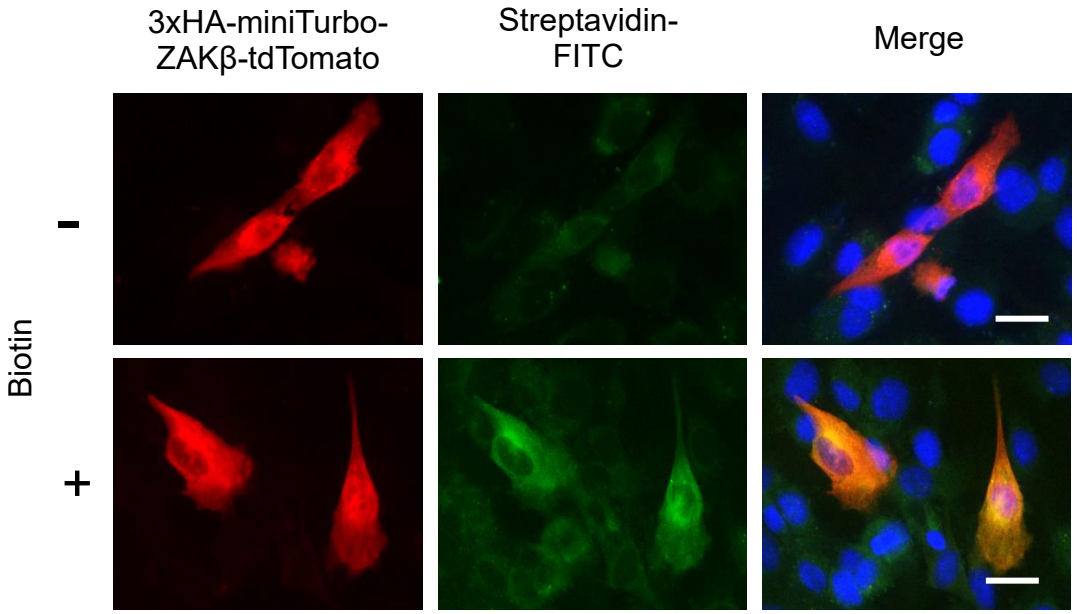

Figure 7.5: Biotinylation confirmed in C2C12 cells transiently transfected with miniTurbo-ZAKβ-tdTomato. Representative images of C2C12 myoblasts transfected with one of the 4 positive clones identified in the restriction digest. Here, the transfection was positive for tdTomato fluorescence indicating the fluorophore intact here and without biotin treatment, streptavidin-FITC staining was negative (Top row). Treatment with biotin prior to fixation shows positive streptavidin-FITC staining in only those cells positive for miniTurbo-ZAKβ-tdTomato indicating that miniTurbo was successful in conjugating biotin molecules to nearby proteins. Scale bar = 100 µm.

7.5 Discussion

Proximity ligation assays are a great way of validating interactions previously identified in other proteomics screens (Dörpholz *et al.*, 2017; Santi *et al.*, 2020). For further analysis of ZAKβ targets identified in the targeted ZAKβ phosphoproteomics screen, proximity ligation assay would offer a unique method of validation.

Proximity ligation allows for the detection of interacting proteins of a protein of interest. The radius of proximity enforces a stringency that narrows the specificity of nearby proteins to that of proteins that directly interact with the protein of interest. As ZAKβ is a MAP3K which phosphorylates serine/threonine residues of downstream targets, this interaction has the potential to be transient. By using miniTurbo, we were able to capture this snapshot of ZAKβ signalling within a one hour window.

By fusing ZAKβ-tdTomato with miniTurbo we generated a construct that was able to transfect in both COS7 and C2C12 cell lines, and showed clear biotinylation within 1 hr of biotin treatment. The aim was to differentiate the transfected C2C12 myoblasts into ZAKβ-miniTurbo-tdTomato-expressing C2C12 myotubes with primitive z-discs. The presence of z-disc structures is more representative of the in vivo environment.

We sought to generate cell lines each stably expressing ZAKβ-tdTomato and miniTurbo-ZAKβ-tdTomato. Unfortunately, the selection process using G418 was highly inefficient, even in untransfected C2C12 cells. Untransfected C2C12 controls were used to assess G418 activity. These controls appeared heavily resistant to the effects of G418 despite increasing the concentration of antibiotic above the usual

levels required for selection. This resulted in multiple passages of transfected cultures with an exponential loss of fluorescence per passage. We next tried to use cloning discs to isolate individual fluorescent colonies and expand from there which proved unsuccessful. We then attempted to generate the stable cell lines using flow cytometry specific for the tdTomato fluorophore. However, this was again unsuccessful as the resultant colonies were negative for fluorescence once expanded. Transient transfection of these constructs into proliferating C2C12 cells which are then differentiated was not an option due to the low proportions of α-actinin positive myotubes observed in previous experiments and the length of time in which it took for myotubes to appear. Going forward, it may be of use to use electroporation as a means to artificially express these constructs *in vitro*. Alternatively, transient transfection may be used so long as transfection efficiency is measured and the batch of C2C12 cell line is capable of high levels of differentiation and fusion. Future experiments may include the electroporation of both ZAKβ-tdTomato and miniTurbo-ZAKβ-tdTomato into mouse skeletal muscle. Through either a high biotin diet, or intramuscular treatment with exogenous biotin, this protocol would enable the pull down of biotinylated proteins and mass spectroscopy identification of interacting targets of ZAKβ *in vivo*.

CHAPTER 8

Results

CHARACTERISATION OF A ZAKβ-DEFICIENT C2C12 CELL LINE

8.1 Introduction

The function of ZAKβ is relatively unknown. ZAKβ was identified as an interacting partner of IGFN1 in a Yeast-two-hybrid assay (Y2H) (Baker *et al.*, 2010). IGFN1 is thought to be a component of the KY protein complex located at the z-disc. The domain structure of IGFN1 is similar to that of other structural sarcomeric proteins which associate with the actin cytoskeleton. These proteins include, but are not limited to, myosin binding protein C, filamin C (FLNC), myotilin, myopalladin and titin (Otey *et al.*, 2009). KY, another protein in the KY protein complex, has recently been implicated in protein turnover (Jokl *et al.*, 2018), in agreement with previous reports showing accumulation of the actin binding crosslinkers FLNC and XIN in muscles from *ky/ky* mice. Filamin C is of particular interest. In addition to IGFN1, Filamin C was identified as an interacting partner of KY (Beatham *et al.*, 2004). Damaged FLNC accumulates in the tissues of both *ky/ky* and $ZAK^{-/-}$ mice (Beatham *et al.*, 2004; Straussberg *et al.*, 2016). Therefore, we hypothesise possible roles for ZAKβ in the regulation of cytoskeletal complexes. ZAK has been implicated in actin organisation and fibre modulation. Not only is ZAK thought to play a role in TGFβ-mediated hypertrophy of cultured cardiomyocytes *in vitro* via an increase in actin polymerisation and organisation, but it also appears to have a role *in vivo* inducing cardiac hypertrophy (Christe *et al.*, 2004; Huang *et al.*, 2004; Hsieh *et al.*, 2015). From the phosphoproteomics screen, we were able to identify possible roles in the regulation of focal and cytoskeletal protein complexes. To gain further insight into the possible mechanisms played by ZAKβ, we generated two ZAK-KO cell lines to validate the hypothesised role concluded from phosphoproteomics. Focusing on certain cellular phenotypes relevant to a role in regulation of focal and cytoskeletal protein complexes we aimed to investigate the ZAK-KO cell line for differences in: migration, fusion, and focal adhesion. These results highlighted cellular fusion and migration as a plausible role for ZAKβ *in vitro*.

8.2 Generation of ZAKβ-KO C2C12 cell lines

Proliferating C2C12 cells were transfected with the CRISPR-Cas9 vector containing two gRNAs specific to the 5' end of *Zakβ* (Figure 2.1). Transfected cells were

incubated in a selective growth medium containing G418. Resistant colonies were serially diluted in a 96 well plate to obtain single resistant cells that were subsequently expanded. Clones were then further expanded for protein extraction after 14 days in differentiation medium (Figure 2.3). By differentiating the cell lines, we were able to visually observe any differentiation or fusion defects due to the loss of ZAK protein. After running protein extracts on Western blots, two clones (clones C10 & D9) were confirmed as deficient for ZAK protein as both were missing the specific 55 kDa band for ZAKβ (Figure 8.1B&C). Though lack of ZAK protein was unequivocally confirmed in both D9 and C10 ZAK-KO cell lines through Western blot, disruption of the ZAK locus was also confirmed through amplification and sequencing of the target gRNA sequences contained within exons 2 and 3. Sequencing of KOD9 exon 2 revealed a homozygous 1 bp deletion resulting in a premature stop codon. Sequencing of exon 3 showed both 7 and 2 bp mutations also producing a premature stop codon. Sequencing of KOC10 revealed a heterozygous 1 bp mutation in exon 2, and a 2 bp heterozygous mutation in exon 3, therefore the genotype of this clone must be a compound heterozygous (Figure 8.2).

In just a few days after the induction of the differentiation programme, WT C2C12 cells are able to differentiate and begin to fuse together to form multinucleated myotubes. After differentiating the ZAK-KO cell lines, we were unable to visually observe the formation of myotubes within the 14 day time frame suggestive of a significant delay in these processes (Figure 8.1A). As a result of this observation, it was decided that the fusion index of both ZAK-KO cell lines would be quantified.

8.3 Evaluation of fusion index in ZAK-KO C2C12 cell line

Throughout the process to generate the ZAK-KO C2C12 cell lines, we noticed the tendency for myoblasts lacking ZAK to peel from the plastic upon induction of the differentiation programme (Figure 8.3A). This propensity to detach called into question the ability for ZAK-KO cells to adhere to a surface. Since cell adhesion was identified as a target process by phosphoproteomics and it is also essential for myoblast fusion, a fusion assay was performed.

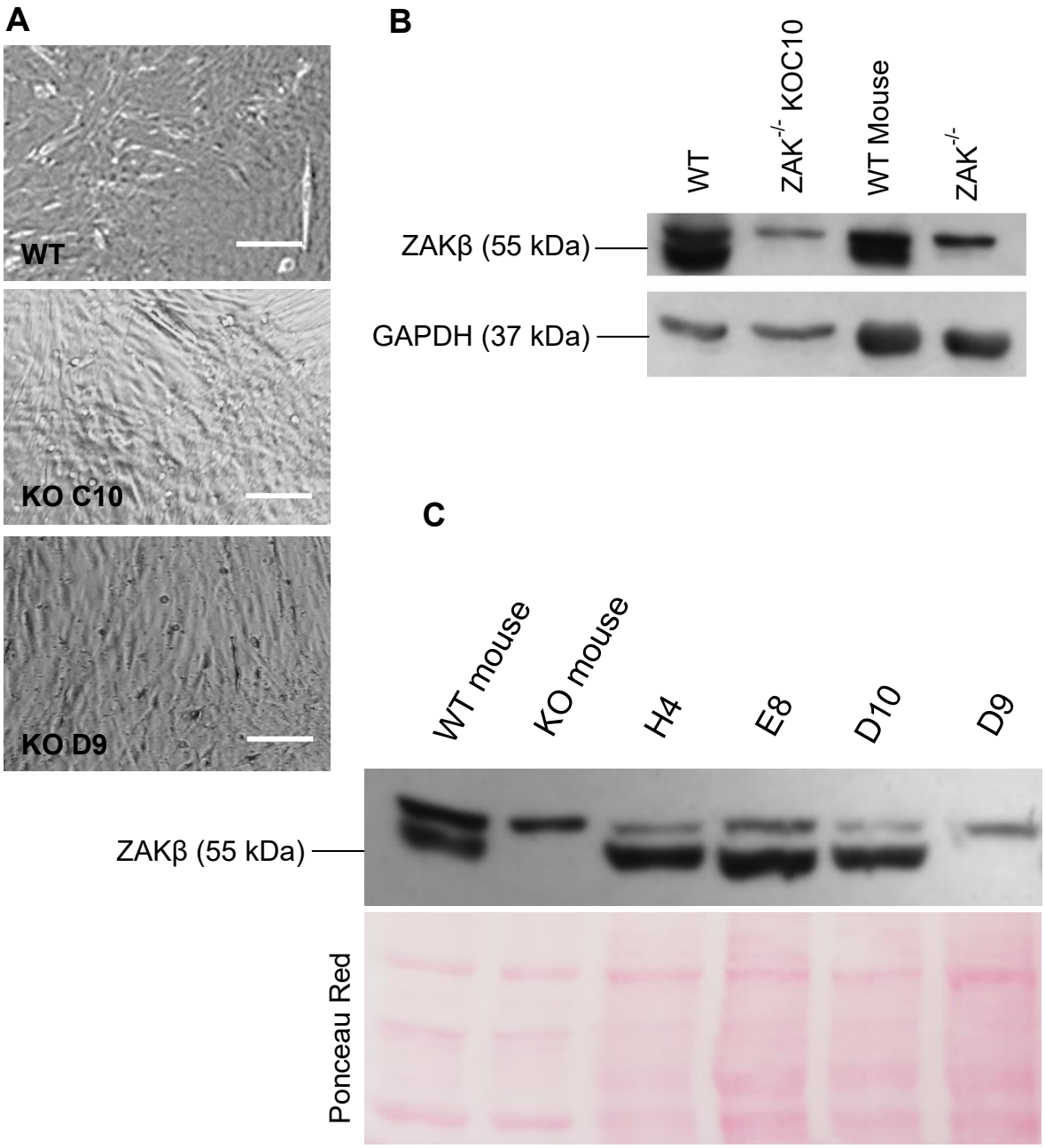

Figure 8.1: Generation of CRISPR-Cas9-mediated ZAK knockout C2C12 cell line. (A) Representative brightfield image of wild-type (WT) or CRISPR-Cas9-targeted ZAK knockout C2C12 clones (KOC10 and KOD9) on day 14 post induction of differentiation. Imaged acquired on EVOS brightfield microscope. Scale bar = 100 µm. (B & C) Protein extracts were obtained from WT, KOC10, KOD9, and other colonies 14 days post differentiation and run alongside validated protein extracts from WT and ZAK$^{-/-}$ mouse gastrocnemius/soleus muscles. The ZAK antibody was not pre-incubated with another blot prior to immunostaining, therefore non-specific bands were present. The Western blot confirms that KOC10 and KOD9 are devoid of ZAKβ. (C) Clones H4, E8, and D10 were not successful.

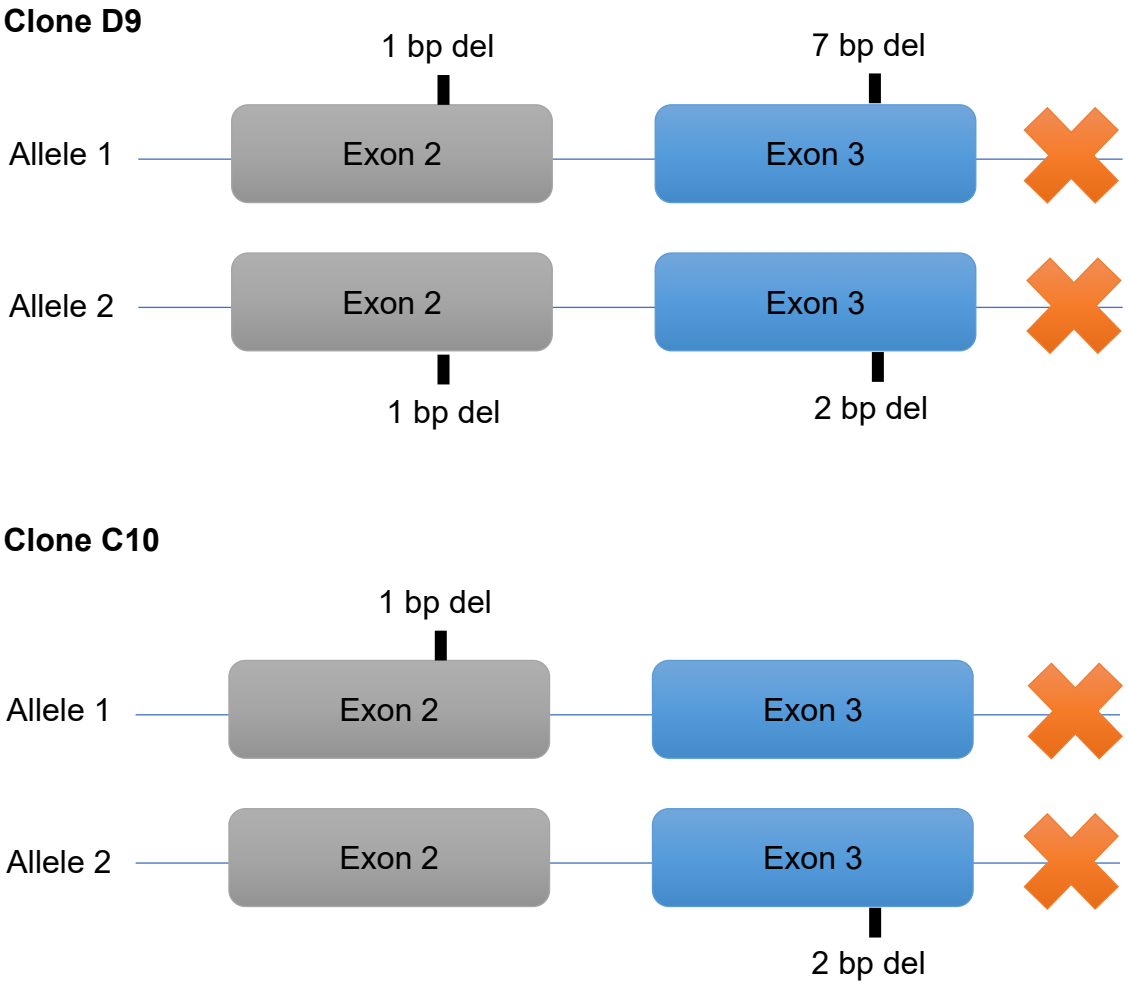

Figure 8.2: Schematic representation of disruptive mutations caused by CRISPR-targeting of exons 2 and 3. (Top) ZAK-KO clone D9 sequenced alleles of exons 2 and 3. Sequencing revealed a 1 bp deletion for both alleles of exon 2, and a 7 bp deletion in one allele of exon 3 with a 2 bp deletion within exon 3 of allele 2. (Bottom) ZAK-KO clone C10 sequenced alleles of exons 2 and 3. Sequencing revealed a 1 bp deletion for one allele of exon 2, and a 2 bp deletion in one allele of exon3.

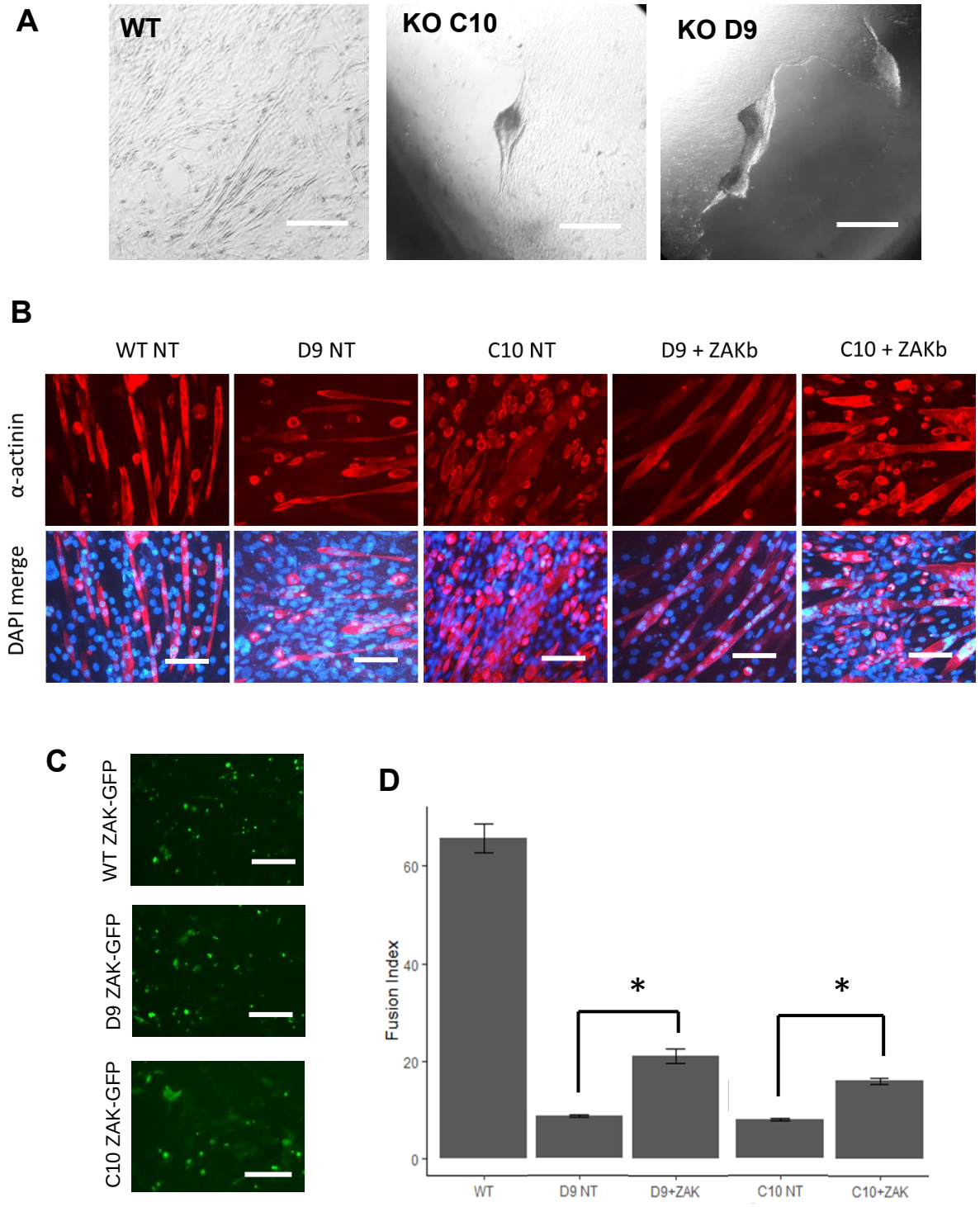

Figure 8.3: ZAK-KO cell lines display fusion defects partially rescued by expression of ZAKβ. (A) ZAK-KO C10 and D9, clones selected following transfection with ZAK-CRISPR-Cas9 plasmid, shows detachment from culture surface upon switching to DF medium, whilst the control C2C12 cell line continues to form myotubes. Scale bar = 40 µm. (B) Representative fluorescence images of C2C12 myoblasts differentiated for 14 days for WT, D9, C10 and D9 & C10 transiently transfected with ZAKβ. Cells were stained for alpha-

actinin (red) representing differentiation and fusion of myotubes and DAPI (blue) (n = 3). Scale bars = 200 µm. (C) Initial transfections of ZAKβ-GFP in WT, KOD9, and KOC10 C2C12 cell lines at Day 0 differentiation. Scale bar = 150 µm. (D) Fusion index calculated as the percentage of alpha-actinin positive cells with three or more nuclei. KOD9 & KOC10 cells have significantly lower fusion index than wildtype and rescued cells. (*) $p<0.01$.

Given that both clones with disruptive exon 2 and 3 mutations on both alleles displayed similar phenotypes, we subject both D9 and C10 for further characterisation. To obtain a more accurate picture of the particular defects caused by loss of ZAK, the fusion index was quantified (Figure 8.3B). ZAKβ-GFP was transiently transfected into WT, KOD9, and KOC10 C2C12 cell lines, the initial transfection efficiency was visible at day 0 (Figure 8.3C). Unfortunately a caveat of the protocol for fixation used for α-actinin immunostaining was the loss of GFP fluorescence at day 14 post differentiation and so the fusion index was quantified using alpha-actinin positive cells. The fusion index, expressed as the percentage of alpha-actinin positive cells with three or more nuclei to the total number of cells expressing alpha-actinin, measured significantly lower than that of the WT C2C12 cell line (Figure 8.3D).

In order to evaluate whether this finding was true of a loss of ZAK mutation, and not of off-target or clonal selection effects, a construct encoding ZAKβ-GFP was transfected into all cell lines (Figure 8.3B). Quantification of fusion index revealed a partial yet significant rescue of fusion (Figure 8.3D), suggesting that ZAKβ plays a role in myoblast fusion.

8.4 Assessment of migratory ability in ZAKβ-deficient C2C12 cell line

Since focal adhesions are key components for adhesion and migration (Chrzanowska-Wodnicka and Burridge, 1996; Ridley *et al.*, 2003; Kirfel *et al.*, 2004), their functions and the proteins which interact with them are important to understand. Phosphoproteomics analysis suggests that ZAKβ signalling is associated with focal adhesion pathways and organisation of the cytoskeleton. Both of which are important for fusion and migration. ZAKβ appears to localise to stress fibres of osmotically shocked U2OS cells *in vitro* (Nordgaard *et al.*, 2022), and z-discs *in vivo*. We next

wanted to evaluate whether the ZAK-KO myoblasts which display reduced fusion, also exhibit defects in cell migration.

An in vitro scratch wound assay was conducted on WT, ZAK-KO D9, and ZAK-KO C10 C2C12 cell lines and the migration was quantified every 3 hours over a 24 hour period (Figure 8.4A). Results showed that both ZAK$^{-/-}$ cell lines are unable to close the wound within the 24 hour period (Figure 8.4B), unlike the WT cell line, therefore indicating that loss of ZAKβ causes delayed migration.

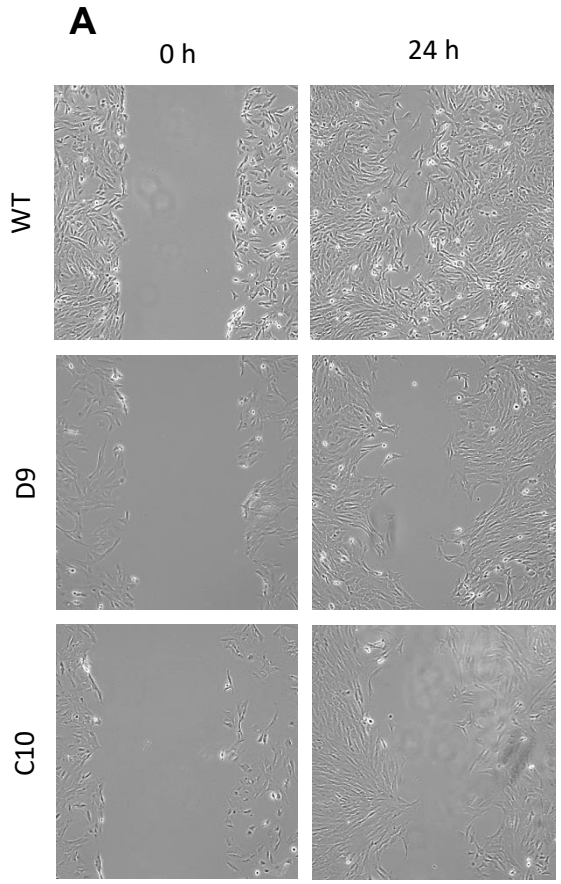

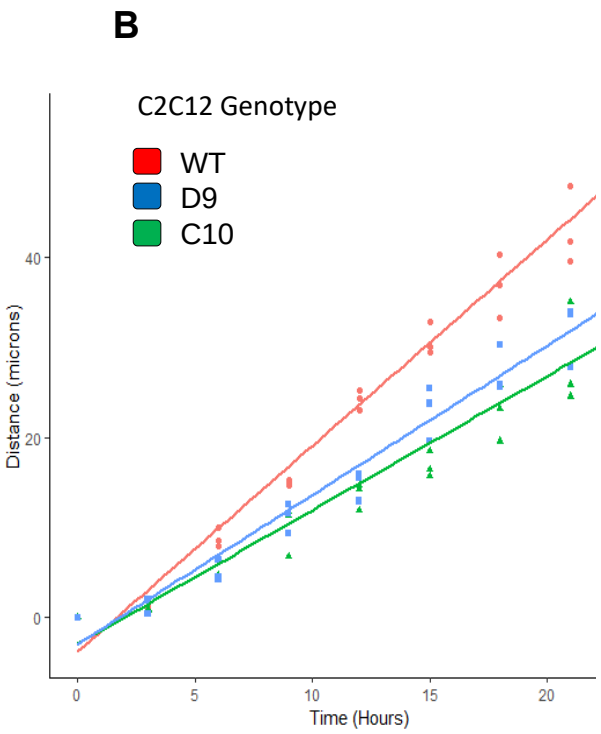

C

C2C12 cell genotype	Mean Speed (time/ distance^{-1})
WT	6.8576
KOD9	4.4615
KOC10	4.9706

Figure 8.4: C2C12 myoblasts lacking ZAK display a reduced migratory ability in culture. (A) In vitro scratch wound assay of WT, ZAK KO D9, and ZAK KO C10. Representative brightfield images taken at 0 h and upon completion at 24 h. (B) Linear plot of the distance travelled to close the wound over a 24 h period. Measurements taken at 3 h intervals with 3 replicates per cell line per time point. WT cells showed full closure within

time frame; however, D9 and C10 cell lines failed to close the gap. (C) Mean speed of each cell line over a 24 hour period calculated from the analysis of linear regression.

8.5 Discussion

Here we attempted to determine the role of ZAKβ more specifically, given the information we have previously generated. The fusion defect and size of myotubes was quantified in both D9 and C10, cell lines with mutations within ZAK exons 2 and 3. Fusion index was significantly reduced, partially rescued by re-expression of ZAKβ, indicating a role in fusion. This observation is consistent with observations that ZAK is thought to play a role in TGFβ-mediated hypertrophy of cultured cardiomyocytes in vitro via an increase in actin polymerisation and organisation, also inducing cardiac hypertrophy (Christe *et al.*, 2004; Huang *et al.*, 2004; Hsieh *et al.*, 2015). The association between ZAKβ and components of the cytoskeleton is relevant, as regulation of these is an important driver of cell adhesion and the ability to fuse. The molecular mechanisms which govern myoblast fusion are still poorly understood. However, it appears as though cytoskeletal remodelling plays an important role. Key regulators of actin remodelling, including the G-protein coupled receptor BAI3 (Hamoud *et al.*, 2014) and its intracellular effector DOCK1 (Laurin *et al.*, 2008), the small G-proteins Rac1 and Cdc42 (Vasyutina *et al.*, 2009), the membrane and Arp2/3 interacting protein CKIP-1 (Baas *et al.*, 2012), the adaptor protein and N-WASP binding partner Grb2 (Mitra and Thanabalu, 2017) and N-WASP itself (Gruenbaum-Cohen *et al.*, 2012) are thought to have a role in mediating cell fusion. Currently, there is no such evidence of the actin nucleating protein COBL in the mediation of myoblast fusion or in the context of adult muscle. Previously, COBL has been shown to be important for G-actin sequestration, weak filament nucleation, powerful filament severing and barbed-end dynamics (Renault, Bugyi and Carlier, 2008; Husson *et al.*, 2011; Jiao *et al.*, 2014).

ZAKβ has been shown to interact with proteins which interact with components of the cytoskeleton or signal transduction pathways. As a MAP3K, ZAKβ may also play a role in signal transduction pathways. These data suggest that ZAKβ has a role in mediating muscle hypertrophy and also modulating cell fusion *in vitro*. ZAKβ has been associated with the CASA-mediating co-chaperone BAG3, both as an interacting

partner of ZAKβ but also as a protein which aggregates co-localising with FLNC in $ZAK^{-/-}$ mouse slow muscle tissue. BAG3 has been shown to localise at the leading edge of migrating COS7 cells alongside actin to control motility, and is important for successful migration (Iwasaki *et al.*, 2010).

During cell migration, the actin cytoskeleton is tightly regulated. Adhesion is mediated by integrin-family proteins attached to the extracellular matrix which are constantly recycled while adhesion molecules are internalised and transported to the leading edge for reuse in cell attachment. Clathrin-mediated endocytosis of integrins has a dominant role at the leading edge of cells. Elevations in recycled/internalised adhesion proteins the leading edge causes a polarity and directs migration. Thus, tightly controlled signalling mechanisms of the actin cytoskeleton and adhesion molecules together regulate cell movement (Klemke *et al.*, 1997; Small *et al.*, 2002; Juliano *et al.*, 2004).

Integrins form an important part of the z-disc/costameric protein structure, linking the muscle fibre with the extracellular matrix and mediating many signalling cascades. Some integrin subunits were identified as directly phosphorylated by ZAKβ in the targeted phosphoproteomics assay, and also co-localise with ZAKβ on stress fibres in vitro (Nordgaard *et al.*, 2022). Therefore, it is plausible that ZAKβ may have a role in modulating the signalling pathways downstream of integrin activation, and aiding the reorganisation of the actin cytoskeleton in response to a stimulus.

CHAPTER 9

Results

STRESS-INDUCED EXACERBATION OF THE ZAKβ-DEFICIENT MOUSE PATHOLOGY

9.1 Introduction

In adulthood, the regulation of muscle mass and fibre cross-sectional area (CSA) is reflective of protein turnover regulation; the balance between protein synthesis and degradation. Muscle atrophy is the shrinkage of myofibres primarily due to a net loss of protein. Acute muscle atrophy occurs in many pathological conditions and is due to hyperactivation of the main cellular degradation pathways, including the ubiquitin-proteasome system (UPS) and the autophagy-lysosome pathways (as reviewed in Bonaldo and Sandri, 2013). Mutations in genes which result in the loss of proteins essential for maintenance of the sarcomere are thought to cause sarcomeric instability and an increase in the levels of damaged proteins in need of degradation (Stedman *et al.*, 1991; Swist *et al.*, 2020). Here, we wanted to establish whether muscles lacking ZAKβ would be inherently more vulnerable to additional stressors and pressures culminating in a phenotype similar to that observed in the human patients. We looked at three different models of muscle stress, induction of acute muscle injury, ageing, and overload-induced resistance exercise. All experiments were performed using the TA muscle, which is non-pathological in young ZAK$^{-/-}$ mice (Figure 3.5).

As muscle atrophy is an obvious sign of muscle maintenance insufficiency, we measured the cross-sectional area (CSA) of the TA muscle in wild-type (WT) and ZAK$^{-/-}$ mice following Barium chloride-induced muscle injury, evaluated the level of central nucleation in the TA muscle in WT and ZAK$^{-/-}$ mice, and quantified the level of FLNC aggregation and CSA of the soleus muscle in WT and ZAK$^{-/-}$ mice soleus muscle after synergistic ablation of the gastrocnemius.

9.2 Myofibre atrophy is observed in Tibialis anterior muscle of ZAK$^{-/-}$ with no visible difference in muscle regeneration following barium chloride injury

In many cases of muscle disease, muscle repair of damage caused by the loss of a protein critical for sarcomeric maintenance becomes impaired (Mann *et al.*, 2011; Allen, Whitehead and Froehner, 2016; Powers *et al.*, 2016). Muscle repair is facilitated by muscle stem cells which differentiate and fuse in a coordinated effort to replace damaged and necrosed fibres (as reviewed in Hawke and Garry, 2001;

Wagers and Conboy, 2005). We know at both transcript and protein levels that ZAKβ is the only ZAK isoform expressed in adult skeletal muscle. However we were interested to see whether ZAK was being expressed at the developmental stages of muscle growth. In order to look at differentiating myoblasts, we utilised the C2C12 immortalised myoblast cell line as a model for the early stages of myogenesis. We identified the expression pattern of ZAK isoforms in proliferating myoblasts through to 7-day differentiated myotubes. The results indicate that both ZAK isoforms are expressed in the proliferating myoblast, however ZAKβ appears to be the only isoform expressed throughout the phases of both proliferation and differentiation (Figure 9.1A). As C2C12 cells differentiate, they begin to fuse together, expressing more components of the skeletal muscle cytoskeleton (Figure 9.1A; a-actinin) and form myotubes (Figure 9.1A; Panels D5 & D7). This is an interesting result showing that in this model of early myogenesis, we see the predominance of the ZAKβ

isoform during the phases of differentiation and fusion.

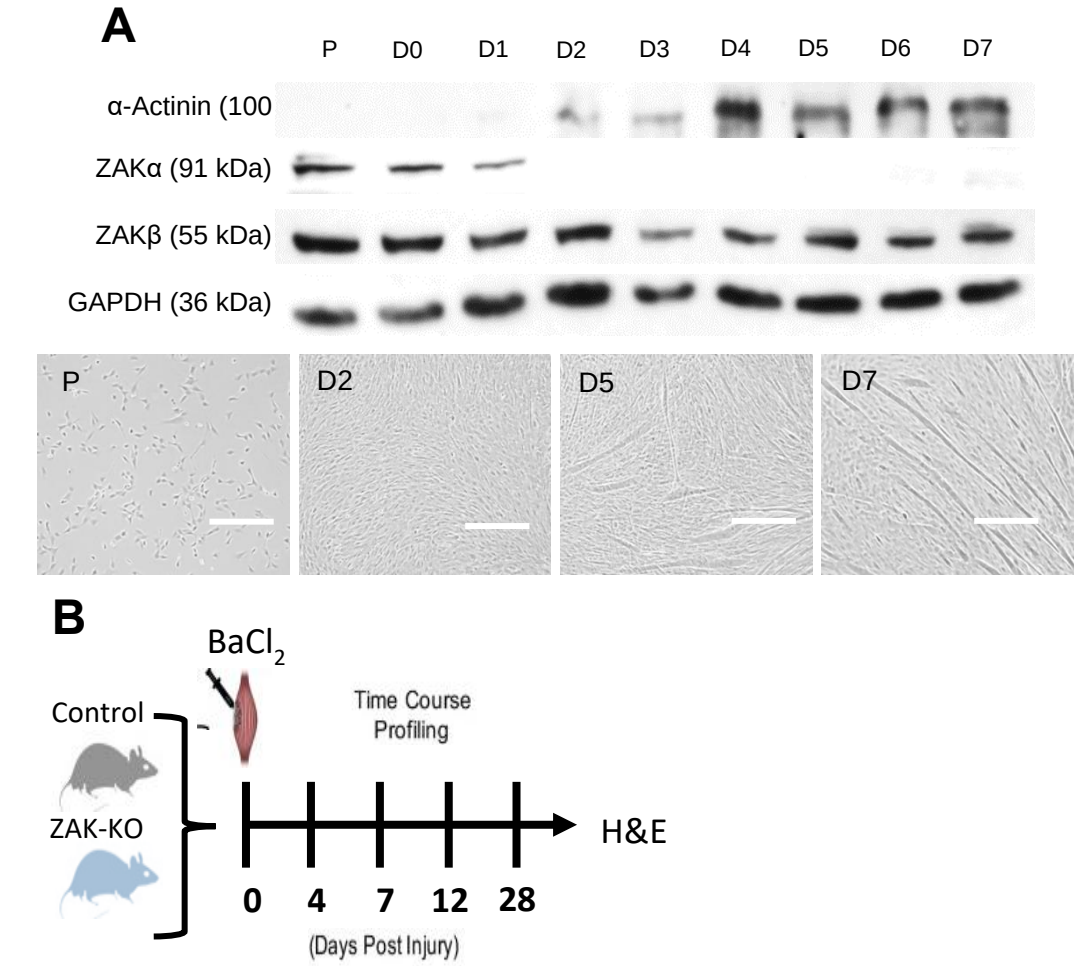

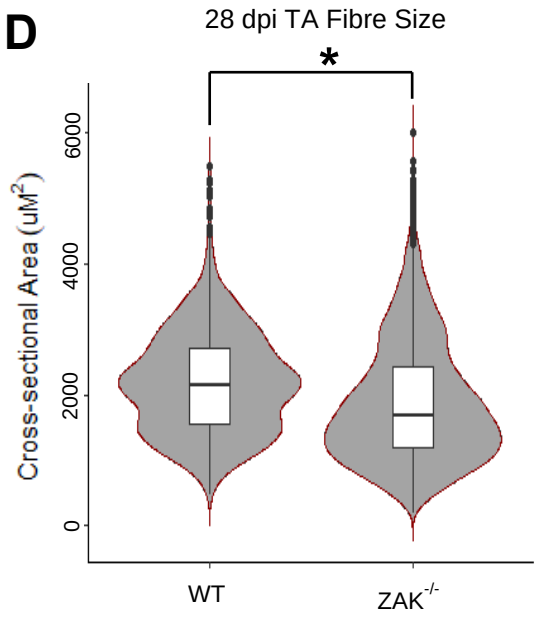

Figure 9.1: Loss of ZAK results in a slight regenerative impairment following $BaCl_2$ injury. (A) (Top) A Western blot showing the expression profile both ZAK isoforms during both proliferation and differentiation, with α-Actinin as a differentiation marker. Loss of expression of ZAKα was observed after differentiation induction, whereas ZAKβ remained present throughout stages of proliferation and differentiation. (A) (Bottom) Representative brightfield images depicting the stages of myotubule growth over a 7 day period; proliferation, confluence, fusion (small myotubes), and fusion (long myotubes). Scale bar = 100 µm. (B) Schematic representation of $BaCl_2$ injury. Control (WT) and ZAK-KO ($ZAK^{-/-}$) TA muscles treated with $BaCl_2$ and left to regenerate for 4, 7, 12, and 28 days before sectioning and H&E staining. (C) Visual comparison of WT and $ZAK^{-/-}$ mouse Tibialis anterior H&E cross sections ranging from 0 to 28 days post injury (dpi) suggests no observable difference in muscle regeneration subsequent to barium chloride injury. Scale bar represents 100 µm. (D) Violin plot represents cross sectional area of 28 dpi wild type (WT) and $ZAK^{-/-}$ muscles including box and whisker plot depicting the mean and interquartile range. Measurement of entire TA muscle containing regeneration. Student's t-test (*= $p<0.01$). $ZAK^{-/-}$ muscles show slight regenerative delay (n=5).

Previously we identified that the soleus muscle exhibits more central nucleation, and by proxy more regeneration, in the $ZAK^{-/-}$ than in the control which is not observed in 8 week TA muscle. From this, we wanted to determine whether the loss of ZAK would impair the regenerative process when the muscle was subject to acute injury and the

stress associated with muscle regeneration. In order to investigate this, we induced an acute muscle injury using barium chloride ($BaCl_2$) toxin on the TA muscles of 8 week WT and $ZAK^{-/-}$ mice. Following injury we measured the progression of regeneration throughout various time points over a period of 28 days (Figure 9.1B). Upon visual inspection of H&E stained TA muscle cross sections from 0, 4, 7, 12, and 28 days post injury (dpi) we did not see any discernible differences in the progression of regeneration (Figure 9.1C). Following the injury performed at 0 dpi, we saw an enormous amount of damage and necrosis at 4 dpi which cleared at 7 dpi leaving only small regenerating cells with centralised nuclei. From 7 dpi onwards, myofibres increased in size whilst maintaining the presence of centralised nuclei. This culminated at 28 dpi with a typical muscle appearance with the exception of the centralised nuclei which are usually present up to three months post injury (Tierney and Sacco, 2016). Interestingly, recent evidence suggests that the nuclei of regenerating fibres of muscles injured using barium chloride have a tendency to remain centralised, forming long chains of centralised nuclei (Mazzotti and Coletti, 2016; Meyer, 2018; Hastings *et al.*, 2020). Cross sectional analysis of 28 dpi muscle fibres revealed a slight significant reduction in fibre CSA of injured $ZAK^{-/-}$ TA muscles (Figure 9.1D). This difference in fibre CSA suggests that the loss of ZAK causes a minor impairment in skeletal muscle regeneration following injury which does not affect the muscle's ability to undergo regeneration. As both isoforms are present in proliferating myoblasts before ZAKα is down-regulated during differentiation, ZAKα could also have a role alongside ZAKβ during muscle growth, repair and regeneration. This fact could account for the level of fusion rescue observed in figure 8.3.

9.3 The effect of ageing on non-pathological TA muscle

Age-related muscle deterioration affects all organisms. The mechanisms which underly age-related muscle loss are not completely understood. Skeletal muscle ageing is the accumulation of numerous structural and functional changes which result in overall physical limitations and age-related muscle diseases. Among these changes are: a decrease in protein synthesis (Welle *et al.*, 1993) , infiltration of adipose tissue and fibrosis (Brack *et al.*, 2007; Addison *et al.*, 2014) , dysregulation of proteasomal degradation pathways (Chondrogianni *et al.*, 2000; Cuervo and Dice, 2000),

mitochondrial dysfunction (Short *et al.*, 2005; Sakellariou *et al.*, 2013) , a reduction of the satellite cell reservoir (Shefer *et al.*, 2006), increased ROS production (Broome *et al.*, 2006; Palomero *et al.*, 2013) and increased inflammation (Fagiolo *et al.*, 1993). Studies have identified some of the structural changes within the ageing muscle, in addition to reduced regenerative capacity and muscle satellite cell number and activity are known to cause age-related muscle loss and increased skeletal muscle stress (Snow, 1977; Schultz and Lipton, 1982; Lexell *et al.*, 1983; Lexell, Downham and Sjöström, 1986; Forsberg *et al.*, 1991; Overend *et al.*, 1992; Ambrosio *et al.*, 2009). It was clear from the 8 week ZAK$^{-/-}$ mouse that the pathology primarily affects the tonically active soleus muscle whereas the TA muscle remained unaffected. In the soleus muscle of the ZAK$^{-/-}$ mice we observe evidence of an age-related muscle degeneration which is characterised by the progressive slow fibre type adaptation and an increase in muscle regeneration more significant than the phenotype of the aged control (Figure 3.4). We next wanted to determine whether the effect of age would have an impact on the pathology of the previously unaffected TA muscle.

Performed alongside a visiting PhD student Aitana Genzor Garbayo from our collaborator's lab in Copenhagen, H&E staining was used to assess the levels of centralised nuclei (Figure 9.2A). From this we calculated the percentage of centralised nuclei across the whole TA muscle and found that aged male and female ZAK$^{-/-}$ mice of 14 months old exhibited a significant increase in the levels of centralised nuclei, and therefore muscle regeneration, than both their WT counterparts and that of the 8 week old mice. This suggests that as the ZAK$^{-/-}$ mice age, the TA too shows evidence of vulnerability. It is plausible that there is a correlation between the level of use of a muscle and the negative effect of loss of ZAK. Muscles like the soleus which are constantly engaged are highly susceptible to the effects of the loss of ZAK, whereas muscles like the TA which are engaged only when needed show evidence of pathology after many months of use.

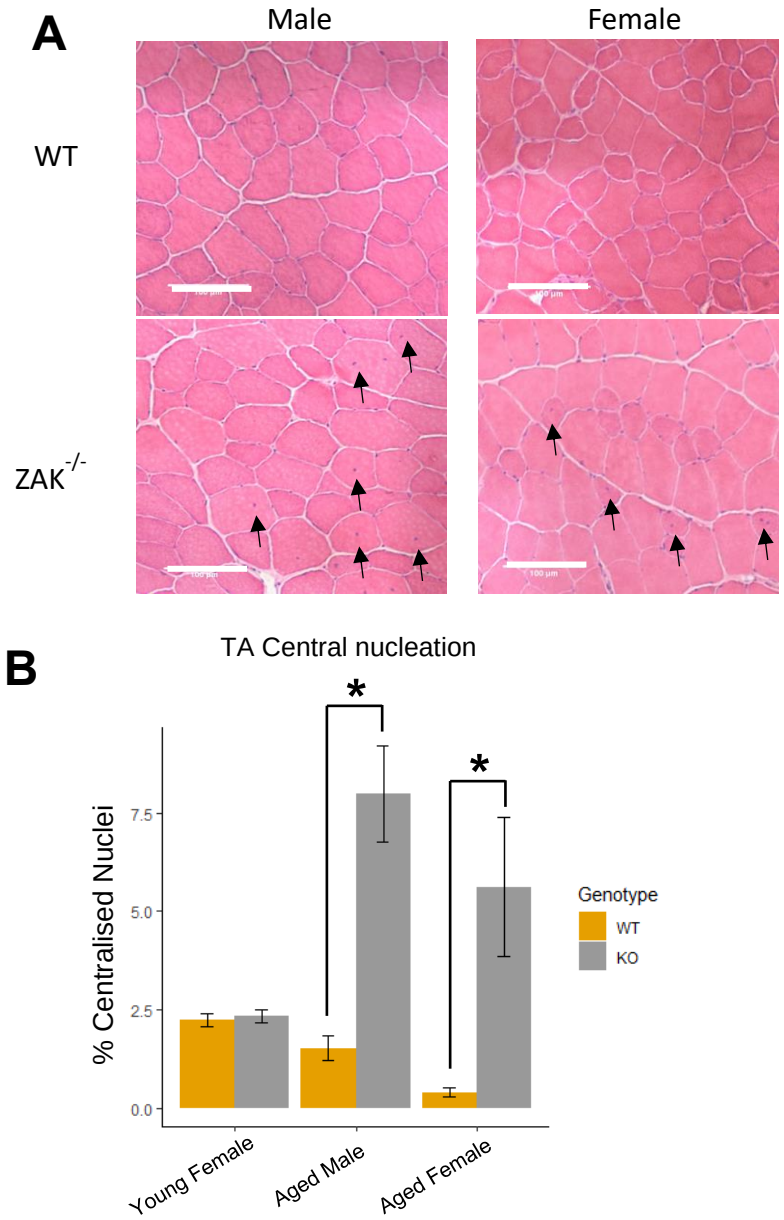

Figure 9.2: Tibialis of 14 month ZAK$^{-/-}$ mice exhibits increase in central nucleation. (A) Representative H&E images of 14 month old male and female, wild type (WT) and ZAK$^{-/-}$ tibialis muscle cross sections. Black arrows indicate presence of centralised nuclei. Scale bar represents 100 µm. (B) Quantification of percentage of centralised nuclei in 8 week female wild type (WT) and ZAK$^{-/-}$ tibialis muscle, and 14 Month old male and female, wild type (WT) and ZAK$^{-/-}$ whole tibialis muscle. ZAK$^{-/-}$ muscle showed evidence of exacerbated pathology with age, as older male and female ZAK$^{-/-}$ mice present with increased centralised nuclei indicative of muscle regeneration not observed in young TA muscle of WT or ZAK$^{-/-}$ mice. One way ANOVA (* $p < 0.01$) (n=6).

9.4 Evaluation of pathology within the soleus following synergistic ablation of the gastrocnemius

Synergistic ablation of skeletal muscle has been used to generate an artificial increase of mechanical load which mimics resistance exercise by forcing synergistic muscles to adapt and bear the weight of the increased demand (Goldberg, 1968; Philp, Hamilton and Baar, 2011; Cui *et al.*, 2020). When quantified previously, the levels of FLNC aggregation between 8 week and 22 week old ZAK$^{-/-}$ soleus muscle appeared to progressively resolve, suggesting that the adaptations undertaken by the muscle aid its ability to clear the damaged FLNC protein. We next wanted to investigate whether the application of additional stress at this late time point (7 months) would be sufficient to damage the muscle further given the apparent successful adaptation of ZAK$^{-/-}$ soleus muscle. Synergistic ablation of the gastrocnemius muscle in only one of WT and ZAK$^{-/-}$ hind limbs generates increased force upon muscles like the soleus which was used here to assess the ability of soleus to cope with persistent overload. The contralateral uninjured leg was used as control. Synergistic ablation of gastrocnemius muscle was performed by another PhD student, Aitana Genzor Garbayo, who then obtained the soleus muscle for further processing and analysis. Due to the extraction, embedding, and sectioning technique, the total cross sectional area of the muscle was not able to be quantified.

At 22 weeks, soleus muscles of ZAK$^{-/-}$ mice exhibit fewer FLNC aggregates than at 8 weeks indicating a progressive amelioration of pathology. However, upon ablation of the gastrocnemius, the soleus muscle of 7 month ZAK$^{-/-}$ mice display a significant visible increase in FLNC positive fibres (Figure 9.3A). When quantified, this difference between control and overloaded leg is staggering (Figure 9.3B). As expected, WT muscles do exhibit evidence of damage with some FLNC accumulation in the overloaded leg. The same protocol in the ZAK$^{-/-}$ mouse produces a significant increase in FLNC aggregates, suggesting that despite the apparent resolution of FLNC aggregates in the older mouse, functional overload of the muscle which results in increased demand and activity reveals once again the acute vulnerability of the muscle to increased contractile forces and correlates the importance of ZAKβ activity with the activity of the muscle. Phosphoproteomics analyses here and previous work in our lab indicate a close but not yet defined relationship between ZAK, the KY protein complex,

FLNC, and BAG3 (Baker *et al.,* 2010; Jokl *et al.,* 2018). These components of the CASA pathway are integral to mediate the degradation of large damaged cytoskeletal components which have become irreversibly unfolded during muscle contraction. Aggregates of FLNC are considered a hallmark of myofibrillar myopathies which become exacerbated by increased muscle stress and mechanical demand. Therefore, the sustained presence of FLNC aggregates within the overloaded ZAK$^{-/-}$ muscle further highlights the importance of ZAKβ in the maintenance of these sarcomeric protein complexes.

Not only does synergistic ablation result in increased muscle stress, it is primarily used as a tool for the enforcement of fibre hypertrophy within the synergistic muscles; in this case, the soleus. Determining whether a protein is important for the maintenance of skeletal muscle is done by the measurement of fibre cross-sectional area (CSA). By comparing the mean difference of soleus CSA before and after synergistic ablation of the gastrocnemius we determined how loss of ZAK affected the intrinsic property of skeletal muscle to adapt to increased mechanical load. From this we generated individual distributions of the data by binning the raw data into small, medium, and large fibres. Ablation of the gastrocnemius muscle in WT mice demonstrates the expected CSA increase in the soleus muscle, evidenced by an upwards shift in the curves representing fibre CSA following synergistic overload (Figure 9.4; WT-orange) when compared to the uninjured control leg (Figure 9.4; WT-blue). Here we saw a significant increase in soleus fibre CSA after ablation. On the other hand, removal of the gastrocnemius in ZAK$^{-/-}$ mice does not produce the same effect. The curves of the overloaded muscles (Figure 9.4; ZAK$^{-/-}$-orange) are unmoved, if not smaller than that of the control leg (Figure 9.4; ZAK$^{-/-}$-blue) and therefore the CSA increase is blunted in the ZAK$^{-/-}$ mice compared to their WT counterparts. This suggests that ZAKβ is somewhat responsible for the facilitation of hypertrophic signalling in response to increased mechanical load. Future directions of this research would be to determine which fibre types are more susceptible to the loss of ZAK by fibre typing these muscle sections and comparing the mean CSA of each fibre type before and after synergistic ablation.

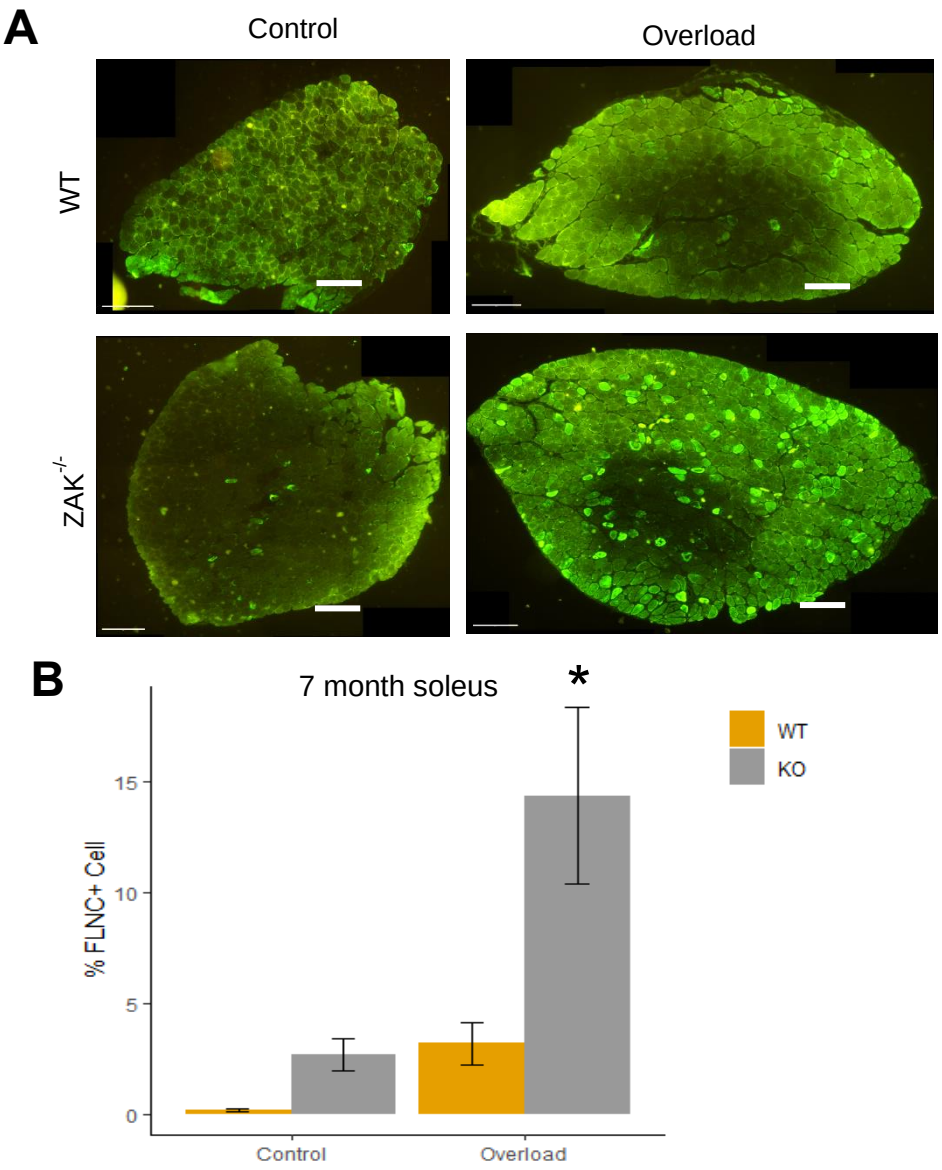

Figure 9.3: Synergistic ablation of mouse gastrocnemius muscle causes significant FLNC aggregation in 7 month ZAK$^{-/-}$ soleus muscle. (A) Representative fluorescence images of 4 month old female wild type (WT) and ZAK$^{-/-}$ soleus muscle cross sections of control and experimental leg muscles from the same mouse (n=6). Muscle sections immunostained using Anti-FLNC RR90. Positive green fibres are representative of FLNC aggregates. (B) Quantification of the FLNC aggregates observed across the whole muscle cross section as a percentage of total fibres. ZAK$^{-/-}$ overloaded leg showed significant increase in FLNC aggregates compared to the overloaded leg of the WT mouse (* $p < 0.05$). Control legs show fewer FLNC aggregates as expected for this age group as observed in 22 week soleus muscle (Stonadge *et al.* In Review). Error bars = mean +/- Standard Error.

Figure 9.4: Loss of ZAK results in an inability to undergo resistance-induced hypertrophy. (Top) Synergistic ablation of the gastrocnemius of wild type (WT) mice and quantification of fibre cross sectional area (CSA) of control and experimental (overload) soleus muscle (n=6). Each mouse is represented here as individuals. After quantification, the majority of experimental muscles display the classical increase in fibre CSA after ablation of gastrocnemius muscles indicative of resistance-induced hypertrophy. (Bottom) Synergistic ablation of the gastrocnemius of ZAK$^{-/-}$ mice and quantification of fibre CSA of control and experimental (overload) soleus muscle (n=6). After quantification, the majority of experimental muscles fail to display the classical increase in fibre CSA after ablation of gastrocnemius muscles indicative of an inability to undergo resistance-induced hypertrophy. Here we compared the means of soleus CSA before and after synergistic ablation. Student's t-test (* $p < 0.05$).

9.5 Discussion

The ability to successfully regenerate following damage is a critical component of skeletal muscle plasticity. Which proteins facilitate this recovery is a fundamental question in skeletal muscle biology. Here we show evidence of the importance of ZAKβ in the maintenance of skeletal muscle throughout periods of intense mechanical stress. As shown with the induction of an acute muscle injury, the loss of ZAK causes a delay in the regeneration time of injured myofibres. Despite $ZAK^{-/-}$ mice being overtly indistinguishable from wild type littermates, the results above confirm that loss of ZAKβ has a small but measurable effect on the muscle regenerative capacity (Figure 9.1). Deletion of ZAK in C2C12 myoblast yields a more striking phenotype whereby myotube formation is significantly impaired (Figure 8.3). Comparatively, the phenotype of the $ZAK^{-/-}$ mouse is less severe, even following acute muscle injury. The fusion of myoblasts into myotubes is one of the most regulated and critical events during skeletal muscle formation and regeneration (as reviewed in Sampath, Sampath and Millay, 2018). It is the role of the skeletal muscle niche however, that heavily influences the ability to proliferate, differentiate, and successfully regenerate (Yin, Price and Rudnicki, 2013). Numerous factors like: neuronal innervation, vasculature, secretion of hormones and extrinsic factors, nutrient availability, and level of damage, all influence muscle regeneration (Jirmanová and Thesleff, 1972; Hansen-Smith, Picou and Golden, 1979; Chanoine *et al.*, 1987; McGeachie and Grounds, 1987; Phillips and Bennett, 1987; Mulvaney, Marple and Merkel, 1988). A lack of this extracellular niche to help promote myoblast fusion and differentiation may account for the fundamental differences in the outcomes of both the $BaCl_2$-induced muscle injury and evaluation of fusion index in ZAK-KO C2C12 myoblasts. A likely explanation is that ZAKβ modulates cell fusion and adhesion complexes, evidenced by the *in vitro* ZAK-KO experiments and phosphoproteomics which culminate in a significant, but not severe, impairment in muscle regeneration following injury *in vivo*. However, an investigation using WT mouse satellite cells would confirm the presence of ZAKα *in vivo* and comparisons of satellite cell proliferation and differentiation *ex vivo* between WT and $ZAK^{-/-}$ mice would confirm the fusion defect *in vivo.*

Another example of the link between muscle overload and muscle regeneration is the mechanosensor, focal adhesion kinase (FAK). FAK is a tyrosine kinase responsible

for coordinating signalling via the focal adhesion complex in response to changes in cellular tension (Schaller *et al.*, 1995). Located primarily within the costamere of skeletal muscle, FAK associates with integrins to signal changes in mechanical loading (Anastasi *et al.*, 2008). FAK is necessary for myoblast fusion and is expressed at higher levels in myotubes than myoblasts (Flück *et al.*, 1999). FAK knock-down prevented myoblast fusion, and satellite cell-specific FAK KO mice have a significantly reduced regenerative capacity following $BaCl_2$-mediated acute muscle injury (Quach *et al.*, 2009), which is considered to be mediated via integrin-FAK complexes. Additionally, FAK is thought to signal via mTOR to regulate skeletal muscle hypertrophy (Gan, Yoo and Guan, 2006). This places ZAKβ in a similar physiological role as FAK in terms of its ability to detect changes in skeletal muscle cytoskeletal tension and mediate hypertrophic signalling and help maintain the regenerative capacity of the muscle once damaged.

The ability of the muscle to detect changes in cytoskeletal tension and initiate the appropriate signalling response is the responsibility of mechanosensors (as reviewed in Martino *et al.*, 2018). Mechanosensors relay this information to alter levels of gene transcription and protein expression (Cho, Irianto and Discher, 2017). Skeletal muscle contains multiple types of mechanosensors with diverse responses to changes in tension (as reviewed in Burkholder, 2007). For many years, the resistance vs endurance exercise paradigm has been well understood. Resistance exercise is known to initiate hypertrophic growth. An artificially created increase of mechanical load upon the muscle results in muscle damage and fibre adaptation by increasing the overall cross-sectional area (CSA) and myofibrillar structure and organisation (Jones *et al.*, 2008; Herman *et al.*, 2010). Conversely, endurance exercise is more suited to an increase in metabolic capacity through low intensity exercise which trains the muscle to become more fatigue resistant (Farup *et al.*, 2012). Here we induced an artificial resistance exercise regime by synergistic ablation of one of the lower limb muscles and forced the synergistic muscles to bear the weight of the mouse and adapt accordingly. We found that $ZAK^{-/-}$ mice were not only unable to undergo hypertrophy, evidenced by the lack of expected CSA increase, but the muscles exhibited aggregations of damaged FLNC which is significantly higher than observed in the WT counterpart. This implicates ZAK in the recognition of stress imposed by resistance exercise, links it with the hypertrophic signalling pathway as has been alluded to

previously, and further highlights the vulnerability within the muscle to increased mechanical load. The generic phenotype observed in the ZAK$^{-/-}$ mouse is likely attributed to skeletal muscle insufficiency to cope with the mechanical load placed upon it, as a result the muscle becomes damaged. This damage is what we observed following overload experiments. Therefore, this once again suggests that ZAKβ is important for maintaining structural integrity throughout periods of increased mechanical demand.

We showed previously that the phenotype of the ZAK$^{-/-}$ mouse progressively deteriorates with age in the soleus, with pathology evident as early as 8 weeks of age. On the other hand, the tibialis anterior does not display a clear pathology at early timepoints, instead displaying a mild pathology at one year of age. As we have seen, a regenerative pathology emerges as the ZAK$^{-/-}$ mice age (Figure 9.2), suggesting that regardless of muscle type, no muscle is exempt from the effect of the loss of ZAK. Despite this, the frequency of use and muscle composition has a significant effect on the development of the pathological phenotype. There are many inherited muscle disorders which preferentially affect specific fibre types, including Duchenne muscular dystrophy (Webster *et al.*, 1988), Myosinopathies (Ortolano *et al.*, 2011), and Pompe disease (Fukuda *et al.*, 2006). In this case however, we observe a phenotype in both fibre types of the soleus (Figure 3.3, 3.4) which is not observed at the early time point in a different muscle like the tibialis. Therefore, the pathology caused by the loss of ZAK is suggested to be linked more with muscle use than with an effect on a particular fibre type. Muscle plasticity deteriorates with age. Several conditions are thought to be responsible for age-related muscle loss: reduced protein synthesis (Welle *et al.*, 1993), infiltration of fat tissue and increased deposition of ECM (Brack *et al.*, 2007; Addison *et al.*, 2014), inflammation (Fagiolo *et al.*, 1993), dysregulation of proteasomal degradation (Chondrogianni *et al.*, 2000; Cuervo and Dice, 2000), and deregulation of autophagy (Joseph *et al.*, 2019). Resistance exercise remains a very effective intervention for increasing mass, strength and quality in older age (Fiatarone *et al.*, 1994). Unfortunately, myopathy patients are often unable to undertake such regimes at the risk of exacerbating their condition, as we have observed using synergistic ablation in the ZAK$^{-/-}$ mouse model. In these circumstances, the management of protein turnover mechanisms is paramount. Clinically it has been suggested that administration of certain compounds such as metformin are able to rebalance protein

turnover and prevent muscle atrophy. For instance, PGC-1α has an essential regulatory role in skeletal muscle aging and atrophy (Petrocelli and Drummond, 2020). Activated PGC-1α can downregulate FOXO3 which prevents muscle atrophy (Sandri *et al.*, 2006), through inhibition of the ubiquitin-proteasome system, and autophagic degradation pathways (Cannavino *et al.*, 2014). Metformin has been demonstrated to promote the expression of PGC-1α in skeletal muscle through the activation of AMPK (Suwa *et al.*, 2006). Metformin treatment was found to improve myofibre atrophy and reduce fibrosis (Hasan *et al.*, 2019). Together, this highlights the importance of understanding the key players in protein turnover mechanisms to improve our clinical knowledge of how we can best treat people who develop muscle diseases. The dual nature of proteins such as ZAKβ; potential regulators of myofibre hypertrophy, yet intrinsically associated with a deregulation of protein degradation when absent, present interesting therapeutic targets to exploit for future treatment of muscle disorders.

CHAPTER 10

DISCUSSION AND FUTURE PLANS

10.1 Overview

The aim of this project was to get insights into the roles of ZAKβ in skeletal muscle, through the characterisation of the phenotype of a $ZAK^{-/-}$ transgenic mouse line, generation and analysis of a C2C12-derived ZAK-KO cell line, and identification of downstream ZAKβ targets. The objectives set out at the beginning of this project were the following:

- **Characterisation of the $ZAK^{-/-}$ mouse pathology.**
- **Determination of the role of ZAKβ in skeletal muscle hypertrophy.**
- **Identification of ZAKβ direct phosphorylation targets in skeletal muscle**.
- **Establishment of the role of ZAKβ under specific physiological stresses.**

A potential molecular signalling pathway was able to be identified from these experiments, which may be delineated through further analysis. We found evidence of a link between ZAKβ and initiation of the hypertrophic response via the canonical hypertrophy associated protein mTOR was identified, potentially acting through various costameric, z-disc, focal adhesion complexes, and the z-disc protein KY. The generation of ZAK-KO C2C12-derived cell lines and a vector capable of biotin ligation of spatially-interacting proteins are essential resources for future characterisations of ZAKβ.

10.2 ZAK and the costamere

In this project, I applied a simple approach for substrate mining that can be used to identify direct, *ex vivo*, downstream substrates of ZAKβ. We were able to identify many novel substrates of ZAKβ that suggest alternative functions for ZAKβ other than classical MAPK signalling, such as FLNC, BAG3, and COBL. We have shown a possible role for ZAKβ in the regulation of COBL expression *in vitro* and have identified aberrant FLNC and BAG3 expression in pathological skeletal muscle of $ZAK^{-/-}$ mice. The FLNC/BAG3 associated pathology within these muscles becomes exacerbated following functional overload, suggestive of a relationship between ZAKβ and mechanically-induced stress. Following a cellular compression stress, ZAKβ has been shown to autophosphorylate and relocate to stress fibres through its unique C-terminal

region. This region contains an isoform-specific stress-fibre binding domain (SFBD) (Nordgaard *et al.*, 2022). Under these conditions, ZAKβ has been shown to activate p38 (Nordgaard *et al.*, 2022). Repeated contractions of Tibialis anterior (TA) muscle also led to p38 activation in a ZAKβ-dependent mechanism (Nordgaard *et al.*, 2022). It would therefore appear that ZAKβ is an early mediator of a contraction-induced mechanical stress, but the mechanism(s) by which ZAKβ senses these stimuli are not yet known. We therefore propose that ZAKβ plays a role in the modulation of z-disc and/or costameric-based protein focal adhesion complexes critical for the maintenance of sarcomeric integrity during muscle contraction and relaxation.

ZAKβ has previously been shown to negatively regulate cancer cell extrusion in RasV12-transformed cells by modulating the activity of Paxillin, Myosin, and Filamin (Maruyama *et al.*, 2020). In this study, ZAK was shown to be a key regulator in the activity and localisation of downstream regulators: Paxillin, Myosin, and Filamin, but was unable to discern exactly how ZAK interacts with these proteins (Maruyama *et al.*, 2020). Since these proteins or their isoforms are also found at the costamere, it is plausible that ZAKβ may perform a similar role in skeletal muscle with these very proteins. Overall, this further supports the hypothesis that ZAKβ may act as a modulator of signal transduction and costameric components.

Based on the results that the α7 integrin isoform was identified as a direct phosphorylation target of ZAKβ, and that the α7 integrin isoform is found differentially expressed in the $ZAK^{-/-}$ mutant, we hypothesise that ZAKβ can modulate the activity of this transmembrane receptor and influence the downstream signal transduction response. When mutated, the α7 integrin isoform is known to cause congenital myopathies (Hayashi *et al.*, 1998). Together with integrin β1 isoform (Belkin *et al.*, 1997), this integrin heterodimer has an extremely important role in cell adhesion and signal transduction at the costamere (Huveneers and Danen, 2009). This relationship may be important for the mediation of signalling specifically via known signal transducers of the integrin pathway such as Focal adhesion kinase (FAK), one of the most characterised mechanosensors known to induce skeletal muscle hypertrophy signalling through Akt/mTOR, ERK1/2, and JNK (Nadruz *et al.*, 2005; Graham, Gallagher and Cardozo, 2015). Overexpression of ZAKβ results in mTOR-dependent fibre hypertrophy. We further propose that ZAKβ modulates the activity of the α7β1

integrin receptor, which ultimately leads to regulation of muscle size, endurance-associated fibre adaptation, and resistance-induced hypertrophy. Since our analyses showed that in the ZAK$^{-/-}$ mouse, synergistic ablation of the gastrocnemius was unable to induce a hypertrophic response in the soleus, and these muscles experience a delay in the regenerative process following barium chloride-induced muscle injury, we suggest that ZAKβ may have a role in supporting the normal function of the costamere and disruption of the complexes found here may affect the typical hypertrophic signalling networks initiated upon detection of mechanical stress.

10.3 ZAK and hypertrophy

ZAK has previously been implicated in actin organisation and fibre modulation. In early studies using H9c2 cardiomyoblasts, overexpression of ZAKβ was associated with an increase in actin fibre organisation and cell size, and loss of ZAK activity correlated with an inability to respond to TGFβ-mediated hypertrophy *in vitro* (Huang et al., 2004; Hsieh et al., 2015). Transgenic expression of ZAKβ in cardiac tissue resulted in differential expression of genes associated with cardiac hypertrophy, and an increase in heart weight to body weight ratio (Christe et al., 2004). Therefore, ZAK was thought to play a regulatory role in cardiac-associated hypertrophy, characterised by increased actin polymerisation and cell size.

Further to this, a novel role of ZAK has also been identified in the transduction of canonical TGFβ signalling (Nyati *et al.*, 2016). Electron microscopy analysis of muscle biopsies of human patients carrying the deleterious mutation within the kinase domain of *ZAK* showed evidence of centralised nuclei tightly surrounded by myofibrils and sarcoplasmic disorganisation (Vasli *et al.*, 2017). Increased load or demand on skeletal muscle results in the stretch-induced stress response which ultimately leads to increased protein synthesis and adaptation of the muscle fibre to withstand future demand (Bloem *et al.*, 2001). Regulation of actin dynamics plays a key role in skeletal muscle hypertrophy. When hypertrophy is induced by mechanical stress, actin reorganisation increases at the barbed end, which is beneficial for the construction of new sarcomeres. These new sarcomeres are added in parallel to the existing sarcomeres and increase the overall cross-sectional area of the myofibre (Gaikis *et*

al., 2013; Haun *et al.*, 2019). The effect of ZAKβ overexpression on fibre CSA leads us to believe that ZAKβ may behave in a similar fashion to that of nebulin and N-WASP which are both required for IGF-1-induced muscle hypertrophy and actin filament formation in myofibrillogenesis via actin nucleation (Takano *et al.*, 2010). In addition to this, the known targets of ZAKβ *in vitro*, p38γ and JNK are important transducers of the stress response (Kyriakis and Avruch, 2001). Collectively, our data suggest that the functional outcome of ZAKβ activation is associated with hypertrophic signalling with mTOR the canonical mediator of such an effect. These findings, alongside the observed general muscle atrophy in human patients (Vasli *et al.*, 2017) and specific atrophy in our mouse model, suggest that ZAKβ could be responsible for initiating a signalling cascade that ultimately results in hypertrophic growth via an increase in cytoskeletal organisation and protein synthesis.

10.4 A potential role for ZAK in the regulation of CASA

In this study, we generated a non-exhaustive list of potential targets of ZAKβ phosphorylation in addition to cross-referencing this with the list of DEGs in the $ZAK^{-/-}$ mouse. From this, and that of the DEGs in the ZAK patients, we reveal an over-representation of genes associated with focal adhesion components of z-disc and costameric protein complexes. Amongst these, the actin filament crosslinking protein FLNC emerged as an interesting target, as FLNC aggregates are a hallmark of the KY-associated muscle conditions (Straussberg *et al.*, 2016). We confirmed the presence of FLNC aggregates in soleus muscle from the $ZAK^{-/-}$ mouse and in skeletal muscle of ZAK patients, suggesting perturbation of FLNC turnover may contribute to the weakening of the muscle fibre.

Effective protein turnover is critical for skeletal muscle integrity. Breakdown of this relationship contributes to a number of different myopathies (Jokl and Blanco, 2016). Loss of KY results in a myofibrillar myopathy characterised by the presence of protein aggregates (Kley *et al.*, 2013; Straussberg *et al.*, 2016), most notably FLNC and BAG3, and an increase in total levels of insoluble BAG3 in soleus (Jokl *et al.*, 2018). Filamin C is a client of the BAG3-mediated chaperone assisted selective autophagy (CASA) pathway, and accumulations of FLNC are known to indicate inefficient protein

turnover via the BAG3-mediated CASA pathway (Leber *et al.*, 2016; Ruparelia *et al.*, 2016).

In this study, we have shown in the ZAK$^{-/-}$ that FLNC co-localised with BAG3 within the fibres of slow twitch muscle. As a co-chaperone of the CASA protein degradation pathway, BAG3 is integral for FLNC turnover whereby both BAG3 and ubiquitinated FLNC are degraded following integration of the whole CASA complex into phagosomes by the p62 cargo. Here we observe an accumulation of BAG3 which colocalised with FLNC (Figure 6.5). This suggests a muscle-specific impairment within the mechanism of protein turnover when ZAKβ is lost.

We also observed the colocalisation between FLNC and Myotilin, another hallmark of myofibrillar myopathies. Myotilin is often found abnormally expressed in other cases of myofibrillar myopathies and can be found alongside FLNC in protein aggregates (Selcen, 2008; Can *et al.*, 2014; Fichna, *et al.*, 2018). Together, this data is suggestive of increased levels of damaged protein. These observations maintain a possible role for ZAK, either in CASA-mediated protein turnover of large, structural z-disc proteins, or for the stabilisation of critical z-disc/costameric protein complexes.

COBL is an actin nucleator known to modulate the actin cytoskeleton (Ahuja *et al.*, 2007). In this study, we observe a relationship between ZAKβ and COBL whereby ZAK modulates the expression pattern of COBL in COS7 cells, and appears to have a role in the stabilisation of the protein in differentiated C2C12 cells. ZAKβ is thought to directly phosphorylate COBL as suggested by the phosphoproteomics assay. In addition to its role in the turnover of damaged z-disc proteins such as FLNC, BAG3 has been reported to regulate the actin cytoskeleton, and modulate cell adhesion and motility through interactions with both Rac and PDZGEF2 (Iwasaki *et al.*, 2007, 2010). Therefore, we hypothesise that the role ZAKβ plays in muscle is not only regulatory of muscle hypertrophy, but a modulator of the actin cytoskeleton via COBL and BAG3.

Here we propose a mechanical stress-associated system utilised by skeletal muscle for the purpose of maintenance of efficient output and integrity. The proteins involved in this system are all key players in the same pathways that overall govern sarcomeric stability and protein turnover at the z-disc. Proteins which include ZAKβ, components of the KY protein complex, and z-disc/costameric protein complexes are intrinsically

linked through established interaction networks. Through localisation at the z-disc, the hub of mechanosensation and transduction, ZAKβ is perfectly situated to modulate signal transduction in response to changes in mechanical load. From the data presented in this thesis, in conjunction with data from previous studies, we observe a stress-induced relationship between ZAKβ, KY, IGFN1, and FLNC as transducers of the stress response and ultimately as regulators of skeletal muscle maintenance through cell adhesion signalling networks and BAG3-mediated protein turnover.

10.5 Future Work

10.5.1 Proximity ligation

An important part of understanding the function of a stress kinase is knowing its unique role in signalling and which proteins it interacts with. With respect to ZAKβ, these questions were largely unanswered. In this project, we began to uncover the molecular mechanisms which govern ZAKβ in the maintenance of skeletal muscle, however more questions remain. We generated a ZAKβ-tdTomato fusion vector with miniTurbo which would enable us to detect any interacting partners in its physiological environment. This assay differs from the whole cell lysate targeted phosphoproteomics undertaken in this study. By using this vector to transfect into C2C12 cells and generate stable cell cultures, we would aim to differentiate and detect any ZAKβ interacting partners at these primitive z-disc target locations, in which ZAKβ has been shown to localise.

10.5.2 KY and ZAK

In previous experiments, ZAKβ has been shown to interact with the KY protein complex via IGFN1 (Baker *et al.*, 2010). The nature of this interaction has yet to be identified. There are many similarities between that of mice and humans lacking the KY protein, and mice and humans lacking ZAK. In $ZAK^{-/-}$ mice, we observe a much milder version of every aspect described in the *ky/ky* mutant, including muscle involvement, slow type adaptation, impaired hypertrophic response, presence of

similar components in apparent aggregates, etc. All suggestive of a milder myofibrillar myopathy in ZAK$^{-/-}$ mice and ZAK patients.

Further to this, we have established a connection between ZAKβ and KY with regards to its importance for hypertrophic signalling upon ZAKβ overexpression in vivo. When KY is lost, ZAKβ overexpression is unable to initiate the characteristic hypertrophic response. Taken altogether we understand that KY acts somewhere downstream of ZAKβ in the activation of mTOR signalling.

Considering all evidence presented here, there is an undoubtable molecular partnership between ZAKβ and KY, of an unknown nature. Further experiments to determine the exact relationship between these two proteins will help delineate the ZAKβ signalling pathway. One avenue of investigation would be the role of the common protein IGFN1 in both KY and ZAKβ signalling, considering the fact that it has been found upregulated in atrophied muscles and muscles of ZAK-null patients (Li *et al.*, 2017; Vasli *et al.*, 2017; Cracknell *et al.*, 2020). Another avenue would be to investigate the relationship between ZAKβ and KY in terms of protein turnover, particularly via chaperone assisted selective autophagy (CASA). It is understood that KY is necessary for efficient CASA turnover of damaged z-disc structural proteins like FLNC. As ZAK$^{-/-}$ muscles exhibit a similar phenotype, it is possible that ZAKβ fits into this pathway alongside KY.

10.5.3 Characterisation of protein aggregates

We see in the ZAK$^{-/-}$ mouse that both BAG3; a CASA co-chaperone, and FLNC; a client of the CASA protein degradation pathway, are implicated in ZAK pathology. Accumulation of misfolded protein is a classical hallmark of myofibrillar myopathies. In the case of the KY mutant, the presence of FLNC aggregates is also characteristic of impairment to the CASA pathway of protein degradation. This type of protein degradation is associated with ubiquitin labelling. By qualifying which proteins have been targeted for degradation through the covalent attachment of ubiquitin molecules, we can try to address the question of what other proteins become misfolded during sarcomeric instability caused by ZAK deficiency. By testing for additional clients of the CASA pathway recently identified, such as ACTN2, MYOZ2, and SPTAN1 (Martin *et*

al., 2021) specific to the sarcomere we aim to test for the presence of z-disc/costameric proteins to further determine the role of ZAKβ in muscle-specific protein turnover.

10.5.4 Electron microscopy of ZAK$^{-/-}$ tissue

In many cases of skeletal muscle myopathies, the resultant pathology can be observed at ultrastructural level. Each myopathy has a set of characteristics, however the severity of such is variable. Such anomalies include z-disc thickening, z-disc dissociation, z-disc streaming, mitochondrial abnormalities, granulofilamentous accumulations, and filamentous bundles and floccular accumulations of thin filamentous material (Fernandez *et al.*, 2005; Claeys *et al.*, 2008). We already knew that ZAKβ interacts with IGFN1 at the z-disc, alongside proteins like FLNC and COBL which are all thought to be important for stabilisation and maintenance of the sarcomere. During this investigation, we found that loss of ZAKβ *in vivo* affects the turnover of both FLNC and BAG3, components of the z-disc and costamere important for sarcomeric and myofibrillar stability. Additionally, ZAKβ activity was shown to modulate COBL activity *in vitro*. As a result, it is possible that loss of ZAKβ results in a lack of regulation of z-disc/costameric complexes and thus pathology at ultrastructural level. A close look at the sarcomeric ultrastructure will allow us to understand the specific effects of the loss of ZAK at single-sarcomere level.

10.6 Summary

Our findings suggest that the ZAK deficiency pathology overlaps with that of other myofibrillar myopathies, in which aggregates containing a small set of z-disc proteins is a common observation. This also places ZAK deficiency myopathies in the category of a myofibrillar myopathy, like that of the KY mutant, instead of a centronuclear myopathy in which it is currently categorised.

We hypothesise that ZAKβ phosphorylates components of the z-disc and costameric protein adhesion and signalling complexes, and the KY protein complex, both thought

to be important for normal muscle function. As a result, we suggest ZAKβ regulates the activity and stability of proteins involved in actin organisation and cell adhesion at the costamere. This ultimately affects the cell's ability to detect and respond to increased mechanical stress in addition to impairment in the cell's motility and protein turnover mechanisms. From what we have discovered, we propose that loss of ZAK causes sarcomeric instability, whereby many proteins responsible for maintaining the structure of the sarcomere become damaged. These damaged proteins accumulate within the fibre and contribute to muscle weakness. We know from other disease models, accumulation of large damaged proteins is detrimental to the health of the organ (Davies, 1987; Davies, Lin and Pacifici, 1987; Williams *et al.*, 2006; Voisine, Pedersen and Morimoto, 2010). The consequences of these aggregates in this scenario are 2-fold. Firstly, the mere presence of protein aggregates results in myofibre weakness through loss of structure and adhesion, and an obstruction to the normal function of the contractile apparatus. But secondly, and arguably more importantly, a decrease in the breakdown of these damaged proteins can be correlated with reduced synthesis of new functional replacement proteins, thus exacerbating the pathology (Homma *et al.*, 2006; Selcen *et al.*, 2009; Kathage *et al.*, 2017).

We know that one of the most obvious phenotypes of the pathology caused by the KY mutation is the presence of FLNC/BAG3 aggregates with an upregulation of clients of the CASA pathway (Jokl *et al.*, 2018). It is from this that we hypothesise that ZAKβ interacts with, and modulates, clients of the CASA pathway which in turn modulates and enhances the turnover of structural proteins specifically targeted for degradation via the CASA pathway.

We now observe a single gene which encodes two distinct protein isoforms that behave remarkably differently. This dichotomy is evident in the tissue-specific expression of each isoform, where ZAKβ is the only isoform expressed in skeletal muscle. Through this investigation into the role of ZAKβ in skeletal muscle, we have found evidence to suggest that ZAKβ is an important regulator of the hypertrophy pathway, activated in response to increased mechanical stress during resistance or overload-based exercises. There appears to be a fundamental relationship between ZAKβ and both the KY protein complex, and the CASA-mediated protein degradation pathway; both critical for the stability of adult skeletal muscle. The exact role of ZAKβ

in skeletal muscle and the nature of its signalling remains unclear, however we are now a little bit closer to answering these questions.

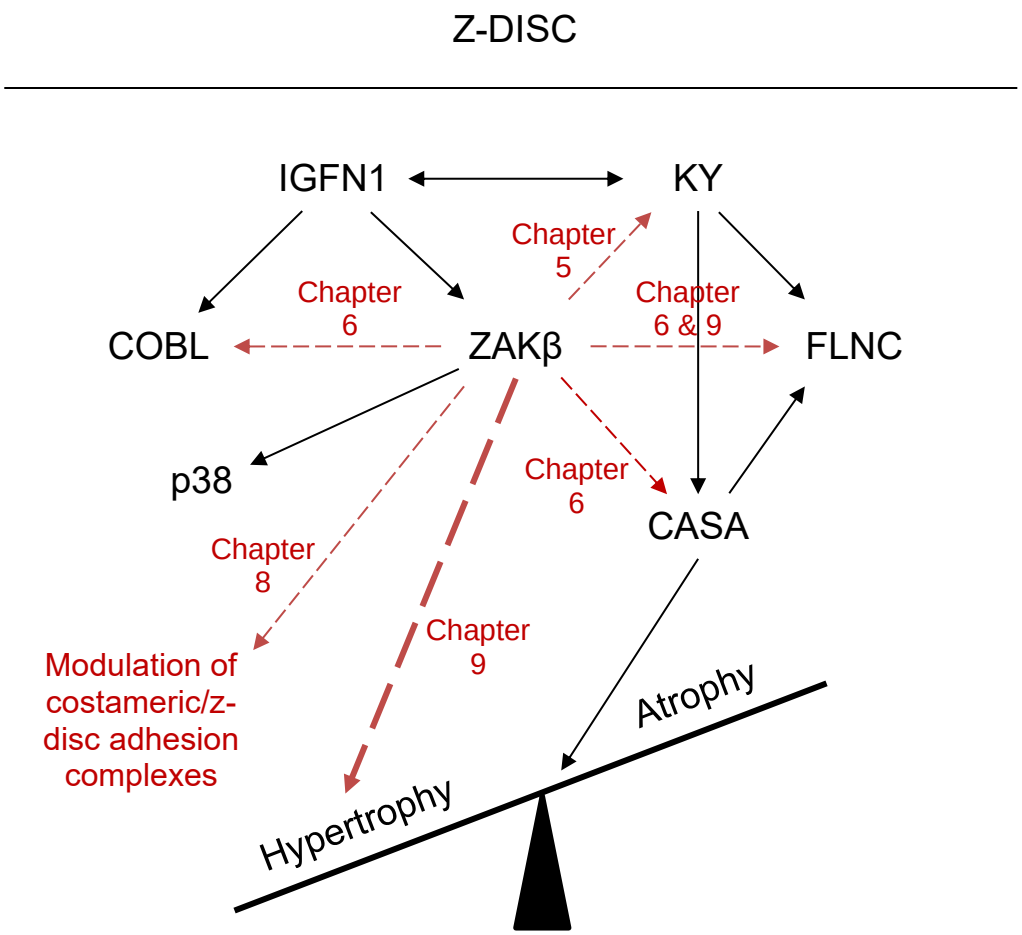

Figure 10.1: Post-project summary of the lines of investigation for the role of ZAKβ in skeletal muscle. Black lines indicate known relationships. Red dashed lines indicate proposed relationships. Each proposed relationship has been investigated in the chapter(s) indicated next to the dashed line.

Glossary of Abbreviations

Abbreviation	Name
ADP	Adenosine diphosphate
AKT	Protein Kinase B
ATP	Adenosine triphosphate
BaCl2	Barium Chloride
BAG3	Bcl2 Associated Athanogen 3
BSA	Bovine serum albumin
C2C12	Skeletal muscle-derived myoblast cell line
CASA	Chaperone Assisted Selective Autophagy
COBL	Cordon-Bleu WH2 Repeat Protein
COS7	CV-1 in Origin, carrying the SV40 genetic material
CRISPR	Clustered regularly interspaced short palindromic repeats
CSA	Cross sectional Area
DAPI	4′,6-diamidino-2-phenylindole
DEG	Differentially-expressed gene
DGC	Dystrophin Glycoprotein Complex
DM	Differentiation Media
DMD	Duchenne muscular dystrophy
DPI	Days post Injury
ECM	Extracellular matrix
EDL	Extensor digitorum
eIF4E	Eukaryotic Translation Initiation Factor 4E
ERK	Extracellular Signal-regulated Kinase
FBS	Foetal bovine serum
FHL1	Four and a half LIM domains protein 1
FLNC	Filamin C
FN	Fibronectin type 3 domain
FOXO	Forkhead Box Transcription Factors
FSBA	5'-4-fluorosulphonylbenzoyladenosine
GAPDH	Glyceraldehyde 3-phosphate dehydrogenase
GM	Growth Media

IG	Immunoglobulin domain
IGF1	Insulin-like growth factor 1
IGF-1R	Insulin-like growth factor 1 Receptor
IGFN1	Immunoglobulin-like and fibronectin type III domain containing 1
IP	Intraperitoneal injection
IRS-1	Insulin Receptor Substrate 1
KY	Kyphoscoliosis peptidase
LC-MS/MS	Liquid Chromatography with tandem mass spectrometry
LZ	Leucine zipper domain
MAPK	Mitogen-activated protein kinase
MFM	Myofibrillar myopathy
MRF	Myogenic regulatory factor
mTOR	Mammalian Target of Rapamycin
MuSC	Muscle stem cell
ON	Overnight
p70S6K	Ribosomal protein s6 kinase beta 1
PAGE	Polyacrylamide gel electrophoresis
PBS	Phosphate-buffered saline
PCR	Polymerase Chain Reaction
PI3K	Phosphatidylinositol 3 kinase
RIPA	Radioimmunoprecipitation assay
RT	Room temperature
SAM	Sterile alpha motif domain
SDS	Sodium dodecyl sulphate
SFBD	Stress fibre binding domain
SMAD2/3	SMAD Family Member 2/3
SR	Sarcoplasmic Reticulum
TA	Tibialis anterior
WGA	Wheat germ agglutinin
WT	Wild-type
XIN	Xin Actin Binding Repeat Containing 1
Y2H	Yeast 2 Hybrid
ZAK	Leucine Zipper-and Sterile Alpha Motif-Containing Kinase

References

Abmayr, S.M. and Pavlath, G.K. (2012) 'Myoblast fusion: lessons from flies and mice', *Development* , 139(4), pp. 641–656.

Addison, O. *et al.* (2014) 'Intramuscular fat and inflammation differ in older adults: the impact of frailty and inactivity', *The journal of nutrition, health & aging*, 18(5), pp. 532–538.

Ahmad, I. *et al.* (2022) 'A novel MAP3K20 mutation causing centronuclear myopathy-6 with fiber-type disproportion in a Pakistani family', *Journal of human genetics*, 68(2), pp. 107–109.

Ahuja, R. *et al.* (2007) 'Cordon-bleu is an actin nucleation factor and controls neuronal morphology', *Cell*, 131(2), pp. 337–350.

Alghannam, A.F., Ghaith, M.M. and Alhussain, M.H. (2021) 'Regulation of Energy Substrate Metabolism in Endurance Exercise', *International journal of environmental research and public health*, 18(9). Available at: https://doi.org/10.3390/ijerph18094963.

Allen, D.G., Whitehead, N.P. and Froehner, S.C. (2016) 'Absence of Dystrophin Disrupts Skeletal Muscle Signaling: Roles of Ca2+, Reactive Oxygen Species, and Nitric Oxide in the Development of Muscular Dystrophy', *Physiological reviews*, 96(1), pp. 253–305.

Ambrosio, F. *et al.* (2009) 'The effect of muscle loading on skeletal muscle regenerative potential: an update of current research findings relating to aging and neuromuscular pathology', *American journal of physical medicine & rehabilitation / Association of Academic Physiatrists*, 88(2), pp. 145–155.

Anantharaman, V., Koonin, E.V. and Aravind, L. (2001) 'Peptide-N-glycanases and DNA repair proteins, Xp-C/Rad4, are, respectively, active and inactivated enzymes sharing a common transglutaminase fold', *Human molecular genetics*, 10(16), pp. 1627–1630.

Anastasi, G. *et al.* (2008) 'Costameric proteins in human skeletal muscle during muscular inactivity', *Journal of anatomy*, 213(3), pp. 284–295.

Andersen, P. and Henriksson, J. (1977). Training induced changes in the subgroups of human type II skeletal muscle fibres. *Acta physiologica Scandinavica*, 99 (1), pp.123–125.

Arif, B. *et al.* (2020) 'A novel homozygous KY variant causing a complex neurological disorder', *European journal of medical genetics*, 63(11), p. 104031.

Arndt, V. *et al.* (2010) 'Chaperone-assisted selective autophagy is essential for muscle maintenance', *Current biology: CB*, 20(2), pp. 143–148.

Augusto, V., Padovani, C. R. and Campos, G. E. R. (2004). SKELETAL MUSCLE FIBER TYPES IN C57BL6J MICE. *Braz. J. morphol. Sci.*, 21 (2), pp.89–94.

Baas, D. *et al.* (2012) 'CKIP-1 regulates mammalian and zebrafish myoblast fusion', *Journal of cell science*, 125(Pt 16), pp. 3790–3800.

Baker, J. *et al.* (2010) 'Identification of a Z-band associated protein complex involving KY, FLNC and IGFN1', *Experimental cell research*, 316(11), pp. 1856–1870.

Bang, M.-L. *et al.* (2006) 'Nebulin-deficient mice exhibit shorter thin filament lengths and reduced contractile function in skeletal muscle', *The Journal of cell biology*, 173(6), pp. 905–916.

Bassel-Duby, R. and Olson, E.N. (2006) 'Signaling pathways in skeletal muscle remodeling', *Annual review of biochemistry*, 75, pp. 19–37.

Beatham, J. *et al.* (2004) 'Filamin C interacts with the muscular dystrophy KY protein and is abnormally distributed in mouse KY deficient muscle fibres', *Human molecular genetics*, 13(22), pp. 2863–2874.
Beatham, J. *et al.* (2006) 'Constitutive upregulations of titin-based signalling proteins in KY deficient muscles', *Neuromuscular disorders: NMD*, 16(7), pp. 437–445.
Belkin, A.M. *et al.* (1997) 'Muscle β1D Integrin Reinforces the Cytoskeleton–Matrix Link: Modulation of Integrin Adhesive Function by Alternative Splicing', *The Journal of cell biology*, 139(6), pp. 1583–1595.
Bischoff, R. (1975) 'Regeneration of single skeletal muscle fibers in vitro', *The Anatomical record*, 182(2), pp. 215–235.
Blake, D.J. *et al.* (2002) 'Function and genetics of dystrophin and dystrophin-related proteins in muscle', *Physiological reviews*, 82(2), pp. 291–329.
Blanco, G. *et al.* (2001) 'The kyphoscoliosis (ky) mouse is deficient in hypertrophic responses and is caused by a mutation in a novel muscle-specific protein', *Human molecular genetics*, 10(1), pp. 9–16.
Blanco, G. *et al.* (2004) 'Molecular phenotyping of the mouse ky mutant reveals UCP1 upregulation at the neuromuscular junctions of dystrophic soleus muscle', *Neuromuscular Disorders*, pp. 217–228. doi:10.1016/j.nmd.2003.09.008.
Bleecker, J.L.D. *et al.* (1996) 'Myofibrillar Myopathy with Abnormal Foci of Desmin Positivity. II. Immunocytochemical Analysis Reveals Accumulation of Multiple Other Proteins', *Journal of Neuropathology and Experimental Neurology*, pp. 563–577. Available at: https://doi.org/10.1097/00005072-199605000-00009.
Bloem, L. J. et al. (2001). Tissue distribution and functional expression of a cDNA encoding a novel mixed lineage kinase. *Journal of molecular and cellular cardiology*, 33 (9), pp.1739–1750.
Bodine, S.C. and Baehr, L.M. (2014) 'Skeletal muscle atrophy and the E3 ubiquitin ligases MuRF1 and MAFbx/atrogin-1', *American journal of physiology. Endocrinology and metabolism*, 307(6), pp. E469–84.
Bodine, S.C. *et al.* (2001) 'Akt/mTOR pathway is a crucial regulator of skeletal muscle hypertrophy and can prevent muscle atrophy in vivo', *Nature cell biology*, 3(11), pp. 1014–1019.
Bonaldo, P. and Sandri, M. (2013) 'Cellular and molecular mechanisms of muscle atrophy', *Disease models & mechanisms*, 6(1), pp. 25–39.
Bottinelli, R. and Reggiani, C. (2000) 'Human skeletal muscle fibres: molecular and functional diversity', *Progress in biophysics and molecular biology*, 73(2-4), pp. 195–262.
Bourdel-Marchasson, I. *et al.* (2016) 'One-Year Mortality in Older Patients with Cancer: Development and External Validation of an MNA-Based Prognostic Score', *PLOS ONE*, p. e0148523. Available at: https://doi.org/10.1371/journal.pone.0148523.
Boyer, J. G. et al. (2019). ERK1/2 signaling induces skeletal muscle slow fiber-type switching and reduces muscular dystrophy disease severity. *JCI insight*, 5 (10). [Online]. Available at: doi:10.1172/jci.insight.127356.
Bozyczko, D. *et al.* (1989) 'Integrin on developing and adult skeletal muscle', *Experimental Cell Research*, pp. 72–91. doi:10.1016/0014-4827(89)90419-9.
Brack, A.S. *et al.* (2007) 'Increased Wnt signaling during aging alters muscle stem cell fate and increases fibrosis', *Science*, 317(5839), pp. 807–810.
Branon, T.C. *et al.* (2017) 'Directed evolution of TurboID for efficient proximity labeling in living cells and organisms', *bioRxiv*. Available at: https://doi.org/10.1101/196980.

Brennan, A. *et al.* (2022) 'An Approach to Derive Functional Peptide Inhibitors of Transcription Factor Activity', *JACS Au*, pp. 996–1006. Available at: https://doi.org/10.1021/jacsau.2c00105.
Brennan, C.M. et al. (2021) 'p38 MAPKs - roles in skeletal muscle physiology, disease mechanisms, and as potential therapeutic targets', JCI insight, 6(12).
Bridges, L.R. *et al.* (1992) 'The neuromuscular basis of hereditary kyphoscoliosis in the mouse', *Muscle & Nerve*, pp. 172–179. Available at: https://doi.org/10.1002/mus.880150208.
Brooks, G.A. (2012) 'Bioenergetics of exercising humans', *Comprehensive Physiology*, 2(1), pp. 537–562.
Broome, C.S. *et al.* (2006) 'Effect of lifelong overexpression of HSP70 in skeletal muscle on age-related oxidative stress and adaptation after nondamaging contractile activity', *FASEB journal: official publication of the Federation of American Societies for Experimental Biology*, 20(9), pp. 1549–1551.
Buckingham, M. and Relaix, F. (2015) 'PAX3 and PAX7 as upstream regulators of myogenesis', *Seminars in cell & developmental biology*, 44, pp. 115–125.
Burkholder, T.J. (2007) 'Mechanotransduction in skeletal muscle', *Frontiers in bioscience: a journal and virtual library*, 12, pp. 174–191.
Burks, T.N. and Cohn, R.D. (2011) 'Role of TGF-β signaling in inherited and acquired myopathies', *Skeletal muscle*, 1(1), p. 19.
Cai, D., McCarron, R.M. and Hallenbeck, J. (2004) 'Cloning and characterization of a forkhead transcription factor gene, FoxO1a, from thirteen-lined ground squirrel', Gene, 343(1), pp. 203–209.
Calabria, E. *et al.* (2009) 'NFAT isoforms control activity-dependent muscle fiber type specification', *Proceedings of the National Academy of Sciences of the United States of America*, 106(32), pp. 13335–13340.
Caldwell, C.J., Mattey, D.L. and Weller, R.O. (1990) 'Role of the basement membrane in the regeneration of skeletal muscle', *Neuropathology and applied neurobiology*, 16(3), pp. 225–238.
Can, T. *et al.* (2014) 'Proteomic analysis of laser capture microscopy purified myotendinous junction regions from muscle sections', *Proteome science*, 12, p. 25.
Cannavino, J. *et al.* (2014) 'PGC1-α over-expression prevents metabolic alterations and soleus muscle atrophy in hindlimb unloaded mice', *The Journal of physiology*, 592(20), pp. 4575–4589.
Cauwer, H.D. *et al.* (2002) 'Workshop report of the 89th ENMC International Workshop: Central Core Disease, 19th–20th January 2001, Hilversum, The Netherlands', *Neuromuscular Disorders*, pp. 588–595. Available at: https://doi.org/10.1016/s0960-8966(02)00002-0.
Celegato, B. et al. (2006). Parallel protein and transcript profiles of FSHD patient muscles correlate to the D4Z4 arrangement and reveal a common impairment of slow to fast fibre differentiation and a general deregulation of MyoD-dependent genes. *PROTEOMICS*, 6 (19), pp.5303–5321. [Online]. Available at: doi:10.1002/pmic.200600056.
Chanoine, C. *et al.* (1987) 'Regulation by thyroid hormones of terminal differentiation in the skeletal dorsal muscle. II. Urodelan amphibians', *Developmental biology*, 123(1), pp. 33–42.
Chen, J.L. *et al.* (2014) 'Elevated expression of activins promotes muscle wasting and cachexia', *The FASEB Journal*, pp. 1711–1723. Available at: https://doi.org/10.1096/fj.13-245894.

Cho, S., Irianto, J. and Discher, D.E. (2017) 'Mechanosensing by the nucleus: From pathways to scaling relationships', *Journal of Cell Biology*, pp. 305–315. Available at: https://doi.org/10.1083/jcb.201610042.

Choi, D.H., Yang, J. and Kim, Y.S. (2019) 'Rapamycin suppresses postnatal muscle hypertrophy induced by myostatin-inhibition accompanied by transcriptional suppression of the Akt/mTOR pathway', Biochemistry and Biophysics Reports, 17, p. 182.

Choi-Rhee, E., Schulman, H. and Cronan, J.E. (2004) 'Promiscuous protein biotinylation by Escherichia coli biotin protein ligase', *Protein science: a publication of the Protein Society*, 13(11), pp. 3043–3050.

Chondrogianni, N. *et al.* (2000) 'Fibroblast cultures from healthy centenarians have an active proteasome', *Experimental gerontology*, 35(6-7), pp. 721–728.

Christe, M. *et al.* (2004) 'Transgenic mice with cardiac-specific over-expression of MLK7 have increased mortality when exposed to chronic β-adrenergic stimulation', *Journal of molecular and cellular cardiology*, 37(3), pp. 705–715.

Claeys, K.G. *et al.* (2008) 'Electron microscopy in myofibrillar myopathies reveals clues to the mutated gene', *Neuromuscular disorders: NMD*, 18(8), pp. 656–666.

Clarke, N.F. (2011) 'Congenital fiber-type disproportion', *Seminars in pediatric neurology*, 18(4), pp. 264–271.

Cohn, R.D. and Campbell, K.P. (2000) 'Molecular basis of muscular dystrophies', *Muscle & nerve*, 23(10), pp. 1456–1471.

Cohn, R.D. and Campbell, K.P. (2000) 'Molecular basis of muscular dystrophies', *Muscle & nerve*, 23(10), pp. 1456–1471.

Collins, C.A. *et al.* (2005) 'Stem cell function, self-renewal, and behavioral heterogeneity of cells from the adult muscle satellite cell niche', *Cell*, 122(2), pp. 289–301.

Collo, G., Starr, L. and Quaranta, V. (1993) 'A new isoform of the laminin receptor integrin alpha 7 beta 1 is developmentally regulated in skeletal muscle', *The Journal of biological chemistry*, 268(25), pp. 19019–19024.

Constantin, B. (2014) 'Dystrophin complex functions as a scaffold for signalling proteins', Biochimica et biophysica acta, 1838(2), pp. 635–642.

Conti, F.J. *et al.* (2009) 'Talin 1 and 2 are required for myoblast fusion, sarcomere assembly and the maintenance of myotendinous junctions', *Development*, pp. 3597–3606. Available at: https://doi.org/10.1242/dev.035857.

Cooper, J.A. (2002) 'Actin dynamics: tropomyosin provides stability', *Current biology: CB*, pp. R523–5.

Cornelison, D.D.W. (2008) 'Context matters: in vivo and in vitro influences on muscle satellite cell activity', *Journal of cellular biochemistry*, 105(3), pp. 663–669.

Cracknell, T. *et al.* (2020) 'Proteomic resolution of IGFN1 complexes reveals a functional interaction with the actin nucleating protein COBL', *Experimental cell research*, 395(2), p. 112179.

Craig, S.W. and Pardo, J.V. (1983) 'Gamma actin, spectrin, and intermediate filament proteins colocalize with vinculin at costameres, myofibril-to-sarcolemma attachment sites', *Cell motility*, 3(5-6), pp. 449–462.

Crist, C.G., Montarras, D. and Buckingham, M. (2012) 'Muscle satellite cells are primed for myogenesis but maintain quiescence with sequestration of Myf5 mRNA targeted by microRNA-31 in mRNP granules', *Cell stem cell*, 11(1), pp. 118–126.

Cuervo, A.M. and Dice, J.F. (2000) ‘Age-related decline in chaperone-mediated autophagy’, *The Journal of biological chemistry*, 275(40), pp. 31505–31513.
Cui, D. *et al.* (2020) ‘A novel voluntary weightlifting model in mice promotes muscle adaptation and insulin sensitivity with simultaneous enhancement of autophagy and mTOR pathway’, *FASEB journal: official publication of the Federation of American Societies for Experimental Biology*, 34(6), pp. 7330–7344.
Cullen, M.J. and Jaros, E. (1988) ‘Ultrastructure of the skeletal muscle in the X chromosome-linked dystrophic (mdx) mouse. Comparison with Duchenne muscular dystrophy’, *Acta neuropathologica*, 77(1), pp. 69–81.
Cullup, T. *et al.* (2012) ‘Mutations in MYH7 cause Multi-minicore Disease (MmD) with variable cardiac involvement’, *Neuromuscular disorders: NMD*, 22(12), pp. 1096–1104.
D’Antona, G. *et al.* (2006) ‘Skeletal muscle hypertrophy and structure and function of skeletal muscle fibres in male body builders’, *The Journal of physiology*, 570(Pt 3), pp. 611–627.
Dalkilic, I. *et al.* (2006) ‘Loss of FilaminC (FLNc) results in severe defects in myogenesis and myotube structure’, *Molecular and cellular biology*, 26(17), pp. 6522–6534.
Davies, K.J., Lin, S.W. and Pacifici, R.E. (1987) ‘Protein damage and degradation by oxygen radicals. IV. Degradation of denatured protein’, *The Journal of biological chemistry*, 262(20), pp. 9914–9920.
Delafontaine, P. (1995) ‘Insulin-like growth factor I and its binding proteins in the cardiovascular system’, *Cardiovascular Research*, pp. 825–834. Available at: https://doi.org/10.1016/0008-6363(95)00163-8.
Delaney, K. et al. (2017) ‘The role of TGF-β1 during skeletal muscle regeneration’, Cell biology international, 41(7), pp. 706–715.
Dickinson, A.G. and Meikle, V.H. (1973) ‘GENETIC KYPHOSCOLIOSIS IN MICE’, *The Lancet*, p. 1186. Available at: https://doi.org/10.1016/s0140-6736(73)91186-0.
Dimachkie, M.M. and Barohn, R.J. (2014) ‘Distal myopathies’, *Neurologic clinics*, 32(3), pp. 817–42, x.
Dörpholz, G. *et al.* (2017) ‘IRS4, a novel modulator of BMP/Smad and Akt signalling during early muscle differentiation’, *Scientific reports*, 7(1), p. 8778.
Dowling, J.J. *et al.* (2008) ‘Kindlin-2 is required for myocyte elongation and is essential for myogenesis’, *BMC cell biology*, 9, p. 36.
Dube, D. k. *et al.* (2014) ‘Expression of Myotilin During Chicken Development’, *The Anatomical Record*, pp. 1596–1603. Available at: https://doi.org/10.1002/ar.22964.
Dubowitz, V. and Everson Pearse, A.G. (1960) ‘OXIDATIVE ENZYMES AND PHOSPHORYLASE IN CENTRAL-CORE DISEASE OF MUSCLE’, *The Lancet*, pp. 23–24. Available at: https://doi.org/10.1016/s0140-6736(60)92665-9.
Dyson, H.J., Jane Dyson, H. and Wright, P.E. (2005) ‘Intrinsically unstructured proteins and their functions’, *Nature Reviews Molecular Cell Biology*, pp. 197–208. Available at: https://doi.org/10.1038/nrm1589.
Ebrahimzadeh-Vesal, R. *et al.* (2018) ‘Identification of a novel nonsense mutation in kyphoscoliosis peptidase gene in an Iranian patient with myofibrillar myopathy’, *Genes & diseases*, 5(4), pp. 331–334.

Engel, A.G., Gomez, M.R. and Groover, R.V. (1971) 'Multicore disease. A recently recognized congenital myopathy associated with multifocal degeneration of muscle fibers', *Mayo Clinic proceedings. Mayo Clinic*, 46(10), pp. 666–681.
Erskine, R.M. and Degens, H. (2013) 'Muscle growth, repair and preservation', in Nutrition and Enhanced Sports Performance. Elsevier, pp. 247–263.
Ervasti, J.M. and Campbell, K.P. (1991) 'Membrane organization of the dystrophin-glycoprotein complex', *Cell*, 66(6), pp. 1121–1131.
Ervasti, J.M. and Campbell, K.P. (1993) 'A role for the dystrophin-glycoprotein complex as a transmembrane linker between laminin and actin', *Journal of Cell Biology*, pp. 809–823. Available at: https://doi.org/10.1083/jcb.122.4.809.
Evans, W.J. (1999) 'Exercise training guidelines for the elderly', *Medicine & Science in Sports & Exercise*, pp. 12–17. Available at: https://doi.org/10.1097/00005768-199901000-00004.
Fagiolo, U. *et al.* (1993) 'Increased cytokine production in mononuclear cells of healthy elderly people', *European journal of immunology*, 23(9), pp. 2375–2378.
Fardeau, M. (1994) 'Congenital myopathies', *Myology*, pp. 1487–1532.
Farup, J. *et al.* (2012) 'Muscle morphological and strength adaptations to endurance vs. resistance training', *Journal of strength and conditioning research / National Strength & Conditioning Association*, 26(2), pp. 398–407.
Fattori, F. *et al.* (2015) 'Centronuclear myopathies: genotype–phenotype correlation and frequency of defined genetic forms in an Italian cohort', *Journal of Neurology*, pp. 1728–1740. Available at: https://doi.org/10.1007/s00415-015-7757-9.
Faulkner, G., Lanfranchi, G. and Valle, G. (2001) 'Telethonin and other new proteins of the Z-disc of skeletal muscle', IUBMB life, 51(5), pp. 275–282.
Feng, Y. and Walsh, C.A. (2004) 'The many faces of filamin: A versatile molecular scaffold for cell motility and signalling', *Nature cell biology*, 6(11), pp. 1034–1038.
Fernandez, C. *et al.* (2005) 'Electron microscopy in neuromuscular disorders', *Ultrastructural pathology*, 29(6), pp. 437–450.
Fiatarone, M.A. *et al.* (1994) 'Exercise training and nutritional supplementation for physical frailty in very elderly people', *The New England journal of medicine*, 330(25), pp. 1769–1775.
Fichna, J.P., Maruszak, A. and Żekanowski, C. (2018) 'Myofibrillar myopathy in the genomic context', *Journal of applied genetics*, 59(4), pp. 431–439.
Fiorillo, C. *et al.* (2016) 'MYH7-related myopathies: clinical, histopathological and imaging findings in a cohort of Italian patients', *Orphanet Journal of Rare Diseases*. Available at: https://doi.org/10.1186/s13023-016-0476-1.
Fitts, R.H. (2008) 'The cross-bridge cycle and skeletal muscle fatigue', *Journal of applied physiology*, 104(2), pp. 551–558.
Flück, M. *et al.* (1999) 'Focal adhesion proteins FAK and paxillin increase in hypertrophied skeletal muscle', *The American journal of physiology*, 277(1), pp. C152–62.
Forsberg, A.M. *et al.* (1991) 'Muscle composition in relation to age and sex', *Clinical science* , 81(2), pp. 249–256.
Foster, W.H., Tidball, J.G. and Wang, Y. (2012) 'p38γ activity is required for maintenance of slow skeletal muscle size', *Muscle & nerve*, 45(2), pp. 266–273.
Franchini, K.G., Clemente, C.F.M.Z. and Marin, T.M. (2009) 'Focal adhesion kinase signaling in cardiac hypertrophy and failure', *Brazilian journal of medical and*

biological research = Revista brasileira de pesquisas medicas e biologicas / Sociedade Brasileira de Biofisica ... [et al.], 42(1), pp. 44–52.
Frontera, W.R. and Ochala, J. (2015) 'Skeletal muscle: a brief review of structure and function', *Calcified tissue international*, 96(3), pp. 183–195.
Fry, A.C. (2004) 'The Role of Resistance Exercise Intensity on Muscle Fibre Adaptations', *Sports Medicine*, pp. 663–679. Available at: https://doi.org/10.2165/00007256-200434100-00004.
Fukuda, T. *et al.* (2006) 'Autophagy and lysosomes in Pompe disease', *Autophagy*, 2(4), pp. 318–320.
Gaikis, L. *et al.* (2013) 'Identifying a role of the actin capping protein CapZ in β-adrenergic receptor signalling', *Acta physiologica* , 207(1), pp. 173–182.
Gallo, K.A. and Johnson, G.L. (2002) 'Mixed-lineage kinase control of JNK and p38 MAPK pathways', *Nature reviews. Molecular cell biology*, 3(9), pp. 663–672.
Gan, B., Yoo, Y. and Guan, J.-L. (2006) 'Association of focal adhesion kinase with tuberous sclerosis complex 2 in the regulation of s6 kinase activation and cell growth', *The Journal of biological chemistry*, 281(49), pp. 37321–37329.
Glass, D.J. (2003) 'Signalling pathways that mediate skeletal muscle hypertrophy and atrophy', *Nature Cell Biology*, pp. 87–90. Available at: https://doi.org/10.1038/ncb0203-87.
Gluzman, Y. (1981) 'SV40-transformed simian cells support the replication of early SV40 mutants', *Cell*, 23(1), pp. 175–182.
Goldberg, A.L. (1968) 'Protein synthesis during work-induced growth of skeletal muscle', *The Journal of cell biology*, 36(3), pp. 653–658.
Goldfarb, L.G. and Dalakas, M.C. (2009) 'Tragedy in a heartbeat: malfunctioning desmin causes skeletal and cardiac muscle disease', The Journal of clinical investigation, 119(7), pp. 1806–1813.
Goldspink, G. (2003) 'Gene expression in muscle in response to exercise', *Journal of muscle research and cell motility*, 24(2-3), pp. 121–126.
Gotoh, I., Adachi, M. and Nishida, E. (2000) 'Identification and Characterization of a Novel MAP Kinase Kinase Kinase, MLTK', *The Journal of biological chemistry*, 276(6), pp. 4276–4286.
Graham, Z.A., Gallagher, P.M. and Cardozo, C.P. (2015) 'Focal adhesion kinase and its role in skeletal muscle', *Journal of muscle research and cell motility*, 36(4-5), pp. 305–315.
Granchi, C. *et al.* (2010) 'Inhibitors of lactate dehydrogenase isoforms and their therapeutic potentials', *Current medicinal chemistry*, 17(7), pp. 672–697.

Green, H. J. et al. (1979). Fiber composition, fiber size and enzyme activities in vastus lateralis of elite athletes involved in high intensity exercise. *European journal of applied physiology and occupational physiology*, 41 (2), pp.109–117.
Gross, E. A. et al. (2002). MRK, a mixed lineage kinase-related molecule that plays a role in gamma-radiation-induced cell cycle arrest. *The Journal of biological chemistry*, 277 (16), pp.13873–13882.
Gruenbaum-Cohen, Y. *et al.* (2012) 'The actin regulator N-WASp is required for muscle-cell fusion in mice', *Proceedings of the National Academy of Sciences of the United States of America*, 109(28), pp. 11211–11216.
Hamoud, N. *et al.* (2014) 'G-protein coupled receptor BAI3 promotes myoblast fusion in vertebrates', *Proceedings of the National Academy of Sciences of the United States of America*, 111(10), pp. 3745–3750.

Hansen-Smith, F.M., Picou, D. and Golden, M.H. (1979) 'Muscle satellite cells in malnourished and nutritionally rehabilitated children', *Journal of the neurological sciences*, 41(2), pp. 207–221.
Hara, K. *et al.* (1997) 'Regulation of eIF-4E BP1 phosphorylation by mTOR', *The Journal of biological chemistry*, 272(42), pp. 26457–26463.
Hasan, M.M. *et al.* (2019) 'Beneficial effects of metformin on muscle atrophy induced by obesity in rats', *Journal of Cellular Biochemistry*, pp. 5677–5686. Available at: https://doi.org/10.1002/jcb.27852.
Hastings, R.L. *et al.* (2020) 'Exclusive vital labeling of myonuclei for studying myonuclear arrangement in mouse skeletal muscle tissue', *Skeletal muscle*, 10(1), p. 15.
Haun, C.T. *et al.* (2019) 'A Critical Evaluation of the Biological Construct Skeletal Muscle Hypertrophy: Size Matters but So Does the Measurement', *Frontiers in physiology*, 10, p. 247.
Hauser, M.A. (2000) 'Myotilin is mutated in limb girdle muscular dystrophy 1A', *Human Molecular Genetics*, pp. 2141–2147. Available at: https://doi.org/10.1093/hmg/9.14.2141.
Hauser, M.A. *et al.* (2002) 'myotilin Mutation Found in Second Pedigree with LGMD1A', *The American Journal of Human Genetics*, pp. 1428–1432. Available at: https://doi.org/10.1086/344532.
Hawke, T.J. and Garry, D.J. (2001) 'Myogenic satellite cells: physiology to molecular biology', *Journal of applied physiology*, 91(2), pp. 534–551.
Hayashi, Y.K. *et al.* (1998) 'Mutations in the integrin α7 gene cause congenital myopathy', *Nature genetics*, 19(1), pp. 94–97.
Hedberg-Oldfors, C. *et al.* (2016) 'A new early-onset neuromuscular disorder associated with kyphoscoliosis peptidase (KY) deficiency', *European journal of human genetics: EJHG*, 24(12), pp. 1771–1777.
Hennebry, A. *et al.* (2009) 'Myostatin regulates fiber-type composition of skeletal muscle by regulating MEF2 and MyoD gene expression', *American Journal of Physiology-Cell Physiology*, pp. C525–C534. Available at: https://doi.org/10.1152/ajpcell.00259.2007.
Herbison, G. J., Jaweed, M. M. and Ditunno, J. F. (1982). Muscle fiber types. *Archives of physical medicine and rehabilitation*, 63 (5), pp.227–230.
Herman, G.E. *et al.* (1999) 'Medical complications in long-term survivors with X-linked myotubular myopathy', *The Journal of pediatrics*, 134(2), pp. 206–214.
Herman, J.R. *et al.* (2010) 'Correlation Between Muscle Fiber Cross-Sectional Area And Strength Gain Using Three Different Resistance-Training Programs In College-Aged Women', *Journal of Strength and Conditioning Research*, p. 1. Available at: https://doi.org/10.1097/01.jsc.0000367128.04768.0a.
Hershko, A. and Ciechanover, A. (1986) 'The Ubiquitin Pathway for the Degradation of Intracellular Proteins', *Progress in Nucleic Acid Research and Molecular Biology*, pp. 19–56. Available at: https://doi.org/10.1016/s0079-6603(08)60019-7.
Heslop, L. *et al.* (2002) 'MS1-2 The roles of stem-like myogenic cells in muscle growth and regeneration', *Acta histochemica et cytochemica* [Preprint]. Available at: https://ci.nii.ac.jp/naid/110003151083/.
Hirsch, N.P. (2007) 'Neuromuscular junction in health and disease', *British journal of anaesthesia*, 99(1), pp. 132–138.

Hoffman, E.P., Brown, R.H., Jr and Kunkel, L.M. (1987) 'Dystrophin: the protein product of the Duchenne muscular dystrophy locus', *Cell*, 51(6), pp. 919–928.
Holt, L.J. *et al.* (2009) 'Global analysis of Cdk1 substrate phosphorylation sites provides insights into evolution', *Science*, 325(5948), pp. 1682–1686.
Homma, S. *et al.* (2006) 'BAG3 deficiency results in fulminant myopathy and early lethality', *The American journal of pathology*, 169(3), pp. 761–773.
Hornberger, T.A. *et al.* (2005) 'Aging does not alter the mechanosensitivity of the p38, $p70^{S6k}$, and JNK2 signaling pathways in skeletal muscle', *Journal of Applied Physiology*, pp. 1562–1566. Available at: https://doi.org/10.1152/japplphysiol.00870.2004.
Hoshijima, M. (2006) 'Mechanical stress-strain sensors embedded in cardiac cytoskeleton: Z disk, titin, and associated structures', American journal of physiology. Heart and circulatory physiology, 290(4), pp. H1313–25.
Hsieh, Y.-L. *et al.* (2015) 'ZAK induces cardiomyocyte hypertrophy and brain natriuretic peptide expression via p38/JNK signaling and GATA4/c-Jun transcriptional factor activation', *Molecular and cellular biochemistry*, 405(1-2), pp. 1–9.
Hu, J. et al. (2011) 'Mutation that blocks ATP binding creates a pseudokinase stabilizing the scaffolding function of kinase suppressor of Ras, CRAF and BRAF', Proceedings of the National Academy of Sciences, 108(15), pp. 6067–6072.
Huang, C.-Y., Chueh, P.J., *et al.* (2004) 'ZAK re-programs atrial natriuretic factor expression and induces hypertrophic growth in H9c2 cardiomyoblast cells', *Biochemical and Biophysical Research Communications*, pp. 973–980. doi:10.1016/j.bbrc.2004.09.156.
Huang, C.-Y., Kuo, W.-W., *et al.* (2004) 'Transforming growth factor-β induces the expression of ANF and hypertrophic growth in cultured cardiomyoblast cells through ZAK', *Biochemical and Biophysical Research Communications*, pp. 424–431. doi:10.1016/j.bbrc.2004.09.067.
Huang, W.A., Boyle, N.G. and Vaseghi, M. (2017) 'Cardiac Innervation and the Autonomic Nervous System in Sudden Cardiac Death', *Cardiac electrophysiology clinics*, 9(4), pp. 665–679.
Husson, C. *et al.* (2011) 'Cordon-Bleu uses WH2 domains as multifunctional dynamizers of actin filament assembly', *Molecular cell*, 43(3), pp. 464–477.
Huveneers, S. and Danen, E.H.J. (2009) 'Adhesion signaling – crosstalk between integrins, Src and Rho', *Journal of Cell Science*, pp. 1059–1069. Available at: https://doi.org/10.1242/jcs.039446.
Huxley, A.F. (1957) 'Muscle structure and theories of contraction', *Progress in biophysics and biophysical chemistry*, 7, pp. 255–318.
Inoki, K. *et al.* (2002) 'TSC2 is phosphorylated and inhibited by Akt and suppresses mTOR signalling', *Nature cell biology*, 4(9), pp. 648–657.
Iwasaki, M. *et al.* (2007) 'BAG3 Regulates Motility and Adhesion of Epithelial Cancer Cells', *Cancer Research*, pp. 10252–10259. Available at: https://doi.org/10.1158/0008-5472.can-07-0618.
Iwasaki, M. *et al.* (2010) 'BAG3 directly associates with guanine nucleotide exchange factor of Rap1, PDZGEF2, and regulates cell adhesion', *Biochemical and Biophysical Research Communications*, pp. 413–418. Available at: https://doi.org/10.1016/j.bbrc.2010.08.092.

Jiao, Y. *et al.* (2014) ‘Mutagenetic and electron microscopy analysis of actin filament severing by Cordon-Bleu, a WH2 domain protein’, *Cytoskeleton* , 71(3), pp. 170–183.
Jirmanová, I. and Thesleff, S. (1972) ‘Ultrastructural study of experimental muscle degeneration and regeneration in the adult rat’, *Zeitschrift fur Zellforschung und mikroskopische Anatomie* , 131(1), pp. 77–97.
Johnson, T.L. and Klueber, K.M. (1991) ‘Skeletal muscle following tonic overload: functional and structural analysis’, *Medicine and science in sports and exercise*, 23(1), pp. 49–55.
Jokl, E.J. and Blanco, G. (2016) ‘Disrupted autophagy undermines skeletal muscle adaptation and integrity’, *Mammalian genome: official journal of the International Mammalian Genome Society*, 27(11-12), pp. 525–537.
Jokl, E.J. *et al.* (2018) ‘Transcriptional upregulation of Bag3, a chaperone-assisted selective autophagy factor, in animal models of KY-deficient hereditary myopathy’, *Disease models & mechanisms*, 11(7). Available at: https://doi.org/10.1242/dmm.033225.
Jones, E.J. *et al.* (2008) ‘Cross-Sectional Area and Muscular Strength’, *Sports Medicine*, pp. 987–994. Available at: https://doi.org/10.2165/00007256-200838120-00003.
Jones, J.I. and Clemmons, D.R. (1995) ‘Insulin-Like Growth Factors and Their Binding Proteins: Biological Actions*’, *Endocrine Reviews*, pp. 3–34. Available at: https://doi.org/10.1210/edrv-16-1-3.
Joseph, G.A. *et al.* (2019) ‘Partial Inhibition of mTORC1 in Aged Rats Counteracts the Decline in Muscle Mass and Reverses Molecular Signaling Associated with Sarcopenia’, *Molecular and cellular biology*, 39(19). Available at: https://doi.org/10.1128/MCB.00141-19.
Joyner, M.J. and Coyle, E.F. (2008) ‘Endurance exercise performance: the physiology of champions’, *The Journal of physiology*, 586(1), pp. 35–44.
Juliano, R.L. *et al.* (2004) ‘Integrin regulation of cell signalling and motility’, *Biochemical Society transactions*, 32(Pt3), pp. 443–446.
Jungbluth, H. (2007) ‘Multi-minicore Disease’, *Orphanet journal of rare diseases*, 2, p. 31.
Kathage, B. *et al.* (2017) ‘The cochaperone BAG3 coordinates protein synthesis and autophagy under mechanical strain through spatial regulation of mTORC1’, *Biochimica et Biophysica Acta, Molecular Cell Research*, 1864(1), pp. 62–75.
Kathage, B. *et al.* (2017) ‘The cochaperone BAG3 coordinates protein synthesis and autophagy under mechanical strain through spatial regulation of mTORC1’, *Biochimica et Biophysica Acta, Molecular Cell Research*, 1864(1), pp. 62–75.
Klemke, R.L. *et al.* (1997) ‘Regulation of cell motility by mitogen-activated protein kinase’, *The Journal of cell biology*, 137(2), pp. 481–492.
Kley, R.A. *et al.* (2013) ‘Impairment of protein degradation in myofibrillar myopathy caused by FLNC/filamin C mutations’, *Autophagy*, 9(3), pp. 422–423.
Kline, W.O. *et al.* (2007) ‘Rapamycin inhibits the growth and muscle-sparing effects of clenbuterol’, *Journal of applied physiology*, 102(2), pp. 740–747.
Knight, J.D. *et al.* (2012) ‘A novel whole-cell lysate kinase assay identifies substrates of the p38 MAPK in differentiating myoblasts’, *Skeletal muscle*, 2, p. 5.
Knuttgen, H.G. and Kraemer, W.J. (1987) ‘Terminology and Measurement in Exercise Performance’, *The Journal of Strength and Conditioning Research*, p. 1. Available at: https://doi.org/10.1519/1533-4287(1987)001<0001:tamiep>2.3.co;2.

Ko, G.J. *et al.* (2017) 'Dietary protein intake and chronic kidney disease', *Current opinion in clinical nutrition and metabolic care*, 20(1), pp. 77–85.
Konigsberg, U.R., Lipton, B.H. and Konigsberg, I.R. (1975) 'The regenerative response of single mature muscle fibers isolated in vitro', *Developmental biology*, 45(2), pp. 260–275.
Krystkowiak, I., Manguy, J. and Davey, N.E. (2018) 'PSSMSearch: a server for modeling, visualization, proteome-wide discovery and annotation of protein motif specificity determinants', *Nucleic acids research*, 46(W1), pp. W235–W241.Kumar, A. *et al.* (2004) 'Loss of dystrophin causes aberrant mechanotransduction in skeletal muscle fibers', *FASEB journal: official publication of the Federation of American Societies for Experimental Biology*, 18(1), pp. 102–113.
Kuang, S. *et al.* (2007) 'Asymmetric self-renewal and commitment of satellite stem cells in muscle', *Cell*, 129(5), pp. 999–1010.
Kyriakis, J.M. and Avruch, J. (2001) 'Mammalian mitogen-activated protein kinase signal transduction pathways activated by stress and inflammation', *Physiological reviews*, 81(2), pp. 807–869.
Laing, N.G. *et al.* (1995) 'Autosomal dominant distal myopathy: linkage to chromosome 14', *American journal of human genetics*, 56(2), pp. 422–427.
Lam, S.S. *et al.* (2015) 'Directed evolution of APEX2 for electron microscopy and proximity labeling', *Nature methods*, 12(1), pp. 51–54.
Laplante, M. and Sabatini, D.M. (2012) 'mTOR signaling in growth control and disease', *Cell*, 149(2), pp. 274–293.
Laplante, M. and Sabatini, D.M. (2013) 'Regulation of mTORC1 and its impact on gene expression at a glance', *Journal of cell science*, 126(Pt 8), pp. 1713–1719.
Laurin, M. *et al.* (2008) 'The atypical Rac activator Dock180 (Dock1) regulates myoblast fusion in vivo', *Proceedings of the National Academy of Sciences of the United States of America*, 105(40), pp. 15446–15451.
Leber, Y. *et al.* (2016) 'Filamin C is a highly dynamic protein associated with fast repair of myofibrillar microdamage', *Human molecular genetics*, 25(13), pp. 2776–2788.
Lecker, S.H. *et al.* (1999) 'Muscle Protein Breakdown and the Critical Role of the Ubiquitin-Proteasome Pathway in Normal and Disease States', *The Journal of Nutrition*, p. 227S–237S. Available at: https://doi.org/10.1093/jn/129.1.227s.
Lee, S. and Dong, H.H. (2017) 'FoxO integration of insulin signaling with glucose and lipid metabolism', *The Journal of endocrinology*, 233(2), pp. R67–R79.
Legate, K.R. *et al.* (2006) 'ILK, PINCH and parvin: the tIPP of integrin signalling', *Nature Reviews Molecular Cell Biology*, pp. 20–31. Available at: https://doi.org/10.1038/nrm1789.
Lepper, C., Partridge, T.A. and Fan, C.-M. (2011) 'An absolute requirement for Pax7-positive satellite cells in acute injury-induced skeletal muscle regeneration', *Development* , 138(17), pp. 3639–3646.
Lessard, S.J. *et al.* (2018) 'JNK regulates muscle remodeling via myostatin/SMAD inhibition', *Nature communications*, 9(1), p. 3030.
Lexell, J. *et al.* (1983) 'Distribution of different fiber types in human skeletal muscles: effects of aging studied in whole muscle cross sections', *Muscle & nerve*, 6(8), pp. 588–595.
Lexell, J., Downham, D. and Sjöström, M. (1986) 'Distribution of different fibre types in human skeletal muscles. Fibre type arrangement in m. vastus lateralis from

three groups of healthy men between 15 and 83 years', *Journal of the neurological sciences*, 72(2-3), pp. 211–222.
Li, R. *et al.* (2013) 'Costamere remodeling with muscle loading and unloading in healthy young men', *Journal of anatomy*, 223(5), pp. 525–536.
Li, X. *et al.* (2013) 'Elucidating human phosphatase-substrate networks', *Science signaling*, 6(275), p. rs10.
Li, X. et al. (2017) 'IGFN1_v1 is required for myoblast fusion and differentiation', PloS one, 12(6), p. e0180217.
Li, Y.-P. et al. (2005) 'TNF-alpha acts via p38 MAPK to stimulate expression of the ubiquitin ligase atrogin1/MAFbx in skeletal muscle', FASEB journal: official publication of the Federation of American Societies for Experimental Biology, 19(3), pp. 362–370.
Lipina, C. *et al.* (2010) 'Mechanisms involved in the enhancement of mammalian target of rapamycin signalling and hypertrophy in skeletal muscle of myostatin-deficient mice', *FEBS Letters*, pp. 2403–2408. Available at: https://doi.org/10.1016/j.febslet.2010.04.039.
Liu, P. *et al.* (2017) 'Sarcopenia as a predictor of all-cause mortality among community-dwelling older people: A systematic review and meta-analysis', *Maturitas*, 103, pp. 16–22.
Liu, T.-C. *et al.* (2000) 'Cloning and Expression of ZAK, a Mixed Lineage Kinase-like Protein Containing a Leucine-Zipper and a Sterile-Alpha Motif', *Biochemical and biophysical research communications*, 274(3), pp. 811–816.
Ma, X.M. and Blenis, J. (2009) 'Molecular mechanisms of mTOR-mediated translational control', *Nature reviews. Molecular cell biology*, 10(5), pp. 307–318.
MacDonald, E.M. and Cohn, R.D. (2012) 'TGFβ signaling: its role in fibrosis formation and myopathies', *Current opinion in rheumatology*, 24(6), pp. 628–634.
Maciejewski, P.M. et al. (1995) 'Mutation of serine 90 to glutamic acid mimics phosphorylation of bovine prolactin', The Journal of biological chemistry, 270(46), pp. 27661–27665.
Mackey, A.L. and Kjaer, M. (2017) 'The breaking and making of healthy adult human skeletal muscle in vivo', *Skeletal Muscle*. Available at: https://doi.org/10.1186/s13395-017-0142-x.
Maharaj, J.N., Cresswell, A.G. and Lichtwark, G.A. (2019) 'Tibialis anterior tendinous tissue plays a key role in energy absorption during human walking', *The Journal of experimental biology*, 222(Pt 11). Available at: https://doi.org/10.1242/jeb.191247.
Malhotra, S.B. *et al.* (1988) 'Frame-shift deletions in patients with Duchenne and Becker muscular dystrophy', *Science*, 242(4879), pp. 755–759.
Mammucari, C. *et al.* (2007) 'FoxO3 controls autophagy in skeletal muscle in vivo', *Cell metabolism*, 6(6), pp. 458–471.
Mann, C.J. *et al.* (2011) 'Aberrant repair and fibrosis development in skeletal muscle', *Skeletal muscle*, 1(1), p. 21.
Manning, B.D. and Cantley, L.C. (2007) 'AKT/PKB Signaling: Navigating Downstream', *Cell*, pp. 1261–1274. Available at: https://doi.org/10.1016/j.cell.2007.06.009.
Mansilla, F. *et al.* (2008) 'Translation elongation factor eEF1A binds to a novel myosin binding protein-C-like protein', *Journal of cellular biochemistry*, 105(3), pp. 847–858.

Maréchal, G. et al. (1996) ‘Isoforms of myosin in growing muscles of ky (kyphoscoliotic) mice’, European journal of biochemistry / FEBS, 241(3), pp. 916–922.
Maréchal, G., Coulton, G.R. and Beckers-Bleukx, G. (1995) ‘Mechanical power and myosin composition of soleus and extensor digitorum longus muscles of ky mice’, *The American journal of physiology*, 268(2 Pt 1), pp. C513–9.
Markesbery, W.R. *et al.* (1974) ‘Late onset hereditary distal myopathy’, *Neurology*, pp. 127–127. Available at: https://doi.org/10.1212/wnl.24.2.127.
Martin, T.G. *et al.* (2021) ‘Cardiomyocyte contractile impairment in heart failure results from reduced BAG3-mediated sarcomeric protein turnover’, *Nature communications*, 12(1), p. 2942.
Martino, F. *et al.* (2018) ‘Cellular Mechanotransduction: From Tension to Function’, *Frontiers in Physiology*. Available at: https://doi.org/10.3389/fphys.2018.00824.
Maruyama, T. *et al.* (2020) ‘ZAK Inhibitor PLX4720 Promotes Extrusion of Transformed Cells via Cell Competition’, *iScience*, 23(7), p. 101327.
Mastroyiannopoulos, N.P. *et al.* (2012) ‘Down-regulation of myogenin can reverse terminal muscle cell differentiation’, *PloS one*, 7(1), p. e29896.
Mathes, S. *et al.* (2019) ‘Evidence for skeletal muscle fiber type-specific expressions of mechanosensors’, *Cellular and Molecular Life Sciences*, pp. 2987–3004. Available at: https://doi.org/10.1007/s00018-019-03026-3.
Matsumura, K. and Campbell, K.P. (1994) ‘Dystrophin-glycoprotein complex: Its role in the molecular pathogenesis of muscular dystrophies’, *Muscle & Nerve*, pp. 2–15. Available at: https://doi.org/10.1002/mus.880170103.
Mauro, A. (1961) ‘Satellite cell of skeletal muscle fibers’, *The Journal of biophysical and biochemical cytology*, 9(2), pp. 493–495.
Mazzotti, A.L. and Coletti, D. (2016) ‘The Need for a Consensus on the Locution “Central Nuclei” in Striated Muscle Myopathies’, *Frontiers in physiology*, 7, p. 577.
McCance, K.L. *et al.* (2019) *Pathophysiology: The Biologic Basis for Disease in Adults and Children*. Elsevier.
McCuller, C., Jessu, R. and Callahan, A.L. (2023) ‘Physiology, Skeletal Muscle’, in *StatPearls*. Treasure Island (FL): StatPearls Publishing.
McGeachie, J.K. and Grounds, M.D. (1987) ‘Initiation and duration of muscle precursor replication after mild and severe injury to skeletal muscle of mice. An autoradiographic study’, *Cell and tissue research*, 248(1), pp. 125–130.
McKinsey, T.A. *et al.* (2000) ‘Signal-dependent nuclear export of a histone deacetylase regulates muscle differentiation’, *Nature*, 408(6808), p. 106.
McNeill, E. *et al.* (2014) ‘Contrasting in vitro vs. in vivo effects of a cell membrane-specific CC-chemokine binding protein on macrophage chemotaxis’, *Journal of molecular medicine* , 92(11), pp. 1169–1178.
McPherron, A.C., Lawler, A.M. and Lee, S.-J. (1997) ‘Regulation of skeletal muscle mass in mice by a new TGF-p superfamily member’, *Nature*, pp. 83–90. Available at: https://doi.org/10.1038/387083a0.
Mertins, P. *et al.* (2014) ‘Ischemia in tumors induces early and sustained phosphorylation changes in stress kinase pathways but does not affect global protein levels’, *Molecular & cellular proteomics: MCP*, 13(7), pp. 1690–1704.
Meyer, G.A. (2018) ‘Evidence of induced muscle regeneration persists for years in the mouse’, *Muscle & nerve*, 58(6), pp. 858–862.

Mitra, P. and Thanabalu, T. (2017) ‘Myogenic differentiation depends on the interplay of Grb2 and N-WASP’, *Biochimica et Biophysica Acta, Molecular Cell Research*, 1864(3), pp. 487–497.
Montarras, D., L’honoré, A. and Buckingham, M. (2013) ‘Lying low but ready for action: the quiescent muscle satellite cell’, *FEBS Journal*, pp. 4036–4050. Available at: https://doi.org/10.1111/febs.12372.
Morissette, M.R. *et al.* (2009) ‘Myostatin inhibits IGF-I-induced myotube hypertrophy through Akt’, *American Journal of Physiology-Cell Physiology*, pp. 1124–1132. Available at: https://doi.org/10.1152/ajpcell.00043.2009.
Morrison, D.K. and Davis, R.J. (2003) ‘Regulation of MAP kinase signaling modules by scaffold proteins in mammals’, *Annual review of cell and developmental biology*, 19, pp. 91–118.
Mulvaney, D.R., Marple, D.N. and Merkel, R.A. (1988) ‘Proliferation of skeletal muscle satellite cells after castration and administration of testosterone propionate’, *Proceedings of the Society for Experimental Biology and Medicine. Society for Experimental Biology and Medicine* , 188(1), pp. 40–45.
Muñoz-Mármol, A.M. *et al.* (1998) ‘A dysfunctional desmin mutation in a patient with severe generalized myopathy’, *Proceedings of the National Academy of Sciences*, pp. 11312–11317. Available at: https://doi.org/10.1073/pnas.95.19.11312.
Nader, G.A. (2005) ‘Molecular determinants of skeletal muscle mass: getting the “AKT” together’, *The international journal of biochemistry & cell biology*, 37(10), pp. 1985–1996.
Nadruz, W., Jr *et al.* (2005) ‘Focal adhesion kinase mediates MEF2 and c-Jun activation by stretch: role in the activation of the cardiac hypertrophic genetic program’, *Cardiovascular research*, 68(1), pp. 87–97.
Nakano, S. *et al.* (1997) ‘Myofibrillar Myopathy. III. Abnormal Expression of Cyclin-dependent Kinases and Nuclear Proteins’, *Journal of Neuropathology and Experimental Neurology*, pp. 850–856. Available at: https://doi.org/10.1097/00005072-199708000-00002.
Nance, J.R. *et al.* (2012) ‘Congenital Myopathies: An Update’, *Current Neurology and Neuroscience Reports*, pp. 165–174. Available at: https://doi.org/10.1007/s11910-012-0255-x.
Nandelstadh, P. von *et al.* (2009) ‘A Class III PDZ Binding Motif in the Myotilin and FATZ Families Binds Enigma Family Proteins: a Common Link for Z-Disc Myopathies’, *Molecular and Cellular Biology*, pp. 822–834. Available at: https://doi.org/10.1128/mcb.01454-08.
Nguyen, J.H. *et al.* (2019) ‘The Microenvironment Is a Critical Regulator of Muscle Stem Cell Activation and Proliferation’, *Frontiers in cell and developmental biology*, 7, p. 254.
Nordgaard, C. et al. (2022) ‘ZAKβ is activated by cellular compression and mediates contraction-induced MAP kinase signaling in skeletal muscle’, The EMBO journal [Preprint]. Available at: https://www.embopress.org/doi/abs/10.15252/embj.2022111650.
North, K.N. *et al.* (2014) ‘Approach to the diagnosis of congenital myopathies’, *Neuromuscular Disorders*, pp. 97–116. Available at: https://doi.org/10.1016/j.nmd.2013.11.003.
Nyati, S. *et al.* (2016) ‘A Requirement for ZAK Kinase Activity in Canonical TGF-β Signaling’, *Translational oncology*, 9(6), pp. 473–481.

Ogasawara, R. *et al.* (2019) 'Resistance Exercise-Induced Hypertrophy: A Potential Role for Rapamycin-Insensitive mTOR', *Exercise and sport sciences reviews*, 47(3), pp. 188–194.
Ohlendieck, K. (2011) 'Skeletal muscle proteomics: current approaches, technical challenges and emerging techniques', *Skeletal muscle*, 1(1), p. 6.
Ohtsuki, I. and Morimoto, S. (2008) 'Troponin: regulatory function and disorders', *Biochemical and biophysical research communications*, 369(1), pp. 62–73.
Ortolano, S. *et al.* (2011) 'A novel MYH7 mutation links congenital fiber type disproportion and myosin storage myopathy', *Neuromuscular disorders: NMD*, 21(4), pp. 254–262.
Ortolano, S. *et al.* (2011) 'A novel MYH7 mutation links congenital fiber type disproportion and myosin storage myopathy', *Neuromuscular disorders: NMD*, 21(4), pp. 254–262.
Otey, C.A. *et al.* (2009) 'Cytoplasmic Ig-domain proteins: cytoskeletal regulators with a role in human disease', *Cell motility and the cytoskeleton*, 66(8), pp. 618–634.
Overend, T.J. *et al.* (1992) 'Thigh composition in young and elderly men determined by computed tomography', *Clinical physiology* , 12(6), pp. 629–640.
Pallafacchina, G. *et al.* (2002) 'A protein kinase B-dependent and rapamycin-sensitive pathway controls skeletal muscle growth but not fiber type specification', *Proceedings of the National Academy of Sciences*, 99(14), pp. 9213–9218.
Palomero, J. *et al.* (2013) 'Aging increases the oxidation of dichlorohydrofluorescein in single isolated skeletal muscle fibers at rest, but not during contractions', *American Journal of Physiology-Regulatory, Integrative and Comparative Physiology*, pp. R351–R358. Available at: https://doi.org/10.1152/ajpregu.00530.2012.
Paolini, C. *et al.* (2007) 'Reorganized stores and impaired calcium handling in skeletal muscle of mice lacking calsequestrin-1', *The Journal of Physiology*, pp. 767–784. Available at: https://doi.org/10.1113/jphysiol.2007.138024.
Pardo, J.V. and Siliciano, J.D. (1983) 'A vinculin-containing cortical lattice in skeletal muscle: transverse lattice elements (" costameres") mark sites of attachment between myofibrils and sarcolemma', *Proceedings of the* [Preprint]. Available at: https://www.pnas.org/content/80/4/1008.short.
Passmore, L.A. and Barford, D. (2004) 'Getting into position: the catalytic mechanisms of protein ubiquitylation', *Biochemical Journal*, 379(Pt 3), pp. 513–525.
Patel, T.J. and Lieber, R.L. (1997) 'Force transmission in skeletal muscle: from actomyosin to external tendons', *Exercise and sport sciences reviews*, 25, pp. 321–363.
Pellegrino, C. and Franzini, C. (1963) 'AN ELECTRON MICROSCOPE STUDY OF DENERVATION ATROPHY IN RED AND WHITE SKELETAL MUSCLE FIBERS', *The Journal of cell biology*, 17(2), pp. 327–349.
Perdiguero, E. et al. (2007) 'Genetic analysis of p38 MAP kinases in myogenesis: fundamental role of p38alpha in abrogating myoblast proliferation', The EMBO journal, 26(5), pp. 1245–1256.
Peterson, A. J. et al. (1997). A domain shared by the Polycomb group proteins Scm and ph mediates heterotypic and homotypic interactions. *Molecular and cellular biology*, 17 (11), pp.6683–6692.
Petrocelli, J.J. and Drummond, M.J. (2020) 'PGC-1α-Targeted Therapeutic Approaches to Enhance Muscle Recovery in Aging', *International Journal of Environmental Research and Public Health*, p. 8650. Available at: https://doi.org/10.3390/ijerph17228650.

Pham, S. and Puckett, Y. (no date) *Physiology, Skeletal Muscle Contraction*. Available at: https://europepmc.org/article/nbk/nbk559006 (Accessed: 1 June 2023).

Phillips, W.D. and Bennett, M.R. (1987) 'Elimination of distributed synaptic acetylcholine receptor clusters on developing avian fast-twitch muscle fibres accompanies loss of polyneuronal innervation', *Journal of neurocytology*, 16(6), pp. 785–797.

Philp, A., Hamilton, D.L. and Baar, K. (2011) 'Signals mediating skeletal muscle remodeling by resistance exercise: PI3-kinase independent activation of mTORC1', *Journal of applied physiology*, 110(2), pp. 561–568.

Pingel, J. and Suhr, F. (2017) 'Are mechanically sensitive regulators involved in the function and (patho)physiology of cerebral palsy-related contractures?', *Journal of Muscle Research and Cell Motility*, pp. 317–330. Available at: https://doi.org/10.1007/s10974-017-9489-1.

Pisconti, A. *et al.* (2010) 'Syndecan-3 and Notch cooperate in regulating adult myogenesis', *The Journal of cell biology*, 190(3), pp. 427–441.

Pisconti, A. *et al.* (2016) 'Loss of niche-satellite cell interactions in syndecan-3 null mice alters muscle progenitor cell homeostasis improving muscle regeneration', *Skeletal muscle*, 6, p. 34.

Ponting, C.P. (1995) 'SAM: a novel motif in yeast sterile and Drosophila polyhomeotic proteins', *Protein science: a publication of the Protein Society*, 4(9), pp. 1928–1930.

Porter, G.A. *et al.* (1992) 'Dystrophin colocalizes with beta-spectrin in distinct subsarcolemmal domains in mammalian skeletal muscle', *The Journal of cell biology*, 117(5), pp. 997–1005.

Potts, G. K. et al. (2017). A map of the phosphoproteomic alterations that occur after a bout of maximal-intensity contractions. *The Journal of physiology*, 595 (15), pp.5209–5226.

Powers, S.K. *et al.* (2016) 'Disease-Induced Skeletal Muscle Atrophy and Fatigue', *Medicine and science in sports and exercise*, 48(11), pp. 2307–2319.

Purcell, N.H. *et al.* (2004) 'Extracellular signal-regulated kinase 2 interacts with and is negatively regulated by the LIM-only protein FHL2 in cardiomyocytes', *Molecular and cellular biology*, 24(3), pp. 1081–1095.

Pyle, W.G. and Solaro, R.J. (2004) 'At the crossroads of myocardial signaling: the role of Z-discs in intracellular signaling and cardiac function', Circulation research, 94(3), pp. 296–305.

Quach, N.L. and Rando, T.A. (2006) 'Focal adhesion kinase is essential for costamerogenesis in cultured skeletal muscle cells', *Developmental biology*, 293(1), pp. 38–52.

Quach, N.L. *et al.* (2009) 'Focal adhesion kinase signaling regulates the expression of caveolin 3 and beta1 integrin, genes essential for normal myoblast fusion', *Molecular biology of the cell*, 20(14), pp. 3422–3435.

Rahimov, F. *et al.* (2011) 'Gene expression profiling of skeletal muscles treated with a soluble activin type IIB receptor', *Physiological Genomics*, pp. 398–407. Available at: https://doi.org/10.1152/physiolgenomics.00223.2010.

Ravenscroft, G. *et al.* (2018) 'Bi-allelic mutations in MYL1 cause a severe congenital myopathy', *Human molecular genetics*, 27(24), pp. 4263–4272.

Reilich, P. *et al.* (2010) 'The p.G154S mutation of the alpha-B crystallin gene (CRYAB) causes late-onset distal myopathy', *Neuromuscular Disorders*, pp. 255–259. Available at: https://doi.org/10.1016/j.nmd.2010.01.012.
Renault, L., Bugyi, B. and Carlier, M.-F. (2008) 'Spire and Cordon-bleu: multifunctional regulators of actin dynamics', *Trends in cell biology*, 18(10), pp. 494–504.
Rhee, H.-W. *et al.* (2013) 'Proteomic mapping of mitochondria in living cells via spatially restricted enzymatic tagging', *Science*, 339(6125), pp. 1328–1331.
Rief, M. *et al.* (1997) 'Reversible Unfolding of Individual Titin Immunoglobulin Domains by AFM', *Science*, pp. 1109–1112. Available at: https://doi.org/10.1126/science.276.5315.1109.
Rochlin, K. *et al.* (2010) 'Myoblast fusion: when it takes more to make one', *Developmental biology*, 341(1), pp. 66–83.
Rodgers, J.T. *et al.* (2014) 'mTORC1 controls the adaptive transition of quiescent stem cells from G0 to GAlert', *Nature*, 510(7505), pp. 393–396.
Rodríguez Cruz, P.M. *et al.* (2020) 'The Neuromuscular Junction in Health and Disease: Molecular Mechanisms Governing Synaptic Formation and Homeostasis', *Frontiers in molecular neuroscience*, 13, p. 610964.

Rommel, C. *et al.* (2001) 'Mediation of IGF-1-induced skeletal myotube hypertrophy by PI(3)K/Akt/mTOR and PI(3)K/Akt/GSK3 pathways', *Nature cell biology*, 3(11), pp. 1009–1013.
Rossi, D. *et al.* (2022) 'The Sarcoplasmic Reticulum of Skeletal Muscle Cells: A Labyrinth of Membrane Contact Sites', *Biomolecules*, 12(4). Available at: https://doi.org/10.3390/biom12040488.

Roux, K.J. *et al.* (2012) 'A promiscuous biotin ligase fusion protein identifies proximal and interacting proteins in mammalian cells', *The Journal of cell biology*, 196(6), pp. 801–810.
Ruparelia, A. *et al.* (2016) 'Filamin C myofibrillar myopathy: Changes in autophagy both cause and can treat the disease', *Neuromuscular Disorders*, pp. S191–S192. Available at: https://doi.org/10.1016/j.nmd.2016.06.382.
Ryan, M.M. *et al.* (2001) 'Nemaline myopathy: A clinical study of 143 cases', *Annals of Neurology*, pp. 312–320. Available at: https://doi.org/10.1002/ana.1080.
Sakellariou, G.K. *et al.* (2013) 'Studies of mitochondrial and nonmitochondrial sources implicate nicotinamide adenine dinucleotide phosphate oxidase(s) in the increased skeletal muscle superoxide generation that occurs during contractile activity', *Antioxidants & redox signaling*, 18(6), pp. 603–621.
Salmikangas, P. (1999) 'Myotilin, a novel sarcomeric protein with two Ig-like domains, is encoded by a candidate gene for limb-girdle muscular dystrophy', *Human Molecular Genetics*, pp. 1329–1336. Available at: https://doi.org/10.1093/hmg/8.7.1329.
Sambasivan, R. *et al.* (2011) 'Pax7-expressing satellite cells are indispensable for adult skeletal muscle regeneration', *Development* , 138(17), pp. 3647–3656.
Sampath, S.C., Sampath, S.C. and Millay, D.P. (2018) 'Myoblast fusion confusion: the resolution begins', *Skeletal Muscle*. Available at: https://doi.org/10.1186/s13395-017-0149-3.
Sandri, M. (2013) 'Protein breakdown in muscle wasting: role of autophagy-lysosome and ubiquitin-proteasome', *The international journal of biochemistry & cell biology*, 45(10), pp. 2121–2129.

Sandri, M. *et al.* (2004) 'Foxo transcription factors induce the atrophy-related ubiquitin ligase atrogin-1 and cause skeletal muscle atrophy', *Cell*, 117(3), pp. 399–412.
Sandri, M. *et al.* (2006) 'PGC-1α protects skeletal muscle from atrophy by suppressing FoxO3 action and atrophy-specific gene transcription', *Proceedings of the National Academy of Sciences*, pp. 16260–16265. Available at: https://doi.org/10.1073/pnas.0607795103.
Sanes, J.R., Marshall, L.M. and McMahan, U.J. (1978) 'Reinnervation of muscle fiber basal lamina after removal of myofibers. Differentiation of regenerating axons at original synaptic sites', *The Journal of cell biology*, 78(1), pp. 176–198.
Santi, S. *et al.* (2020) 'PCAF Involvement in Lamin A/C-HDAC2 Interplay during the Early Phase of Muscle Differentiation', *Cells* , 9(7). Available at: https://doi.org/10.3390/cells9071735.
Santulli, G., Lewis, D.R. and Marks, A.R. (2017) 'Physiology and pathophysiology of excitation-contraction coupling: the functional role of ryanodine receptor', *Journal of muscle research and cell motility*, 38(1), pp. 37–45.
Sartori, R. *et al.* (2009) 'Smad2 and 3 transcription factors control muscle mass in adulthood', *American journal of physiology. Cell physiology*, 296(6), pp. C1248–57.
Sartori, R. *et al.* (2013) 'BMP signaling controls muscle mass', *Nature Genetics*, pp. 1309–1318. Available at: https://doi.org/10.1038/ng.2772.
Schaller, M.D. *et al.* (1995) 'Focal adhesion kinase and paxillin bind to peptides mimicking beta integrin cytoplasmic domains', *The Journal of cell biology*, 130(5), pp. 1181–1187.
Schiaffino, S. and Reggiani, C. (1996) 'Molecular diversity of myofibrillar proteins: gene regulation and functional significance', *Physiological reviews*, 76(2), pp. 371–423.
Schiaffino, S. and Reggiani, C. (2011) 'Fiber Types in Mammalian Skeletal Muscles', *Physiological reviews*, 91(4), pp. 1447–1531.
Schoenauer, R. *et al.* (2005) 'Myomesin is a molecular spring with adaptable elasticity', *Journal of molecular biology*, 349(2), pp. 367–379.
Schultz, E. and Lipton, B.H. (1982) 'Skeletal muscle satellite cells: Changes in proliferation potential as a function of age', *Mechanisms of ageing and development*, 20(4), pp. 377–383.
Schultz, E. and McCormick, K.M. (1994) 'Skeletal muscle satellite cells', *Reviews of physiology, biochemistry and pharmacology*, 123, pp. 213–257.
Schultz, E., Gibson, M.C. and Champion, T. (1978) 'Satellite cells are mitotically quiescent in mature mouse muscle: an EM and radioautographic study', *The Journal of experimental zoology*, 206(3), pp. 451–456.
Scott, W., Stevens, J. and Binder-Macleod, S. A. (2001). Human skeletal muscle fiber type classifications. *Physical therapy*, 81 (11), pp.1810–1816.
Seale, P. and Rudnicki, M.A. (2000) 'A New Look at the Origin, Function, and "Stem-Cell" Status of Muscle Satellite Cells', *Developmental biology*, 218(2), pp. 115–124.
Selcen, D. (2008) 'Myofibrillar myopathies', *Current opinion in neurology*, 21(5), pp. 585–589.
Selcen, D. (2011) 'Myofibrillar myopathies', *Neuromuscular disorders: NMD*, 21(3), pp. 161–171.
Selcen, D. and Engel, A.G. (2005) 'Mutations inZASP define a novel form of muscular dystrophy in humans', *Annals of Neurology*, pp. 269–276. Available at: https://doi.org/10.1002/ana.20376.

Selcen, D. *et al.* (2009) ‘Mutation in BAG3 causes severe dominant childhood muscular dystrophy’, *Annals of neurology*, 65(1), pp. 83–89.
Selcen, D. *et al.* (2011) ‘Reducing bodies and myofibrillar myopathy features in FHL1 muscular dystrophy’, *Neurology*, 77(22), pp. 1951–1959.
Shear, C.R. and Bloch, R.J. (1985) ‘Vinculin in subsarcolemmal densities in chicken skeletal muscle: localization and relationship to intracellular and extracellular structures’, *The Journal of cell biology*, 101(1), pp. 240–256.
Shefer, G. *et al.* (2006) ‘Satellite-cell pool size does matter: defining the myogenic potency of aging skeletal muscle’, *Developmental biology*, 294(1), pp. 50–66.
Sheikh, F. *et al.* (2008) ‘An FHL1-containing complex within the cardiomyocyte sarcomere mediates hypertrophic biomechanical stress responses in mice’, *The Journal of clinical investigation*, 118(12), pp. 3870–3880.
Shi, H. *et al.* (2008) ‘Modulation of skeletal muscle fiber type by mitogen-activated protein kinase signaling’, *The FASEB Journal*, pp. 2990–3000. Available at: https://doi.org/10.1096/fj.07-097600.
Shi, X. and Garry, D.J. (2006) ‘Muscle stem cells in development, regeneration, and disease’, *Genes & development*, 20(13), pp. 1692–1708.
Short, K.R. *et al.* (2005) ‘Decline in skeletal muscle mitochondrial function with aging in humans’, *Proceedings of the National Academy of Sciences of the United States of America*, 102(15), pp. 5618–5623.
Sjöblom, B., Salmazo, A. and Djinović-Carugo, K. (2008) ‘α-Actinin structure and regulation’, *Cellular and molecular life sciences: CMLS*, 65(17), pp. 2688–2701.
Small, J.V. *et al.* (2002) ‘The lamellipodium: where motility begins’, *Trends in cell biology*, 12(3), pp. 112–120.
Smythe, G.M. and Forwood, J.K. (2012) ‘Altered mitogen-activated protein kinase signaling in dystrophic (mdx) muscle’, *Muscle & nerve*, 46(3), pp. 374–383.
Snow, M.H. (1977) ‘The effects of aging on satellite cells in skeletal muscles of mice and rats’, *Cell and tissue research*, 185(3), pp. 399–408.
Spangenburg, E.E. *et al.* (2008) ‘A functional insulin-like growth factor receptor is not necessary for load-induced skeletal muscle hypertrophy’, *The Journal of physiology*, 586(1), pp. 283–291.
Spielmann, M. *et al.* (2016) ‘Exome sequencing and CRISPR/Cas genome editing identify mutations of ZAK as a cause of limb defects in humans and mice’, *Genome research*, 26(2), pp. 183–191.
Spiro, A.J., Shy, G.M. and Gonatas, N.K. (1966) ‘Myotubular myopathy. Persistence of fetal muscle in an adolescent boy’, *Archives of neurology*, 14(1), pp. 1–14.
Squire, J. (2019) ‘The actin-myosin interaction in muscle: Background and overview’, *International journal of molecular sciences*, 20(22), p. 5715.
Stedman, H.H. *et al.* (1991) ‘The mdx mouse diaphragm reproduces the degenerative changes of Duchenne muscular dystrophy’, *Nature*, 352(6335), pp. 536–539.
Stewart, C.E.H. and Rittweger, J. (2006) ‘Adaptive processes in skeletal muscle: molecular regulators and genetic influences’, *Journal of musculoskeletal & neuronal interactions*, 6(1), pp. 73–86.
Straussberg, R. *et al.* (2016) ‘Kyphoscoliosis peptidase (KY) mutation causes a novel congenital myopathy with core targetoid defects’, *Acta Neuropathologica*, pp. 475–478. Available at: https://doi.org/10.1007/s00401-016-1602-9.
Stréter, F. A. et al. (1973). Synthesis by Fast Muscle of Myosin Light Chains characteristic of Slow Muscle in Response to Long-term Stimulation. *Nature New Biology*, 241 (105), pp.17–19. [Online]. Available at: doi:10.1038/newbio241017a0.

Suwa, M. *et al.* (2006) 'Metformin increases the PGC-1alpha protein and oxidative enzyme activities possibly via AMPK phosphorylation in skeletal muscle in vivo', *Journal of applied physiology*, 101(6), pp. 1685–1692.

Swist, S. *et al.* (2020) 'Maintenance of sarcomeric integrity in adult muscle cells crucially depends on Z-disc anchored titin', *Nature communications*, 11(1), p. 4479.

Szikora, S., Görög, P. and Mihály, J. (2022) 'The Mechanisms of Thin Filament Assembly and Length Regulation in Muscles', *International journal of molecular sciences*, 23(10). Available at: https://doi.org/10.3390/ijms23105306.

Tajsharghi, H. *et al.* (2003) 'Myosin storage myopathy associated with a heterozygous missense mutation inMYH7', *Annals of Neurology*, pp. 494–500. Available at: https://doi.org/10.1002/ana.10693.

Takano, K. et al. (2010) 'Nebulin and N-WASP cooperate to cause IGF-1-induced sarcomeric actin filament formation', *Science*, 330(6010), pp. 1536–1540.

Tanner, S.M. *et al.* (1999) 'Skewed X-inactivation in a manifesting carrier of X-linked myotubular myopathy and in her non-manifesting carrier mother', *Human genetics*, 104(3), pp. 249–253.

Tatsumi, R. *et al.* (1998) 'HGF/SF is present in normal adult skeletal muscle and is capable of activating satellite cells', *Developmental biology*, 194(1), pp. 114–128.

Taylor, W.E. *et al.* (2001) 'Myostatin inhibits cell proliferation and protein synthesis in C_2C_{12} muscle cells', *American Journal of Physiology-Endocrinology and Metabolism*, pp. E221–E228. Available at: https://doi.org/10.1152/ajpendo.2001.280.2.e221.

Tierney, M.T. and Sacco, A. (2016) 'Inducing and Evaluating Skeletal Muscle Injury by Notexin and Barium Chloride', *Methods in molecular biology* , 1460, pp. 53–60.

Tisdale, M.J. (2005) 'The ubiquitin-proteasome pathway as a therapeutic target for muscle wasting', *The journal of supportive oncology*, 3(3), pp. 209–217.

Tosti, E. *et al.* (2004) 'The stress kinase MRK contributes to regulation of DNA damage checkpoints through a p38gamma-independent pathway', *The Journal of biological chemistry*, 279(46), pp. 47652–47660.

Trendelenburg, A.U. *et al.* (2009) 'Myostatin reduces Akt/TORC1/p70S6K signaling, inhibiting myoblast differentiation and myotube size', *American Journal of Physiology-Cell Physiology*, pp. C1258–C1270. Available at: https://doi.org/10.1152/ajpcell.00105.2009.

Tsekoura, M. *et al.* (2017) 'Sarcopenia and Its Impact on Quality of Life', *Advances in experimental medicine and biology*, 987, pp. 213–218.

Tskhovrebova, L. and Trinick, J. (2003) 'Titin: properties and family relationships', *Nature reviews. Molecular cell biology*, 4(9), pp. 679–689.

Tubridy, N., Fontaine, B. and Eymard, B. (2001) 'Congenital myopathies and congenital muscular dystrophies', *Current Opinion in Neurology*, pp. 575–582. Available at: https://doi.org/10.1097/00019052-200110000-00005.

Uezu, A. *et al.* (2016) 'Identification of an elaborate complex mediating postsynaptic inhibition', *Science*, 353(6304), pp. 1123–1129.

Ulbricht, A. and Höhfeld, J. (2013) 'Tension-induced autophagy: may the chaperone be with you', *Autophagy*, 9(6), pp. 920–922.

Ulbricht, A. *et al.* (2013) 'Cellular mechanotransduction relies on tension-induced and chaperone-assisted autophagy', *Current biology: CB*, 23(5), pp. 430–435.

Ulbricht, A. *et al.* (2015) 'Induction and adaptation of chaperone-assisted selective autophagy CASA in response to resistance exercise in human skeletal muscle', *Autophagy*, 11(3), pp. 538–546.
Vasli, N. *et al.* (2017) 'Recessive mutations in the kinase ZAK cause a congenital myopathy with fibre type disproportion', *Brain: a journal of neurology*, 140(1), pp. 37–48.
Vasyutina, E. *et al.* (2009) 'The small G-proteins Rac1 and Cdc42 are essential for myoblast fusion in the mouse', *Proceedings of the National Academy of Sciences of the United States of America*, 106(22), pp. 8935–8940.
Venugopal, V. and Pavlakis, S. (2022) 'Duchenne Muscular Dystrophy', in *StatPearls*. Treasure Island (FL): StatPearls Publishing.
Vihola, A. et al. (2003). Histopathological differences of myotonic dystrophy type 1 (DM1) and PROMM/DM2. *Neurology*, 60 (11), pp.1854–1857.
Vind, A.C. *et al.* (2020) 'ZAKα Recognizes Stalled Ribosomes through Partially Redundant Sensor Domains', *Molecular Cell*, pp. 700–713.e7. Available at: https://doi.org/10.1016/j.molcel.2020.03.021.
Voisine, C., Pedersen, J.S. and Morimoto, R.I. (2010) 'Chaperone networks: tipping the balance in protein folding diseases', *Neurobiology of disease*, 40(1), pp. 12–20.
Vorgerd, M. *et al.* (2005) 'A mutation in the dimerization domain of filamin c causes a novel type of autosomal dominant myofibrillar myopathy', *American journal of human genetics*, 77(2), pp. 297–304.
Vracko, R. and Benditt, E.P. (1972) 'BASAL LAMINA: THE SCAFFOLD FOR ORDERLY CELL REPLACEMENT', *Journal of Cell Biology*, pp. 406–419. Available at: https://doi.org/10.1083/jcb.55.2.406.
Wachsstock, D.H., Wilkins, J.A. and Lin, S. (1987) 'Specific interaction of vinculin with α-actinin', *Biochemical and biophysical research communications*, 146(2), pp. 554–560.
Wackerhage, H. *et al.* (2019) 'Stimuli and sensors that initiate skeletal muscle hypertrophy following resistance exercise', *Journal of applied physiology*, 126(1), pp. 30–43.
Wagers, A.J. and Conboy, I.M. (2005) 'Cellular and molecular signatures of muscle regeneration: current concepts and controversies in adult myogenesis', *Cell*, 122(5), pp. 659–667.
Wakayama, Y. *et al.* (1979) 'Quantitative ultrastructural study of muscle satellite cells in Duchenne dystrophy', *Neurology*, pp. 401–401. Available at: https://doi.org/10.1212/wnl.29.3.401.
Webster, C. *et al.* (1988) 'Fast muscle fibers are preferentially affected in Duchenne muscular dystrophy', *Cell*, 52(4), pp. 503–513.
Weeds, A. G. et al. (1974). Myosin from cross-reinnervated cat muscles. *Nature*, 247 (5437), pp.135–139.
Welle, S. *et al.* (1993) 'Myofibrillar protein synthesis in young and old men', *The American journal of physiology*, 264(5 Pt 1), pp. E693–8.
Whitmarsh, A.J. (2006) 'The JIP family of MAPK scaffold proteins', *Biochemical Society transactions*, 34(Pt 5), pp. 828–832.
Williams, A. *et al.* (2006) 'Aggregate-Prone Proteins Are Cleared from the Cytosol by Autophagy: Therapeutic Implications', in *Current Topics in Developmental Biology*. Academic Press, pp. 89–101.
Witt, C.C. *et al.* (2006) 'Nebulin regulates thin filament length, contractility, and Z-disk structure in vivo', *The EMBO journal*, 25(16), pp. 3843–3855.

Xie, S.-J. et al. (2018) ‘Inhibition of the JNK/MAPK signaling pathway by myogenesis-associated miRNAs is required for skeletal muscle development’, Cell death and differentiation, 25(9), pp. 1581–1597.
Yaffe, D. and Saxel, O. (1977) ‘Serial passaging and differentiation of myogenic cells isolated from dystrophic mouse muscle’, *Nature*, 270(5639), pp. 725–727.
Yang H, Wang H, Jaenisch R (2014) Generating genetically modified mice using CRISPR/Cas-mediated genome engineering. *Nat Protoc* 9: 1956–1968
Yang, J.-J. (2002) ‘Mixed lineage kinase ZAK utilizing MKK7 and not MKK4 to activate the c-Jun N-terminal kinase and playing a role in the cell arrest’, *Biochemical and biophysical research communications*, 297(1), pp. 105–110.
Yin, H., Price, F. and Rudnicki, M.A. (2013) ‘Satellite cells and the muscle stem cell niche’, *Physiological reviews*, 93(1), pp. 23–67.
Yogev, Y. *et al.* (2017) ‘Progressive hereditary spastic paraplegia caused by a homozygous KY mutation’, *European journal of human genetics: EJHG*, 25(8), pp. 966–972.
Yuan *et al.* (2011) ‘FoxO1 regulates muscle fiber-type specification and inhibits calcineurin signaling during C2C12 myoblast differentiation’, *Molecular and Cellular Biochemistry*, pp. 77–87. Available at: https://doi.org/10.1007/s11010-010-0640-1.
Zammit, P.S. *et al.* (2002) ‘Kinetics of myoblast proliferation show that resident satellite cells are competent to fully regenerate skeletal muscle fibers’, *Experimental cell research*, 281(1), pp. 39–49.
Zayia, L.C. and Tadi, P. (2022) ‘Neuroanatomy, Motor Neuron’, in *StatPearls*. Treasure Island (FL): StatPearls Publishing.
Zemljic-Harpf, A., Manso, A.M. and Ross, R.S. (2009) ‘Vinculin and talin: focus on the myocardium’, *Journal of investigative medicine: the official publication of the American Federation for Clinical Research*, 57(8), pp. 849–855.
Zhang, M. *et al.* (2007) ‘Identification of CAP as a costameric protein that interacts with filamin C’, *Molecular biology of the cell*, 18(12), pp. 4731–4740.
Zhao, J. *et al.* (2007) ‘FoxO3 coordinately activates protein degradation by the autophagic/lysosomal and proteasomal pathways in atrophying muscle cells’, *Cell metabolism*, 6(6), pp. 472–483.
Zou, K. *et al.* (2011) ‘The α7β1-integrin increases muscle hypertrophy following multiple bouts of eccentric exercise’, *Journal of applied physiology*, 111(4), pp. 1134–1141.

Appendix

Supplementary Table 1: Summary table of known KY mutations in patients

Family	P.1	P.1	P.1	P.1	P.1	P.1	P.1	P.1	P.2	P.3	P.3	A.1	B.1	B.1	C.1	D.1	D.1	D.1	D.1
Individual	III:2	III:9	IV:2	IV:3	IV:6	IV:11	IV:12	V:3	II:3	III:3	IV:1	I	I:1	I:2	I	III:6	III:7	III:8	IV:2
Source*	1	1	1	1	1	1	1	1	1	1	1	2	3	3	4	5	5	5	5
Sex	M	M	F	M	M	F	F	F	F	F	F	F	M	M	M	M	M	F	F
Age at examination	34	53	9	3	11	12	14	5	4.5	22	2.8	7.5	23	34	29	NA	NA	NA	NA
Age at onset	<1	<1	<1	<1	<1	1	<1	1.4	<1	<1	1	2	<1	<1	3	6	6	6	6
Mutation	1	1	1	1	1	1	1	1	1	1	1	2	3	3	4	5	5	5	5
Progressive deterioration	+	+	+	+	+	+	+	+	+	+	+	+	+	+	+	+	+	+	+
Toe walking	+	+	+	+	+	+	+	+	+	+	+	+	+	+	+	+	+	+	+
Weakness upper limb	-	+	-	+	-	-	-	-	-	-	-	-	+	-	-	-	-	-	-
Weakness lower limb	-	+	-	+	-	-	-	-	-	-	+	+	+	+	+	+	+	+	+
Atrophy upper limb	-	+	-	+	-	-	-	+	-	-	-	-	+	-	-	-	-	-	-
Atrophy lower limb	-	+	-	+	-	-	-	+	-	-	-	+	+	+	+	+	+	+	+
Kyphosis	+	+	-	+/-	+	+	+	-	+/-	+/-	-	-	+	+	-	-	-	-	-
Scoliosis	+	+	-	-	-	-	+	-	-	-	-	-	+	-	+	-	-	-	-
Tongue atrophy	NA	+	-	-	+	-	+	+	-	+	-	NA	+	+	NA	NA	NA	NA	NA

* 1 = (Yogev et al., 2017)
* 2 = (Hedberg-Oldfors et al., 2016)
* 3 = (Straussberg et al., 2016)
* 4 = (Ebrahimzadeh-Vesal et al., 2018)
* 5 = (Arif et al., 2020)

1 = NM_178554.6:c.51_52insTATCGACATGTGCTGTATCTATCGACAT;p.(Val18TyrfsTer56) (Yogev et al., 2017) frameshift

2 = NM_178554.6:c.1071delG;p.(Thr358LeufsT er3) (Hedberg-Oldfors et al., 2016) frameshift, introduction of a premature stop codon, producing a smaller truncated protein
3 = NM_178554.6:c.405C>A;p.(Tyr135Ter) (Straussberg et al., 2016) resulting in a premature stop codon suggested to cause nonsense-mediated mRNA decay
4 = NM_178554.6:c.415C>T;p.(Arg139Ter) (Ebrahimzadeh-Vesal et al., 2018) nonsense
5 = NM_178554.6:c.842_855del; p.(Val281GlyfsTer18) (Arif et al., 2020) missense

Supplementary Table 2: Summary table of known ZAK mutations in patients

Family	I	II	II	III	III	III	IV	IV	IV	IV	IV	IV	IV
Individual	I-1	II-1	II-2	III-1	III-2	III-3	IV-3	IV-4	IV-5	IV-6	IV-7	IV-10	V-1
Source	1	1	1	1	1	1	2	2	2	2	2	2	2
Sex	M	F	F	F	M	M	M	M	F	M	M	F	F
Age at examination	27	37 (deceased)	33	32	26	NA	(deceased early childhood)	(deceased early childhood)	(deceased early childhood)	(deceased early childhood)	34	29	27
Age at onset	2	4	2	5	2	<1	<1	<1	<1	<1	<1	<1	<1
Mutation	1	2	2	3	3	3	4	4	4	4	4	4	4
Progressive deterioration	+	+	+	+	+	+	+	+	+	+	+	+	+
Toe walking	-	-	-	+	+	-	-	-	-	-	-	-	-
Weakness upper limb	+	-	-	+	-	-	+	+	+	+	+	+	+
Weakness lower limb	+	+	+	+	+	+	+	+	+	+	+	+	+
Atrophy upper limb	+	-	-	-	-	-	-	-	-	-	-	-	-
Atrophy lower limb	+	+	+	+	+	-	+	+	+	+	+	+	+
Kyphosis	-	-	-	-	-	-	-	-	-	-	-	-	-
Scoliosis	+	+	+	+	+	+	+	+	+	+	+	+	+
Tongue atrophy	-	-	-	-	NA	NA	NA	NA	NA	NA	NA	NA	NA

* 1 = (Vasli *et al.*, 2017)
* 2 = (Ahmad *et al.*, 2022)
1 = NM_133646: c.490_491delATp.Met164fs*24 Frameshift
2 = NM_133646: c.515G>Ap.Trp172* Nonsense
3 = NM_133646: c.280_281insTp.Asn95* Frameshift
4 = NM_133646:c.456delTp.Phe152Leufs*49 frameshift variant that leads to premature termination of translation

Article

SOURCE DATA | TRANSPARENT PROCESS | OPEN ACCESS

THE EMBO JOURNAL

ZAKβ is activated by cellular compression and mediates contraction-induced MAP kinase signaling in skeletal muscle

Cathrine Nordgaard[1], Anna Constance Vind[1], Amy Stonadge[2], Rasmus Kjøbsted[3], Goda Snieckute[1], Pedro Antas[4], Melanie Blasius[1], Marie Sofie Reinert[1], Ana Martinez Del Val[5], Dorte Breinholdt Bekker-Jensen[5], Peter Haahr[6], Yekaterina A Miroshnikova[7], Abdelghani Mazouzi[6], Sarah Falk[8], Emeline Perrier-Groult[9], Christopher Tiedje[1], Xiang Li[2], Jens Rithamer Jakobsen[10], Nicolas Oldenburg Jørgensen[3], Jørgen FP Wojtaszewski[3], Frederic Mallein-Gerin[9], Jesper Løvind Andersen[1,10], Cristian Pablo Pennisi[11], Christoffer Clemmensen[8], Moustapha Kassem[12,13], Abbas Jafari[12], Thijn Brummelkamp[6,14,15,16], Vivian SW Li[4], Sara A Wickström[7], Jesper Velgaard Olsen[5], Gonzalo Blanco[2] & Simon Bekker-Jensen[1,*]

Abstract

Mechanical inputs give rise to p38 and JNK activation, which mediate adaptive physiological responses in various tissues. In skeletal muscle, contraction-induced p38 and JNK signaling ensure adaptation to exercise, muscle repair, and hypertrophy. However, the mechanisms by which muscle fibers sense mechanical load to activate this signaling have remained elusive. Here, we show that the upstream MAP3K ZAKβ is activated by cellular compression induced by osmotic shock and cyclic compression *in vitro*, and muscle contraction *in vivo*. This function relies on ZAKβ's ability to recognize stress fibers in cells and Z-discs in muscle fibers when mechanically perturbed. Consequently, ZAK-deficient mice present with skeletal muscle defects characterized by fibers with centralized nuclei and progressive adaptation towards a slower myosin profile. Our results highlight how cells in general respond to mechanical compressive load and how mechanical forces generated during muscle contraction are translated into MAP kinase signaling.

Keywords mechanobiology; muscle contraction; myopathy; ZAKβ
Subject Categories Musculoskeletal System; Post-translational Modifications & Proteolysis
DOI 10.15252/embj.2022111650 | Received 12 May 2022 | Revised 28 May 2022 | Accepted 22 June 2022 | Published online 28 July 2022
The EMBO Journal (2022) 41: e111650

Introduction

The MAP kinases p38 and JNK are central transducers of cellular stress-signaling pathways (Wagner & Nebreda, 2009). In general,

1 Center for Healthy Aging, Department of Cellular and Molecular Medicine, University of Copenhagen, Copenhagen, Denmark
2 Department of Biology, University of York, York, UK
3 Department of Nutrition, Exercise and Sports, University of Copenhagen, Copenhagen, Denmark
4 Stem Cell and Cancer Biology Laboratory, The Francis Crick Institute, London, UK
5 Mass Spectrometry for Quantitative Proteomics, Proteomics Program, Faculty of Health and Medical Sciences, The Novo Nordisk Foundation Center for Protein Research, University of Copenhagen, Copenhagen, Denmark
6 Division of Biochemistry, The Netherlands Cancer Institute, Amsterdam, The Netherlands
7 Stem Cells and Metabolism Research Program, Faculty of Medicine and Helsinki Institute of Life Science, University of Helsinki, Helsinki, Finland
8 Novo Nordisk Foundation Center for Basic Metabolic Research, Faculty of Health and Medical Sciences, University of Copenhagen, Copenhagen, Denmark
9 Institut de Biologie et Chimie des Protéines, CNRS UMR5305, Lyon, France
10 Department of Orthopedic Surgery M, Institute of Sports Medicine Copenhagen, Bispebjerg Hospital, Copenhagen, Denmark
11 Regenerative Medicine Group, Department of Health Science and Technology, Aalborg University, Aalborg, Denmark
12 Department of Cellular and Molecular Medicine, Novo Nordisk Foundation Center for Stem Cell Biology (DanStem), University of Copenhagen, Copenhagen, Denmark
13 Department of Endocrinology and Metabolism, University Hospital of Odense and University of Southern Denmark, Odense, Denmark
14 Oncode Institute, Division of Biochemistry, The Netherlands Cancer Institute, Amsterdam, The Netherlands
15 CeMM Research Center for Molecular Medicine of the Austrian Academy of Sciences, Vienna, Austria
16 Cancer Genomics Center, Amsterdam, The Netherlands
*Corresponding author (lead contact). Tel: +45 35 25 50 24; E-mail: sbj@sund.ku.dk

they control inflammatory cytokine production, and they are essential due to their impact on a vast array of signaling pathways that control cell fate decisions such as apoptosis and differentiation. p38 and JNK are activated upon exposure of cells to a number of stress agents like UV light, ribosomal impairment, oxidative stress, and heat or osmotic shock (Davis, 2000). In addition, p38 and JNK are activated by a number of extracellular signaling molecules such as growth factors, hormones, and cytokines (Wagner & Nebreda, 2009). MAP kinases are generally activated through signal transduction cascades involving upstream MAP kinase kinases (MAP2Ks) and MAP kinase kinase kinases (MAP3Ks). For extracellular ligand-mediated MAP kinase activation, the signaling from upstream pathway components and transmembrane receptors has largely been deduced. However, how the same kinases are activated by endogenous stress signals is only poorly elucidated and this represents a considerable gap in our knowledge about MAP kinase signaling pathways. Targeting of p38 and JNK holds great potential for the treatment of a range of diseases but is associated with detrimental side effects due to the broad and general functions of these kinases (Hammaker & Firestein, 2010). Elucidation of pathways for context-dependent and stimulus-specific MAP kinase activation thus represents a major scientific challenge and an untapped opportunity for medical exploitation.

With a few exceptions, we know virtually nothing about the molecular/chemical nature of the stress signals, their cellular sensors, or the MAP3Ks responsible for initiating the kinase cascades. The best-studied case of such a signal-sensor relationship is that of the oxidative stress-responsive MAP3K ASK1. This kinase is normally kept in an inactive oligomeric state through an interaction with the reduced form of thioredoxin (Saitoh *et al*, 1998). In the presence of Reactive Oxygen Species (ROS), thioredoxin is oxidized and the inhibition of ASK1 kinase activity is relieved (Tobiume *et al*, 2002). In this scenario, ROS molecules themselves constitute the signal and thioredoxin performs the role of a sensor. Another example is the sensing of translation-impairing ribosomal lesions (ribotoxic stress) by the MAP3K ZAKα (MAP3K20 / MLTK / MRK / MLK7—long transcript). This kinase contains two ribosome-binding domains in its C-terminus that in combination serve as a molecular sensing module (Vind *et al*, 2020b). The nature of the ribosomal signal that ZAKα responds to is still elusive and can involve the collision of ribosomes (Wu *et al*, 2020; Vind *et al*, 2020a). Several MAP3Ks have been reported to be activated by stress treatments such as UV light and osmotic shock. Besides their best understood cellular effects (damage to DNA and reduction in cell volume, respectively), these treatments are highly pleiotropic and likely give rise to several p38- and JNK-activating stress signals that are sensed by diverse and still elusive mechanisms. Rather than being redundant, individual MAP3Ks are activated upon the generation of specific and nonoverlapping physiological signals, the complexity of which we do not yet appreciate.

Physiologically relevant mechanical perturbations of cells include stretching, compression, increased pressure, and fluid flow. Cellular perception of mechanical cues is ensured primarily through the activation of mechanosensing proteins (Kechagia *et al*, 2019). Such sensors are found associated with the cell membrane, caveolae, the primary cilium, the cytoskeleton, and focal adhesions. Mechanosensation underlies physiological phenomena such as the senses of touch and hearing and impacts cellular processes such as cell differentiation, migration, invasion, and tissue homeostasis. Prominent among cellular mechanosensors are the piezo channels, which open upon membrane deformation, causing the influx of cations such as calcium (Wu *et al*, 2017). These ions activate several kinases and mediate a multitude of cellular effector pathways, including a recently described stretching-induced nuclear softening response (Nava *et al*, 2020). Mechanical perturbations also give rise to p38- and JNK-activating stress signals (Hoffman *et al*, 2017) (and references herein), the identities of which are poorly understood. One mechanism operates through piezo channel opening (Fukuno *et al*, 2011; Blythe *et al*, 2019), and a calcium-activated calmodulin-dependent kinase has been reported to phosphorylate and activate the MAP3K TAK1 (Liu *et al*, 2008). In support of this model, piezo channels and TAK1 are required for bone homeostasis (Swarnkar *et al*, 2015; Wang *et al*, 2020), likely by coupling mechanical load to remodeling in this tissue.

The physiology of several other tissues depends on precisely dosed mechanical stress sensing and MAP kinase signaling. A prime example is a skeletal muscle, where the contraction of the individual muscle fibers generates cellular stress signals that are transformed into MAP kinase activation (Nelson *et al*, 2019). Such signaling is critically important for local and systemic adaptation to exercise, muscle repair, and homeostasis (Kramer & Goodyear, 2007). The identities of MAP kinase activating signals relevant to muscle use are elusive, as are the corresponding sensing mechanisms and responsible MAP3Ks. Here, we show that the ubiquitously expressed but poorly described MAP3K20/ZAK/MLTK/MRK/MLK7 splice form ZAKβ is activated by osmotic shock and mechanical compression of cells. This process is mediated through a C-terminal domain that responds to the mechanical perturbation of cytoskeletal stress fibers. In skeletal muscle, Z-disc localized ZAKβ responds to muscle fiber contraction to mediate MAP kinase activation and is required to prevent muscle pathology.

Results

The short isoform of the MAP3K ZAK is activated by osmotic shock

To identify proteins controlling p38 activation upon osmotic shock, we designed a genetic screen in the human haploid cell line HAP1 (Brockmann *et al*, 2017). This unbiased approach was based on the random insertion of gene-traps, FACS-assisted sorting of cells with high and low levels of phospho-p38 and deep sequencing to map insertions (Fig EV1A). Next to p38 and MAP2K6, the MAP3K genes TAK1 (also shown by (Huangfu *et al*, 2006; Inagaki *et al*, 2008)) and ZAK appeared as the only hits in the MAPK signaling pathway (Fig 1A; Dataset EV1). The result for the latter could be validated both in ZAK-deleted HAP1 and U2OS cells, where p38 activation by the ribotoxic stress-inducing agent anisomycin was completely abolished as previously shown (Vind *et al*, 2020b), and sorbitol-induced p38 activation was clearly reduced (Figs 1B and EV1B). The ZAK gene in vertebrates encodes two alternatively spliced transcripts that give rise to two MAP3K proteins with distinct C-termini (Gross *et al*, 2002; Fig 1C). The longer of these, ZAKα, is a sensor of ribotoxic stress by virtue of two ribosome-binding domains in its unique C-terminus (Wu *et al*, 2020; Vind *et al*, 2020b). Its shorter

counterpart ZAKβ is expressed roughly 10-fold higher than ZAKα, is not activated by ribotoxic stress, and remains functionally uncharacterized. Further analysis of the ZAK-specific gene-trap sequences (Figs 1A and EV1A) revealed a lack of bias in insertions at ZAKα-specific intron-exon boundaries in the "low" vs "high" populations, indicating that the α isoform is not critical for this effect. This was in stark contrast to a previously published anisomycin screen (Brockmann *et al*, 2017) where such insertions were strongly biased towards the low p-p38 cell pool (Fig 1D). The nature of gene disruption by insertional gene-traps and the presence of only a single unique last exon in ZAKβ precluded us from conducting a similar analysis for this isoform, but these results indicated to us that the shorter isoform of ZAK is activated upon osmotic shock. In support, strep-HA-tagged ZAKβ and the atypical MAP kinase ERK5 displayed a massive gel mobility shift when cells were challenged with osmotic stress agents (Sorbitol, NaCl). This was not observed with other p38- and JNK-activating stimuli such as ribotoxic stressors (anisomycin, UV), an inflammatory cytokine (IL1β), or oxidative stress (arsenite) (Fig 1E). This mobility shift was titratable with increasing concentrations of sorbitol in the medium (Fig EV1C), could be observed also for endogenous ZAKβ (Fig EV1D), and was abolished by incubation of lysates with phosphatase or interference with ZAKβ catalytic activity (Fig EV1D and E). The positive impact of ZAK on p38 and JNK phosphorylation was evident as early as 5 min after sorbitol addition (Fig EV1F), and the phosphorylation state of these kinases was quickly reset upon normalization of osmotic pressure (Fig EV1G). Finally, *in vitro* kinase activity of ZAKβ increased when the kinase was freshly purified from sorbitol-treated cells (Fig 1F). Together, these results led us to conclude that ZAKβ is activated and engages in autophosphorylation when cells are challenged by osmotic shock. Through rescue experiments and isoform-specific knockdown, we were able to determine that both α and β isoforms could compensate for deletion of the ZAK gene with respect to osmotic shock-induced activation of p38 and JNK (Figs 1G and EV1H). This initially puzzling observation indicated to us that osmotic shock triggers not only both ZAKα-activating ribotoxic stress but also a range of other stress signals that are recognized by several MAP3Ks, including ZAKβ. This notion was supported by the fact that rescue by ZAKα required the integrity of the two ribosome-binding domains in this isoform (Vind *et al*, 2020a; Fig EV1I). We thus concluded that osmotic shock induces both a known stress signal sensed by ZAKα (ribotoxic stress) and an unknown signal that leads to activation of ZAKβ (Fig 1H).

Other MAP3Ks have been implicated in p38/JNK activation after osmotic shock, such as MEKK2 and TAK1 (Uhlik *et al*, 2003; Huangfu *et al*, 2006). siRNA-mediated depletion of these kinases in ZAK-deficient U2OS cells removed the last traces of p38 and JNK phosphorylation (Figs 1I and 2A, and EV2A). Our careful analysis thus allowed us to compile an inventory of MAP3Ks (ZAKα, ZAKβ, TAK1, and MEKK2) that are responsible for p38 and JNK activation upon osmotic shock in an additive fashion. Although this list is likely not complete and may be impacted by differences in MAP3K expression across cell lines, our data clearly highlight that the uncharacterized MAP3K ZAKβ substantially contributes to p38 and JNK activation in cells exposed to osmotic shock.

ZAKβ is recruited to stress fibers after osmotic shock

Both ZAK isoforms primarily localize to the cytoplasm; however, upon osmotic shock, ZAKβ adopts a remarkable and extraction-resistant localization to the nuclear lamina and discrete nuclear domains (Fig 2A and B). Here, ZAKβ co-localizes with Lamin A/C (Figs 2A and EV2B) and the DNA damage response (DDR) factor 53BP1 (Figs 2C and EV2B). The latter of these structures have been previously described to be related to mechanical stress responses and accrue a host of DDR factors such as ATR, ATRIP, and 53BP1 (Kumar *et al*, 2014; Xia *et al*, 2018). These 53BP1-ZAKβ foci do not contain DNA lesions, as determined by the absence of γ-H2AX (Fig EV2C), and ZAKβ is also not recruited to Ionizing Radiation-Induced Foci (IRIF) (Fig EV2D). Thus, these osmotic shock triggered foci represent noncanonical DDR complexes with unknown

Figure 1. Osmotic shock-induced activation of p38 and JNK requires both ZAK isoforms.

A Gene-trap-based genetic screen in haploid human cells for regulators of p38 kinase activation (p38 Thr180/Tyr182 phosphorylation) in response to hyperosmotic shock (500 mM Sorbitol, 1 h). Per gene (dots), the frequency of gene-trap insertions in the "high" phospho-p38 population divided by the frequency of insertions in the "low" population is plotted as mutation index (y-axis) against the total number of insertions assigned to the gene (x-axis). Significant negative and positive regulators are colored in orange and blue, respectively (two-sided Fisher's exact test, false discovery rate-corrected, $P \leq 0.05$).

B Human U2OS cells and cells deleted for ZAK (ΔZAK) were treated with anisomycin (1 h) or 500 mM sorbitol (1 h). Lysates were analyzed by immunoblotting as indicated.

C Schematic of ZAK protein isoforms. LZ—leucine zipper; SAM—sterile alpha-motif; S—sensor domain; CTD—C-terminal domain; SFBD—stress fiber-binding domain.

D Unique gene-trap insertions (dots) mapped to the genomic ZAK locus (x-axis) identified in the low (blue) and high (orange) channels of two individual haploid genetic screens for stress-induced p38 activation (Sorbitol (Fig 1A) and Anisomycin; Brockmann *et al*, 2017). The total number of identified insertions was similar for each channel within the individual screens. For visual purposes, insertion dots were spread on the y-axis, and exons in the ZAK gene body schematic have been scaled up (compared with introns).

E U2OS/S-HA-ZAKβ cells were induced for expression with doxycycline (DOX) and subjected to the indicated drugs and treatments (1 h). Lysates were analyzed by immunoblotting with the indicated antibodies. Sorb.—sorbitol; Ani.—anisomycin; Ars.—arsenite.

F U2OS cells stably expressing WT and kinase-dead (KD) versions of S-HA-ZAKβ were pretreated with ZAK inhibitor (ZAKi - 0.5 h) and 500 mM sorbitol (1 h) as indicated. Whole-cell extracts (WCE) were analyzed by immunoblotting, and strep-pull-down material was used in a kinase assay, separated by SDS–PAGE and analyzed by autoradiography.

G U2OS and ΔZAK cells rescued with S-HA-ZAKβ, were DOX-induced, and treated with 500 mM sorbitol (1 h) as indicated. Lysates were analyzed by immunoblotting with the indicated antibodies.

H Osmotic shock activates p38 both via a ZAKα-dependent ribotoxic stress response and a previously uncharacterized ZAKβ-dependent stress response.

I U2OS and ΔZAK cells were transfected with the indicated siRNAs and treated with sorbitol (500 mM, 1 h) as indicated. Lysates were analyzed by immunoblotting with the indicated antibodies. T1—TAK1; M2—MEKK2.

Source data are available online for this figure.

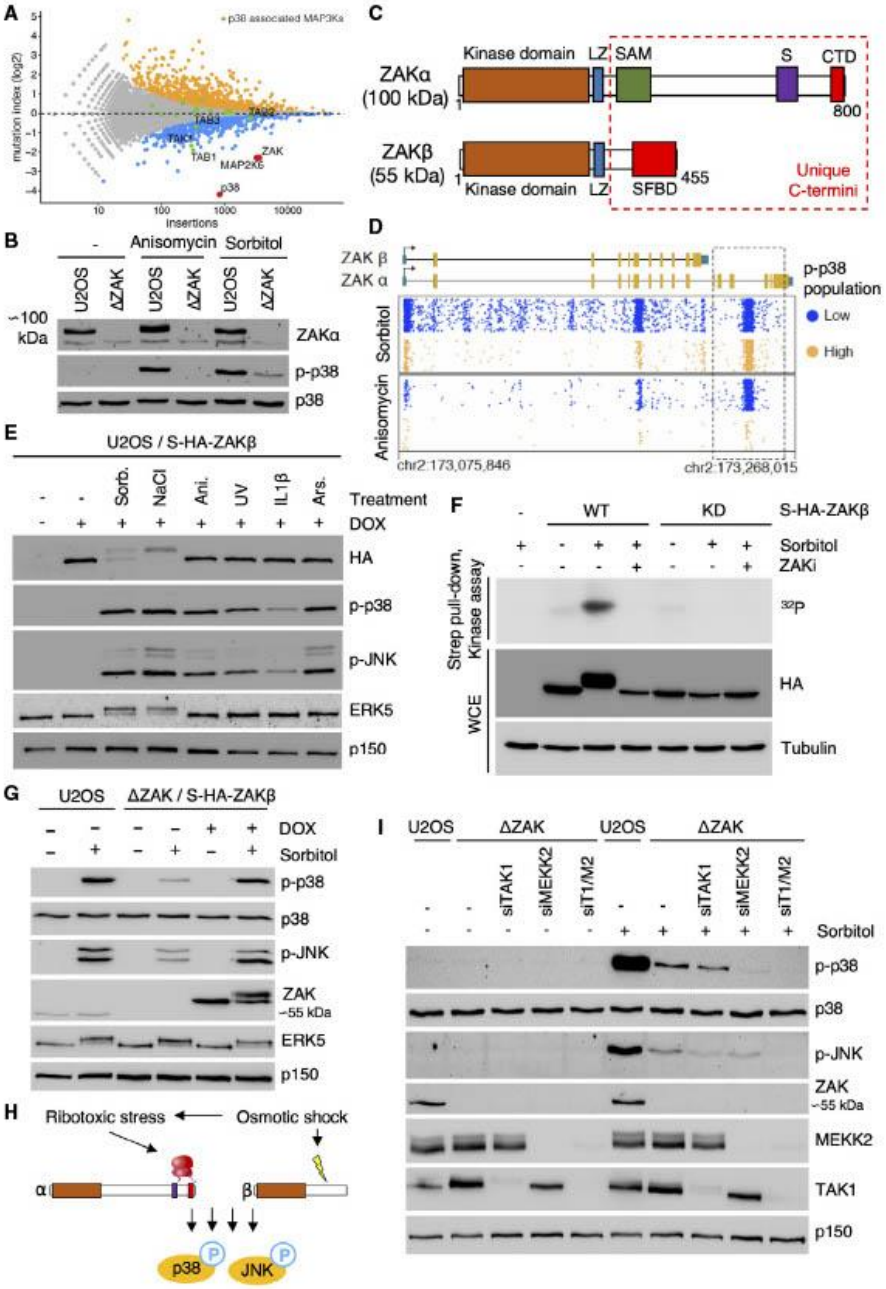

Figure 1.

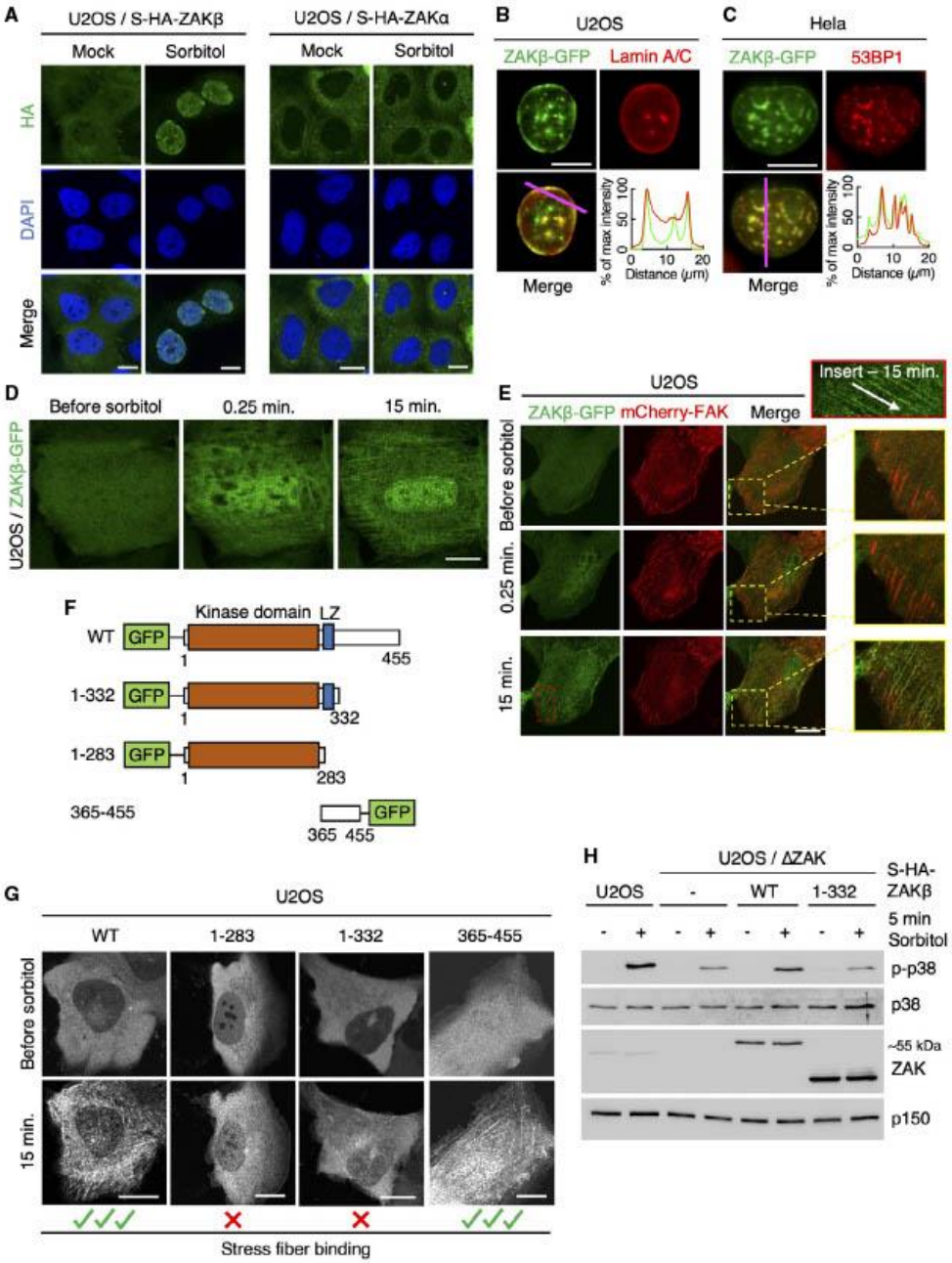

Figure 2.

Figure 2. ZAKβ redistributes to nuclear domains and stress fibers after osmotic shock.

A U2OS cells stably expressing Strep-HA-ZAKβ or -ZAKα were treated with sorbitol (500 mM, 1 h) as indicated. Cells were fixed, immunostained with HA antibody, and counterstained with DAPI.

B U2OS cells stably expressing ZAKβ-GFP were treated with sorbitol (500 mM, 1 h), pre-extracted, fixed, and immunostained with Lamin A/C antibody. Lower right: Intensity distribution graph showing fluorescence intensities along the magenta line.

C As in (B) except that Hela cells were transfected with ZAKbeta-GFP and immunostained with 53BP1 antibody.

D Cells from (B) were imaged by live-cell fluorescence microscopy. Sorbitol (final concentration 500 mM) was added after the acquisition of the first frame.

E As in (D), except that cells were co-transfected with mCherry-FAK. Inserts show higher magnification of the yellow and red regions, white arrow indicates the direction of stress fibers.

F Schematic of GFP-tagged ZAKβ truncation constructs.

G U2OS cells were transfected with constructs from (F) and imaged by live-cell fluorescence microscopy. Sorbitol (final concentration 500 mM) was added after the acquisition of the first frame.

H U2OS and ΔZAK cells stably expressing the indicated Strep-HA-tagged ZAKβ constructs were treated with sorbitol (500 mM, 5 min). Lysates were analyzed by immunoblotting with the indicated antibodies.

Data information: All scale bars, 10 μm.
Source data are available online for this figure.

functions. The same dramatic localization change was not observed for the ZAKα isoform (Fig 2A). Live-cell imaging furthermore revealed a dramatic and rapid sorbitol-induced assembly of ZAKβ-GFP on filament-like structures resembling the cytoskeleton (Figs 2D and EV2E; Movie EV1). Of note, this localization was reversed almost immediately upon normalization of culture medium osmolarity (Fig EV2F). Also, this behavior was specific for the short ZAK isoform, as GFP-ZAKα localization was not impacted by osmotic shock (Fig EV2G). We hypothesized that these filaments could be related to the contractile machinery of cells. This was supported by the co-localization of ZAKβ-GFP with SiR-actin, a live-cell probe for F-actin (Fig EV2H), the stress fiber marker α-actinin1 (Fig EV2I), and the focal adhesion marker FAK (Fig 2E; Movie EV2). In search of molecular determinants of ZAKβ's osmotic shock-induced recruitment to stress fibers, we generated a series of GFP-tagged truncation constructs (Fig 2f) that were transfected into U2OS cells and analyzed by live-cell imaging. Upon sorbitol treatment, only full-length ZAKβ and a fragment containing the C-terminus of the protein (AA 365–455) were recruited to stress fiber-like structures (Fig 2G; Movie EV3). This region, which we named the stress fiber-binding domain (SFBD, Fig 1C), appeared to be obligatory for ZAKβ activation. Thus, ZAK-deleted U2OS cells expressing a doxycycline-inducible C-terminal truncation of ZAKβ (AA 1–332) did not rescue acute sorbitol-induced p38 activation (Fig 2H).

Activation of ZAKβ upon mechanical compression requires an isoform-specific stress fiber-binding domain

Osmotic shock confers considerable mechanical stress on cells due to a sudden compression and reduction in volume (Finan & Guilak, 2010). To investigate whether ZAKβ is also activated by mechanical compression, we casted U2OS cells into agarose that we subjected to cyclic compression. Fully in line with the observations above, this treatment led to a pronounced, ZAK-dependent activation of p38 and JNK (Fig 3A and B). This activation defect could be rescued by re-introducing WT Strep-HA-ZAKβ but not its SFBD-deleted counterpart into ZAK-deleted U2OS cells (Fig 3C). To elucidate whether ZAKβ is activated also by other mechanical stimuli, we exposed cells to cyclic uniaxial and equibiaxial stretching. While these treatments activated p38 and JNK as reported (Hoffman *et al*, 2017), this process was surprisingly not impacted by ZAKβ (Fig 3A and D). Instead, it was fully dependent on TAK1 as previously reported (Fukuno *et al*, 2011; Fig 3E). We conclude that ZAKβ is specifically activated by a compressive load but not the other mechanical perturbations tested here. Conversely, TAK1 performs the same function upon cell stretching (Fig 3F). Our data point towards the SFBD in ZAKβ acting as a mechano-responsive module through its recognition of perturbed stress fibers.

Figure 3. ZAKβ responds to cellular compression but not stretching.

A Schematic of mechanical perturbation of cells by compression and stretching.

B U2OS and ΔZAK cells were embedded in agarose and subjected to cyclic compression (0.5 h). Lysates were analyzed by immunoblotting with the indicated antibodies.

C U2OS and ΔZAK cells stably expressing the indicated Strep-HA-tagged ZAKβ constructs were embedded in agarose and subjected to cyclic compression for 5 or 30 min. Lysates were analyzed as in (B).

D U2OS and ΔZAK cells were pretreated with ZAK inhibitor (ZAKi) for 30 min and subjected to equibiaxial (Equi) or uniaxial (Uni) cyclic stretch (0.5 h) as indicated. Lysates were analyzed as in (B).

E U2OS and ΔZAK cells were transfected with the indicated siRNAs and subjected to equibiaxial cyclic stretch (5 min) as indicated. Lysates were analyzed as in (B).

F Model of MAP3Ks involved in p38- and JNK-activating signaling in mechanically stimulated cells. ZAKβ is activated upon compressive load (left), in a manner dependent on stress fiber binding. TAK1 is activated by cell stretching (right).

G Expression levels of MAP3 kinase genes in human skeletal muscle (GTEx Portal). TPM—transcripts per million.

H Murine C2C12 myoblasts can be differentiated into myotubes by incubation in a myotube differentiation (diff.) medium for 6 days.

I C2C12 cells were incubated in diff. Medium for 3 or 6 days. Lysates were analyzed for ZAK isoform expression by immunoblotting.

J C2C12 myoblasts and myotubes (6 d differentiation) were pretreated with ZAK inhibitor (ZAKi, 0.5 h) and treated with 500 mM sorbitol (1 h) as indicated. Lysates were analyzed by immunoblotting with the indicated antibodies.

Source data are available online for this figure.

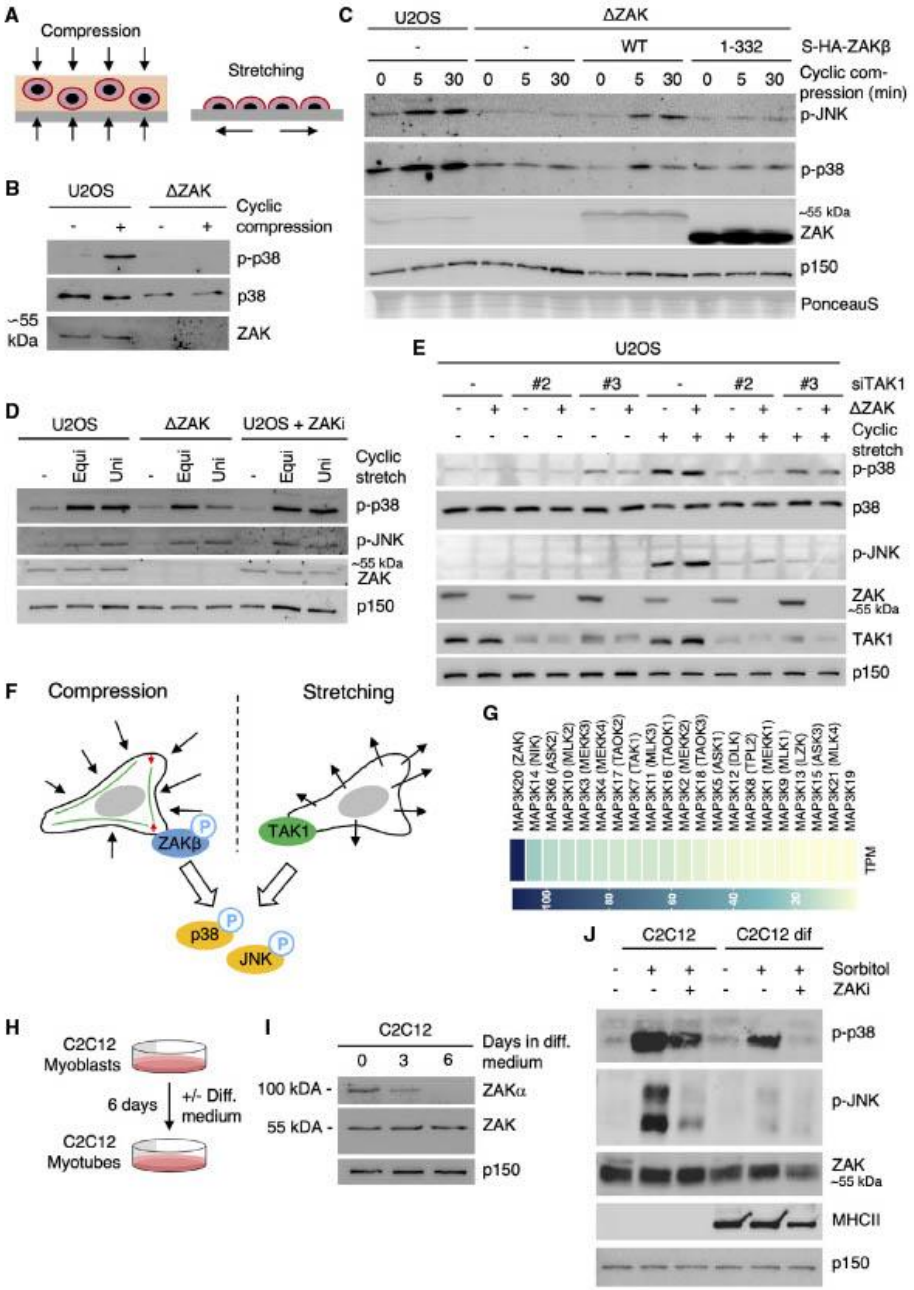

Figure 3.

Stretch-induced signaling has clear physiological counterparts and has been linked to essential processes such as growth regulation and differentiation in the skin, heart physiology, and urinary function in the bladder (Le *et al*, 2016; Aragona *et al*, 2020; Marshall *et al*, 2020; Jiang *et al*, 2021). In contrast, cell compression has been much less studied. In search of a potential *in vivo* role for compression-induced ZAKβ activation, we noticed that skeletal muscle has the highest expression of the ZAK gene among human tissues (data from gtexportal.org). In addition, skeletal muscle only expresses the β (but not α) isoform of ZAK, and this gene codes for the p38- and JNK-directed MAP3K with the highest expression in skeletal muscle (Fig 3G). The asymmetric relationship between the two ZAK isoforms in muscle was underscored by differentiation experiments with the murine myoblast cell line C2C12. These cells express both ZAKα and ZAKβ, however upon differentiation to multinucleated myotubes, expression of the former is lost (Fig 3H and I). Contrary to p38 (Cuenda & Cohen, 1999), inhibition of ZAK kinase activity did not negatively impact this differentiation process as judged by the appearance of myotubes and expression of a muscle-specific myosin isoform (Fig EV3A and B). Also in this cell system, stretching was accompanied by ZAK-independent p38 activation (Fig EV3C). For technical reasons, we were not able to apply agarose embedding and mechanical compression on C2C12 myotubes, but osmotic shock resulted in clear activation of p38 and JNK in a ZAK activity-dependent manner in these cells (Fig 3J). These observations led us to speculate that muscle contraction could represent a physiologically relevant ZAKβ-activating event.

In situ muscle contraction activates p38 and *JNK* via Z-disc localized *ZAKβ*

To determine the importance of ZAKβ function at the level of a mammalian organism, we interrupted the ZAK gene in mice with CRISPR technology. Our guide-RNA was designed to target the second exon of the gene, and we isolated a C57BL/6 line with a frameshift mutation (Fig 4A). In view of conflicting reports about the essentiality of ZAK (Jandhyala *et al*, 2016; Spielmann *et al*, 2016), our approach was highly successful and completely eliminated both ZAKα and ZAKβ expression in all tissues and cells we analyzed. Consistent with above, mouse skeletal muscle only expressed the ZAKβ isoform, while ZAKα was enriched in the liver (Fig 4B). In $ZAK^{+/-}$ breeding experiments, KO mice were born at the expected Mendelian frequency (Fig EV3D) that displayed normal fertility when interbred (Fig EV3E). $ZAK^{-/-}$ mice were also indistinguishable from their WT littermates with respect to weight (Fig EV3F), and a macroscopic examination of all organs did not reveal any obvious pathologies or developmental abnormalities. The phenotype of mouse embryonic fibroblasts (MEF) from $ZAK^{-/-}$ mice closely matched our observations in human cell lines (Figs 1B and EV1B), as they displayed reduced activation of p38 and JNK following osmotic shock (Fig 4C) and were completely refractory to activate the same kinases upon treatment with the ribotoxic stressors anisomycin and cycloheximide (Fig EV3G). To induce muscle contraction in these mice, we exposed one of the lower hindlimbs of anesthetized WT and $ZAK^{-/-}$ mice to a 10 min. *in situ* contraction protocol (Movie EV4) followed by the immediate harvesting of the tibialis anterior (TA) and extensor digitorum longus (EDL) muscles from both legs (Fig 4D). This procedure induced the expected depletion of glycogen and an increase in uptake and clearance of glucose irrespective of genotype (Fig EV3H). Western blotting of muscle lysates revealed that Zak knockout was associated with a severe repression of the normal contraction-induced activation of p38 and JNK without affecting the activation of unassociated kinases such as AMPK and ERK1/2 (Nelson *et al*, 2019; Figs 4E and EV3I–K). We even detected a mild decrease in p38 phosphorylation in the noncontracted muscles of $ZAK^{-/-}$ mice, suggesting that our experimental protocol also mildly stimulated ZAKβ activity in the muscles of the contralateral leg. We also conducted a phospho-proteomic analysis of lysates from noncontracted and *in situ* contracted TA muscles from WT and $ZAK^{-/-}$ mice (Fig 4D; Dataset EV2). Here, we observed a clear separation of the four samples on the level of phosphorylation sites (Fig EV4A), but not at the whole-proteome level

Figure 4. Z-disc localized ZAKβ is activated by muscle contraction.

A Genomic location of guide-RNA sequence (blue) and a derived knockout allele in exon 2 of the murine ZAK gene. PAM—protospacer adjacent motif.

B Skeletal muscle (tibialis anterior, TA) and liver from WT and $ZAK^{-/-}$ mice were lysed and analyzed for ZAK isoform expression by immunoblotting. Ponceau staining of the membrane indicates equal loading.

C Mouse embryonic fibroblasts (MEF) isolated from WT and $ZAK^{-/-}$ mice were treated with 500 mM sorbitol (1 h). Lysates were analyzed by immunoblotting with the indicated antibodies. *—unspecific band.

D Schematic of *in situ* muscle contraction experiments. Mice were anesthetized, and one of the lower hindlimbs was subjected to electrically stimulated contraction (10 min.). Upon euthanization, tibialis anterior (TA) and extensor digitorum longus (EDL) muscles were isolated. Tissue homogenates were processed for immunoblotting (e) or proteins were subjected to trypsin digestion, phospho-peptide enrichment, and label-free quantification by mass spectrometry.

E 16-18-week-old WT and $ZAK^{-/-}$ male mice ($n = 3$ biological replicates) were subjected to the protocol in (D). TA lysates were analyzed by immunoblotting with the indicated antibodies.

F ZAKβ S335 and S339 phosphorylation sites upregulated in WT TA muscles from (D). Values indicate absolute phospho-peptide abundances and error bars represent the standard deviation ($n = 3$ biological replicates).

G TA muscle in an 8-week-old WT male mouse was electroporated with a ZAKβ-tdTomato construct. After 7 days the muscle was harvested, sectioned longitudinally, and immunostained with an antibody against the Z-disc marker α-actinin1. The right panel shows a higher magnification of the region highlighted in yellow.

H C2C12 cells were differentiated into myotubes for 14 days and transfected with the indicated GFP-ZAKβ constructs. Cells were fixed and immunostained with an antibody against α-actinin1.

I Schematic of electroporation rescue experiments. TA muscles were electroporated with GFP-ZAKβ constructs. After 3 days the muscles were exposed to in situ contraction and processed for immunoblotting.

J 16-18-week-old WT and $ZAK^{-/-}$ male mice were subjected to the experimental protocol in (I). TA muscle lysates were analyzed by immunoblotting with the indicated antibodies.

Data information: All scale bars, 20 μm.
Source data are available online for this figure.

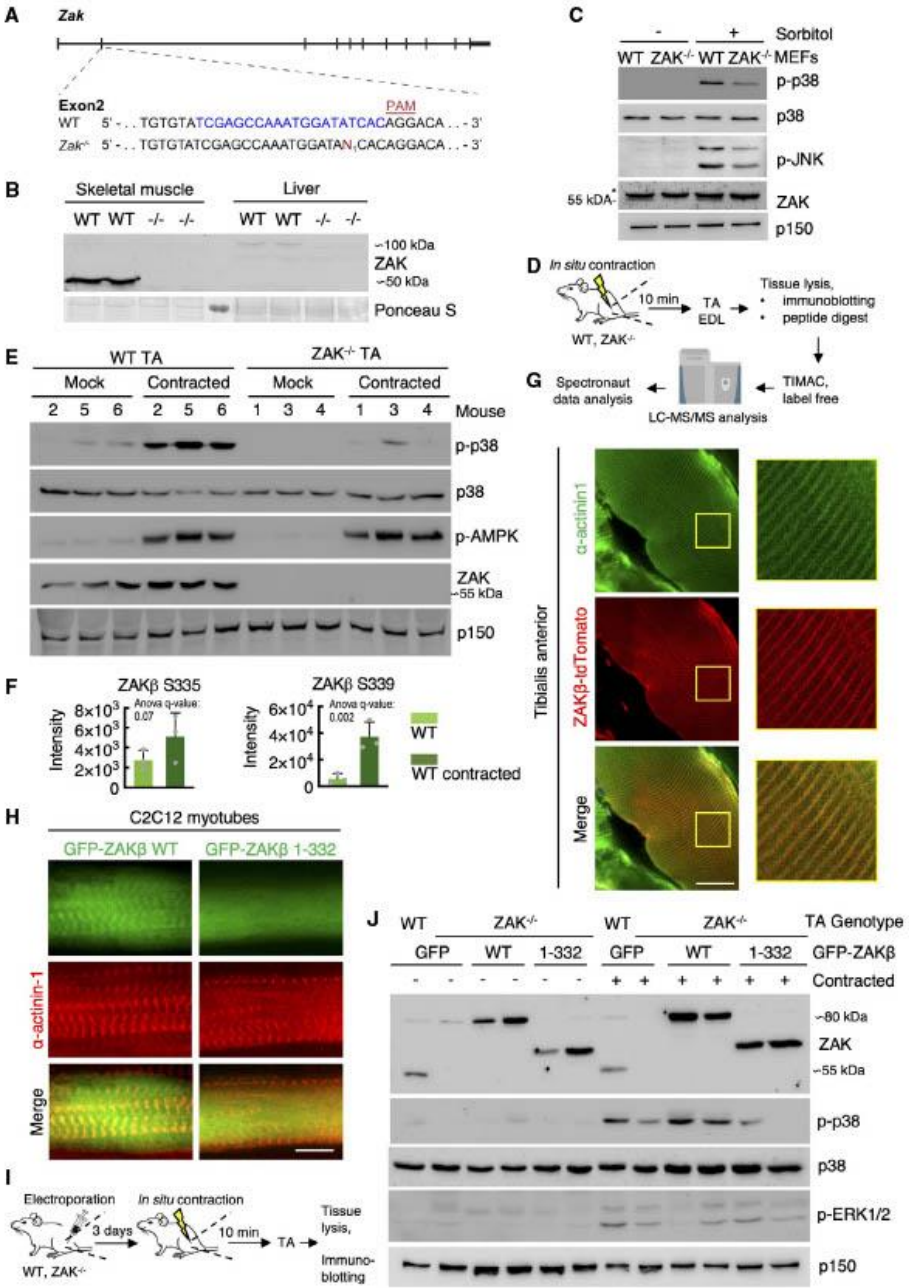

Figure 4.

(Fig EV4B), as judged by a principal component analysis. Among the many contraction-induced phosphorylation events, we detected two sites on ZAKβ (Fig 4F) that likely result from autophosphorylation as also observed *in vitro* and in cell culture (Figs 1F and EV1D and E). One of these, S339, was also previously found to be upregulated in human subjects undergoing high-intensity cycle-ergometer exercise (Hoffman *et al*, 2015). Clustering analysis allowed us to highlight an excess of 3,000 differentially regulated phosphorylation sites, with the cluster representing ZAK-dependent decrease enriched for GO-terms related to muscle function (Fig EV4C). Electroporation of fluorescently tagged ZAKβ into TA muscle revealed a characteristic striated pattern, which we determined to be the Z-disc by co-staining with an antibody against α-actinin1 (Fig 4G). This observation made perfect sense to us, as the muscle Z-disc has some compositional overlap with cellular stress fibers (Luther, 2009), to which ZAKβ is recruited upon osmotic shock (Figs 2D and E, and EV2H and I). The localization was dependent on the ZAKβ SFBD, as our deletion mutant lacking this domain (Fig 2F) largely displayed a diffuse sarcoplasmic localization when electroporated into muscle fibers (Fig EV4D). This difference in localization was even more striking when the constructs were transfected into C2C12 myotubes (Fig 4H). Consequently, while electroporated WT GFP-ZAKβ perfectly rescued p38 activation upon contraction of ZAK$^{-/-}$ TA muscle, its SFBD-deleted counterpart was markedly compromised in this ability (Fig 4I and J). These results led us to conclude that muscle contraction induces an important physiological activation signal for ZAKβ.

ZAKβ is required for skeletal muscle maintenance

The ZAK gene has been found mutated in a small number of patients suffering from congenital myopathy (Vasli *et al*, 2017), and we proceeded by looking for signs of muscle pathology in our mouse model. To this end, we isolated fast-twitch (TA), slow-twitch (soleus), and intermediate (gastrocnemius) muscles from the lower leg of the mice. The weight of these muscles did not indicate any anomalies (Fig EV4E), but morphological analysis of H&E stained sections revealed the presence of centralized nuclei specifically in the muscle fibers of the soleus (Figs 5A and B, and EV4F–H), a clear sign of pathology and active muscle regeneration. This phenotype progressed with age (Fig 5A and B, and EV4F), indicating that it is not developmental but rather linked to muscle use. Muscle fiber typing of the soleus revealed a marked shift from a roughly equal distribution of the slow-twitch type I fibers and fast-twitch type II fibers to a clear overrepresentation of type I fibers in adult mice (Figs 5C and D, and EV5A), indicating an adaptive change towards the more fatigue-resistant slow-twitch muscle fiber profile. These hallmarks are similar to histopathological features to those observed in Zak-deficient human patients (Vasli *et al*, 2017). Finally, we determined that both type I and type II fibers were clearly atrophic in the soleus from ZAK$^{-/-}$ mice (Fig 5E).

To glean more insight into these phenotypic muscle changes, we submitted soleus and TA muscles from WT and ZAK$^{-/-}$ mice to sequencing-based transcriptome analysis (Fig 5F). At the global level, principal component analysis (Fig 5G), correlation analysis (Fig EV5B), and comparison of the number of differentially expressed genes (DEG) (Fig EV5C) clearly indicated a large separation of pathological soleus (but not nonpathological TA) dependent on genotype. Additionally, the few DEGs in the unaffected TA were largely identified among the many likely pathology-associated DEGs found in soleus (Figs 5H and EV5D and E; Dataset EV3). These data suggest that tonically active slow-twitch muscles are more susceptible to ZAKβ deficiency than fast muscles, likely because they are permanently stimulated to generate tension to support body weight against gravity. Despite the clear soleus pathology, but perhaps because other fast-twitch muscles appear largely unaffected, ZAK$^{-/-}$ mice behaved similarly to their WT counterparts in an open field assay, both with respect to the distance covered, speed of movement, and time spent exploring the surroundings (Fig EV5F and G).

Discussion

We describe here the function of the MAP3K ZAKβ as an upstream activator of p38 and JNK upon cellular compression (Fig 5I). This function is mediated by a C-terminal domain that recognizes mechanically perturbed stress fibers. ZAKβ is the shorter of the two isoforms encoded by the human Zak gene. The longer isoform, ZAKα, mediates MAP kinase activation in the presence of a very different signal, ribotoxic stress, through ribosome-binding sensor domains in its C-terminus (Vind *et al*, 2020b). Zak is thus a rather unique case of a single gene coding for two kinases that are

Figure 5. ZAKβ guards against skeletal muscle pathology in mice.

A H&E staining of soleus muscle cross-sections from 8- and 22-week-old WT and ZAK$^{-/-}$ male mice. Arrows indicate the presence of centralized nuclei. Scale bars, 50 μm.

B Quantification of (A). Values indicate the percentage of fibers displaying centralized nuclei and error bars represent the standard deviation ($n = 3$ biological replicates). **$P < 0.01$ and ***$P < 0.001$ in *t*-test with the Bonferroni–Dunn correction for multiple comparison.

C Muscles from (A) were immunostained for type I (red) and type IIa (green) fibers using myosin isoform-specific antibodies. Scale bars, 500 μm.

D Quantification of (C). Values indicate the percentage of fibers positive for type I myosin and error bars represent the standard deviation ($n = 3$ biological replicates). **$P < 0.01$ and ns, not significant in *t*-test with the Bonferroni–Dunn correction for multiple comparison.

E Cross-sectional area of type I and type IIa fibers in soleus from 8-week-old WT and ZAK$^{-/-}$ male mice. Values indicate the mean from one specimen and error bars represent the standard deviation ($n = 3$ biological replicates). *$P < 0.05$ in 2-way ANOVA corrected for multiple comparison using FDR (Benjamini, Krieger, and Yekutieli).

F Schematic of muscle transcriptomic analysis. Soleus and TA muscles were isolated from 16-18-week-old WT and ZAK$^{-/-}$ female mice ($n = 4$ biological replicates). Purified RNA was subjected to polyA capture and deep sequencing.

G Principal component analysis of the data obtained from (F).

H Venn diagram from (F) of the overlap of differentially expressed genes (DEG) in soleus (Sol, blue) and TA (brown).

I Mechanical perturbation of cells by osmotic shock, compression, and muscle contraction activates ZAKβ and downstream kinases p38 and JNK. These reactions are dependent on sensing of stress fiber/Z-disc deformation by the ZAKβ SFBD domain.

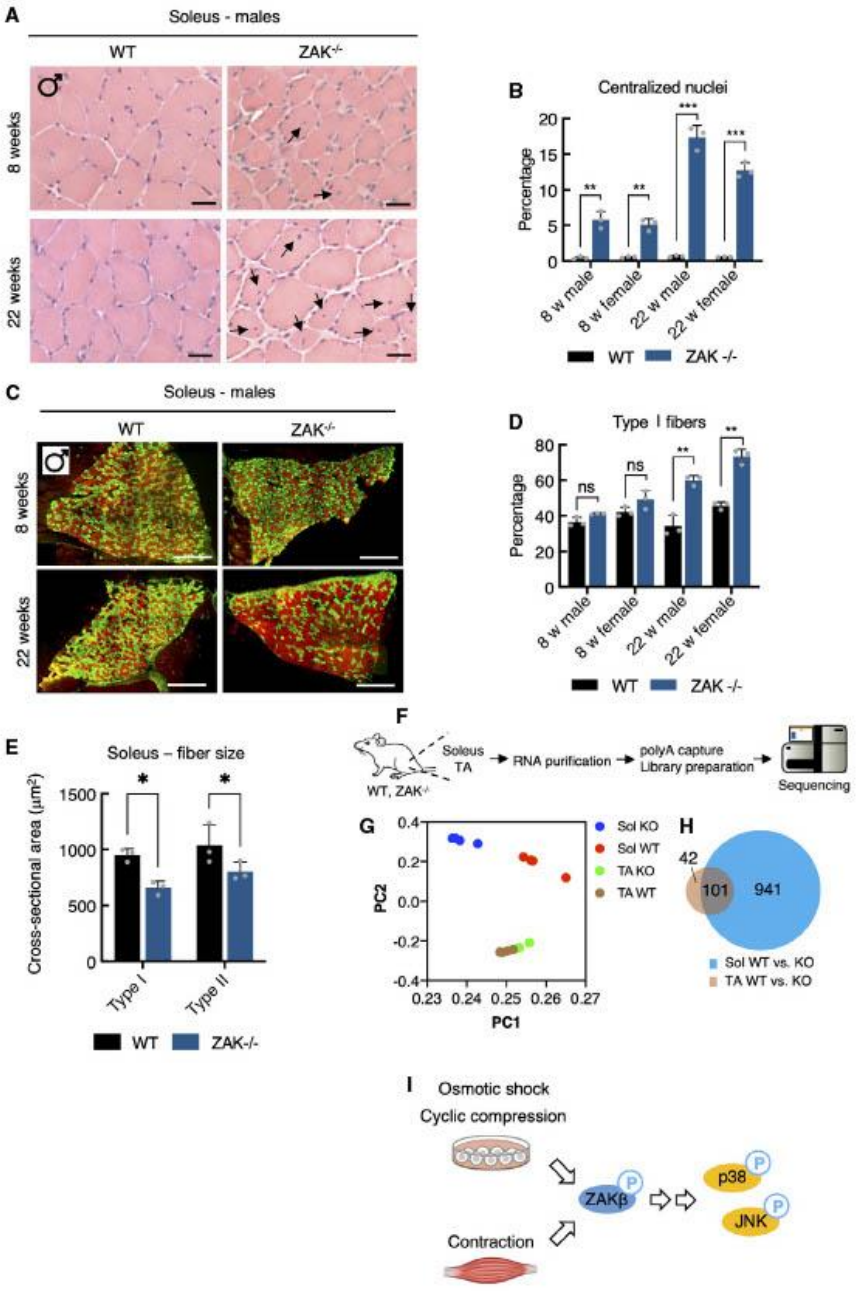

Figure 5.

activated by clearly different signals. Curiously, while only the α isoform is encoded in the *C. elegans* genome, some higher organisms like zebrafish code for clear ZAKα and β homologs in two independent genes.

ZAKβ is ubiquitously expressed among cultured cell lines, where it mounts stress responses upon acute cell compression. It is also found in most tissues of the body, suggesting that this mechanism is generally important for cell function. Skeletal muscle is a tissue where the role of this kinase is especially clear, and ZAKβ is strongly activated upon muscle fiber contraction. Besides the general implications for cell physiology, our discovery of ZAKβ function addresses important outstanding questions regarding how muscles sense and respond to the extent of mechanical load they are exposed to. In the absence of a detailed biophysical examination of the process, and without knowing the exact identity of its direct binding partner on stress fibers, we cannot unequivocally state that ZAKβ acts as a molecular sensor in this process. Instead, we speculate that ZAKβ could be detecting a mechanically induced conformational change in a protein component in stress fibers that would expose a binding platform. Future work is needed to unravel the key upstream event linking cellular compression and ZAKβ recruitment to stress fibers.

ZAKβ is a rare case of a protein that is specifically activated upon compression of cells but does not appear to respond to stretching, for which the inventory of known sensors is much larger (Martino *et al*, 2018). Muscle contraction is traditionally associated with stretching of Z-lines and build-up of tension, and our discovery of ZAKβ as a compression-sensitive kinase that is activated in this process could appear controversial. A review on mechano-transduction in cardiomyocytes describes how mechanosensors that are oriented perpendicular to the direction of stress fibers would only be affected by the compressive force and not stretching (Chen-Izu & Izu, 2017). It is also becoming evident that the degree of deformation is critical for the cellular response (Liu *et al*, 2020). This is likely to be relevant for various extrinsic forces with importance for muscle physiology (Randhawa & Wakeling, 2018; Wakeling *et al*, 2020). Upon contraction, muscle fibers deform with constant volume. Thus, when subjected to tension in one direction, the muscle develops internal stresses that cause constriction in the perpendicular plane (Burkholder, 2007). Thus, both compressive and tensile strains are likely to be relevant in muscle physiology.

Skeletal muscle is a remarkably plastic organ that is remodeled upon exercise stimuli. Endurance exercise generally increases the oxidative capacity of the muscle (Powers, 2017), while resistance exercise primarily stimulates the growth of fast-twitch type II muscle fibers (hypertrophy) (Bamman *et al*, 2018). Contraction-induced MAP kinase signaling has recently been linked to the establishment of this dichotomy (Lessard *et al*, 2018). Specifically, contraction-activated JNK was reported to phosphorylate the SMAD2 transcription factor to alleviate suppression of muscle growth by the myokine myostatin. Consequently, mice with conditional knockout of JNK1 and JNK2 in skeletal muscle are defective for resistance to exercise-induced hypertrophy (Lessard *et al*, 2018). In our experiments, ZAKβ was required for contraction-induced JNK activation (Fig EV3I). The p38 pathway, the other prominent downstream target of ZAKβ (Figs 4E and EV3I), plays equally important roles for exercise adaptation in muscles. A key role is in the control of production and release of myokines with both systemic and local effects (Pedersen & Febbraio, 2008; Lee & Jun, 2019).

In sum, our work establishes the MAP3K ZAKβ as a kinase activated upon cellular compression, with a particularly pronounced function in skeletal muscle, where it mediates contraction-induced activation of p38 and JNK. Besides the general implications for cell biology, our work addresses important outstanding questions regarding how muscles sense and respond to the extent of mechanical load they are exposed to.

Materials and Methods

Cell culture and reagents

Human U2OS osteosarcoma (ATCC, HTB-96), human Hela malignant cervical epithelial cells (ATCC, CCL-2), human HEK293 embryonic kidney cells (ATCC, CRL-1573) and murine C2C12 myoblast (ATCC, CRL-1772) were cultured in Dulbecco's modified eagle's medium (DMEM, Biowest) supplemented with 10% fetal bovine serum (FBS, Biowest), L-Glutamine, penicillin, and streptomycin (P/S). Human HAP1 haploid cells (EMBL-EBI, RRID: CVCL_5G07) were cultured in Iscove Modified Dulbecco Medium (IMDM, Gibco) supplemented with 10% FBS and P/S. All cell lines were regularly tested for mycoplasma infection. Cells were maintained at 37°C in a humidified 5% CO_2 cell incubator. Stable cell lines were created by transfecting cells with a plasmid carrying the gene of interest and subsequently cultured for weeks with appropriate antibiotic selection (Zeocin (0.2 μg/ml, Thermo Fisher), Blasticidin S (5 μg/ml, Thermo Fisher), G418 (0.4 mg/ml, Gibco/Invitrogen)). To generate inducible cell lines, pcDNA4/TO-constructs were co-transfected with the pcDN6/TR construct (Life Technology) in a 1:4 ratio. Individual clones were picked and screened by immunofluorescence and western blot. U2OS ΔZAK cells were previously published (Vind *et al*, 2020b). C2C12 was differentiated from myoblasts to myotubes by replacing DMEM with 10% FBS for DMEM with 2% horse serum (Biowest). Medium was replaced every second day, and cells were left to differentiate for 3, 6, or 14 days. Chemicals and inhibitors used in this paper included doxycycline (1 μg/ml), sorbitol (500 mM, unless stated otherwise), NaCl (500 mM), anisomycin (1 μM), cycloheximide (10 μM), Interleukin 1 beta (IL1β, 2 ng/ml, Preprotech), Arsenite (0.5 mM). ZAK inhibitor (Chang *et al*, 2017) (10 μM) was a kind gift from Xiaoyun Lu (Jinan University, China). To induce DSBs, cells were exposed to 4 Gy of X-rays (ionizing radiation—IR) using a Y.SMART tube (YXLON A/S) at 6 mA and 160 kV through a 3-mm aluminum filter. UV-C light (40 J/m^2) was delivered in a BS-02 irradiation chamber equipped with 254 nm bulbs (Gröbel Elektronik, Germany).

FACS-based haploid genetic screen

The haploid genetic screen was carried out as described before in detail (Brockmann *et al*, 2017). In short, a clonal HAP1 cell line generated for other unrelated purposes (carrying a doxycycline-inducible TET1-transgene; cells were used in a noninduced state) was mutagenized and 30 billion cells were then treated with 500 mM Sorbitol for 1 h. Cells were harvested by trypsinization, washed with ice-cold PBS followed by fixation with BD Fix buffer I (BD Phosflow™) for 10 min at 37°C and permeabilization with Permeabilization buffer III (BD Phosflow™) for 30 min on ice. Cells

were then resuspended in PBS supplemented with 10% FBS, hereafter referred to as FACS buffer. Cells were stained using anti-phospho Thr180/Tyr182 p38 (1:400, Cell Signaling, D3F9, #4511) for 2 h at room temperature (RT). After washing with FACS buffer, secondary antibody anti-rabbit-AlexaFluor-488 (Invitrogen #A-11008) and DAPI (Invitrogen #D1306) was added for 1 h at RT. Cells were then washed and resuspended in FACS buffer. Sorting was performed on a FACSAria™ Fusion cell sorter (BD Biosciences) until 12e6 cells for both the 5% highest- and lowest phospho-p38 signal were retrieved. Only G1-cells were gated to prevent contamination with diploid HAP1 cells. Sorted cells were collected and isolation of genomic DNA, library preparation, next-generation sequencing, and analysis were performed as described (Brockmann *et al*, 2017). Briefly, sequence reads were aligned to hg19 tolerating a single mismatch and assigned to nonoverlapping protein-coding gene regions (Refseq). The number of in-sense gene-trap integrations in each gene was compared between the high and low phospho-p38 population by means of a two-sided Fisher's exact test false discovery rate-corrected, $P \leq 0.05$.

Plasmids and siRNAs

Full length and truncated ZAKα and ZAKβ were PCR-cloned into the pcDNA4/TO/Strep-HA and pcDNA4/TO/GFP vectors using NotI restriction sites or into peGFP-N1 using XhoI and BamHI restrictions sites. To generate the pDEST47_ZAKβ_tdTomato plasmid, tdTomato from pRSET-B_tdTomato (a kind gift of Dr. Paul Pryor) was cloned into pcDNA-DEST47 using NheI and BstBI, and restriction sites. This destination vector was then used to generate the final plasmid using the Gateway cloning protocol following the manufacturer's instructions (Life Technologies). Constructs carrying internal deletions and point mutations were made by site-directed mutagenesis using Phusion DNA polymerase (New England Biolabs) as described in the manufacturer's protocol. mCherry-Alpha-actinin-1 (#54975) and mCherry-FAK (#55044) were obtained from Addgene. All constructs were verified by sequencing. Plasmid transfection and siRNA transfection were performed using FUGENE6 (Promega) and RNAiMAX (Life Technologies), respectively, as described in the manufacturer's instruction. Plasmid transfection of C2C12 myotubes was carried out using the TransIT-X2 Dynamic delivery system (Mirus, MIR6004) as described in manufacturer's instruction. siRNA sequences used in this study were: ZAKα: GTGCCCAUUAAGTAUCAA (dTdT), ZAKβ: AUGCAAGCCAAGCAGAAU (dTdT), ZAKα+β: GCUUAAAGAACGAGAAAGA (dTdT), siMEKK2 #1: CACUAGAAGAUUUGGAUAA (dTdT), siTAK1 #2: AAGAUGGUAUAUACCAAGUUA (dTdT) and siTAK1 #3: UGGCUUAUCUUACACUGGA (dTdT).

Western blot and pull-down

Cells were lysed using EBC buffer (50 mM Tris, pH 7.5, 150 mM NaCl, 1 mM EDTA, 0.5% NP-40, protease and phosphatase inhibitors). For phosphatase treatment, cells were lysed in either the lysis buffer mentioned above or in EBC buffer w/o EDTA supplemented with 1 mM $MnCl_2$ and then incubated with NEBuffer for Protein Metallophosphatases and Lambda Protein Phosphatase (NEB, P0753L) at 30°C for 30 min at 800 rpm. Strep pull-downs were carried out with Strep-Tactin sepharose for 1 h at 4°C (IBA Life Sciences). Samples were mixed with Laemmli sample buffer and boiled before they were resolved by SDS–PAGE and transferred to nitrocellulose gels. Membranes were blocked in PBS-T + 5% milk, after which they were incubated with antibodies overnight. Antibodies used for western blot in this study: phospho-p38 (T180/Y182, Cell Signaling, 9216, mouse and 4511S, rabbit), p38 (T180/Y182, Cell Signaling, 9212, rabbit), phospho-JNK (T183/Y185, Cell Signaling, 9255, mouse), ZAK (BioSite. 14945-1-AP, rabbit), MEKK2 (Abcam, ab33918, rabbit), ERK5 (Cell Signaling, 3372, rabbit), phospho-AMPK (T172, Cell Signaling, 2535, rabbit), phospho-ERK1/2 (T202/Y204, Cell Signaling, 9106, mouse), phospho-p70 S6K (T389, Cell Signaling, rabbit), Myosin Heavy Chain (MHCII, Novus Biologicals, MAB4470, mouse), p150 (BD biosciences, 610473, mouse), actin (Merck, MAB1501, mouse), α-tubulin (Sigma, T9026, mouse), HA (Santa Cruz, sc-7392, mouse), GFP (Torrey Pines, TP401, rabbit) and phospho-Tyrosine (Millipore, 05–0511, mouse). The membranes were subsequently washed in PBS-T and incubated for 1 h with Goat Anti-Rabbit or Goat Anti-Mouse IgG Antibody (H + L) Peroxidase (Vector laboratories). PBS-T washing was repeated, and the antibody signal was visualized by chemiluminescence (Clarity Western ECL substrate, Bio-Rad) using the Bio-Rad Chemidoc imaging system. Quantification of western blots was carried out using ImageJ gel plot lane function.

Immunofluorescence and microscopy

For immunofluorescence, cells were grown on coverslips and treated as indicated before they were fixed for 15 min in paraformaldehyde (Lillys væske, Ampliqon) and permeabilized with 0.2% TritonX-100 for 5 min. For pre-extraction, cells were incubated for 1 min in 0.2% TritonX-100 prior to fixation. Primary antibody incubation was carried out at RT for 1 h using the following antibodies diluted in DMEM: HA (Santa Cruz, sc-7392, mouse), 53BP1 (Santa Cruz, sc-22760, rabbit), Lamin A/C (Cell Signaling, 4777, mouse), and γH2AX (Millipore, JBW301, mouse). Coverslips were washed with PBS and incubated with secondary antibody diluted in DMEM for 30 min at RT. The following secondary antibodies were used: Alexa Fluor 488 goat anti-mouse (A11001), Alexa Fluor 568 goat anti-mouse (A11004), and Alexa Fluor 568 goat anti-rabbit (A11011). Finally, coverslips were washed with PBS and rinsed in water before mounted in a mounting medium containing DAPI (Vectashield, H-1200). Images were acquired through a 63X oil immersion objective on a LAS X widefield microscope (Leica). For live confocal images, cells were grown in 4-chamber Lab-tek glass-bottom dishes (Nunc) and acquired through a 40X water immersion objective on an LSM 880 microscope (Carl Zeiss). For SiRActin live imaging, SiRActin (50 nM, Spirochrome) was added 15 min prior to acquisition. For immunofluorescence of frozen muscle samples, the snap-frozen muscle tissue was first sectioned using a cryostat machine, and slides were stored at −80°C. Slides were removed from −80°C and left to thaw at RT until condensation had evaporated. Blocking was performed in 4% Bovine Serum Albumin (BSA) in 1x PBS. Sections were incubated with the following primary antibodies ON at 4°C; 1:150 anti-α-actinin (EA-53, SIGMA), 1:100 anti-MyHC1 (A4.840, DSHB), and 1:100 anti-MyHC2a (SC-71, DSHB) in blocking solution. Sections were subject to 3x 5 min washes in 1x PBS and incubated with the following secondary antibodies at RT for 1 h; 1:200 goat anti-mouse IgG-AlexaFluor 488 or 594 (R37120 or A32742, Invitrogen), 1:150 goat anti-mouse IgG-

FITC (F9006, Sigma) and 1:150 goat anti-mouse IgM-TRITC (SAB3701196, Sigma). Sections were again subject to 3x 5 min washes in 1x PBS. Slides were mounted with Mowiol mounting medium with DAPI. A coverslip was added and compressed avoiding the formation of air bubbles.

In vitro kinase assay

Cell lysates were incubated with Strep-Tactin Sepharose beads (IBA Lifesciences) overnight at 4°C. Following this, pull-downs were washed twice in EBC buffer, twice in EBC buffer w/o EDTA, and finally, twice in kinase buffer (40 mM Tris–HCl pH 7.5, 40 mM $MgCl_2$, 0.1 mg/ml BSA, 50 μM DTT, 12.5 mM beta-glycerophosphate). Beads were incubated for 45 min at 37°C in 20 μl kinase buffer supplemented with 0.0625 μCi ^{32}P-ATP (Perkin Elmer) and boiled in Laemmli sample buffer. Samples were resolved by SDS–PAGE and transferred to nitrocellulose membranes. Incorporation of ^{32}P was detected by SDS–PAGE and subsequent exposure to X-ray films (Amersham).

Hematoxylin and eosin staining (H&E)

Snap-frozen muscle tissue was first sectioned using a cryostat machine and slides were stored at −80°C. Slides were removed from −80°C and left to thaw at RT until condensation had evaporated. Slides were fixed in acetone for 10 s and then incubated in Gill's Hematoxylin for 2 min. Slides were then washed in tap water for 1 min. Sections were incubated in Scott's water for 1 min and subsequently washed again in tap water for 1 min. Afterward, the sections were incubated in eosin for 45 s and then washed in tap water for 1 min. Sections were washed first in 70% ethanol for 1 min, then in 100% ethanol for 1 min, and finally in HistoClear (National Diagnostics) for an additional 1 min. Slides were mounted with Histomount medium and a coverslip and compressed to prevent the formation of air bubbles.

Image analysis

Cells and muscle fibers

For intensity distribution, a line was drawn across the region of interest and the intensity of the different channels was measured along this line using a plot profile (ImageJ). The percent of maximum intensity was calculated for each channel and plotted against the respective position on the line.

Muscle fibers

For fiber typing of soleus muscle sections, relative numbers of type I and type IIa fibers were determined manually by counting the total of fibers expressing each myosin isoform. The fiber cross-sectional area was calculated as an average of three individual muscles. To avoid regional fiber size variation in the TA muscle to confound comparisons, a scale factor (average area of electroporated: average area nonelectroporated) was obtained from at least three electroporated regions within the muscle, which were then averaged to produce a single data point per muscle. For morphological analyses of H&E stained sections, 10x magnification images were captured using the Leica brightfield microscope (DM2500), camera and imaging software (SPOT Insight FireWire; Diagnostic instruments). Centralized nuclei were counted manually. The number of fibers displaying centralized nuclei was expressed as a percentage of the total number of myofibers to create one single data point per muscle. An average of the percentage of fibers with centralized nuclei was calculated across three mice per genotype. Data were compared using a one-way ANOVA test followed by a Tukey's HSD *post hoc* test. *P* values less than 0.05 were deemed significant.

RNA sequencing

Muscles were snap-frozen in liquid nitrogen and homogenized twice for 2 min at 30 Hz using Tissuelyser II (Qiagen). Total RNA was isolated using the TRIzol reagent as above. Total RNA was sent to BGI Europe for RNA sequencing. Here, a polyA-selected mRNA library was prepared from the total RNA and subjected to PE100 sequencing with 20 M pair reads using the DNBSEQ platform. Low-quality reads were filtered with SOAPnuke 1.5.2 and the remaining reads were mapped to version GCF_000001635.26_GRCm38.p6 of the *Mus musculus* genome. After alignment using Bowtie2 2.2.5, the expression level of each gene was calculated by RSEM 1.2.12, and differential expression analysis was performed using DESeq2 1.4.5 with the parameters fold change ≥2 and adjusted *P* value ≤ 0.001. The sequencing data analysis, including principal component analysis (PCA) and Venn diagram creation, was performed using BGI Dr. Tom 2.0.

Mechanical manipulation of cells

Cyclic stretch

Cyclic mechanical stretching of cells was performed with the Flexcell FX-5000 Tension System (Flexcell International Corporation, Burlington, NC). This system takes advantage of vacuum-based stretching of elastic membranes over an equibiaxial loading post. To impose a uniaxial strain state on the cells we used a custom-made rectangular loading post. Cells were grown on flexible-bottomed collagen I-coated culture plates and subjected to cyclic stretch at a frequency of 1 Hz. The imposed strain was 15%.

Cyclic compression

U2OS and U2OS ΔZAK cells were trypsinized and embedded in 2% agarose gels at a density of 2×10^6 cells/ml as described (Bougault *et al*, 2009). The constructs were subjected to compression using a previously characterized model system (Bougault *et al*, 2012). Cyclic compression of 60 kPa in a sine waveform at a frequency of 0.5 Hz was applied. Control constructs were uncompressed. For protein extraction, agarose constructs were frozen in liquid nitrogen, freeze-dried, resuspended in 200 μl Laemmli sample buffer, and boiled immediately for 5 min. To eliminate most of the agarose, the samples were then allowed to gel at room temperature. The gels were cut into pieces and transferred to Handee Mini-Spin Column (Pierce). These empty columns have a paper filter resistant to clogging from cellular debris. Samples were centrifuged at 12,000 *g* for 20 min at room temperature. The paper filter with the agarose gel was discarded and the proteins solubilized in the extraction buffer were frozen at −20°C.

Generation, genotyping, and husbandry of ZAK knockout mice

Husbandry

In Denmark, mice were housed at the animal facility of the Department of Experimental Medicine at the University of Copenhagen, and the research was monitored by the Institutional Animal Care and Use Committee. All of the mouse work was performed in compliance with Danish and European regulations. In the United Kingdom, all animal regulated procedures were carried out according to Project License constraints (PEF3478B3) and Home Office guidelines and regulations. In Denmark, animal experiments were approved by the Danish Experimental Animal Inspectorate. Mice were kept on a 12 light/12 dark cycle in ventilated cages at room temperature and fed regular rodent chow.

Generation of ZAK knockout mice

Generation of Cas9 mRNA and sgRNA was performed as previously described (Yang *et al*, 2014). *In vitro* transcription of Cas9 mRNA was done using the mMESSAGE Machine T7 Kit and MEGAclear kit following the manufacturer's instruction. sgRNA was transcribed using the MEGAshortscript T7 kit, as per the kit protocol. C57BL/6 X CBA(F1) female mice were used as embryo donors and foster mothers. Superovulated female mice (7–8 weeks old) were mated to males, and fertilized embryos were collected from oviducts. Cas9 mRNAs (10 ng from a 100 ng/µl stock) were injected into zygotes, and sgRNA (25 ng from 50 ng/µl stock) was injected into the cytoplasm of fertilized eggs with well-recognized pronuclei in M2 medium. Genotyping was performed by targeted gene sequencing in the Illumina Miseq System according to the manufacturer's instructions (Fw: 5′-tcgtcggcagcgtcagatgtg tataagagacagtttctgaactcatcgggcct-3′; Rw: 5′-gtctcgtgggctcggagatgtgtat aagagacagttgggaaggagcctcatgga-3′). FastQ reads were mapped to the *Mus musculus* genome version 9 (mm9). Several alleles were successfully germline transmitted. Animals harboring Mutation 2 (M2) were maintained as *Zak-null* mouse strains.

Genotyping

For routine genotyping, a 700 bp PCR product was amplified from genomic DNA extracted from ear clippings (Fw: 5′-gcaaggggtgaaaatagggag-3′; Rw: 5′-gtgagtgctttcatttcgacttg-3′). The PCR products were digested with EcoRV, with the M2 mutation disrupting a single EcoRV restriction site in the WT product (WT bands, 430 and 270 bp; M2 band, 700 bp).

Muscle glucose uptake during *in situ* contraction

Fed mice were anesthetized by an intraperitoneal injection of pentobarbital and left to recover on a heating plate (30°C) for ~ 20 min. Subsequently, an electrode was placed on a single common peroneal nerve followed by 10 min *in situ* contraction of EDL and TA muscle. The contralateral leg served as a sham-operated resting control. The *in situ* contraction protocol consisted of 0.5-s trains repeated every 1.5 s (frequency: 100 Hz; duration; 0.1 ms; voltage; 5 V). To determine muscle glucose uptake during contraction, mice were subjected to a retroorbital injection of [3H]-2-deoxyglucose (12.3 Mbq/kg body weight) dissolved in a 0.9% saline solution immediately prior to *in situ* contraction and tail blood was collected at the time point 0, 5, and 10 min. [3H]-2-deoxyglucose uptake was determined by analyzing the accumulation of [3H]-2-deoxyglucose-6-phosphate in muscle and [3H]-2-deoxyglucose-specific activity in plasma. Muscle glucose clearance was calculated by dividing the muscle glucose uptake rate by the average blood glucose concentration during *in situ* contraction.

Muscle glycogen content

Glycogen content in muscle was assessed by a fluorometric method and measured as glycosyl units after acid hydrolysis of whole muscle protein homogenate.

In vivo electroporation of muscle

Plasmid DNA was diluted in a sterile 0.9% saline solution to a final concentration of 2 µg/µl. Two hours after hyaluronidase treatment of TA muscle (one injection of 30 units, 1 unit/µl), 50 µg of DNA was injected and electroporation was performed (ECM 830—Square Wave Electroporation System; voltage: 75 V; pulse length: 10 ms; Interval: 1 s; pulses: 15). Three and six days after electroporation TA muscles were dissected, placed in cryo-embedding medium (Tissue-Tek, O.C.T. Compound) and immersed in precooled isopentane for ~30 s before frozen in liquid nitrogen for later analyses.

Muscle processing

Muscles were lysed in ice-cold buffer (10% glycerol, 20 mM sodium pyrophosphate, 1% NP-40, 2 mM phenylmethylsulfonyl fluoride, 150 mM sodium chloride, 50 mM HEPES, 20 mM b-glycerophosphate, 10 mM sodium fluoride, 1 mM EDTA, 1 mM EGTA, 10 mg/ml aprotinin, 10 mg/ml leupeptin, 3 mM benzamidine, and 2 mM sodium orthovanadate, pH 7.5) using steel beads and a TissueLyzer II (QIAGEN, Hilden, Germany). Homogenates were rotated end over end for 1 h before centrifuged at 16,000 *g* for 20 min. The supernatant (lysate) was collected, frozen in liquid nitrogen, and stored at −80°C for later western blot analyses.

Mouse open field test

General locomotor activity was evaluated using an open field test. In brief, following 7 days of acclimatization to the procedure room, mice were placed in a 50x50x50cm white arena and moving patterns were recorded using ceiling-mounted Logitech C920 Pro cameras. Tracing of mouse movement during a 10-min test period was quantified using Noldus EthoVision XT software. For analysis, a 4x4 grid was applied to the arena and the four middle sections were defined as the center zone.

Proteomics

Sample preparation for MS analysis

Snap-frozen and ground muscle samples were transferred to a Precellys tube, with three beads (2.8 mm) and 750 µl of boiling lysis buffer containing 5% SDS, 100 mM Tris–HCl pH 8.5, 1 mM NaF, 1 mM beta-glycerol-phosphate, 1 mM Sodium Orthovanadate and cOmplete, Mini, EDTA-free Protease Inhibitor Cocktail (Sigma Aldrich). Samples were homogenized using 12,000 *g* for 20 s. After clarification, samples were reduced and alkylate in 5 mM TCEP and 10 mM CAA for 10 min at 95°C. Samples were further homogenized by sonication with a probe for 2 min (1 s ON, 1 s OFF, 70%

amplitude). Samples were centrifuged at 16,000 *g* for 5 min and supernatants were collected. Protein concentration was measured by BCA. Afterwards, samples were digested overnight using the PAC protocol (Batth *et al*, 2019) implemented for the KingFisher robot as described previously (Bekker-Jensen *et al*, 2020b). Samples were acidified after digestion to a final concentration of 1% trifluoroacetic acid (TFA), and peptides were loaded onto Sep-Pak cartridges (C18 1 cc Vac Cartridge, 50 mg—Waters). Eluted peptides from the Sep-Pak were concentrated in a Speed-Vac, and 200 µg of peptides (measured by A280 Nanodrop) were used for phosphor-enrichment. Phospho-enrichment was performed as described previously (Bekker-Jensen *et al*, 2020a) using 20 µl of TiIMAC-HP beads (MagResyn). Eluted phosphopeptides were acidified with 10% TFA to pH <3 and loaded into Evotips for further MS analysis.

LC–MS/MS analysis

Samples were analyzed on the Evosep One system using an in-house packed 15 cm, 150 µm i.d. capillary column with 1.9 µm Reprosil-Pur C18 beads (Dr. Maisch, Ammerbuch, Germany) using the preprogrammed gradients for 60 samples per day (SPD) for phospho-proteome samples and 30SPD for total proteome. The column temperature was maintained at 60°C using an integrated column oven (PRSO-V1, Sonation, Biberach, Germany) and interfaced online with the Orbitrap Exploris 480 MS. Spray voltage was set to 2.0 kV, funnel RF level at 40, and heated capillary temperature at 275°C. Full MS resolutions were set to 120,000 at m/z 200, and full MS AGC target was 30% with an IT of 45 ms. Mass range was set to 350–1,400. Full MS scan was followed by a DIA scan comprised of 49 windows of 13.7 Da with an overlap of 1 Da, scanning from 472 to 1,143 Da for phospho-proteome and 361 to 1,033 Da for total proteome. Resolution was set to 15,000 and IT to 22 ms. Normalized collision energy was set at 27%. AGC target value for fragment spectra was set at 1000%. All data were acquired in profile mode using positive polarity and peptide match was set to off, and isotope exclusion was on.

Raw data processing

Raw files were searched in Spectronaut (v14) using a library-free approach (directDIA). Carbamylation of cysteines was set as a fixed modification, whereas oxidation of methionines, acetylation of protein N-termini, and in phosphor-proteomics samples phosphorylation of serine, threonine, and tyrosine were set as possible variable modifications. Mus musculus FASTA database (UniprotKB/Swiss-prot 22888 entries) and a common contaminants database were used. For phospho-proteomics samples, PTM localization cutoff was set as 0.75. Cross-run normalization was on. Phospho-peptide quantification data were exported and collapsed to site information using the Perseus plugin described in Bekker-Jensen *et al* (Bekker-Jensen *et al*, 2020b).

Data analysis

Phospho-site and proteome datasets were processed using R (v3.6.2). Data were log2 transformed and two valid values in at least one experimental group were required to preserve the phospho-site for further analysis. Imputation of missing values was performed using the data analysis pipeline of Prostar (v 1.18.4) (Wieczorek *et al*, 2017). First, partially observed values (*i.e.*, values missing within a condition in which there are valid quantitative values) were imputed using the function KNN (10 neighbors) and labeled with blue in Table S2; second. Values missing in an entire condition were imputed using the detQuant function (quantile = 1, factor = 1) and labeled with orange in Table S2. Next, data were exported into Perseus (v1.6.5.0) (Tyanova *et al*, 2016) for differential expression analysis using ANOVA (5% FDR) followed by a *post hoc* test to evaluate significant pairs. Gene Ontology enrichment annotation was performed in Perseus (v1.6.5.0), using GO BP, MF, and CC names and slim names. Significance of the enrichment was calculated using the Fisher's exact test (two-sided) with the Benjamini–Hochberg FDR correction.

Principal component analysis was performed in Perseus (v1.6.5.0) using as input the data obtained after imputation.

Western blot quantification and statistical analysis

Band intensity of western blots was quantified using ImageJ. Fold changes to the control sample were calculated, and data were compared using the statistical test described in the figure legends.

Statistical analysis

Sample sizes were decided in order to use a minimum number of mice. Animals and samples were not randomized, and the researcher was not blinded. Inclusion criteria were based on weight and the healthy appearance of mice. Data in bar and line graphs are presented as mean ± standard deviation. Statistical analyses were performed in GraphPad Prism 9 applying statistical tests as described in figure legends. ns., nonsignificant; $*P < 0.05$; $**P < 0.01$; $***P > 0.001$, $****P < 0.0001$.

Data availability

The mass spectrometry proteomics data have been deposited to the ProteomeXchange Consortium via the PRIDE partner repository with the dataset identifier PXD028548 (https://www.ebi.ac.uk/pride/archive/projects/PXD028548). Fastq RNA sequencing files from this study have been deposited in the NCBI BioProject database under accession code PRJNA816072 (https://www.ncbi.nlm.nih.gov/bioproject/?term=PRJNA816072). All other data supporting the findings of this study are available within the article and its supplementary data.

Expanded View for this article is available online.

Acknowledgements

We thank Dr. Andres Lopez-Contreras (University of Copenhagen, Denmark) for support with mouse husbandry, and Drs. Xiaoyun Lu, Ke Ding (both Jinan University, China), and Paul Pryor (University of York, UK) for providing reagents. We thank Drs. Atul Deshmukh and Alba Gonzalez-Franquesa (both University of Copenhagen, Denmark) for help with C2C12 culture. For providing access to confocal and time-lapse microscopy we acknowledge the Danstem and NNF-CPR imaging platform (University of Copenhagen, Denmark). and Michele M. Nava (University of Helsinki) for help with mechanical manipulations. The Genotype-Tissue Expression (GTEx) Project was supported by the Common Fund of the Office of the Director of the National Institutes

of Health, and by NCI, NHGRI, NHLBI, NIDA, NIMH, and NINDS. Work in the Bekker-Jensen lab was supported by grants from the Lundbeck Foundation (R190-2014-4037), The Danish Medical Research Council (9039-00007B), The Novo Nordisk Foundation (NNF21OC0071475), The NEYE Foundation, The Nordea Foundation, and the European Research Council (ERC) under the European Union's Horizon 2020 research and innovation program (grant agreement 863911 - PHYRIST). Anna Constance Vind is supported by the BRIDGE—Translational Excellence Program funded by the Novo Nordisk Foundation (NNF20SA0064340). Christoffer Clemmensen receives funding from the Lundbeck Foundation (Fellowship R238-2016-2859) and the Novo Nordisk Foundation (grant number NNF17OC0026114). Novo Nordisk Foundation Center for Basic Metabolic Research is an independent Research Center, based on the University of Copenhagen, Denmark, and partially funded by an unconditional donation from the Novo Nordisk Foundation (www.cbmr.ku.dk) (Grant number NNF18CC0034900). Work in the Wojtaszewski lab was supported by a grant from the Danish Council for Independent Research—Medical Sciences (FSS 8020-00288) and a research grant to Rasmus Kjøbsted from the Danish Diabetes Academy, which is funded by the Novo Nordisk Foundation (NFF 17SA0031406). Work in Jesper Olsen's lab at The Novo Nordisk Foundation Center for Protein Research (CPR) is funded in part by a generous donation from the Novo Nordisk Foundation (Grant number NNF14CC0001).

Author contributions

Cathrine Nordgaard: Data curation; formal analysis; investigation; methodology; project administration. **Anna Constance Vind:** Conceptualization; data curation; formal analysis; investigation; methodology. **Amy Stonadge:** Data curation; formal analysis; investigation; methodology. **Rasmus Kjøbsted:** Data curation; formal analysis; methodology. **Goda Snieckute:** Data curation; investigation; methodology. **Pedro Antas:** Resources. **Melanie Blasius:** Data curation; investigation. **Marie Sofie Reinert:** Data curation; investigation. **Ana Martinez del Val:** Data curation; software; visualization; methodology. **Dorte Breinholdt Bekker-Jensen:** Formal analysis; methodology. **Peter Haahr:** Data curation; methodology. **Yekaterina Miroshnikova:** Supervision; methodology. **Abdelghani Mazouzi:** Resources. **Sarah Falk:** Data curation; methodology. **Emeline Perrier-Groult:** Data curation; methodology. **Christopher Tiedje:** Supervision; investigation. **Xiang Li:** Resources; methodology. **Jens Rithamer Jakobsen:** Data curation. **Nicolas Oldenburg Jørgensen:** Methodology. **Jørgen Wojtaszewski:** Supervision. **Frederic Mallein-Gerin:** Supervision. **Jesper Løvind Andersen:** Methodology. **Cristian Pablo Pennisi:** Supervision; methodology. **Christoffer Clemmensen:** Supervision; funding acquisition; methodology. **Moustapha Kassem:** Methodology. **Abbas Jaffari:** Methodology. **Thijn R Brummelkamp:** Resources; supervision; investigation. **Vivian SW Li:** Supervision; methodology. **Sara A Wickström:** Resources; supervision; writing – review and editing. **Jesper Velgaard Olsen:** Methodology. **Gonzalo Blanco:** Conceptualization; formal analysis; supervision; methodology. **Simon Bekker-Jensen:** Conceptualization; supervision; funding acquisition; writing – original draft; project administration.

Disclosure and competing interests statement

The authors have no positions, patents, or financial interests to declare.

References

Aragona M, Sifrim A, Malfait M, Song Y, Van Herck J, Dekoninck S, Gargouri S, Lapouge G, Swedlund B, Dubois C *et al* (2020) Mechanisms of stretch-mediated skin expansion at single-cell resolution. *Nature* 584: 268 – 273

Bamman MM, Roberts BM, Adams GR (2018) Molecular regulation of exercise-induced muscle fiber hypertrophy. *Cold Spring Harb Perspect Med* 8: a029751

Batth TS, Tollenaere MAX, Ruther P, Gonzalez-Franquesa A, Prabhakar BS, Bekker-Jensen S, Deshmukh AS, Olsen JV (2019) Protein aggregation capture on microparticles enables multipurpose proteomics sample preparation. *Mol Cell Proteomics* 18: 1027 – 1035

Bekker-Jensen DB, Bernhardt OM, Hogrebe A, Martinez-Val A, Verbeke L, Gandhi T, Kelstrup CD, Reiter L, Olsen JV (2020a) Rapid and site-specific deep phosphoproteome profiling by data-independent acquisition without the need for spectral libraries. *Nat Commun* 11: 787

Bekker-Jensen DB, Martinez-Val A, Steigerwald S, Ruther P, Fort KL, Arrey TN, Harder A, Makarov A, Olsen JV (2020b) A compact quadrupole-orbitrap mass spectrometer with FAIMS interface improves proteome coverage in short LC gradients. *Mol Cell Proteomics* 19: 716 – 729

Blythe NM, Muraki K, Ludlow MJ, Stylianidis V, Gilbert HTJ, Evans EL, Cuthbertson K, Foster R, Swift J, Li J *et al* (2019) Mechanically activated Piezo1 channels of cardiac fibroblasts stimulate p38 mitogen-activated protein kinase activity and interleukin-6 secretion. *J Biol Chem* 294: 17395 – 17408

Bougault C, Aubert-Foucher E, Paumier A, Perrier-Groult E, Huot L, Hot D, Duterque-Coquillaud M, Mallein-Gerin F (2012) Dynamic compression of chondrocyte-agarose constructs reveals new candidate mechanosensitive genes. *PLoS One* 7: e36964

Bougault C, Paumier A, Aubert-Foucher E, Mallein-Gerin F (2009) Investigating conversion of mechanical force into biochemical signaling in three-dimensional chondrocyte cultures. *Nat Protoc* 4: 928 – 938

Brockmann M, Blomen VA, Nieuwenhuis J, Stickel E, Raaben M, Bleijerveld OB, Altelaar AFM, Jae LT, Brummelkamp TR (2017) Genetic wiring maps of single-cell protein states reveal an off-switch for GPCR signalling. *Nature* 546: 307 – 311

Burkholder TJ (2007) Mechanotransduction in skeletal muscle. *Front Biosci* 12: 174 – 191

Chang Y, Lu X, Shibu MA, Dai YB, Luo J, Zhang Y, Li Y, Zhao P, Zhang Z, Xu Y *et al* (2017) Structure based design of N-(3-((1H-Pyrazolo[3,4-b]pyridin-5-yl)ethynyl)benzenesulfonamides as selective leucine-zipper and sterile-alpha motif kinase (ZAK) inhibitors. *J Med Chem* 60: 5927 – 5932

Chen-Izu Y, Izu LT (2017) Mechano-chemo-transduction in cardiac myocytes. *J Physiol* 595: 3949 – 3958

Cuenda A, Cohen P (1999) Stress-activated protein kinase-2/p38 and a rapamycin-sensitive pathway are required for C2C12 myogenesis. *J Biol Chem* 274: 4341 – 4346

Davis RJ (2000) Signal transduction by the JNK group of MAP kinases. *Cell* 103: 239 – 252

Finan JD, Guilak F (2010) The effects of osmotic stress on the structure and function of the cell nucleus. *J Cell Biochem* 109: 460 – 467

Fukuno N, Matsui H, Kanda Y, Suzuki O, Matsumoto K, Sasaki K, Kobayashi T, Tamura S (2011) TGF-beta-activated kinase 1 mediates mechanical stress-induced IL-6 expression in osteoblasts. *Biochem Biophys Res Commun* 408: 202 – 207

Gross EA, Callow MG, Waldbaum L, Thomas S, Ruggieri R (2002) MRK, a mixed lineage kinase-related molecule that plays a role in gamma-radiation-induced cell cycle arrest. *J Biol Chem* 277: 13873 – 13882

Hammaker D, Firestein GS (2010) "go upstream, young man": Lessons learned from the p38 saga. *Ann Rheum Dis* 69: i77 – i82

Hoffman L, Jensen CC, Yoshigi M, Beckerle M (2017) Mechanical signals activate p38 MAPK pathway-dependent reinforcement of Actin via mechanosensitive HspB1. *Mol Biol Cell* 28: 2661 – 2675

Hoffman NJ, Parker BL, Chaudhuri R, Fisher-Wellman KH, Kleinert M, Humphrey SJ, Yang P, Holliday M, Trefely S, Fazakerley DJ *et al* (2015) Global phosphoproteomic analysis of human skeletal muscle reveals a network of exercise-regulated kinases and AMPK substrates. *Cell Metab* 22: 922 – 935

Huangfu WC, Omori E, Akira S, Matsumoto K, Ninomiya-Tsuji J (2006) Osmotic stress activates the TAK1-JNK pathway while blocking TAK1-mediated NF-kappaB activation: TAO2 regulates TAK1 pathways. *J Biol Chem* 281: 28802 – 28810

Inagaki M, Omori E, Kim JY, Komatsu Y, Scott G, Ray MK, Yamada G, Matsumoto K, Mishina Y, Ninomiya-Tsuji J (2008) TAK1-binding protein 1, TAB1, mediates osmotic stress-induced TAK1 activation but is dispensable for TAK1-mediated cytokine signaling. *J Biol Chem* 283: 33080 – 33086

Jandhyala DM, Wong J, Mantis NJ, Magun BE, Leong JM, Thorpe CM (2016) A novel ZAK knockout mouse with a defective ribotoxic stress response. *Toxins* 8: 259

Jiang F, Yin K, Wu K, Zhang M, Wang S, Cheng H, Zhou Z, Xiao B (2021) The mechanosensitive Piezo1 channel mediates heart mechano-chemo transduction. *Nat Commun* 12: 869

Kechagia JZ, Ivaska J, Roca-Cusachs P (2019) Integrins as biomechanical sensors of the microenvironment. *Nat Rev Mol Cell Biol* 20: 457 – 473

Kramer HF, Goodyear LJ (2007) Exercise, MAPK, and NF-kappaB signaling in skeletal muscle. *J Appl Physiol* 1985: 388 – 395

Kumar A, Mazzanti M, Mistrik M, Kosar M, Beznoussenko GV, Mironov AA, Garre M, Parazzoli D, Shivashankar GV, Scita G *et al* (2014) ATR mediates a checkpoint at the nuclear envelope in response to mechanical stress. *Cell* 158: 633 – 646

Le HQ, Ghatak S, Yeung CY, Tellkamp F, Gunschmann C, Dieterich C, Yeroslaviz A, Habermann B, Pombo A, Niessen CM *et al* (2016) Mechanical regulation of transcription controls Polycomb-mediated gene silencing during lineage commitment. *Nat Cell Biol* 18: 864 – 875

Lee JH, Jun HS (2019) Role of Myokines in regulating skeletal muscle mass and function. *Front Physiol* 10: 42

Lessard SJ, MacDonald TL, Pathak P, Han MS, Coffey VG, Edge J, Rivas DA, Hirshman MF, Davis RJ, Goodyear LJ (2018) JNK regulates muscle remodeling via myostatin/SMAD inhibition. *Nat Commun* 9: 3030

Liu A, Yu T, Young K, Stone N, Hanasoge S, Kirby TJ, Varadarajan V, Colonna N, Liu J, Raj A *et al* (2020) Cell mechanical and physiological behavior in the regime of rapid mechanical compressions that lead to cell volume change. *Small* 16: e1903857

Liu X, Yao M, Li N, Wang C, Zheng Y, Cao X (2008) CaMKII promotes TLR-triggered proinflammatory cytokine and type I interferon production by directly binding and activating TAK1 and IRF3 in macrophages. *Blood* 112: 4961 – 4970

Luther PK (2009) The vertebrate muscle Z-disc: Sarcomere anchor for structure and signalling. *J Muscle Res Cell Motil* 30: 171 – 185

Marshall KL, Saade D, Ghitani N, Coombs AM, Szczot M, Keller J, Ogata T, Daou I, Stowers LT, Bonnemann CG *et al* (2020) PIEZO2 in sensory neurons and urothelial cells coordinates urination. *Nature* 588: 290 – 295

Martino F, Perestrelo AR, Vinarsky V, Pagliari S, Forte G (2018) Cellular mechanotransduction: From tension to function. *Front Physiol* 9: 824

Nava MM, Miroshnikova YA, Biggs LC, Whitefield DB, Metge F, Boucas J, Vihinen H, Jokitalo E, Li X, Garcia Arcos JM *et al* (2020) Heterochromatin-driven nuclear softening protects the genome against mechanical stress-induced damage. *Cell* 181: 800 – 817.e22

Nelson ME, Parker BL, Burchfield JG, Hoffman NJ, Needham EJ, Cooke KC, Naim T, Sylow L, Ling NX, Francis D *et al* (2019) Phosphoproteomics reveals conserved exercise-stimulated signaling and AMPK regulation of store-operated calcium entry. *EMBO J* 38: e102578

Pedersen BK, Febbraio MA (2008) Muscle as an endocrine organ: Focus on muscle-derived interleukin-6. *Physiol Rev* 88: 1379 – 1406

Powers SK (2017) Exercise: Teaching myocytes new tricks. *J Appl Physiol* 1985: 460 – 472

Randhawa A, Wakeling JM (2018) Transverse anisotropy in the deformation of the muscle during dynamic contractions. *J Exp Biol* 221: jeb175794

Saitoh M, Nishitoh H, Fujii M, Takeda K, Tobiume K, Sawada Y, Kawabata M, Miyazono K, Ichijo H (1998) Mammalian thioredoxin is a direct inhibitor of apoptosis signal-regulating kinase (ASK) 1. *EMBO J* 17: 2596 – 2606

Spielmann M, Kakar N, Tayebi N, Leettola C, Nurnberg G, Sowada N, Lupianez DG, Harabula I, Flottmann R, Horn D *et al* (2016) Exome sequencing and CRISPR/Cas genome editing identify mutations of ZAK as a cause of limb defects in humans and mice. *Genome Res* 26: 183 – 191

Swarnkar G, Karuppaiah K, Mbalaviele G, Chen TH, Abu-Amer Y (2015) Osteopetrosis in TAK1-deficient mice owing to defective NF-kappaB and NOTCH signaling. *Proc Natl Acad Sci U S A* 112: 154 – 159

Tobiume K, Saitoh M, Ichijo H (2002) Activation of apoptosis signal-regulating kinase 1 by the stress-induced activating phosphorylation of pre-formed oligomer. *J Cell Physiol* 191: 95 – 104

Tyanova S, Temu T, Sinitcyn P, Carlson A, Hein MY, Geiger T, Mann M, Cox J (2016) The Perseus computational platform for comprehensive analysis of (prote)omics data. *Nat Methods* 13: 731 – 740

Uhlik MT, Abell AN, Johnson NL, Sun W, Cuevas BD, Lobel-Rice KE, Horne EA, Dell'Acqua ML, Johnson GL (2003) Rac-MEKK3-MKK3 scaffolding for p38 MAPK activation during hyperosmotic shock. *Nat Cell Biol* 5: 1104 – 1110

Vasli N, Harris E, Karamchandani J, Bareke E, Majewski J, Romero NB, Stojkovic T, Barresi R, Tasfaout H, Charlton R *et al* (2017) Recessive mutations in the kinase ZAK cause a congenital myopathy with fibre type disproportion. *Brain* 140: 37 – 48

Vind AC, Genzor AV, Bekker-Jensen S (2020a) Ribosomal stress-surveillance: Three pathways is a magic number. *Nucleic Acids Res* 48: 10648 – 10661

Vind AC, Snieckute G, Blasius M, Tiedje C, Krogh N, Bekker-Jensen DB, Andersen KL, Nordgaard C, Tollenaere MAX, Lund AH *et al* (2020b) ZAKalpha recognizes stalled ribosomes through partially redundant sensor domains. *Mol Cell* 78: 700 – 713.e7

Wagner EF, Nebreda AR (2009) Signal integration by JNK and p38 MAPK pathways in cancer development. *Nat Rev Cancer* 9: 537 – 549

Wakeling JM, Ross SA, Ryan DS, Bolsterlee B, Konno R, Dominguez S, Nigam N (2020) The energy of muscle contraction. I. Tissue force and deformation during fixed-end contractions. *Front Physiol* 11: 813

Wang L, You X, Lotinun S, Zhang L, Wu N, Zou W (2020) Mechanical sensing protein PIEZO1 regulates bone homeostasis via osteoblast-osteoclast crosstalk. *Nat Commun* 11: 282

Wieczorek S, Combes F, Lazar C, Giai Gianetto Q, Gatto L, Dorffer A, Hesse AM, Coute Y, Ferro M, Bruley C *et al* (2017) DAPAR & ProStaR: Software to perform statistical analyses in quantitative discovery proteomics. *Bioinformatics* 33: 135 – 136

Wu CC, Peterson A, Zinshteyn B, Regot S, Green R (2020) Ribosome collisions trigger general stress responses to regulate cell fate. *Cell* 182: 404 – 416.e4

Wu J, Lewis AH, Grandl J (2017) Touch, tension, and transduction - the function and regulation of piezo ion channels. *Trends Biochem Sci* 42: 57 – 71

Xia Y, Pfeifer CR, Cho S, Discher DE, Irianto J (2018) Nuclear mechanosensing. *Emerg Top Life Sci* 2: 713 – 725

Yang H, Wang H, Jaenisch R (2014) Generating genetically modified mice using CRISPR/Cas-mediated genome engineering. *Nat Protoc* 9: 1956 – 1968